2016

Design and Implementation of QCM Virtual Sensing Schemes for Analyses of Volatile Organic Compounds

Nicholas Colby Speller
Louisiana State University and Agricultural and Mechanical College, nspell1@lsu.edu

DESIGN AND IMPLEMENTATION OF QCM VIRTUAL SENSING SCHEMES FOR ANALYSES OF VOLATILE ORGANIC COMPOUNDS

A Dissertation

Submitted to the Graduate Faculty of the
Louisiana State University and
Agricultural and Mechanical College
in partial fulfillment of the
requirements for the degree of
Doctor of Philosophy

in

The Department of Chemistry

by
Nicholas Colby Speller
B.S., Morehouse College, 2011
B.S., Morehouse College, 2011
August 2016

I dedicate this dissertation to:

My beautiful mother and father who are the perpetual “Sun and Moon” that have guided the “orbit and tides” of my life. Who have instilled poise and self confidence within me from the beginning, along with the virtues of hard work, dedication, and perseverance

May this milestone bring them great joy and pride in seeing the growth of the seed that they sowed and tended to with great toil imbued with unending love

My sisters who are sources of love, happiness, inspiration, compassion, and understanding

May my path also be a source of inspiration, happiness, and pride

My grandparents who are sources of love, wisdom, and inspiration

May they take pride in this achievement as it is a culmination of the values they impressed upon their children and ultimately upon me

My aunts, uncles, and cousins who are sources love, happiness, wisdom, and inspiration

May they take pride in my path and may it serve as a source of inspiration and guidance for those who may walk it after me

ACKNOWLEDGEMENTS

My journey towards a PhD has only been realized with the help and contributions of others. Hence, I give these efforts a fitting and much deserved acknowledgement.

First, I acknowledge my advisor, Professor Isiah Warner. You have been the invaluable source of knowledge and guidance that has propelled me throughout my graduate education. Your trust, compassion and understanding provided an environment under which I was able to flourish and develop into a scientist. We have spoken many times about my uncertainty about what the future holds for me. However, the past is unchanging, and thus one thing is for certain. I truly believe that without you, I would not have made this journey towards a PhD. I am forever indebted to you for all of your time and effort expended on my behalf. Thank you for taking me under your tutelage and being the unwavering, assiduous mentor and person that you are.

I acknowledge my post doc Dr. Noureen Siraj. Thank you for being another beacon of wisdom and compassion. I have truly benefited from your support, discussion, and advice on countless topics throughout my graduate years. Thank you from the bottom of my heart.

I thank my PhD committee for their time, insights, and valuable discussions throughout my graduate education.

I acknowledge Professor Randy Duran and Dr. Zakiya Wilson for their recruitment to LSU and subsequent support. Without them the door to embarking on this journey may not have opened or may have closed prematurely. Thank you for enabling this experience.

I acknowledge all of my coworkers, past and present, within the Warner Research Group, friends, and peers that have made my graduate experience in Baton Rouge a fruitful and memorable endeavor. Thank you for your guidance, compassion, wisdom, and caring throughout my graduate years.

Last but not least, I acknowledge my family without whom I would have never made this journey. Thank you for your love, compassion, and reassurance.

TABLE OF CONTENTS

ACKNOWLEDGEMENTS iii

ABSTRACT viii

CHAPTER 1. INTRODUCTION 1
1.1 Volatile Organic Compounds Importance and Analysis 1
1.1.1 Volatile Organic Compounds 1
1.1.2 Importance of VOC Detection and Determination 1
1.1.3 VOCs Analysis 2
1.1.4 Cross Reactive Sensor Arrays 4
1.1.5 Multisensor Arrays 4
1.1.6 Virtual Sensor Arrays 6
1.2 Quartz Crystal Microbalance based Sensors for VOC analysis 7
1.2.1 Desire for Quartz based Devices 8
1.2.2 Quartz Crystal Microbalance 8
1.2.3 Piezoelectricity 8
1.2.4 Quartz Crystal Resonators 10
1.2.5 Acoustic Shear Waves and Basic QCM Principle of Operation 12
1.2.6 Overtones 13
1.2.7 QCR Resonance 14
1.2.8 Quartz Crystal Microbalance with Dissipation Monitoring Technique 16
1.2.9 Gravimetric and Non-gravimetric Sensing in Air using the QCM 17
1.2.10 Chemosensitive Materials for QCM based VOC Sensors 20
1.2.11 Ionic Liquids and GUMBOS 21
1.2.12 Ionic Liquid based QCM Sensor Arrays 22
1.3 Statistical Analysis 24
1.3.1 Principal Component Analysis (PCA) 25
1.3.2 Discriminant Analysis (DA) 27
1.4 Scope of Dissertation 28
1.5 References 30

CHAPTER 2. RATIONAL DESIGN OF QCM-D VIRTUAL SENSOR ARRAYS BASED ON FILM THICKNESS, VISCOELASTICITY AND HARMONICS FOR VAPOR DISCRIMINATION* 41
2.1 Introduction 41
2.2 Experimental Section 44
2.2.1 Preparation of Stock Solutions 44
2.2.2 Preparation of Sensing Films 44
2.2.3 QCM-D Data Acquisition 44
2.2.4 Data Analysis 45
2.3 Results and Discussion 46
2.3.1 Preparation and Characterization of Sensing Films 46
2.3.2 Examination of the Effect of Film Thickness on Gas-sensing Response 46
2.3.3 Fabrication and Evaluation of Virtual Sensor Arrays 49
2.4 Conclusions 60
2.5 References 61

CHAPTER 3. QCM VIRTUAL SENSOR ARRAY: VAPOR IDENTIFICATION AND MOLECULAR WEIGHT APPROXIMATION 66
3.1 Introduction 66
3.1.1 Approach 68
3.1.2 Theory of QCM based Molecular Weight Approximation 70
3.1.3 Theory of QCM based Virtual Sensing 71
3.2 Experimental Section 72
3.2.1 Reagents and Materials 72
3.2.2 Instrumentation 72
3.2.3 Synthesis of Ionic Liquid 72
3.2.4 Preparation of Stock Solutions 73
3.2.5 Preparation of Sensing Films 73
3.2.6 Film Characterization 73
3.2.7 QCM-D Data Acquisition 73
3.2.8 Data Analysis 74
3.3 Results and Discussion 74
3.3.1 Preparation and Characterization of Sensing Films 74
3.3.2 Examination of the Effect of Film Thickness on Gas-sensing Response of Ionic Liquid-Polymer Composites 75
3.3.3 Fabrication and Evaluation of a Virtual Sensor Array for Discrimination and Molecular Weight Approximation 78
3.3.4 Evaluation of a Virtual Sensor Array for Discrimination of Alcohols and Isomers 80
3.4 Conclusions 85
3.5 References 86

CHAPTER 4. ASSESSMENT OF QCM ARRAY SCHEMES FOR MIXTURE IDENTIFICATION: CITRUS SCENTED ODORS 90
4.1 Introduction 90
4.2 Approach 92
4.2.1 Array Fabrication 92
4.2.2 QCM Virtual Sensor Arrays 93
4.2.3 QCM Virtual Multisensor Arrays 95
4.3 Experimental Section 96
4.3.1 Reagents and Materials 96
4.3.2 Preparation of Stock Solutions 96
4.3.3 Preparation of Sensing Films 96
4.3.4 QCM-D Data Acquisition 97
4.3.5 Data Analysis 97
4.4 Results and Discussion 98
4.4.1 Sensor Response of ILs to Odors 98
4.4.2 Evaluation of a Multisensor Array for Odor Recognition 98
4.4.3 Evaluation of Virtual Sensor Arrays for Odor Recognition 101
4.4.4 Evaluation of Virtual Multisensor Sensor Arrays for Odor Recognition 103
4.5 Conclusion 108
4.6 References 109

CHAPTER 5. QCM VIRTUAL MULTISENSOR ARRAY FOR FUEL DISCRIMINATION AND DETECTION OF GASOLINE ADULTERATION 111

5.1 Introduction 111
5.2 Experimental Section 114
5.2.1 Reagents and Materials 114
5.2.2 Preparation of Stock Solutions 114
5.2.3 Preparation of Sensing Films 114
5.2.4 Preparation of Fuel Samples 115
5.2.5 Preparation of Adulterated Samples 115
5.2.6 Array Fabrication 115
5.2.7 Data Acquisition 116
5.2.8 Data Analysis 116
5.3 Results and Discussion 117
5.3.1 Fuel Discrimination using a QCM V-MSA 117
5.3.2 Gasoline Grade Discrimination using a QCM V-MSA 119
5.3.3 Detection of Gasoline Adulteration using a QCM V-MSA 121
5.4 Conclusion 125
5.5 References 125

CHAPTER 6. CONCLUSIONS AND FUTURE WORK 130
6.1 Conclusions 130
6.2 Future Work 132

APPENDIX A: SUPPORTING INFORMATION FOR CHAPTER TWO 134

APPENDIX B: SUPPORTING INFORMATION FOR CHAPTER THREE 153

APPENDIX C: SUPPORTING INFORMATION FOR CHAPTER FOUR 156

APPENDIX D: SUPPORTING INFORMATION FOR CHAPTER FIVE 164

APPENDIX E: LETTER OF PERMISSION 195

VITA 196

ABSTRACT

Sensor arrays have evolved as powerful approaches for providing detection and discrimination of volatile organic compounds (VOCs) as required across numerous analytical applications. Such systems typically comprise a number of cross reactive sensor elements, which generate analyte specific response patterns upon exposure to VOCs, and are known as multisensor arrays. When evaluated using statistical methods, these response patterns facilitate classification of VOCs. As an alternative, a single dynamically operated sensor could also be used to generate analyte specific response patterns. This approach is known as a virtual sensor array (VSA) and can exhibit significant advantages when compared to MSAs. Some advantages include lower power consumption, sensor drift, material cost, and experimental preparatory time. Furthermore, several dynamically operated sensors could be used in tandem (using the MSA and VSA scheme in a complementary fashion) to fabricate virtual multisensor arrays (V-MSAs). Such systems would exhibit greater data density than either the MSA or VSA, and are promising for samples that are particularly challenging to discriminate.

Among the various systems utilized for VOC discrimination, sorption based systems hold considerable promise because they are simple and inexpensive yet highly effective. This dissertation is focused on the development of array sensing schemes using ionic liquids (ILs), a group of uniform materials based on organic salts (GUMBOS), and binary blends of either IL or GUMBOS with polymer as recognition elements and the quartz crystal microbalance (QCM) as the transducer. Towards this end, ILs, which are defined as organic salts with melting points below 100 °C, and group of uniform materials based on organic salts (GUMBOS) which extend the melting range of ILs to 250 °C to encompass similar solid phase salts, were used to design the first examples of QCM based VSAs, and V-MSAs, for pure VOC and complex mixture analyses. Furthermore binary blends of organic salts and polymer were used to fabricate the first

VSA with the capability to identify and approximate molecular weight of pure VOCs. By and large, the studies presented here demonstrate the excellent potential of these materials and techniques for advancement of vapor phase measurement science.

CHAPTER 1. INTRODUCTION

1.1 Volatile Organic Compounds Importance and Analysis

1.1.1 Volatile Organic Compounds

Volatile organic compounds (VOCs) are a ubiquitous class of organic chemicals, which readily evaporate or sublimate under ambient conditions. Typically, VOCs exhibit molecular weights below 300 Da and weak intermolecular forces. As a result, they exhibit low boiling points and high vapor pressures. In fact, VOCs have been defined by the World Health Organization as organic compounds with boiling points from about 50°C to about 260°C.[1] Notably, VOCs are emitted from numerous sources, both natural and artificial. Furthermore, complex mixtures of VOCs constitute many familiar odors or aromas. Moreover, natural sources, such as plants, animals, and microorganisms, emit a large variety of VOCs, for a number of reasons.[2] These might include communication,[3–7] self-preservation,[8–10] or as metabolic byproducts.[9,11–13] Artificial sources, such as industrialization, are also major contributors to global VOC emissions, evidenced by environmental concern and regulatory efforts.[14–19] When considering the ubiquitous nature and societal impact of VOCs, it is not surprising that it would be important to detect and analyze this class of chemicals.

1.1.2 Importance of VOC Detection and Determination

While some VOCs are innocuous, many can be harmful. Acute and chronic exposure to harmful VOCs can have numerous health and environmental effects.[20,21] Some of the most deleterious health effects caused by VOC exposure, include cancer, as well as damage to the central nervous system, kidneys, liver and lungs. Other, less severe, effects include headache, irritation, allergic reactions, nausea, fatigue and dizziness. Notably, concentrations of certain VOCs can be many times higher indoors vs outdoors depending on usage/function of the space.[1,22–25] This may have direct implications on life quality as many people spend the majority of their time indoors.

Thus, development of gas sensing approaches for detection and identification/discrimination of VOCs has attracted considerable research interest. In this regard, research is driven by requirements to monitor VOCs in many sectors including environmental protection, industry, health, and safety.[12,13,26–36] Since VOCs are characteristic of the emission source, they can be used as markers for identification of various conditions. As a result, VOC analyses can be used for many applications including assessment of food quality,[29,37–39] detection of disease states,[11–13,40,41] or the presence of explosives.[42–44] With such a large variety in potential applications, many different methods have been devised to analyze VOCs.

1.1.3 VOCs Analysis

GC-MS has long been regarded as the “gold standard” method for VOC analysis.[45] However, such instrumentation is expensive and requires significant expertise to employ effectively.[20,45] As a result, researchers have endeavored to find sensitive, simplistic, and cost effective alternatives for VOCs analysis. In this regard, sorption based gas sensor technology has proven increasingly attractive. Generally, such sensors are comprised of a recognition element coupled with an appropriate transducer. A recognition element is composed of a chemosensitive material, which exhibits a change of physical or chemical properties upon interaction with analytes. Transducers convert the change in properties to an electronic signal that allows quantification of the interaction. In this regard, most commonly employed transducers fall within four main classes of transduction e.g. electrochemical, thermometric, optical and gravimetric transduction.

Electrochemical transducers typically measure change in conductivity, resistance, permittivity or impedance.[46] The most common examples of these devices in sorption based VOCs sensing are chemicapacitors and chemiresistors.[46] Well known examples of chemicapacitive sensors are demonstrated in Micro-Electro-Mechanical

Systems (MEMS) sensors[47] while examples of chemiresistive sensors are Metal Oxide Semiconductor (MOS) sensors.[48] Such sensors are characteristic of the internal components in many commercially fabricated electronic noses.[48]

Thermal transducers, as the name suggests, measure change in thermal energy. Chemical sensors that employ this transducer are based on the first law of thermodynamics which states: when internal energy of a system changes, heat is either absorbed or produced.[46] This is important because many chemical reactions absorb or produce heat (endothermic or exothermic). Hence, these sensors have been designed to quantify heat transfer during such chemical reactions. The most common examples of this sensor class when employed for VOC sensing are calorimetric and catalytic sensors.[49–53]

Optical transducers measure interaction of the electromagnetic spectrum with chemicals or chemosensitive materials. In this regard, many spectroscopic techniques can be applied as a transducer to create optical sensors for VOC detection. These sensors are widely used in literature, and popular examples include fluorescence,[43,54,55] UV-VIS,[20,28,56–58] and surface plasmon resonance based sensors.[59–61]

Gravimetric transducers measure mass change. Common examples of sensors that employ gravimetric transduction include surface acoustic wave (SAW) sensors,[48,62,63] thickness shear mode (TSM) sensors,[48,62,63] and mircocantilevers.[62,64] These transducers, typically fabricated from a piezoelectric material, quantify change in mass as a function of change in frequency or vibrational properties. This dissertation will focus on the quartz crystal microbalance (QCM) which is a member of the TSM class of acoustic wave sensors. Herein, applications in VOC sensing will be explored. Further detail on operation of the QCM will be explained in section 1.2. While many types of sensors have proven robust for detection of gases, as individual entities, they are typically not the most efficient means for analyses of gases.

1.1.4 Cross Reactive Sensor Arrays

A popular approach for analyzing volatile organic compounds (VOCs) is use of cross-reactive sensor arrays (CRSAs).[20,28,29,35,37,48,65–69] The advantage of these systems lies in their ability to identify/ discriminate samples, without the need to identify individual VOCs. In fact, the operating principle was developed to mimic the excellent performance of biological olfactory systems.[67] For example, the typical olfactory system employs numerous cross reactive receptors that generate response signals from odor stimuli. The aggregate of these responses is then processed by the brain to identify a particular odor. CRSAs mimic this operating principle, on a smaller scale, by employing cross reactive sensors/ sensing schemes. A schematic for the operating principle of CRSAs is depicted in Figure 1.1. With regard to quartz crystal microbalance based sensor arrays, there are two main array schemes employed by CRSAs reported in literature: 1) Multisensor array 2) Virtual Sensor Array. Each scheme will be explored within this dissertation.

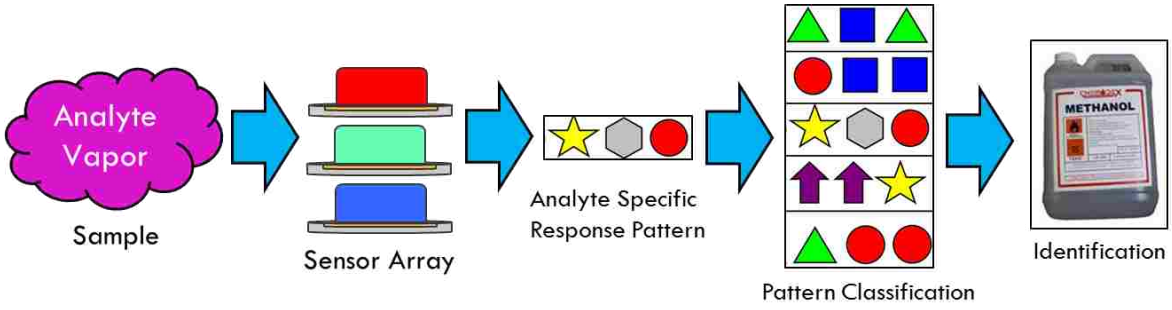

Figure 1.1 Schematic of CRSA operating principle.

1.1.5 Multisensor Arrays

The majority of CRSAs reported in the literature are known as multisensor arrays (MSAs). In this array scheme, several cross reactive sensors are employed in a tandem fashion. Subsequently, these sensors are exposed to an analyte of interest. Each sensor

responds to all analytes however to varying degrees. In this regard, the sensors exhibit differential responses. When taken in aggregate, the responses of all sensors constitute and analyte specific response pattern. Such patterns are then employed using pattern classification techniques or statistical approaches to identify or discriminate analytes. Statistical approaches will be discussed in further detail in section 1.3. An example of a multisensor array scheme for the QCM is depicted in Figure 1.2.

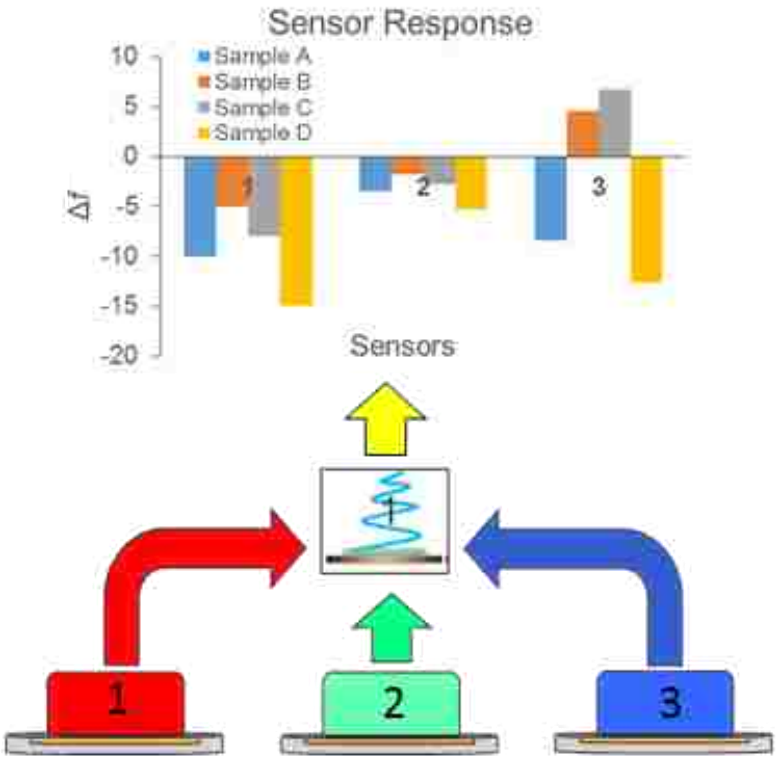

Figure 1.2 Schematic of a QCM based multisensor array, where 1, 2, and 3 represent chemically distinct sensors and the small sensor labeled one represents a single harmonic.

This array scheme effectively converts the limitation of partial selectivity, which is observed for many chemosensitive materials and their corresponding sensors, into an advantage. Although a very robust scheme, MSAs, suffer from a number of limitations. A few examples might include sensor drift, increased preparative time, and requirement

of judicious selection of sensing materials and numerous physical sensors are a few among others. To address these limitations, researchers have strived to develop effective alternative array schemes. Hence, virtual sensor arrays (VSAs) were developed as a viable alternative.

1.1.6 Virtual Sensor Arrays

VSAs consist of a small number of sensors or only a single sensor that can contribute many quasi-independent responses to the resultant array output pattern.[69] In simpler terms, this sensing scheme is based on dynamic operation of physical sensors to generate additional sensor responses. This mimics inclusion of a larger number of physical sensors within an array however these sensors are nonexistent i.e. virtual sensors. This approach can address limitations in sensor drift, data dimensionality, cost, and complexity that are encountered with use of a MSA.[69] Notably, the operating principle is largely similar to that employed by an MSA. In this regard, a number of (single) dynamically operated sensor(s) are (is) exposed to an analyte and measurements are obtained. The aggregate of sensor responses form an analyte specific response pattern. Since pattern classification is independent of the data collection method these measurements are subject to the same statistical treatment utilized by MSAs. Dynamic operation as exploited by VSAs, typically employs an easily tunable variable or factor that suitably alters sensor response. Such variables might include temperature, exposure time, excitation energy, data windows, frames, or carrier gas etc.[69] Incidentally, devices based on temperature variation, such as metal oxide sensors and field effect transistor (MOSFET) devices, represent the most extensively reported examples of VSAs.[70,71] Other non-conventional VSAs involving the use of tandem methods have also been documented.[41,42,72] Within this dissertation, two types of dynamically operated arrays are distinguished. In this regard, VSAs comprising only a single sensor are termed VSAs, while those comprising multiple sensors are termed

Virtual Multisensor Arrays. (V-MSAs). An example of a virtual sensor array scheme for a QCM is depicted in Figure 1.3.

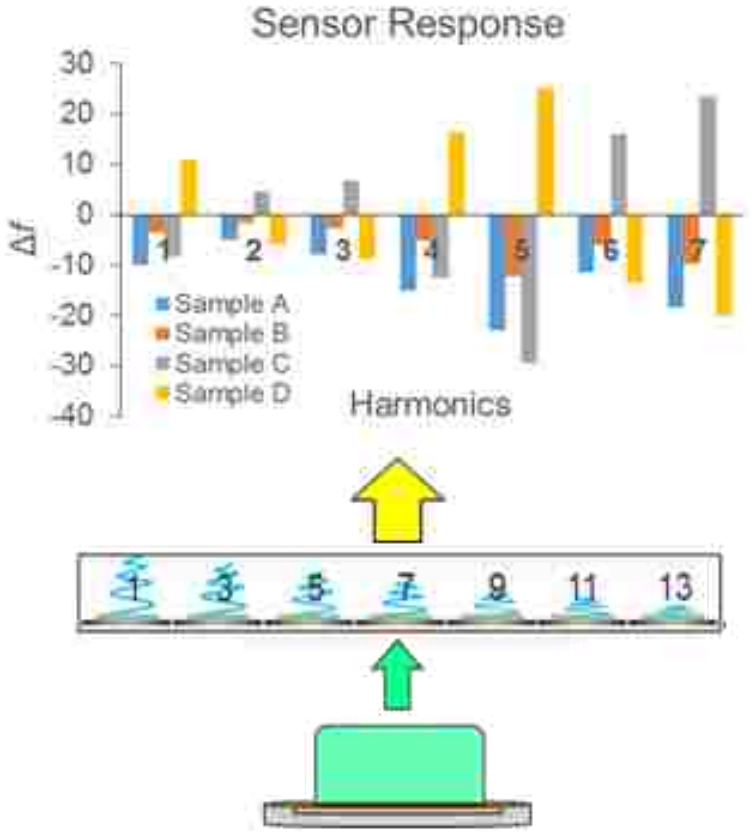

Figure 1.3 Schematic of a QCM based virtual sensor array, where sensors 1-13 represent seven harmonics utilized for dynamic operation.

1.2 Quartz Crystal Microbalance based Sensors for VOC analysis

Quartz crystal microbalance based sensors are comprised of a QCM transducer coupled with an appropriate chemsosensitive adlayer for detection of a desired analyte. The selected coupling of chemosensitive material (recognition element) and transducer is essential for successful operation of sensors and the sensor arrays which they comprise. Section 1.2 will detail fundamental background on the QCM as well as explore promising chemosensitive materials which have been employed as adlayers.

1.2.1 Desire for Quartz based Devices

To discuss the development of the quartz crystal microbalance, it is worth briefly mentioning the developmental history of quartz based devices. The original desire for quartz based devices stemmed from the development of quartz based clocks and radios among other military and civilian technologies.[73,74] Such devices employed quartz crystal oscillators to supply their various functions. Within each device the quartz crystal was typically sequestered away from the surrounding environment because their proper function was sensitive to environmental changes. Interestingly, it is exactly this non ideal scenario of quartz within a clock or radio that made it attractive for fabrication of a sensitive instrument.

1.2.2 Quartz Crystal Microbalance

The quartz crystal microbalance (QCM) is a simple, yet sensitive, tool for monitoring changes in force along the quartz surface. In simplest terms, the device comprises a power source, interface electronics and quartz oscillator. In this regard, the device uses the power source to drive the oscillator and interface electronics are used to monitor environmental changes that come in contact with the oscillator surface. This oscillator, more specifically termed a quartz crystal resonator (QCR), operates based on the converse piezoelectric effect, and is the centerpiece of the device. Incidentally, there have been several types of oscillators, circuits and interface electronics developed to generate optimal QCM devices. The remainder of section 1.2 will explore the discovery of piezoelectricity, development of quartz resonators and design and application of the QCM.

1.2.3 Piezoelectricity

Central to the development of quartz based technology is a foundational understanding of piezoelectricity. In this regard, piezoelectricity is a form of electrical energy generated from mechanical deformation of crystalline materials that exhibit

asymmetrically charged unit cells.[74] The term piezoelectricity was coined by Hankel.[75] However, this phenomenon was discovered by physicists Pierre and Jacques Curie when examining asymmetric crystalline structures in 1880, and termed the piezoelectric effect.[74] At this time, the Curie brothers established the existence of the piezoelectric effect using crystalline materials such as quartz, topaz, and Rochelle salt. In 1881, Gabriel Lippman mathematically deduced that the converse piezoelectric effect should exist,[76] and this deduction was experimentally proven by the Curies thereafter.[77] A visual example of the piezoelectric effect using a mock quartz unit cell is depicted in Figure 1.4, while Figure 1.5 is a depiction of the converse piezoelectric effect. The converse piezoelectric effect, which states that application of an electric voltage to a piezoelectric material causes a mechanical deformation, is particularly important to the function of the quartz crystal microbalance. Notably these discoveries have allowed quartz (as well as

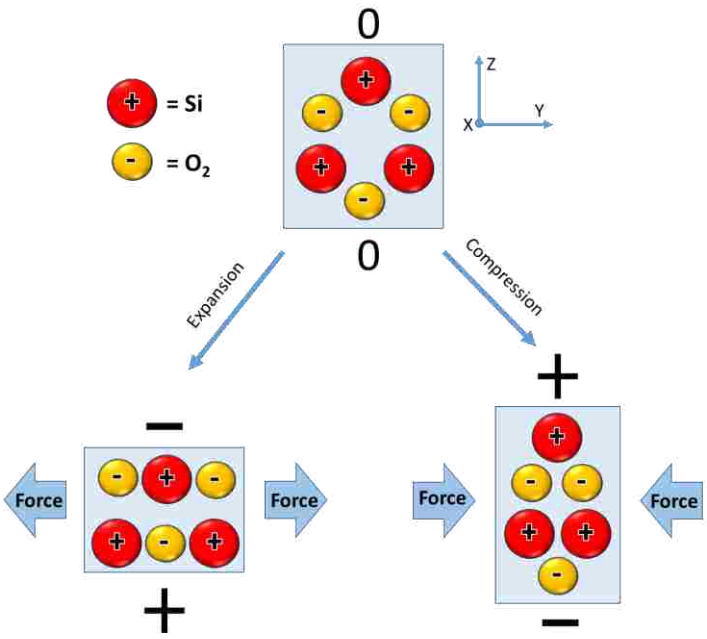

Figure 1.**4** Schematic of the piezoelectric effect in a quartz crystal lattice. Adapted from https://www.creationscience.com/onlinebook/Radioactivity2.html (Accessed 2/2016)

other piezoelectric materials) to be employed in applications ranging from time keeping to telecommunications. However for successful implementation of the piezoelectric properties of quartz to occur, specific cuts had to be developed. In this regard the quartz resonator employed in the QCM is no different.

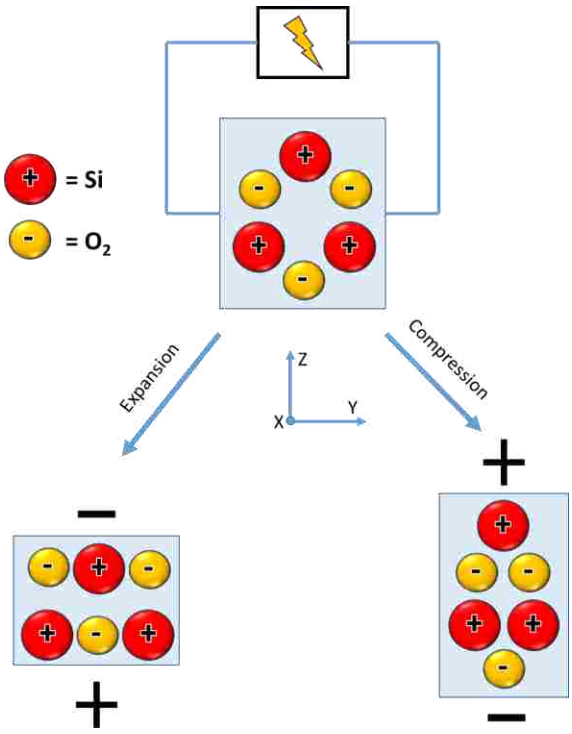

Figure 1.5 Schematic of the converse piezoelectric effect in a quartz crystal lattice.

1.2.4 Quartz Crystal Resonators

About 40 years after the discovery of piezoelectricity, the first quartz resonator was developed and employed for frequency stabilization.[73,74] Unfortunately these devices suffered from temperature-frequency coupling. This is a condition where temperature adversely effects crystal oscillation causing undesirable frequency shifts. To overcome this limitation, two temperature compensated crystal cuts were developed by Koga in the 1930's.[73,74,78] These cuts, termed AT and BT shear cuts are still employed today. The cutting scheme for AT cut quartz is depicted in Figure 1.6. The angle of the cut relative

to the axes of the quartz determines the temperature-frequency coupling characteristics. There are other cuts in existence however only the AT cut is relevant to the QCM employed herein. The QCR utilized within this dissertation employs an AT cut quartz wafer with electrodes on both sides. In this regard, gold electrodes were utilized on the QCRs employed, since they are robust and chemically inert.

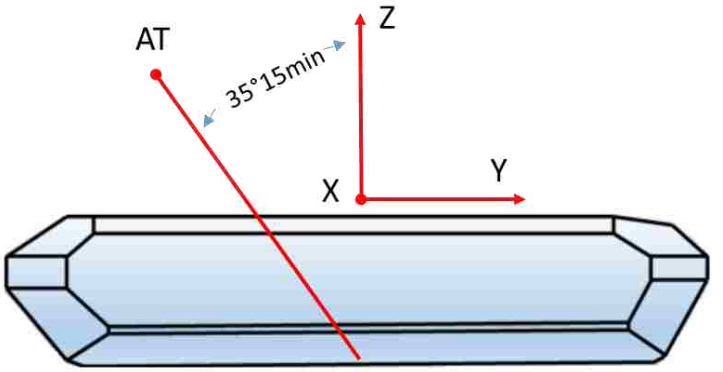

Figure 1.6. Schematic of AT cut quartz

A schematic of a typical QCR used in a QCM is depicted in Figure 1.7. These resonators are known as thickness shear mode resonators and under AC voltage generate an acoustic wave from the surface that is essential to QCM operation. Section 1.2.5 will discuss the basic operating principles of QCRs that contribute to the function of the QCM.

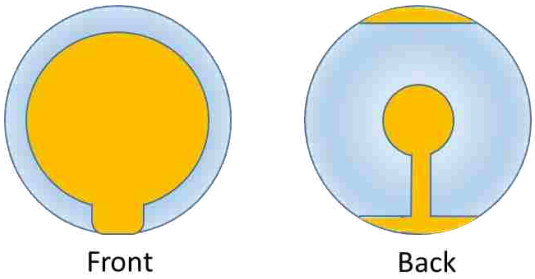

Figure 1.7 Schematic representation of a quartz crystal resonator with gold electrodes.

1.2.5 Acoustic Shear Waves and Basic QCM Principle of Operation

From the converse piezoelectric effect, applying an AC voltage across a QCR should result in a mechanical deformation or in this case crystal oscillations. These oscillations ultimately give rise to an acoustic wave. A schematic of crystal oscillation under applied voltage for a QCR is depicted in Figure 1.8. It should be noted that the oscillation of the crystal is parallel to the crystal surface which is typical of a thickness shear mode resonator. Specifically, QCR oscillations exhibit sine wave behavior, with nodes inside the crystal and antinodes at the crystal surface, under resonance conditions. This behavior generates an acoustic wave that propagates perpendicular to the QCR surface with a wavelength that is approximately twice the QCR thickness at the fundamental frequency. This relationship is given by equation 1.1.[73]

$$f = \frac{c_q}{\lambda} = \frac{c_q}{2\left(d_q + d_f\right)} \qquad (1.1),$$

Where *f* is frequency, c_q is speed of sound, d_q is thickness of the QCR, and d_f is the film thickness. This acoustic wave is known as the resonance frequency.[73] It is one of the two parameters exploited for measurements with the quartz crystal microbalance. (The other is dissipation which is discussed in section 1.2.7) If sorption of an analyte or deposition of a material on the surface of a QCR is considered increasing the thickness of the QCR, it is easy to see why the QCM would be sensitive to change in surface mass. In this regard, increases in QCR thickness, would result in decreases of resonance frequency. This relationship was discovered by Gunter Sauerbrey in the 1960's and is the basis of gravimetric sensing (use of the QCM as a mass detector) using the QCM. Equation 1.2 denotes the Sauerbrey equation.[79] Where Δf is change in

$$\Delta f = -\frac{n}{c}\Delta m = -\frac{n}{c}\rho_f t_f \qquad (1.2),$$

resonance frequency, n is harmonic number, c is mass sensitivity which is 17.7 ngcm^{-2}Hz^{-1} for the 5MHz AT cut crystal used herein, ρ_f is the density of the film, and t_f is film thickness.

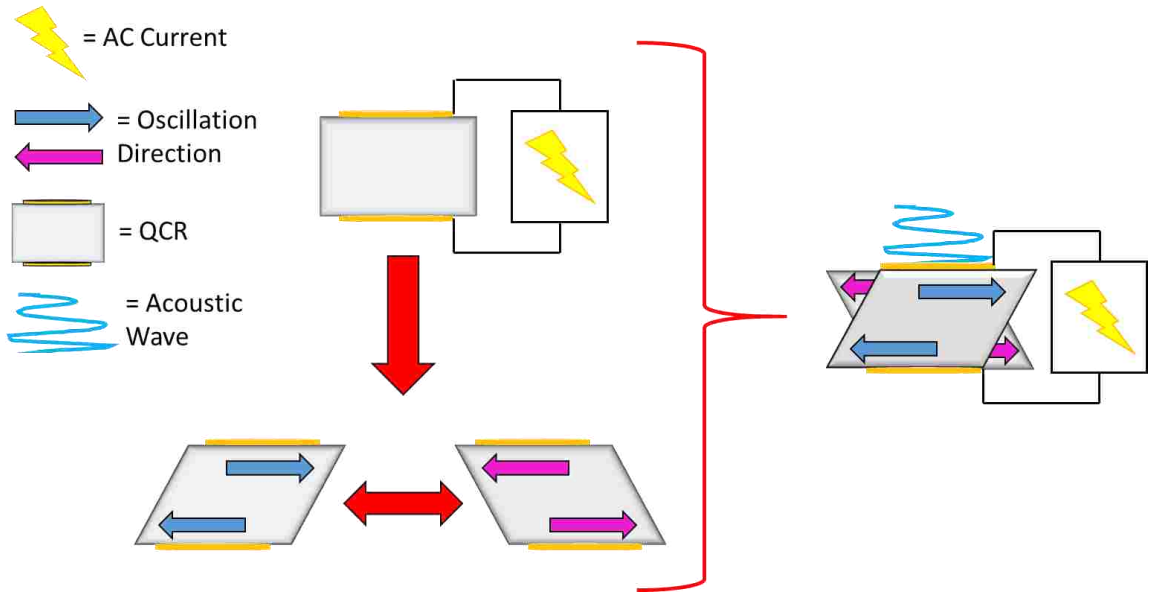

Figure 1.8 Schematic of QCR under applied voltage

1.2.6. Overtones

Since resonance conditions of the QCR are achieved electrically, it is possible to excite the QCR to higher energy resonances. This process results in the generation of overtones or harmonics of the fundamental frequency. Interestingly, it is only possible to excite odd harmonics due to reverse polarity of the electrodes on the QCR surface. Examples of wave behavior exhibited by the QCR are depicted in Figure 1.9. It should be noted from the figure that it is possible to have multiple resonances with nodes in the center of the crystal. In this regard, a wave with a single node is characteristic of the fundamental frequency (1st harmonic), while a wave with three nodes is characteristic of

the 3rd harmonic. Hence, the number of nodes parallel to the resonator surface corresponds to the overtone number. Moreover, as the number of nodes increases, the wavelength decreases resulting in an increase in frequency. Thus, each overtone represents a higher frequency than the fundamental frequency. As the frequency of the acoustic wave increases, the penetration depth of the acoustic wave decreases. Incidentally, at higher frequencies, sensitivity increases however, so does instrumental noise. Additionally, it is worth noting that penetration depth of the acoustic wave is also dependent upon the density and viscosity of the environment in contact with QCR surface. The mathematical relationship for penetration depth is depicted in equation 1.3.

$$\delta = \sqrt{\frac{2\eta}{\rho\omega}} \quad where\ is\ \omega = 2\pi f \qquad (1.3),$$

Where σ = penetration depth, η= viscosity of the adlayer, ρ= density of the adlayer, ω is the angular frequency and *f* is frequency. Multiple harmonics have been employed for the work presented within this dissertation.

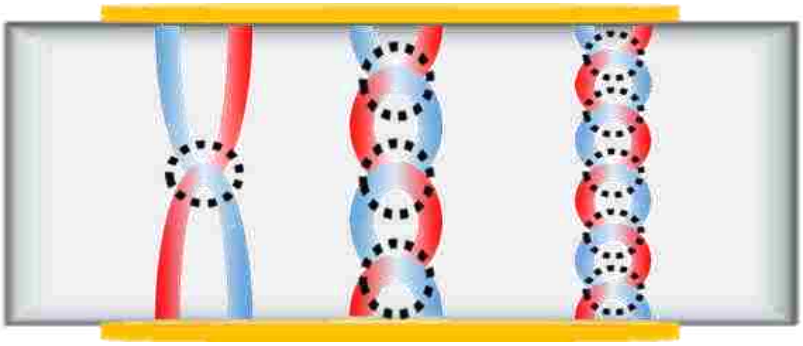

Figure 1.9 Schematic of wave behavior inside the QCR.

1.2.7 QCR Resonance

The QCM technique utilized in this dissertation employs QCRs under resonance conditions. Such resonances are found by electrically exciting the QCR, across a range

of frequencies, and monitoring conductance of the system. In this regard, resonance occurs at those frequencies that exhibit peak conductance as depicted in Figure 1.10. Each QCR is capable of several resonances and this is directly related to overtones. For example, the first resonance of the QCRs employed herein would be exhibited at 5 MHz (fundamental frequency). Thus, overtones would be exhibited at odd multiples of this frequency. Therefore the 3rd harmonic would exhibit resonance at 15 MHz, the 5Th harmonic at 25 MHz, 7th harmonic at 35 MHz and so on. Another parameter that can be obtained from the conductance plot of a QCR under resonance conditions is the bandwidth, which is related to energy dissipation of the oscillating crystal. Bandwidth corresponds to the full width at half maximum of the conductance curve at the resonance frequency. The relationship between dissipation and bandwidth is given by equation 1.4

$$D = \frac{2\Gamma}{f} \qquad (1.4)$$

Where *D*= dissipation factor, Γ= bandwidth and *f*= resonance frequency. Specifically,

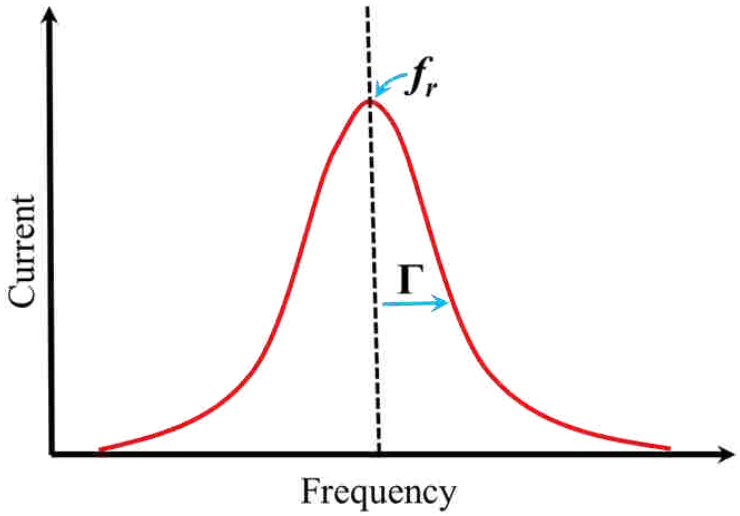

Figure 1.10 Plot of current versus frequency.

dissipation is a measurement of the energy lost during oscillation and can be calculated as $D = E_{dissipated}/2\pi E_{stored}$ where $E_{dissipated}$ is the energy lost per oscillation cycle, and E_{stored} is the total energy stored in the oscillation system. Importantly, dissipation is the second parameter commonly employed for QCM measurements.

1.2.8 Quartz Crystal Microbalance with Dissipation Monitoring Technique

The resonance behavior of QCRs is utilized for development of the quartz crystal microbalance. In regard to the QCM-D technique, two parameters of the oscillating QCR are typically monitored. These parameters are resonance frequency and dissipation. The operating principle of the QCM-D utilized within this dissertation, employs a ring down approach. This approach is based on impulse excitation of the QCR, which is essentially a process of briefly exciting the QCR and monitoring the amplitude of resonance decay. The amplitude of decay is governed by the sine expression denoted in equation 1.5.

$$A_t = A_0 e - \pi \sin(\omega t + \varphi) + c, t \geq 0 \qquad (1.5)$$

Where A_t is the amplitude at time t, A_0 is the amplitude $t = 0$, τ is the decay time constant, ω is the angular frequency, φ is the phase, and c is the dc offset. Hence the dissipation factor can be calculated as:

$$D = \frac{2}{\omega\tau} \qquad (1.6)$$

Where D= dissipation factor, τ is the decay time constant, and ω is the angular frequency Figure 1.11 depicts a plot of resonance decay as a function of time. Due to use of impulse excitation, it is possible for the QCM-D to progressively probe multiple harmonics in short succession. In this regard the fundamental frequency is excited and

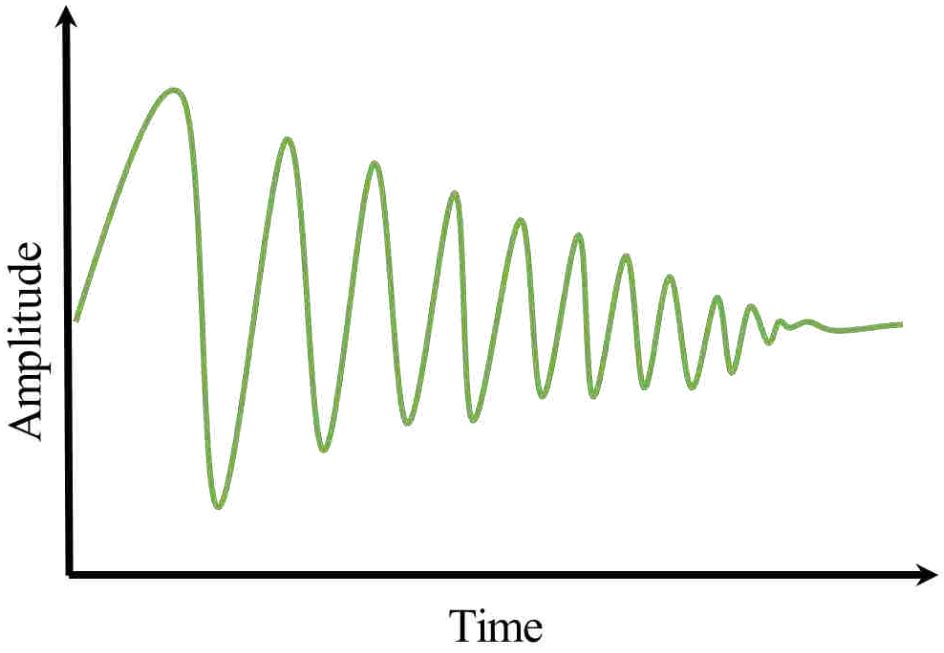

Figure 1.11 Schematic of amplitude change versus time

the resonance decay is monitored, then a higher resonance is excited and that resonance decay is monitored. This process takes milliseconds, and it was possible to monitor up to 7 overtones (odd harmonics 1st through 13th) for the work presented herein.

1.2.9 Gravimetric and Non-gravimetric Sensing in Air using the QCM

Gravimetric sensing, as related to the QCM, can be defined as the detection or determination of analyte mass. In fact, this is the same function as a standard balance, thus the name quartz crystal microbalance. In this regard, the QCM has been widely employed as a mass detector. The measurement principle is based on the Sauerbrery equation, as introduced in 1960, by German physicist Gunter Sauerbrey.[79] The Sauerbrey equation is denoted here:

$$\Delta f = -\frac{n}{c}\Delta m = -\frac{n}{c}\rho_f t_f \qquad (1.7)$$

where Δf is change in resosnance frequency, n is harmonic number, c is mass sensitivity which is 17.7 $ngcm^{-2}Hz^{-1}$ for the 5 MHz AT cut crystal used herein, ρ_f is the density of the film, and t_f is film thickness. In simple terms, this equation states that the change in resonance frequency of a QCR is directly proportional to the mass deposited on the surface. Specifically, resonance frequency should decrease with the addition of mass on the QCR surface. This behavior is known as ideal Sauerbrey behavior and is only valid for loadings that are rigid, uniform, and thin (thickness) relative to the wavelength of the acoustic wave used to interrogate the sensor. For such films, dissipation values are typically small. However, if these conditions are not met, deviation from ideal Sauerbrey behavior occurs.[80, 81] In fact, this is true for many non-rigid i.e. soft films (such as those comprised by various chemosensitive adlayers including ionic liquids and polymers), and films not in the thin film or Sauerbrey regime (thick films). These films typically exhibit larger dissipation values. The sensor response of these films may be influenced by a variety of effects including viscoelasticity, film thickness, or film resonance.[73,80] Viscoelasticity is a property of soft films where they exhibit both viscous and elastic characteristics. Soft films which exhibit viscoelastic properties behave differently under resonant conditions as compared to rigid films. Ultimately, this difference in behavior affects sensor response in various ways, depending upon how viscoelastic/ how thick a film may be.[73,80] A plot adapted from a study on how viscoelasticity and film thickness affect sensor response is depicted in figure 1.12.[80] Film resonance is a condition that occurs when a soft films' thickness reaches ¼ the wavelength of the acoustic wave interrogating the sensor. During this condition, resonance frequency increases with increases in film thickness.[73] In fact, film resonance

is represented by the extrema seen on plots of Figure 1.12. At this point sensor response can become progressively positive. Notably, film resonance is dependent on harmonic as an increase in harmonic decreases the wavelength of acoustic wave. Furthermore, occurrence of film resonance is dependent upon softness of the film as increasing film softness decreases acoustic wavelength as well. Finally, film resonance may be dependent of film properties such as swelling, because if a film swells during sorption of an analyte, film thickness increases. Thus, for a given soft film, film resonance would more likely be exhibited at higher harmonics. Such deviations from ideal Sauerbrey behavior fall within the realm of non-gravimetric QCM sensing and opens new possibilities for QCM based measurement. Typically, film resonance

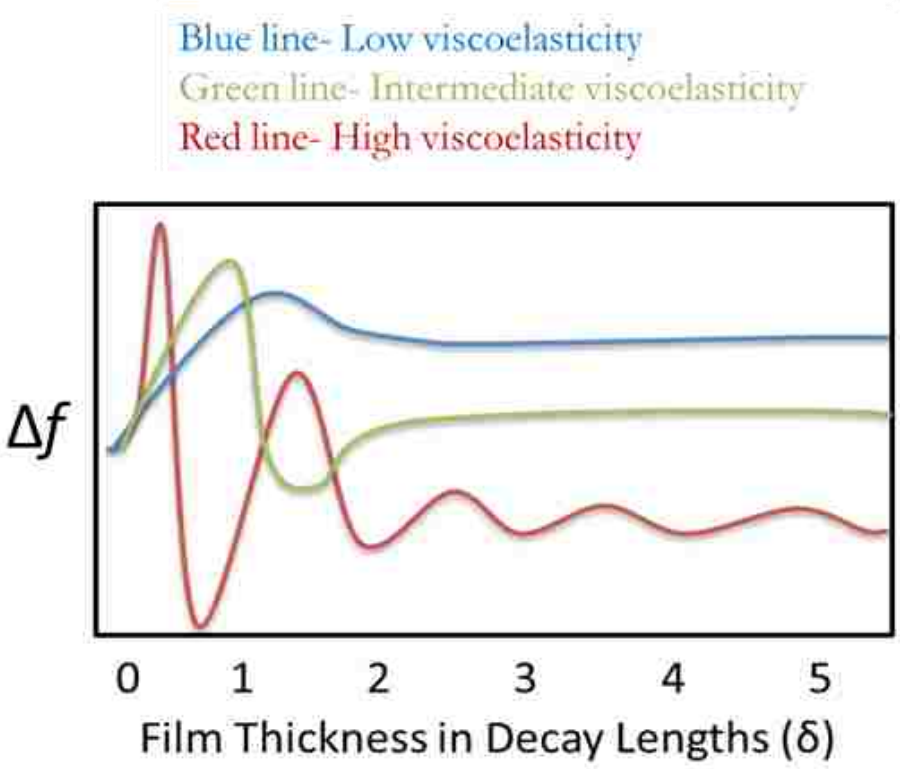

Figure 1.12 Schematic of Sensor response depending upon viscoelasticity and film thickness

conditions are avoided for QCM measurements as modeling for extraction of parameters important for some studies does not yield good agreement. Lesser deviations to ideal Sauerbrey behavior can be modeled using equations that account for viscoelastic contributions to sensor response. Examples of these models include the Maxwell and Kelvin-Voigt equations.[81–83] Notably, these corrections are primarily important for applications which seek to approximate certain parameters outside of frequency or dissipation change. However, for other applications such as the sensor arrays presented in this dissertation non gravimetric behavior of soft films coated on the QCM is essential to proper function.

1.2.10 Chemosensitive Materials for QCM based VOC Sensors

Sensors, which comprise QCM sensor arrays, typically employ a QCM transducer in conjunction with chemosensitive material. This is because the transducer is inherently non-selective. Thus, chemosensitive materials are of paramount importance for the proper function of QCM based chemosensors. These materials, typically employed as adlayers (thin films) on the QCR surface, affect the sensitivity and selectivity of the sensor. Moreover, in the case of gas phase QCM sensors, such materials influence the sorption-desorption profiles of analytes which directly impacts sensor performance. Thus, the development of novel chemosensitive materials has been an active area of research. Ideally, these materials should be inexpensive, stable under operating conditions, exhibit reversible sorption, and be sensitive to desired analytes. Furthermore, for application in sensor arrays, these materials should exhibit partial selectivity. To satisfy these criteria, researchers have employed a plethora of materials including ordinary polymers,[26,84,85] molecularly imprinted polymers,[86–88] metal complexes,[89] calixarenes,[90,91] carbon nanotubes,[92] metalloporphyrins and phthalocyanines,[93–96] and ceramic materials[97] among others. One class of materials that has proven promising in the last decade are organic salts, specifically Ionic Liquids

and GUMBOS. In fact, the application of these materials in QCM based VOC discrimination is expanded upon within this dissertation. The following will give a brief introduction on Ionic Liquids and GUMBOS, as well as a history on the application of such materials for QCM sensor arrays.

1.2.11 Ionic Liquids and GUMBOS

Due to shortcomings observed in many chemosensitive materials, a search for materials that are both easily tunable and sensitive began. Organic salts are a class of materials that can satisfy these requirements. Specifically, Ionic Liquids and GUMBOS are a subset of organic materials composed of organic cations and anions that contain favorable properties. In fact, they can exhibit a number of interactions that can be tailored to specific analytes. The ability to tune the properties of ILs and GUMBOS stems from the interactions of the constituent cations and anions. Furthermore, these ions contain large structural diversity and can be flexibly interchanged via simple ion exchange methods allowing specificity to a broad range of analytes. Figure 1.13 depicts many commonly employed cations and anions. Ionic liquids (ILs), which are defined as organic salts having a melting point below 100°C, are typically composed of bulky cations and/or anions.[98] They can be divided into two classes, namely room temperature ionic liquids (RTILs) and frozen ionic liquids (FILs). The first, RTILS, are ILs which have a melting point below room temperature and have been shown to exhibit a number of properties such as low vapor pressure,[99] high conductivity,[100] high thermal stability,[101] wide solvation range,[102] and recyclability.[103] Furthermore, functionalizing their constituent ions can tune their properties for specific applications. Examples of these task specific ionic liquids (TSILs) include those that are magnetic, antimicrobial, anticancer, and fluorescent. This class of materials has seen an increase in applications across various fields such as catalysis,[98,104] electrochemistry,[104–106] separations,[103,107] and synthesis.[98] The second class, known as FILs, are defined as ILs, which melt at temperatures above

room temperature and have been applied in controlled nanoparticle synthesis and as rewritable surfaces.[108] The term **G**roup of **U**niform **M**aterials **B**ased on **O**rganic **S**alts (GUMBOS) has recently been introduced by the Warner research group to encompass a range of solid phase organic salts exhibiting melting points between 25°C and 250°C. GUMBOS exhibit the same highly tunable properties and ease of synthesis characteristic of ILs. Furthermore, particles in the nanoscale derived from GUMBOS i.e. nanoGUMBOS can possess the favorable properties of GUMBOS in addition to the unique physicochemical properties of nanoparticles. GUMBOS have found application in numerous areas including medicine,[109–114] energy generation and sustainability,[115–117] nanomaterials,[111,112,114,115,118–128] sensors/sensor arrays,[93,129–131] and matrices for MALDI mass spectrometry.[132]

1.2.12 Ionic Liquid based QCM Sensor Arrays

Within the last 15 years, several ILs and GUMBOS based QCM sensors/ sensor arrays for VOCs analysis have been reported. In fact, the first application of ionic liquids as chemosensitive adlayers for QCM sensors was presented by Liang and colleagues in 2002.[133] This work utilized the favorable viscosity, diffusion, and vapor pressure properties of ionic liquids to detect organic vapors using the QCM. This seminal publication set the stage for development of many types of IL based QCM sensors,[133] including those that employ composites,[134] or chemical reactions to enhance film properties or sensitivity respectively. Furthermore, this work paved the way for development of IL sensor arrays which are the primary focus of this dissertation. Hence, Jin *et al.* constructed the first QCM based ionic liquid sensor array a few years later.[101] In this regard, an IL sensor array for discrimination of gases at elevated temperatures (e.g., 120°C) was presented. This study utilizes the negligible vapor pressure and high thermal stability exhibited by ILs to develop the presented sensor array. The array data

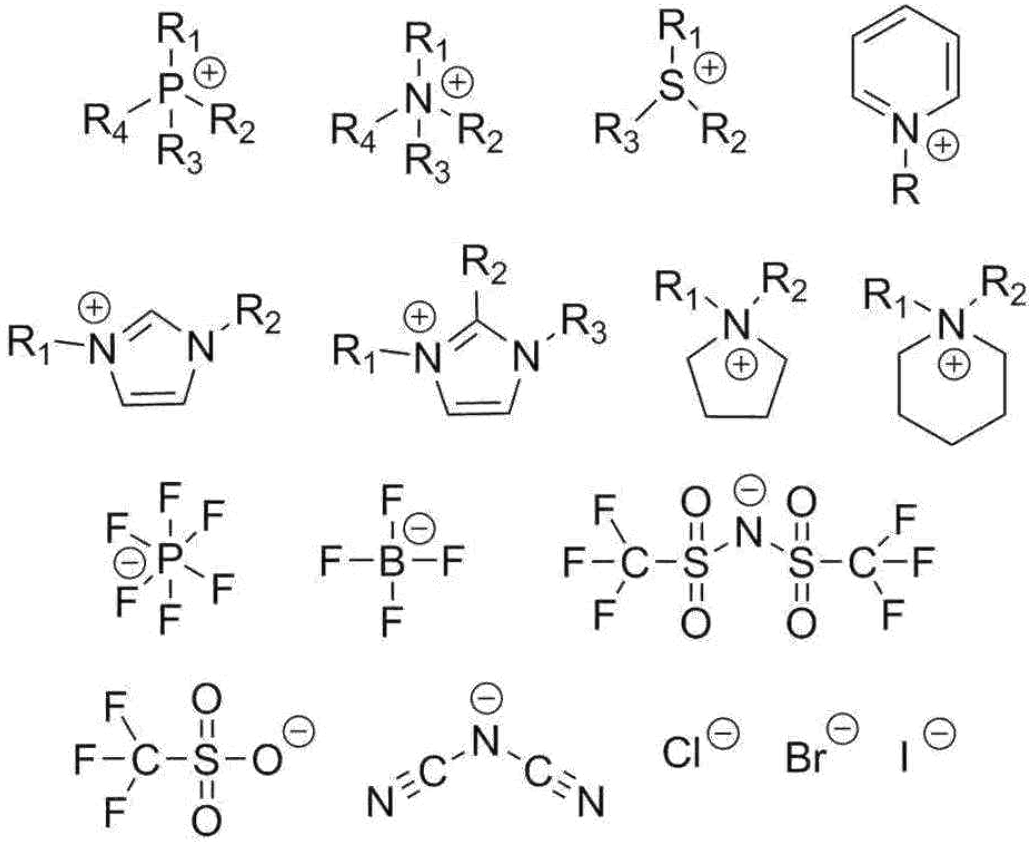

Figure 1.13 Common ions used to prepare ionic liquids and GUMBOS

was classified using LDA to accurately discriminate between several VOCs. Subsequently, Xu *et al.* employed an IL based QCM sensor array for ambient discrimination of VOCs utilizing artificial neural networks (ANN) to accurately analyze the array data.[135] Later, Toniolo et al. reported a IL based QCM sensor array for potentially monitoring food quality.[37] The presented array was capable of discriminating between 31 VOCs allowing classes to be visualized using PCA. Furthermore, the array was able to discriminate between two complex mixtures of VOCs represented by two distinct cinnamon odors. This study represents the first example of a IL based QCM sensor array applied for real sample analysis. Most recently, I reported the development of an IL based QCM VSA.[136] This study utilized the viscoelastic properties of ionic liquids

coupled with dynamic operation of the QCM to discriminate between 18 closely related VOCs. Furthermore, two complex mixtures represented by petroleum ether and kerosene were discriminated. Discrimination accuracies were obtained using QDA and LDA. This study represents the first example of a QCM based VSA.

While each study is more promising than the last, more elaborate studies are required to investigate the full potential of organic salts as recognition elements for QCM sensor arrays. Moreover, additional studies are required to elevate QCM sensing approaches within the measurement sciences. The work within this dissertation is a small step in furthering each of these aims.

1.3 Statistical Analysis

Statistics is a field of mathematics developed by scientist and mathematicians to study data, events, probabilities and patterns.[137,138] This field specifically focuses on development of analysis methods that allow for conclusions to be drawn from observed data. In this regard, statistical analysis provides a means for interpretation and presentation of data. Such topics are of pivotal importance for the successful fabrication of sensor arrays as discussed in this dissertation.

Statistics can be divided into two major types i.e descriptive and inferential statistics. The former consists of methods for organizing and summarizing data, while the later consists of methods for drawing conclusions and inferences from data.[138] To expound upon this, descriptive statistics includes all types of data presentation and commonplace calculations (graphs, tables, histograms, averages, means, etc.) as well as univariate and bivariate analysis techniques. In contrast, inferential statistics includes methods for scaling, prediction, estimation, and classification of data (MANOVA, discriminant analysis, linear regression, etc.) This dissertation employs several elements from each category however the emphasis of this brief introduction will be placed on the less common place inferential techniques employed herein.

1.3.1 Principal Component Analysis (PCA)

Principal component analysis (PCA) is a technique commonly employed to display and reduce the dimensionality of data sets.[139,140] The mathematical basis of which was pioneered by Pearson in 1901.[141] However, with the advent of computerized computation, the tedious mathematics employed have been streamlined into software packages such as SAS, MATLAB, and R, making this method accessible to data analyst at large. More in depth discussions on PCA can be found here.[139,140,142–144] Herein, a non-mathematically rigorous example of the function and importance of PCA as applied for sensor arrays is provided.

When considering array data sets, it is commonplace for such measurements to exhibit multidimensionality. A good example of this is color data, such as that obtained from a colorimetric sensor array. A 6 sensor colorimetric sensor array mock up that will be used as an aid in this discussion is depicted in Figure 1.14. In colorimetric sensor arrays, sensors change color upon interaction with chemical analytes and measurements of the sensor colors are obtained. Each color measurement of the individual sensors yields a Red, Green, Blue (RGB) value. Thus, the data set for even a single sensor measurement is multidimensional. Typically, a series of analytes are introduced and the aggregate of all sensor measurements are collected to form a data set further enhancing the dimensionality. For clarity, 5 replicate measurements of 5 samples were obtained. If this data set was then arranged into a matrix, with the columns representing sensors and the rows representing sensor response, the first table in Figure 1.14 would obtained. Examining the columns, this data set has 18 dimensions. (6 sensors 3 RGB values per sensor) Drawing meaningful conclusions from this data set using conventional graphical techniques would prove challenging. However, PCA, which reduces the dimensionality of data sets, is ideally suited to this situation.[140,142,143] Typically, sensor responses are quasi -independent and so this process is able to

reduce the data to a small set of orthogonal (linearly independent) variables known as

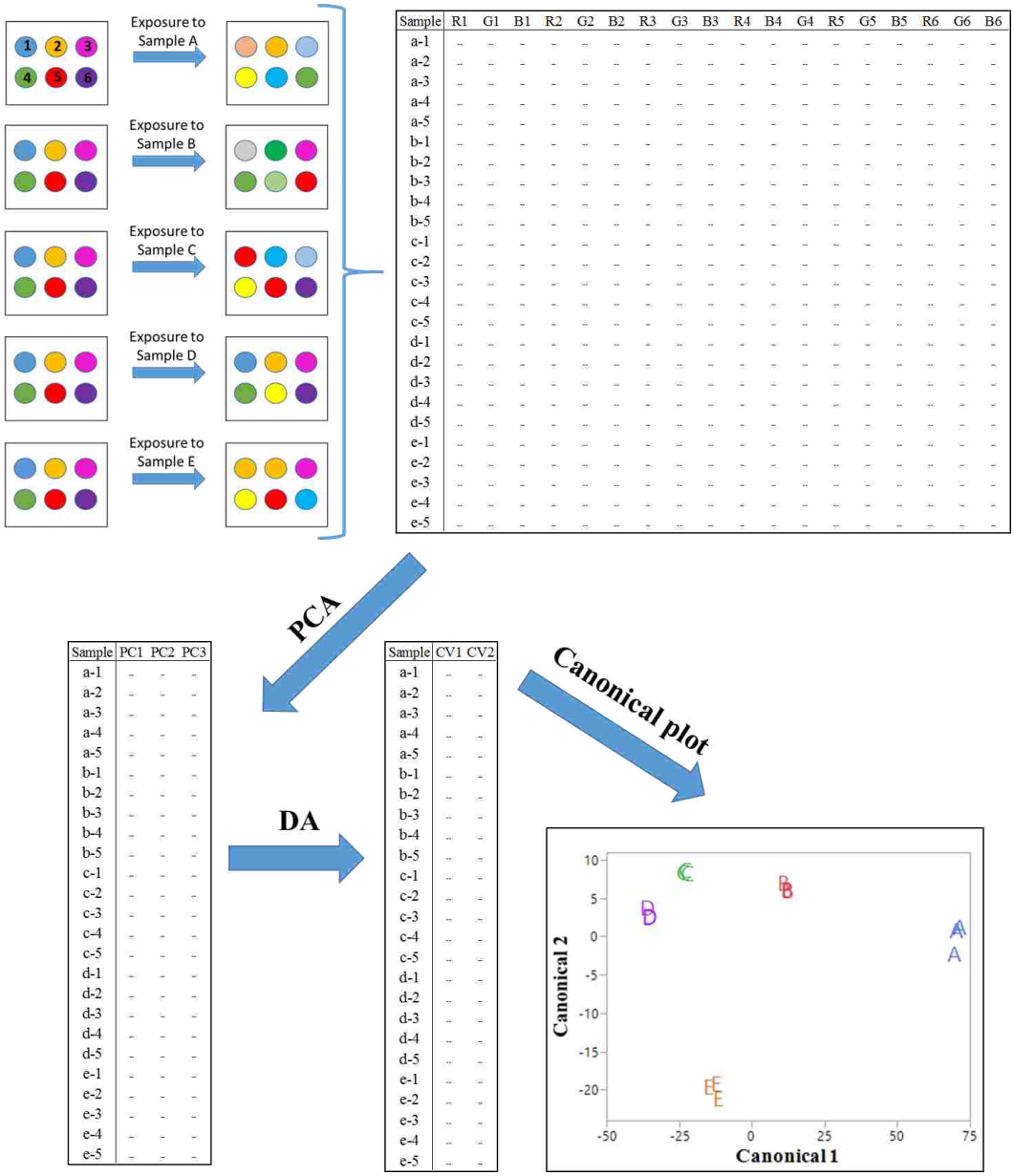

Figure 1.14 Schematic representation of a statistical analysis work flow

principal components. Reduction of dimensionality is accomplished by performing an orthogonal liner transformation of this matrix, which projects the original data onto a different coordinate space where the proportions of the variance in the original data set

correspond with the new coordinates in a sequential fashion. In this regard, the first coordinate comprises the most variance, while the second coordinate comprises the second most variance and so on until 100% of the variance in the original data set is accounted. These coordinates also termed variables are called principal components. Within this dissertation, a set of principal components accounting for 99% of the variance in the original data set are kept for further analysis. A schematic of a reduction that might occur for the example colorimetric sensor array is depicted in Figure 1.14. The principal components can then be displayed using graphical means such as scatter plots, to obtain a qualitative survey of the data. However, to obtain a quantitative assessment of discrimination, as is typically desired for sensor arrays, methods such as discriminant analysis must be performed.[139,140] In this regard, the principal components generated from PCA can be used as input variables for quantitative analysis.

1.3.2 Discriminant Analysis (DA)

Discriminant analysis broadly describes a set of supervised (requires that group membership is known) techniques that are useful for identifying and classifying the patterns within data. These techniques analyze input variables and construct new canonical axes that best maximize separation of data groups.[140] Group membership is determined by distance from the point to the group mean in multivariate space known as the Mahalanobis distance. In this regard, samples are classified to the group where the Mahalanobis distance is shortest from the group mean. To quantify classification accuracy, cross validation is performed. Within this dissertation two types of DA are employed specifically linear discriminant analysis (LDA) and quadratic discriminant analysis (QDA) in conjunction with cross validation. More detailed explanations of each process can be found here.[140,145–147]

The former, LDA, was first developed by Fisher in 1936, and is based on maximizing the ratio of variance between groups divided by the variance within

groups.[148] This ratio bears the developers name and is called the Fisher ratio. Effectively, this technique clusters group members of the same group while maximizing separation between groups. This is accomplished as stated above. LDA assumes a common covariance matrix and the number of canonicals can never exceed the number of variables or number of groups minus one. The latter, QDA, is closely related to LDA except that it is assumed that the covariance matrix is different for each group. This requires that a quadratic discriminant function be employed. The advantage of QDA is that it allows better fit of the data; however this technique may not be applicable for small data sets. An example of a DA canonical plot is depicted in Figure 1.14.

To quantify classification accuracy of DA, the cross validation method was employed. Specifically, the leave one out cross validation method was utilized within this dissertation. Cross validation is a statistical method employed for assessing how a statistical model would classify an independent sample set. In other words, it is a method for assessing how a statistical model would perform in a real test run. This method, as the name suggests, excludes one sample (removes the sample and treats it as an unknown) from the data set and uses the rest of the data to create a predictive model. Then, the excluded sample's group membership is determined based on the predicative model. This process is performed iteratively for every sample within the data set, to determine an error rate from which the classification accuracy can be obtained. This method is known to generate a highly unbiased estimate of classification accuracy.[140]

1.4 Scope of Dissertation

This dissertation focuses on design, development, and implementation of novel sensing schemes for vapor phase QCM based sensor arrays. The objective of this work was to introduce sensing schemes, alternative to the conventional MSA, which would address current limitations while advancing the field of QCM based measurement science. Although, organic salts were employed as chemosensitive materials in each of

the following chapters, the techniques presented herein should prove applicable for any chemosensitive material that sorbs analyte and is suitably viscoelastic.

The first alternative sensing scheme developed is introduced in chapter 2. In this regard, the theory, design, and implementation of the first example of a QCM based VSA is examined. The VSAs presented comprise a single dynamically operated sensor employing ionic liquid recognition elements. As a proof of concept, the VSAs were employed to distinguish between 18 closely related VOCs as well as two complex mixtures. Notably, excellent identification accuracy was achieved. Thus, this system proved an interesting platform for further optimization due to its considerable promise for vapor phase analyses.

In Chapter 3, the VSA approach developed in the previous chapter was further optimized as a step towards developing a sophisticated QCM based analytical method. In this regard, a VSA with the capability to simultaneously identify pure VOCs while independently approximating their respective molecular weights was developed. This was accomplished by expanding the approach presented in the previous chapter while employing an ionic liquid-polymer composite as the chemosensitive material. To benchmark this system, several alcohols including isomers were tested. This approach resulted in excellent identification accuracy with strong molecular weight correlations. These results further extol the virtue of the VSA approach.

Whenever a new array sensing scheme is developed, the question of how does it compare to the conventional scheme arises. A direct comparison of the VSA versus MSA is presented in chapter 4. Furthermore, the second alternative sensing scheme i.e. the V-MSA, is introduced and the systematic design is explored. Effectively, it is a logical fusion of the MSA and VSA schemes. To benchmark the capabilities of each system, a set of complex mixtures represented by citrus type odors were tested and identification accuracies were obtained. The newly introduced V-MSA proved particularly promising

for complex mixture analyses.

Utilizing the knowledge on V-MSAs gained in chapter 4, a V-MSA was subsequently applied for another real world application. Chapter 5, contains studies on the implementation of a QCM based V-MSA for fuel discrimination and detection of gasoline adulteration. In this regard, petroleum based fuels, gasoline grades, and gasoline adulteration were all identified with extremely high accuracy. This is a first for QCM sensor arrays and was only possible using the newly developed V-MSA scheme.

To conclude this dissertation, a summary of the findings, and discussion on the foreseeable implications as well as future directions are presented in chapter 6. Taken in aggregate, this work is a promising step towards advancing the field of QCM based measurement science.

1.5 References

1. Wolkoff, P. & Nielsen, G. D. Organic compounds in indoor air—their relevance for perceived indoor air quality? *Atmos. Environ.* **35,** 4407–4417 (2001).

2. Guenther, A. *et al.* A global model of natural volatile organic compound emissions. *J. Geophys. Res.* **100,** 8873 (1995).

3. Weller, A. Human pheromones: Communication through body odour. *Nature* **392,** 126–127 (1998).

4. Wyatt, T. D. *Pheromones and Animal Behaviour: Communication by Smell and Taste*. (Cambridge University Press, 2003).

5. Blande, J. D., Holopainen, J. K. & Li, T. Air pollution impedes plant-to-plant communication by volatiles: Ozone-facilitated communication breakdown. *Ecol. Lett.* **13,** 1172–1181 (2010).

6. Shorey, H. H. *Animal Communication by Pheromones*. (Academic Press, 2013).

7. Agosta, W. C. *Chemical Communication: The Language Of Pheromones*. (Macmillan, 1992).

8. Kessler, A. Defensive Function of Herbivore-Induced Plant Volatile Emissions in Nature. *Science* **291,** 2141–2144 (2001).

9. Kesselmeier, J. & Staudt, M. Biogenic Volatile Organic Compounds (VOC): An Overview on Emission, Physiology and Ecology. *J. Atmospheric Chem.* **33,** 23–88 (1999).

10. Baldwin, I. T., Kessler, A. & Halitschke, R. Volatile signaling in plant–plant–herbivore interactions: what is real? *Curr. Opin. Plant Biol.* **5,** 351–354 (2002).

11. Mazzone, P. J. *et al.* Diagnosis of lung cancer by the analysis of exhaled breath with a colorimetric sensor array. *Thorax* **62,** 565–568 (2007).

12. Di Natale, C. *et al.* Lung cancer identification by the analysis of breath by means of an array of non-selective gas sensors. *Biosens. Bioelectron.* **18,** 1209–1218 (2003).

13. Machado, R. F. *et al.* Detection of Lung Cancer by Sensor Array Analyses of Exhaled Breath. *Am. J. Respir. Crit. Care Med.* **171,** 1286–1291 (2005).

14. McConnell, V. D. & Schwab, R. M. The Impact of Environmental Regulation on Industry Location Decisions: The Motor Vehicle Industry. *Land Econ.* **66,** 67 (1990).

15. Current, R. B. C. T. EPA Proposes Mandatory Methane Reduction Despite Declining Emissions. *Policy* (2015).

16. Simon, H., Reff, A., Wells, B., Xing, J. & Frank, N. Ozone Trends Across the United States over a Period of Decreasing NOx and VOC Emissions. *Environ. Sci. Technol.* **49,** 186–195 (2015).

17. Weinhold, B. The future of fracking: new rules target air emissions for cleaner natural gas production. *Environ. Health Perspect.* **120,** A272 (2012).

18. Matsumoto, N., Elder, M. & Ogihara, A. Japan's policy to reduce emissions of volatile organic compounds: factors that facilitate industry participation in voluntary actions. *J. Clean. Prod.* **108,** 931–943 (2015).

19. Derwent, R. G. in *Issues in Environmental Science and Technology* (eds. Harrison, R. M. & Hester, R. E.) **4,** 1–16 (Royal Society of Chemistry, 1995).

20. Suslick, B. A., Feng, L. & Suslick, K. S. Discrimination of Complex Mixtures by a Colorimetric Sensor Array: Coffee Aromas. *Anal. Chem.* **82,** 2067–2073 (2010).

21. Kampa, M. & Castanas, E. Human health effects of air pollution. *Environ. Pollut.* **151,** 362–367 (2008).

22. Ohura, T. *et al.* Comparative study on indoor air quality in Japan and China: Characteristics of residential indoor and outdoor VOCs. *Atmos. Environ.* **43,** 6352–6359 (2009).

23. Adgate, J. L. *et al.* Outdoor, Indoor, and Personal Exposure to VOCs in Children. *Environ. Health Perspect.* **112,** 1386–1392 (2004).

24. Chao, C. Y. & Chan, G. Y. Quantification of indoor VOCs in twenty mechanically ventilated buildings in Hong Kong. *Atmos. Environ.* **35,** 5895–5913 (2001).

25. Jia, C., Batterman, S. & Godwin, C. VOCs in industrial, urban and suburban neighborhoods, Part 1: Indoor and outdoor concentrations, variation, and risk drivers. *Atmos. Environ.* **42,** 2083–2100 (2008).

26. Ayad, M. M. & Torad, N. L. Alcohol vapours sensor based on thin polyaniline salt film and quartz crystal microbalance. *Talanta* **78,** 1280–1285 (2009).

27. Hierlemann, A., Weimar, U., Kraus, G., Schweizer-Berberich, M. & Göpel, W. Polymer-based sensor arrays and multicomponent analysis for the detection of hazardous oragnic vapours in the environment. *Sens. Actuators B Chem.* **26,** 126–134 (1995).

28. Carey, J. R. *et al.* Rapid Identification of Bacteria with a Disposable Colorimetric Sensing Array. *J. Am. Chem. Soc.* **133,** 7571–7576 (2011).

29. Capone, S. *et al.* Monitoring of rancidity of milk by means of an electronic nose and a dynamic PCA analysis. *Sens. Actuators B Chem.* **78,** 174–179 (2001).

30. Buratti, S., Benedetti, S., Scampicchio, M. & Pangerod, E. C. Characterization and classification of Italian Barbera wines by using an electronic nose and an amperometric electronic tongue. *Anal. Chim. Acta* **525,** 133–139 (2004).

31. Bello, A. *et al.* Potentialities of a modified QCM sensor for the detection of analytes interacting via H-bonding and application to the determination of ethanol in bread. *Sens. Actuators B Chem.* **125,** 321–325 (2007).

32. Ponrathnam, T., Cho, J., Kurup, P., Nagarajan, R. & Kumar, J. Investigation of QCM Sensors with Azobenzene Functionalized Coatings for the Detection of Nitroaromatics. *J. Macromol. Sci. Part A* **48,** 1031–1037 (2011).

33. Wang, F., Gu, H. & Swager, T. M. Carbon Nanotube/Polythiophene Chemiresistive Sensors for Chemical Warfare Agents. *J. Am. Chem. Soc.* **130,** 5392–5393 (2008).

34. Rehman, A. *et al.* Differential Solute Gas Response in Ionic-Liquid-Based QCM Arrays: Elucidating Design Factors Responsible for Discriminative Explosive Gas Sensing. *Anal. Chem.* **83,** 7823–7833 (2011).

35. Bourgeois, W., Romain, A.-C., Nicolas, J. & Stuetz, R. M. The use of sensor arrays for environmental monitoring: interests and limitations. *J. Environ. Monit.* **5,** 852 (2003).

36. Stetter, J. R., Jurs, P. C. & Rose, S. L. Detection of hazardous gases and vapors: pattern recognition analysis of data from an electrochemical sensor array. *Anal. Chem.* **58,** 860–866 (1986).

37. Toniolo, R. *et al.* Room Temperature Ionic Liquids As Useful Overlayers for Estimating Food Quality from Their Odor Analysis by Quartz Crystal Microbalance Measurements. *Anal. Chem.* **85,** 7241–7247 (2013).

38. Barié, N., Bücking, M. & Rapp, M. A novel electronic nose based on miniaturized SAW sensor arrays coupled with SPME enhanced headspace-analysis and its use for rapid determination of volatile organic compounds in food quality monitoring. *Sens. Actuators B Chem.* **114,** 482–488 (2006).

39. Schaller, E., Bosset, J. O. & Escher, F. 'Electronic Noses' and Their Application to Food. *LWT - Food Sci. Technol.* **31,** 305–316 (1998).

40. Brunner, C. *et al.* Discrimination of cancerous and non-cancerous cell lines by headspace-analysis with PTR-MS. *Anal. Bioanal. Chem.* **397,** 2315–2324 (2010).

41. Chen, X. *et al.* A study of an electronic nose for detection of lung cancer based on a virtual SAW gas sensors array and imaging recognition method. *Meas. Sci. Technol.* **16,** 1535–1546 (2005).

42. Staples, E. J. & Viswanathan, S. Ultrahigh-speed chromatography and virtual chemical sensors for detecting explosives and chemical warfare agents. *IEEE Sens. J.* **5,** 622–631 (2005).

43. Zhu, W. *et al.* A Rapid and Efficient Way to Dynamic Creation of Cross-Reactive Sensor Arrays Based on Ionic Liquids. *Chem. - Eur. J.* **19,** 11603–11612 (2013).

44. Yinon, J. Peer Reviewed: Detection of Explosives by Electronic Noses. *Anal. Chem.* **75,** 98 A-105 A (2003).

45. Delgado-Rodríguez, M. *et al.* Use of electronic nose and GC-MS in detection and monitoring some VOC. *Atmos. Environ.* **51,** 278–285 (2012).

46. Snow, E. S., Perkins, F. K., Houser, E. J., Badescu, S. C. & Reinecke, T. L. Chemical Detection with a Single-Walled Carbon Nanotube Capacitor. *Science* **307,** 1942–1945 (2005).

47. Yamazoe, N. & Shimanoe, K. New perspectives of gas sensor technology. *Sens. Actuators B Chem.* **138,** 100–107 (2009).

48. James, D., Scott, S. M., Ali, Z. & O'Hare, W. T. Chemical Sensors for Electronic Nose Systems. *Microchim. Acta* **149,** 1–17 (2005).

49. Lerchner, J., Caspary, D. & Wolf, G. Calorimetric detection of volatile organic compounds. *Sens. Actuators B Chem.* **70,** 57–66 (2000).

50. Hagleitner, C. *et al.* Smart single-chip gas sensor microsystem. *Nature* **414,** 293–296 (2001).

51. Gentry, S. J. & Jones, T. A. The role of catalysis in solid-state gas sensors. *Sens. Actuators* **10,** 141–163 (1986).

52. Sasahara, T., Kato, H., Saito, A., Nishimura, M. & Egashira, M. Development of a ppb-level sensor based on catalytic combustion for total volatile organic compounds in indoor air. *Sens. Actuators B Chem.* **126,** 536–543 (2007).

53. Hagleitner, C., Lange, D., Hierlemann, A., Brand, O. & Baltes, H. CMOS single-chip gas detection system comprising capacitive, calorimetric and mass-sensitive microsensors. *IEEE J. Solid-State Circuits* **37,** 1867–1878 (2002).

54. Hu, Z., Deibert, B. J. & Li, J. Luminescent metal–organic frameworks for chemical sensing and explosive detection. *Chem Soc Rev* **43,** 5815–5840 (2014).

55. Zhang, M. *et al.* Two-Dimensional Metal–Organic Framework with Wide Channels and Responsive Turn-On Fluorescence for the Chemical Sensing of Volatile Organic Compounds. *J. Am. Chem. Soc.* **136,** 7241–7244 (2014).

56. Spadavecchia, J., Ciccarella, G., Vasapollo, G., Siciliano, P. & Rella, R. UV-Vis absorption optosensing materials based on metallophthalocyanines thin films. *Sens. Actuators B Chem.* **100,** 135–138 (2004).

57. Janzen, M. C., Ponder, J. B., Bailey, D. P., Ingison, C. K. & Suslick, K. S. Colorimetric Sensor Arrays for Volatile Organic Compounds. *Anal. Chem.* **78,** 3591–3600 (2006).

58. Suslick, K. S., Rakow, N. A. & Sen, A. Colorimetric sensor arrays for molecular recognition. *Tetrahedron* **60,** 11133–11138 (2004).

59. Cheng, C.-S., Chen, Y.-Q. & Lu, C.-J. Organic vapour sensing using localized surface plasmon resonance spectrum of metallic nanoparticles self assemble monolayer. *Talanta* **73,** 358–365 (2007).

60. Bingham, J. M., Anker, J. N., Kreno, L. E. & Van Duyne, R. P. Gas Sensing with High-Resolution Localized Surface Plasmon Resonance Spectroscopy. *J. Am. Chem. Soc.* **132,** 17358–17359 (2010).

61. Kreno, L. E., Hupp, J. T. & Van Duyne, R. P. Metal−Organic Framework Thin Film for Enhanced Localized Surface Plasmon Resonance Gas Sensing. *Anal. Chem.* **82,** 8042–8046 (2010).

62. Fanget, S. *et al.* Gas sensors based on gravimetric detection—A review. *Sens. Actuators B Chem.* **160,** 804–821 (2011).

63. Bodenhöfer, K., Hierlemann, A., Noetzel, G., Weimar, U. & Göpel, W. Performances of Mass-Sensitive Devices for Gas Sensing: Thickness Shear Mode and Surface Acoustic Wave Transducers. *Anal. Chem.* **68,** 2210–2218 (1996).

64. Vashist, S. K. A review of microcantilevers for sensing applications. *J Nanotechnol.* **3,** 1–18 (2007).

65. Galpothdeniya, W. I. S. *et al.* Ionic liquid-based optoelectronic sensor arrays for chemical detection. *RSC Adv* **4,** 7225–7234 (2014).

66. Kwon, H., Samain, F. & Kool, E. T. Fluorescent DNAs printed on paper: sensing food spoilage and ripening in the vapor phase. *Chem. Sci.* **3,** 2542 (2012).

67. Albert, K. J. *et al.* Cross-Reactive Chemical Sensor Arrays. *Chem. Rev.* **100,** 2595–2626 (2000).

68. Reimann, P. & Schütze, A. in *Gas Sensing Fundamentals* (eds. Kohl, C.-D. & Wagner, T.) **15,** 67–107 (Springer Berlin Heidelberg, 2013).

69. Stetter, J. R. & Penrose, W. R. Understanding Chemical Sensors and Chemical Sensor Arrays(Electronic Noses): Past, Present, and Future. *Sens. Update* **10,** 189 (2002).

70. Ankara, Z., Kammerer, T., Gramm, A. & Schütze, A. Low power virtual sensor array based on a micromachined gas sensor for fast discrimination between H2, CO and relative humidity. *Sens. Actuators B Chem.* **100,** 240–245 (2004).

71. Schutze, A., Gramm, A. & Ruhl, T. Identification of Organic Solvents by a Virtual Multisensor System With Hierarchical Classification. *IEEE Sens. J.* **4,** 857–863 (2004).

72. Sim, C. O. *et al.* Chemometric Classification of Herb – Orthosiphon stamineus According to Its Geographical Origin Using Virtual Chemical Sensor Based Upon Fast GC. *Sensors* **3,** 458–471 (2003).

73. Johannsmann, D. *The Quartz Crystal Microbalance in Soft Matter Research: Fundamentals and Modeling*. (Springer, 2014).

74. Heywang, W., Lubitz, K. & Wersing, W. *Piezoelectricity: Evolution and Future of a Technology*. (Springer Science & Business Media, 2008).

75. Hankel, W. Ueber die Entwickelung polarer Electricität in hemimorphen Krystallen durch Aenderung des Druckes in der Richtung der unsymmetrisch ausgebildeten Axen. *Ann. Phys.* **249,** 640–644 (1881).

76. Lippman, G. Principe de la conservation de l'électricité. in *Annales de chimie et de physique* **24,** 381–394 (1881).

77. Curie, J. & Curie, P. Contractions et dilatations produites par des tensions électriques dans les cristaux hémièdres à faces inclinées. *Comptes-Rendus L'Académie Sci.* **93,** 1137–1140 (1881).

78. Koga, I. Notes on Piezoelectric Quartz Crystals. *Proc. IRE* **24,** 510–531 (1936).

79. Sauerbrey, G. Z. Use of quartz vibration for weighing thin films on a microbalance. *J Phys.* **155,** 206–212 (1959).

80. McHale, G., Lücklum, R., Newton, M. I. & Cowen, J. A. Influence of viscoelasticity and interfacial slip on acoustic wave sensors. *J. Appl. Phys.* **88,** 7304 (2000).

81. Vogt, B. D., Lin, E. K., Wu, W. & White, C. C. Effect of Film Thickness on the Validity of the Sauerbrey Equation for Hydrated Polyelectrolyte Films. *J. Phys. Chem. B* **108,** 12685–12690 (2004).

82. Voinova, M. V., Jonson, M. & Kasemo, B. Internal and interfacial friction in the dynamics of soft/solid interfaces. *ArXivcond-Mat9906415* (1999).

83. Voinova, M. V., Rodahl, M., Jonson, M. & Kasemo, B. Viscoelastic Acoustic Response of Layered Polymer Films at Fluid-Solid Interfaces: Continuum Mechanics Approach. *Phys. Scr.* **59,** 391–396 (1999).

84. Strashilov, V. L., Alexieva, G. E., Velichkov, V. N., Mateva, R. P. & Avramov, I. D. Polymer-Coated Quartz Microbalance Sensors for Volatile Organic Compound Gases. *Sens. Lett.* **7,** 203–211 (2009).

85. Si, P., Mortensen, J., Komolov, A., Denborg, J. & Møller, P. J. Polymer coated quartz crystal microbalance sensors for detection of volatile organic compounds in gas mixtures. *Anal. Chim. Acta* **597,** 223–230 (2007).

86. Matsuguchi, M. & Uno, T. Molecular imprinting strategy for solvent molecules and its application for QCM-based VOC vapor sensing. *Sens. Actuators B Chem.* **113,** 94–99 (2006).

87. Kikuchi, M., Tsuru, N. & Shiratori, S. Recognition of terpenes using molecular imprinted polymer coated quartz crystal microbalance in air phase. *Sci. Technol. Adv. Mater.* **7,** 156–161 (2006).

88. Jha, S. K., Liu, C. & Hayashi, K. Molecular imprinted polyacrylic acids based QCM sensor array for recognition of organic acids in body odor. *Sens. Actuators B Chem.* **204,** 74–87 (2014).

89. Yang, M., He, J., Hu, X., Yan, C. & Cheng, Z. CuO Nanostructures As Quartz Crystal Microbalance Sensing Layers for Detection of Trace Hydrogen Cyanide Gas. *Environ. Sci. Technol.* **45,** 6088–6094 (2011).

90. Kalchenko, V. I. *et al.* Calixarene-based QCM sensors array and its response to volatile organic vapours. *Mater. Sci.* **20,** 73–88 (2002).

91. Koshets, I. A., Kazantseva, Z. I., Shirshov, Y. M., Cherenok, S. A. & Kalchenko, V. I. Calixarene films as sensitive coatings for QCM-based gas sensors. *Sens. Actuators B Chem.* **106,** 177–181 (2005).

92. Su, P.-G., Sun, Y.-L. & Lin, C.-C. A low humidity sensor made of quartz crystal microbalance coated with multi-walled carbon nanotubes/Nafion composite material films. *Sens. Actuators B Chem.* **115,** 338–343 (2006).

93. Regmi, B. P. *et al.* Phthalocyanine- and porphyrin-based GUMBOS for rapid and sensitive detection of organic vapors. *Sens. Actuators B Chem.* **209,** 172–179 (2015).

94. Fietzek, C. *et al.* Soluble phthalocyanines as coatings for quartz-microbalances: specific and unspecific sorption of volatile organic compounds. *Sens. Actuators B Chem.* **57,** 88–98 (1999).

95. Tasaltin, C. *et al.* Synthesis and DMMP sensing properties of fluoroalkyloxy and fluoroaryloxy substituted phthalocyanines in acoustic sensors. *Sens. Actuators B Chem.* **150,** 781–787 (2010).

96. Kumar, A. *et al.* Tetra-tert-butyl copper phthalocyanine-based QCM sensor for toluene detection in air at room temperature. *Sens. Actuators B Chem.* **210,** 398–407 (2015).

97. Latif, U., Rohrer, A., Lieberzeit, P. A. & Dickert, F. L. QCM gas phase detection with ceramic materials—VOCs and oil vapors. *Anal. Bioanal. Chem.* **400,** 2457–2462 (2011).

98. Welton, T. Room-Temperature Ionic Liquids. Solvents for Synthesis and Catalysis. *Chem. Rev.* **99,** 2071–2084 (1999).

99. Earle, M. J. & Seddon, K. R. Ionic liquids. Green solvents for the future. *Pure Appl. Chem.* **72,** 1391–1398 (2000).

100. Galiński, M., Lewandowski, A. & Stępniak, I. Ionic liquids as electrolytes. *Electrochimica Acta* **51,** 5567–5580 (2006).

101. Jin, X., Yu, L., Garcia, D., Ren, R. X. & Zeng, X. Ionic Liquid High-Temperature Gas Sensor Array. *Anal. Chem.* **78,** 6980–6989 (2006).

102. Wilkes, J. S. A short history of ionic liquids—from molten salts to neoteric solvents. *Green Chem.* **4,** 73–80 (2002).

103. Huddleston, J. G., Willauer, H. D., Swatloski, R. P., Visser, A. E. & Rogers, R. D. Room temperature ionic liquids as novel media for 'clean' liquid–liquid extraction. *Chem Commun* 1765–1766 (1998).

104. Sun, W., Gao, R. & Jiao, K. Electrochemistry and Electrocatalysis of Hemoglobin in Nafion/nano-$CaCO_3$ Film on a New Ionic Liquid $BPPF_6$ Modified Carbon Paste Electrode. *J. Phys. Chem. B* **111,** 4560–4567 (2007).

105. Liu, H. *et al.* An ionic liquid-type carbon paste electrode and its polyoxometalate-modified properties. *Electrochem. Commun.* **7,** 1357–1363 (2005).

106. Zhao, Y. *et al.* Selective detection of dopamine in the presence of ascorbic acid and uric acid by a carbon nanotubes-ionic liquid gel modified electrode. *Talanta* **66,** 51–57 (2005).

107. Deng, N. *et al.* Highly efficient extraction of phenolic compounds by use of magnetic room temperature ionic liquids for environmental remediation. *J. Hazard. Mater.* **192,** 1350–1357 (2011).

108. Rutten, F. J. M., Tadesse, H. & Licence, P. Rewritable Imaging on the Surface of Frozen Ionic Liquids. *Angew. Chem. Int. Ed.* **46,** 4163–4165 (2007).

109. Cole, M., Hobden, J. & Warner, I. Recycling Antibiotics into GUMBOS: A New Combination Strategy to Combat Multi-Drug-Resistant Bacteria. *Molecules* **20,** 6466–6487 (2015).

110. Cole, M. R. *et al.* Minimizing human infection from Escherichia coli O157:H7 using GUMBOS. *J. Antimicrob. Chemother.* **68,** 1312–1318 (2013).

111. Dumke, J. C. *et al.* In vitro activity studies of hyperthermal near-infrared nanoGUMBOS in MDA-MB-231 breast cancer cells. *Photochem. Photobiol. Sci.* **13,** 1270 (2014).

112. Siraj, N., Kolic, P. E., Regmi, B. P. & Warner, I. M. Strategy for Tuning the Photophysical Properties of Photosensitizers for Use in Photodynamic Therapy. *Chem. - Eur. J.* **21,** 14440–14446 (2015).

113. Magut, P. K. S. *et al.* Tunable Cytotoxicity of Rhodamine 6G via Anion Variations. *J. Am. Chem. Soc.* **135,** 15873–15879 (2013).

114. Bwambok, D. K. *et al.* Near-Infrared Fluorescent NanoGUMBOS for Biomedical Imaging. *ACS Nano* **3,** 3854–3860 (2009).

115. Jordan, A. N., Siraj, N., Das, S. & Warner, I. M. Tunable near-infrared emission of binary nano- and mesoscale GUMBOS. *RSC Adv.* **4,** 28471 (2014).

116. Sarkar, A. *et al.* Electro-optical characterization of cyanine-based GUMBOS and nanoGUMBOS. *Electron. Mater. Lett.* **10,** 879–885 (2014).

117. Jordan, A. N. *et al.* Anion-controlled morphologies and spectral features of cyanine-based nanoGUMBOS – an improved photosensitizer. *Nanoscale* **4,** 5031 (2012).

118. de Rooy, S. L. *et al.* Fluorescent one-dimensional nanostructures from a group of uniform materials based on organic salts. *Chem. Commun.* **47,** 8916 (2011).

119. de Rooy, S. L. *et al.* Ionically Self-Assembled, Multi-Luminophore One-Dimensional Micro- and Nanoscale Aggregates of Thiacarbocyanine GUMBOS. *J. Phys. Chem. C* **116,** 8251–8260 (2012).

120. Lu, C. *et al.* Irradiation Induced Fluorescence Enhancement in PEGylated Cyanine-Based NIR Nano- and Mesoscale GUMBOS. *Langmuir* **28,** 14415–14423 (2012).

121. Hamdan, S. *et al.* Ionic liquid crosslinkers for chiral imprinted nanoGUMBOS. *J. Colloid Interface Sci.* **463,** 29–36 (2016).

122. Hamdan, S. *et al.* Strategies for controlled synthesis of nanoparticles derived from a group of uniform materials based on organic salts. *J. Colloid Interface Sci.* **446,** 163–169 (2015).

123. Wright, A. R. *et al.* Soft- and hard-templated organic salt nanoparticles with the Midas touch: gold-shelled nanoGUMBOS. *J Mater Chem C* **2,** 8996–9003 (2014).

124. Dumke, J. C. *et al.* Photothermal Response of Near-Infrared-Absorbing NanoGUMBOS. *Appl. Spectrosc.* **68,** 340–352 (2014).

125. Das, S. *et al.* Tunable Size and Spectral Properties of Fluorescent NanoGUMBOS in Modified Sodium Deoxycholate Hydrogels. *Langmuir* **28,** 757–765 (2012).

126. Das, S. *et al.* Nontemplated Approach to Tuning the Spectral Properties of Cyanine-Based Fluorescent NanoGUMBOS. *Langmuir* **26,** 12867–12876 (2010).

127. Dumke, J. C. *et al.* Lanthanide-Based Luminescent NanoGUMBOS. *Langmuir* **26,** 15599–15603 (2010).

128. Tesfai, A. *et al.* Magnetic and Nonmagnetic Nanoparticles from a Group of Uniform Materials Based on Organic Salts. *ACS Nano* **3,** 3244–3250 (2009).

129. Regmi, B. P. *et al.* A novel composite film for detection and molecular weight determination of organic vapors. *J. Mater. Chem.* **22,** 13732 (2012).

130. Regmi, B. P. *et al.* Molecular weight sensing properties of ionic liquid-polymer composite films: theory and experiment. *J Mater Chem C* **2,** 4867–4878 (2014).

131. Galpothdeniya, W. I. S. *et al.* Tunable GUMBOS-based sensor array for label-free detection and discrimination of proteins. *J Mater Chem B* **4,** 1414–1422 (2016).

132. Al Ghafly, H. *et al.* GUMBOS matrices of variable hydrophobicity for matrix-assisted laser desorption/ionization mass spectrometry: GUMBOS matrices of variable hydrophobicity for MALDI-MS. *Rapid Commun. Mass Spectrom.* **28,** 2307–2314 (2014).

133. Liang, C., Yuan, C.-Y., Warmack, R. J., Barnes, C. E. & Dai, S. Ionic Liquids: A New Class of Sensing Materials for Detection of Organic Vapors Based on the Use of a Quartz Crystal Microbalance. *Anal. Chem.* **74,** 2172–2176 (2002).

134. Goubaidoulline, I., Vidrich, G. & Johannsmann, D. Organic Vapor Sensing with Ionic Liquids Entrapped in Alumina Nanopores on Quartz Crystal Resonators. *Anal. Chem.* **77,** 615–619 (2005).

135. Xu, X., Cang, H., Li, C., Zhao, Z. K. & Li, H. Quartz crystal microbalance sensor array for the detection of volatile organic compounds. *Talanta* **78,** 711–716 (2009).

136. Speller, N. C. *et al.* Rational Design of QCM-D Virtual Sensor Arrays Based on Film Thickness, Viscoelasticity, and Harmonics for Vapor Discrimination. *Anal. Chem.* **87,** 5156–5166 (2015).

137. Shalizi, C. R. Advanced data analysis from an elementary point of view. *URL Httpwww Stat Cmu EducshaliziADAfaEPoV13* **24,** (2013).

138. Isotalo, J. Basics of statistics. *Finl. Univ. Tamp.* (2001).

139. Abdi, H. & Williams, L. J. Principal component analysis. *Wiley Interdiscip. Rev. Comput. Stat.* **2,** 433–459 (2010).

140. Morgan, S. L. & Bartick, E. G. in *Forensic Analysis on the Cutting Edge* (ed. Blackledge, R. D.) 333–374 (John Wiley & Sons, Inc., 2007).

141. Pearson, K. Principal components analysis. *Lond. Edinb. Dublin Philos. Mag. J. Sci.* **6,** 559 (1901).

142. Jolliffe, I. in *Wiley StatsRef: Statistics Reference Online* (eds. Balakrishnan, N. et al.) (John Wiley & Sons, Ltd, 2014).

143. Wold, S., Esbensen, K. & Geladi, P. Principal component analysis. *Chemom. Intell. Lab. Syst.* **2,** 37–52 (1987).

144. Bro, R. & Smilde, A. K. Principal component analysis. *Anal. Methods* **6,** 2812 (2014).

145. Izenman, A. J. *Modern Multivariate Statistical Techniques*. (Springer New York, 2008).

146. Klecka, W. R. *Discriminant Analysis*. (SAGE, 1980).

147. McLachlan, G. *Discriminant Analysis and Statistical Pattern Recognition*. (John Wiley & Sons, 2004).

148. Fisher, R. A. THE USE OF MULTIPLE MEASUREMENTS IN TAXONOMIC PROBLEMS. *Ann. Eugen.* **7,** 179–188 (1936).

CHAPTER 2. RATIONAL DESIGN OF QCM-D VIRTUAL SENSOR ARRAYS BASED ON FILM THICKNESS, VISCOELASTICITY AND HARMONICS FOR VAPOR DISCRIMINATION*

2.1 Introduction

Acute and chronic exposure to volatile organic compounds (VOCs) can have numerous and far-reaching consequences with regard to health effects. Thus, development of novel gas sensing materials and systems for detection and discrimination of VOCs has attracted considerable research interests in recent years. Research involving VOC sensing is driven by requirements to monitor VOCs in different kinds of samples including ambient air monitoring,[1-3] biomedical diagnostics,[4-6] food quality assurance,[7-9] and military and civilian counterterrorism.[10-12] A conventional technique for VOC monitoring is GC-MS. However, this technique requires expensive instrumentation, as well as highly skilled and dedicated operators. Therefore, a current trend is to develop simple low-cost devices for accurate and real-time monitoring of VOCs.

A large fraction of the currently used gas sensing systems employ multisensor arrays (MSAs), popularly referred to as electronic noses.[2, 12-22] This concept effectively converts the limitation of partial selectivity, which is observed for many sensors, into an advantage. The creation of MSAs has allowed vast improvements in the chemical diversity and chemical selectivity with which analytes can be discriminated. A typical configuration for an MSA consists of a collection of several partially selective sensors, where each of the sensor elements interact with all or most analytes, but to varying degrees. In other words, an MSA comprises a number of cross-reactive sensors.[16-18] The collective responses from an MSA are best analyzed by use of pattern recognition techniques such as principal component analysis (PCA), discriminant analysis (DA), and

* Reprinted with permission from N. C. Speller, N. Siraj, B. P. Regmi, H. Marzoughi, C. Neal and I. M. Warner, *Anal. Chem.*, 2015, **87**, 5156-5166.Copyright 2015 American Chemical Society.

artificial neural networks (ANN) that facilitate identification and classification of such analytes. In such cases, a judicious selection of sensing materials is critical for discrimination between structurally similar analytes. One important consideration is that MSAs should be simple and inexpensive for optimal implementation.

A very promising approach, alternative and/or complementary to MSA, which allows generation of analyte-specific response patterns is to use a single physical sensor that can produce multiple responses.[23-25] This approach, which is generally known as a virtual sensor array (VSA) or virtual multisensors, relies on dynamic operation of a single sensor that gives analyte-specific response patterns similar to that obtained from an MSA.[24, 25] The most extensively reported examples of VSAs are metal oxide sensors and field effect transistor devices that discriminate between different analytes by use of temperature variations.[25, 26] Other non-conventional VSAs involving use of tandem methods have also been documented.[27-29] In fact, VSAs offer several distinct advantages, and in this regard, cost, complexity, and problems associated with sensor drift are minimized in VSAs as compared to MSAs.[24]

The detection principle of a gas sensor depends on both the chemosensitive film and the transducer. With regard to transducers, the quartz crystal microbalance (QCM) has been increasingly adopted for construction of gas sensing devices[1, 5, 9, 12, 14, 15, 30-33] because it is sensitive, offers potential for miniaturization,[34] and is amenable to fabrication of sensor arrays. A QCM sensor is typically fabricated by immobilizing a thin film of suitable sensing material onto the surface of an AT-cut quartz crystal. In this regard, ionic liquids (ILs) have proved to be promising sensing materials for detection and discrimination of a wide range of organic vapors.[14, 15, 31-34] This is because ILs, which are defined as organic salts with melting point below 100 °C, are highly tunable materials with low vapor pressures and reversible capture of organic vapors. In addition, ILs have also been shown to possess viscoelastic properties,[33, 35, 36] which are particularly

relevant to the studies presented in this chapter. In this chapter, my desire is to create sensor arrays by exploiting the viscoelastic properties of ILs, rather than utilizing differences in chemical affinity as is usually done.

Herein, I report an IL-based virtual sensor array (VSA) fabricated by depositing a thin film of IL on the surface of a QCM-D transducer. The films utilized in this study consisted of an IL, 1-octyl-3-methylimidazolium bromide ([OMIm][Br]) or 1-octyl-3-methylimidazolium thiocyanate ([OMIm][SCN]), at two different thicknesses. These four individual QCM-D sensors were then exposed to a range of different organic vapors at various concentrations and the frequency shift (Δf) at multiple harmonics were measured. Due to the viscoelastic properties of the IL coating, both increases and decreases in Δf were observed depending on the analyte, harmonic number, and film thickness. Variable harmonics have been used previously by a number of researchers for examination of binding, adhesion, interaction forces, and, viscoelastic modeling .[37-43] Moreover, use of dynamic methods can be categorized under the general heading of "higher order sensing".[44] In contrast, harmonics has been used in this chapter for the first time as a sensor element on the basis of different decay lengths. In developing this sensor array, focus is placed on intraclass discrimination as opposed to the typical interclass discrimination commonly reported in the literature. For proof of concept, discrimination of members of four homologous series (alcohols, hydrocarbons, nitriles, chlorohydrocarbons) was investigated. Furthermore, interclass discrimination potential was also evaluated. Lastly, discrimination of two related complex mixtures (petroleum ether and kerosene) was examined. Responses obtained at different harmonics were subsequently analyzed using PCA and DA, and examination of the resultant data demonstrated that discrimination of analytes can be achieved with very high accuracy. The high level of discrimination achieved by use of this approach truly underscores the potential of QCM based VSAs for analyses of organic vapors in a wide range of

applications. To the best of my knowledge, my work is the first report of a QCM based virtual sensor array, as well as an experimental sensor array that is based primarily on viscoelasticity, film thickness, and harmonics.

2.2 Experimental Section

2.2.1 Preparation of Stock Solutions

Stock solutions of [OMIm][Br] or [OMIm][SCN] (1mg/mL) were prepared in DCM using 20 mL borosilicate glass scintillation vials. Synthesis of ionic liquids is detailed in appendix A.

2.2.2 Preparation of Sensing Films

Electrospray was used to prepare thin films and details are provided in appendix A. All films were coated under similar conditions onto a clean quartz crystal resonator so that film variation was purely time dependent. Regular coating time intervals were chosen to study the effect of film thickness. After coating, all films were dried using nitrogen, followed by storage in a desiccator.

2.2.3 QCM-D Data Acquisition

A schematic of the experimental system is depicted in Figure 2.1. The system consists of two independent gas flow channels i.e. one channel for the sample vapors and the other channel for the carrier gas. Before data collection, ultrapure argon was purged through the system until a stable frequency was achieved. Afterwards, chemical vapors were introduced via bubbling of argon gas through the sample reservoir, which was filled with pure liquid phase analyte of interest to generate a sample of saturated vapor pressure. As the sample channel and carrier channel merge, the sample flow is diluted yielding various concentrations which are represented here in terms of partial pressure, $p_a/p_o = 0.2, 0.3, 0.4$, where p_a is the partial pressure of the VOC and p_o is the saturated vapor pressure. The flow rate was controlled by use of digital mass flow controllers and adjusted to a total flow rate of 100 sccm. After sufficient mixing over the

length of the tubing (1 m), the vapors are passed over the QCM sensor crystal placed inside a flow module. The chamber temperature was precisely regulated (22 °C). Finally, to remove sample vapors, the system was purged with ultrapure argon until recovery of the baseline.

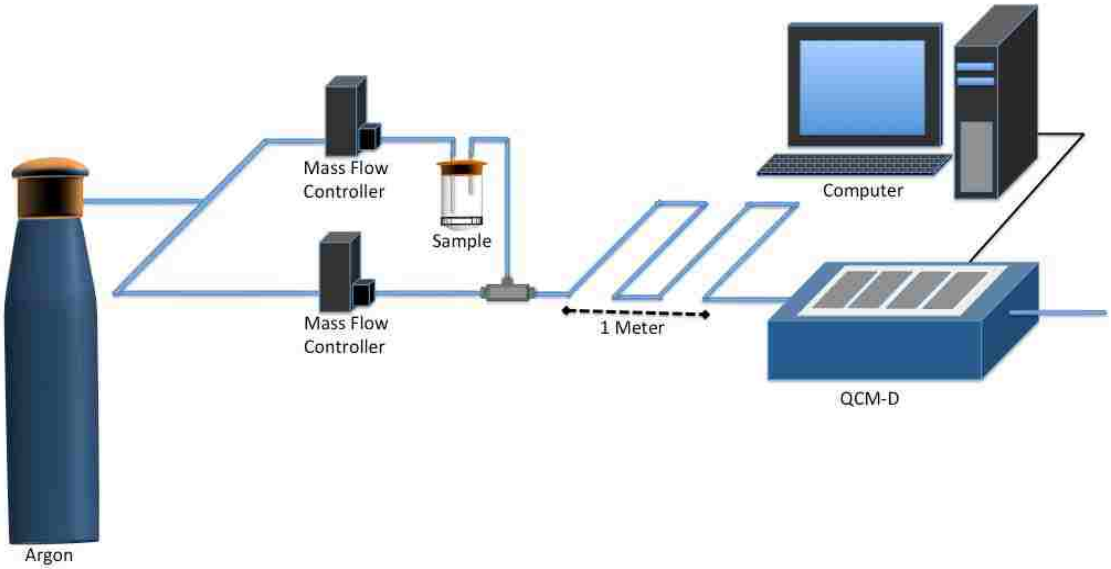

Figure 2.1 Schematic of the experimental system

2.2.4 Data Analysis

Multiple harmonic data generated from these experiments were used to design statistical models for identification of analytes. Predictive models were developed using Δf values obtained using multiple harmonics. As a first step in data analysis, principal component analysis (PCA) was used to reduce the dimensionality of the predictor space. The goal of this analysis was to create a smaller number of predictors based on the full set of original measured variables that retain as much of the variability in the original variables as possible. In all cases, up to five principal components were sufficient to account for 99% of the variability in the original variables. The indices created by PCA were used as input variables to QDA or LDA for the purpose of developing models that could accurately distinguish among and specifically identify the various analytes within

each homologous series and 18 analyte set. In order to accurately assess the predictive ability of the developed models, cross-validation was used to estimate classification error rates of the models.

2.3 Results and Discussion

2.3.1 Preparation and Characterization of Sensing Films

As previously noted, thin composite films were prepared using an electrospray method due to its high material deposition efficiency.[45] These films were then imaged using SEM and EDS. Representative micrographs for four different films, corresponding to either [OMIm][Br] or [OMIm][SCN] coated for 1.5, and 3 minutes respectively, are shown in Figure A1. Based on these SEM images, it was evident that all films were heterogeneous and comprised of isolated islands/droplets of varying sizes. SEM images and EDS spectra further show that the surface coverage increases with coating time (Figure A2). Furthermore, EDS point mapping confirms that the ionic liquid coating material is represented in black while the grey areas of the images correspond to the gold surface (Figure A3). By using AFM, it was found that the Z-depth of droplets increases proportional to droplet size in the x-y dimension. (Figure A4) Increased coating time leads to larger droplets in the x-y dimension and proportionally the z-dimension. Moreover, an increased population of larger sized droplets was also observed as compared to smaller sized droplets on the QCR surface, which resulted in an average increase in Z depth.

2.3.2 Examination of the Effect of Film Thickness on Gas-sensing Response

Four QCRs coated with either [OMIm][Br] or [OMIm][SCN] films of two different thicknesses were installed into the QCM-D system. The frequency change at the first harmonic for each sensor after coating was found to be ~ -1000 Hz, and ~ -2000 Hz, for coating times of 1.5, and 3 minutes respectively. As the coating time is increased, there is an increase in both surface coverage and thickness. All sensors were subsequently

exposed to a number of different analyte vapors belonging to four classes of organic compounds (See Table A1)[46] at different concentrations (p_a/p_o = 0.2, 0.3, 0.4), and the changes in frequency were measured. It was found that sensor response varied between films of the same chemical composition, depending upon coating thickness for the QCR and concentration of the analyte. Additionally, it is noted that for each sensor the baseline is stable and response is very reproducible. (Figure A5-A8) Moreover, as expected, sensor response varied between coatings of different chemical composition. The values of Δf plotted against thickness (coating time) for five analytes (methanol, ethanol, DCM, n-hexane, and acetonitrile) across several concentrations (p_a/p_o = 0.2, 0.3, 0.4) is depicted in Figure 2.2 Depending on the thickness of the coating, positive and negative shifts in frequency were observed. Simply by changing thickness, the response pattern for the five analytes is altered. Furthermore, it is noted that these virtual sensor elements display a cross-reactive response to different analytes, and cross-reactivity is a requirement for array based sensing. This thickness-dependent response can be attributed to relative changes in the mass and viscoelastic contributions to the sensor response. A number of theoretical treatments have been presented in the literature that supports these observations. In this regard, McHale and colleagues introduced a model that can account for changes as a function of film thickness and viscoelasticity ranging from liquid to amorphous solid coatings.[47] The conclusion from this model illustrates that it is possible to obtain both positive and negative frequency shift depending upon film thickness and viscoelastic properties of the coating material. Moreover, Vogt et al.,[48] after examination of the effect of film thickness on validity of the Sauerbrey equation using a polyelectrolyte film, found that as the coating thickness increases, so does the effect of its viscoelasticity, leading to deviations from the Sauerbrey equation. Finally, at least one research group has sought to model and quantify the relationship between mass change and frequency shift of a QCM in contact

with viscoelastic media.[49] In agreement with theoretical models, I was able to obtain both positive and negative resonant frequency changes using these coating materials

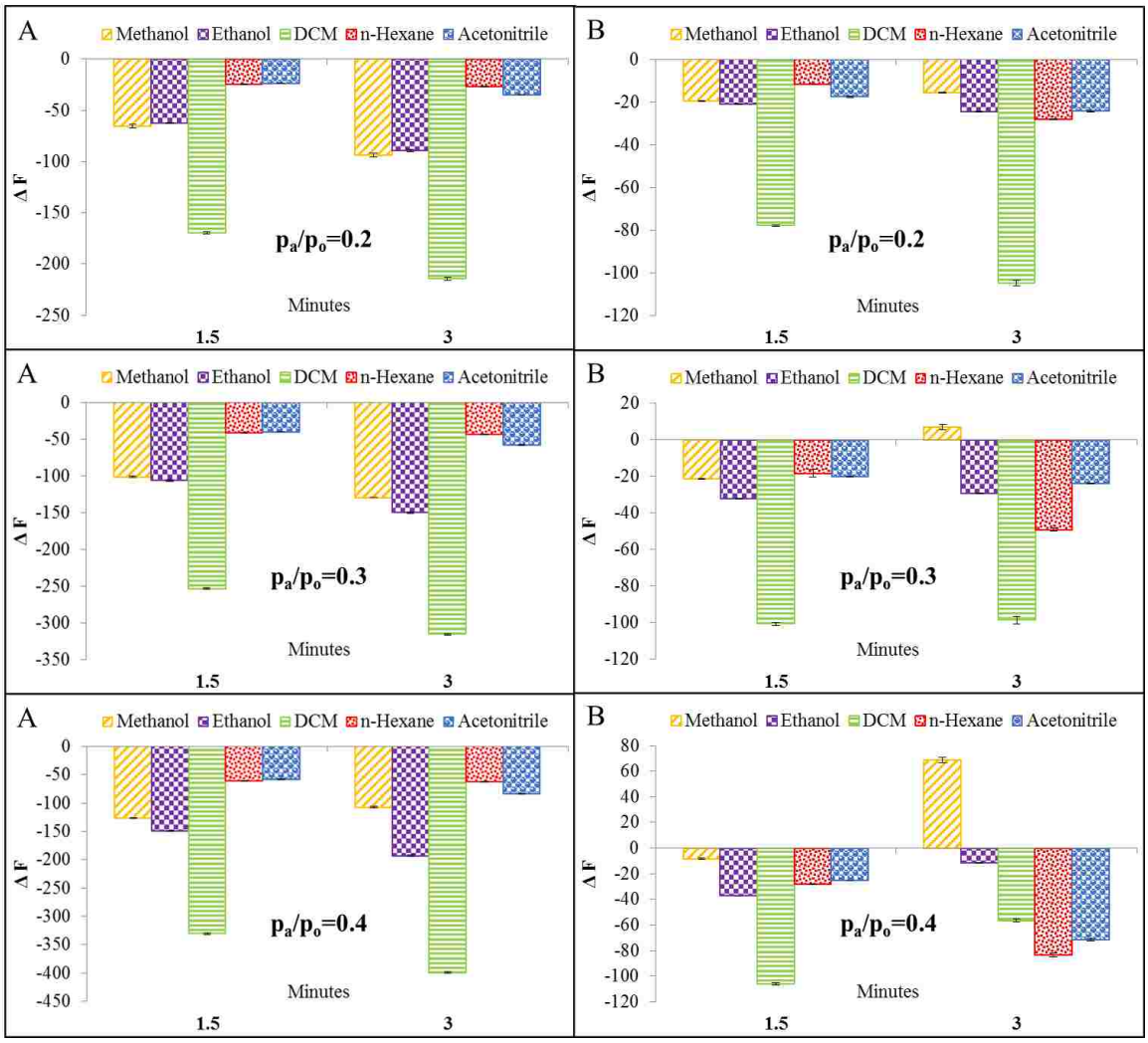

Figure 2.2 *Δf* (Hz) response patterns of 5 analytes generated by four sensors at different concentration of vapors. A) first harmonic frequency change of [OMIm][Br] sensors coated for 1.5 and 3 minutes and B) first harmonic frequency of [OMIm][SCN] sensors coated for 1.5 and 3 minutes. Error bars represent three replicate measurements.

after exposure to organic vapors. Based on the above results and discussions, I concluded that a sensor array based solely upon viscoelasticity could be fabricated by changes in film thickness.

2.3.3 Fabrication and Evaluation of Virtual Sensor Arrays

Since cross-reactive responses to different analytes can be obtained by simply changing the coating thickness, similar responses are expected to be obtained when measuring the frequency response at different harmonics using a QCM-D sensor. There is equivalence between measurements of multiple thicknesses at a single harmonic and a fixed thickness at multiple harmonics which can be better understood by considering the following equation:

$$\delta = \sqrt{\frac{2\eta}{\rho\omega}} \quad where,\ \omega = 2\pi f \qquad (2.1)$$

where δ is penetration depth, i.e. the distance at which the amplitude of the wave decreases to 1/e of its value at the surface; η is the viscosity of the coating; ρ is the density of the coating; ω is angular frequency, and f is the frequency. From this equation, it is evident that as frequency increases, the penetration depth of the acoustic wave decreases. In addition, as the penetration depth decreases, the acoustic wave probes progressively closer to the QCR surface (Figure 2.3). In other words, for a coating of fixed thickness on the QCR surface, as the frequency of waves increases, the thickness perceived by the waves also increases. Therefore, probing a single sensor at multiple harmonics should provide analyte-specific response patterns similar to those obtained by probing multiple sensors of different thickness at a single harmonic. Using the QSense QCM-D, it is possible to measure the resonance frequency at up to seven different harmonics (odd harmonics from 1st through 13th). Different harmonics are successively probed within a range of milliseconds.[50] In order to obtain data from multiple harmonics, a film of suitable thickness is required, and for this reason, two QCRs coated for shorter times 1.5 and 3 minutes, were chosen to perform further studies. Typically, as film thickness increases, the number of harmonics that can be measured decreases. In this regard, 7 harmonics were obtained for the thinner films (1.5

min coatings) and 6 harmonics were obtained for the thicker films (3 min coatings). To the best of my knowledge, variations in harmonics have never been used to create

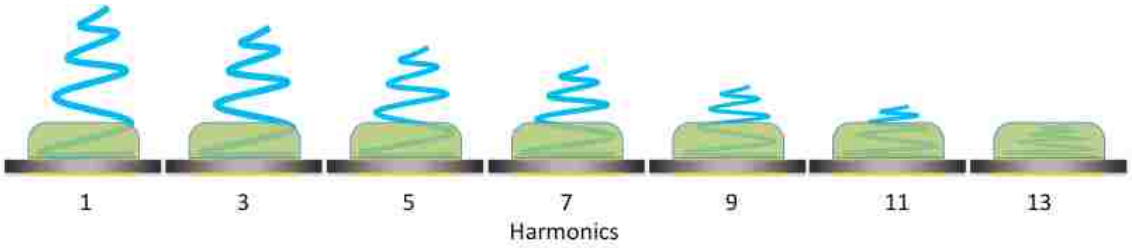

Figure 2.3 Schematic showing that change in harmonic number alters the penetration depth of the shear waves.

sensor arrays. Although Q-sense markets their instrument with the ability to excite various harmonics, to date there are few practical applications in gas sensing that employ multiple harmonics simultaneously.[51] In this chapter, I present a novel concept of using multiple harmonics to create virtual sensor arrays for QCM transducers via the aforementioned thickness equivalencies. The QCM-D sensors were exposed to 18 different analyte vapors, which are listed in Table 2.1. To evaluate the gas discrimination power of a single-sensor-based virtual sensor array, I investigated analytes belonging to the same class, as well as different classes. In this regard, four classes of organic vapors, namely, alcohols, chlorohydrocarbons, hydrocarbons, and nitriles, were selected as analytes. The QCM-D sensor was then exposed to different concentrations of each analyte and the changes in frequency were measured at each harmonic. The baseline for all tested sensors was very stable and the signal was highly reproducible as depicted in Figure A5-A8. A flow-type system was employed for gas generation, and the vapor coming from a liquid after bubbling a carrier gas was assumed to be saturated. Figure 2.4 contains plots of the sensor response (Δf) versus harmonic number for a single class of analytes, e.g. alcohols, at p_a/p_o=0.2 for all sensors. It should be noted that by simply changing the harmonics, a suitably varied response was achieved. Moreover, it is clear

that film thickness and chemical composition of the coating have a marked effect on sensor response. In changing the chemical composition, i.e. anion of the ionic liquid, many properties of the material change such as viscosity, hydrophobicity, and chemical affinity. This is clearly represented by the vast differences in sensor response obtained using [OMIm][Br] and [OMIm][SCN] based sensors. Finally, by varying the thickness of coatings comprised of the same ionic liquid, it is also possible to generate varied response. This result is only logical based upon previous works which suggest thin films exhibit more Sauerbrey behavior while thicker films experience deviations from this behavior due to increased viscoelasticity. Due to this revelation, evaluation of these sensors to create VSAs was initiated.

A VSA has been defined as an array that consists of a small number of sensors

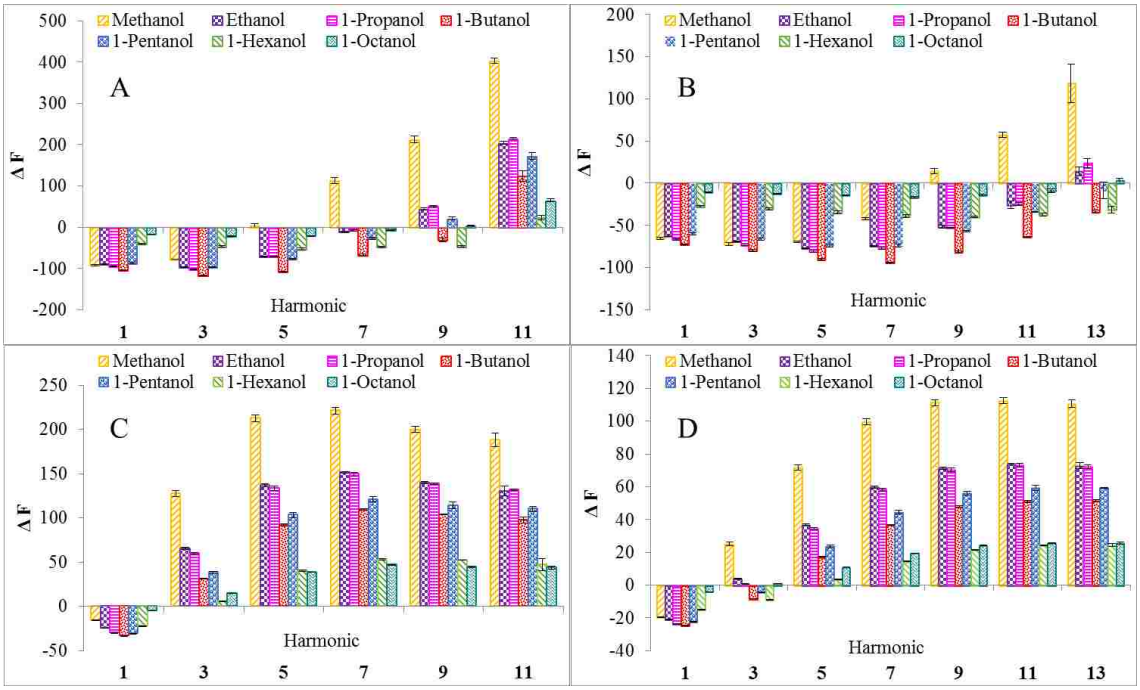

Figure 2.4 Δ*f* (Hz) as a function of harmonic number for a single sensor on exposure to p_a/p_o = 0.2 of a series of alcohols A) 3 minute [OMIm][Br] B) 1.5 minute [OMIm][Br] C) 3 minute [OMIm][SCN] D) 1.5 minute [OMIm][SCN]. Error bars represent three replicate measurements.

or only one sensor that can contribute many responses to the output pattern.[23] By using viscoelasticity as the discriminating factor, it was possible to apply the VSA scheme to the QCM-D transducer. Significant advantages arise when using a VSA scheme in comparison to MSAs. Although MSAs are widely used, there are several limitations associated with the use of these arrays. For instance, MSAs require stringent selection of multiple coating materials based on chemical affinity in addition to multiple readout electronics.[24] Additionally, the signal drift associated with even a single sensor deteriorates the performances of such MSAs.[24, 52] As a result of these limitations, there has been growing interest in the creation of virtual sensor arrays.[24, 53-55]

ILs were selected for the present study because they are viscoelastic, exhibit rapid absorption and desorption of analytes, and IL-based QCM sensors show minimal signal drift.[33] Three different concentrations of vapors were tested for all analytes, ranging from p_a/p_o = 0.2-0.4. I note that these concentrations are typically high for trace VOC detection. However, they are appropriate for real samples that use concentrations up to saturated vapor pressure. Therefore, I explore such concentrations herein.[18, 56-58] Moreover, I have also investigated discrimination of a set of analytes at lower concentrations. For clarity, data at p_a/p_o = 0.2 are presented here. In Figure 2.5, Δf response patterns for each class of analytes obtained at multiple harmonics for a A) 3 minute [OMIm][SCN] coating and B) 3 minute [OMIm][Br] coating based sensors are shown. Plots of Δf response patterns for 1.5 minute coating based sensors are shown in figure A9. It is observed that different analytes exhibit different response patterns. Principal component analysis (PCA) and quadratic discriminant analysis (QDA) were performed for each class of analytes, as well as for the complete set of analytes. PCA is a technique for data dimension reduction and display, which allows a qualitative survey of the possible discriminating power of the array. QDA is a method that allows quantitative classification of group membership, specifically using the method of cross

validation, and data display. This approach yields a quantitative survey of the possible discriminating power of the array. In this regard, I have depicted QDA canonical plots for further analyses. These analyses were based on a data matrix of Δ*f* values, where the columns represent harmonics and the rows represent the analytes. Three replicate measurements for three concentrations (p_a/p_o = 0.2, 0.3, 0.4) were considered for each analyte, for a total of 9 measurements per analyte. Data were baseline shifted to account for positive and negative responses and normalized to adjust for concentration related magnitude changes. Canonical plots for each of the tested classes for a A) 3 minute [OMIm][Br] coating based VSA and a B) 3 minute [OMIm][SCN] coating based VSA are depicted in Figure 2.6. Plots for 1.5 minute coating based VSAs for all classes are presented in Figure A10. Ellipses and Ellipsoids represent 95% confidence. In each case extremely high accuracy was achieved independent of the coating material or thickness. For each of the classes, it was possible to discriminate each class member with 100% accuracy over a range of concentrations for each three minute VSA with the exception of alcohols for [OMIm][Br] where one observation of ethanol was confused for 1-propanol, yielding 98.4% accuracy. In regard to the 1 minute VSAs, 100% accuracy was achieved for each class of analytes tested independent of coating material. These results indicate that this approach is truly promising for discrimination of members of the same homologous series. It is important to recognize that several previously published studies have reported on discrimination of completely unrelated analytes[14, 59] (e.g., polar, nonpolar, from different classes etc.). In contrast, herein I strive to discriminate between closely related analytes within a chosen class. In fact, electronic nose technology has been found to be successful in discrimination of compounds belonging to different homologous series, while distinction of members within a chemical class still remains a challenge.[60] Additionally, I have evaluated the discriminating power of the VSAs towards all 18 analytes, independent of the class. The data for the 18 analyte set were similarly

analyzed using PCA and QDA techniques; canonical plots for each VSA are depicted in appendix A Figures A11-A15. Accuracies of 97.6% and 98.7% were achieved for 3 minute [OMIm][Br] and [OMIm][SCN] based VSAs, respectively. In the case of the 3 minute [OMIm][Br] based VSA, 4 out of 162 total samples were misclassified, specifically 3 chloroform samples were confused for acrylonitrile and 1 acrylonitrile sample was confused for chloroform. This discrepancy is a result of the large degree of sample overlap within the corresponding canonical plots. (Figure A11) When considering the 3 minute [OMIm][SCN] VSA, 2 out of 162 total samples were misclassified, specifically 1 sample of DCM was confused for methanol and acrylonitrile, respectively. Again this is supported by a large degree of overlap between the three vapors in the corresponding canonical plots. (Figure A12) In regard to the 1 minute VSAs, QDA accuracies of 99.4%, corresponding to 1 misclassification out of 162 total samples, were achieved independent of coating composition. For the 1 minute [OMIm][Br] based VSA, 1 sample of chloroform was confused for acrylonitrile(Figure A13), while for a 1 minute [OMIm][SCN] based VSA, 1 sample of dichloromethane was confused for methanol (Figure A14). Overall, the 1 minute VSAs outperformed the thicker film counterparts. However, these VSAs exhibited lower signal. Furthermore, VSAs of the same chemical composition exhibited the same types of misclassification, suggesting that anion variation, which produces variations in the properties of the material, plays an important role in performance of these virtual sensor arrays. Finally, since confused samples are not chemically related, this suggests that viscoelasticity and not chemical affinity is the primary discriminating factor at work in these arrays.

To demonstrate capability for trace VOC detection, the most sensitive class of analytes, chlorohydrocarbons, was tested at a low concentration range. (p_a/p_o = 0.02-0.15) In this case, only the three minute VSAs were considered since they exhibited superior signal at low concentrations. Three replicate measurements over four

concentrations (p_a/p_o = 0.02, 0.05, 0.10, 0.15) were considered for a total of 12 measurements per analyte. QDA canonical plots are depicted in Figure 2.7. Again, each VSA was able to classify class members with 100% accuracy over the range of concentrations tested. When all data are taken in aggregate, these results demonstrate the excellent potential of this approach for discriminating pure organic vapors, whether from the same or different chemical classes at high or low vapor concentrations. Finally, to provide a more stringent test of these VSAs, I have investigated the discriminating power towards similar complex mixtures. In this regard, two industrially relevant petroleum distillates, petroleum ether and kerosene, were chosen as representative samples. During the refining process, petroleum ether contains a fraction of hydrocarbons distilled prior to kerosene. As a result, petroleum ether is a mixture of lower boiling hydrocarbons while kerosene contains higher boiling hydrocarbons. Hydrocarbon complex mixtures were chosen since hydrocarbons have been previously shown to be the least sensitive class tested for each array. In Figure 2.8, Δf response patterns for petroleum ether and kerosene exposed to p_a/p_o= 0.2 obtained at multiple harmonics for A) 3 minute [OMIm][Br] based VSA and B) 3 minute [OMIm][SCN] coating based VSA are depicted. LDA plots for analyses of five replicate measurements of each of the two analytes at a single concentration (p_a/p_o= 0.2) are shown in Figure A16. for each array, suggesting that this approach is very promising for discrimination of similar complex mixtures. All experimental results have been summarized in Table A2. Overall, the results presented here suggest that use of a material property, such as viscoelasticity, for pure analyte and mixture discrimination is indeed a viable approach for fabrication of arrays, as well as a viable alternative to chemical affinity. Moreover, the VSA methodology presented here is a promising alternative to the conventional MSA approach used for QCM based gas discrimination, whether for analyses of pure samples or complex mixtures.

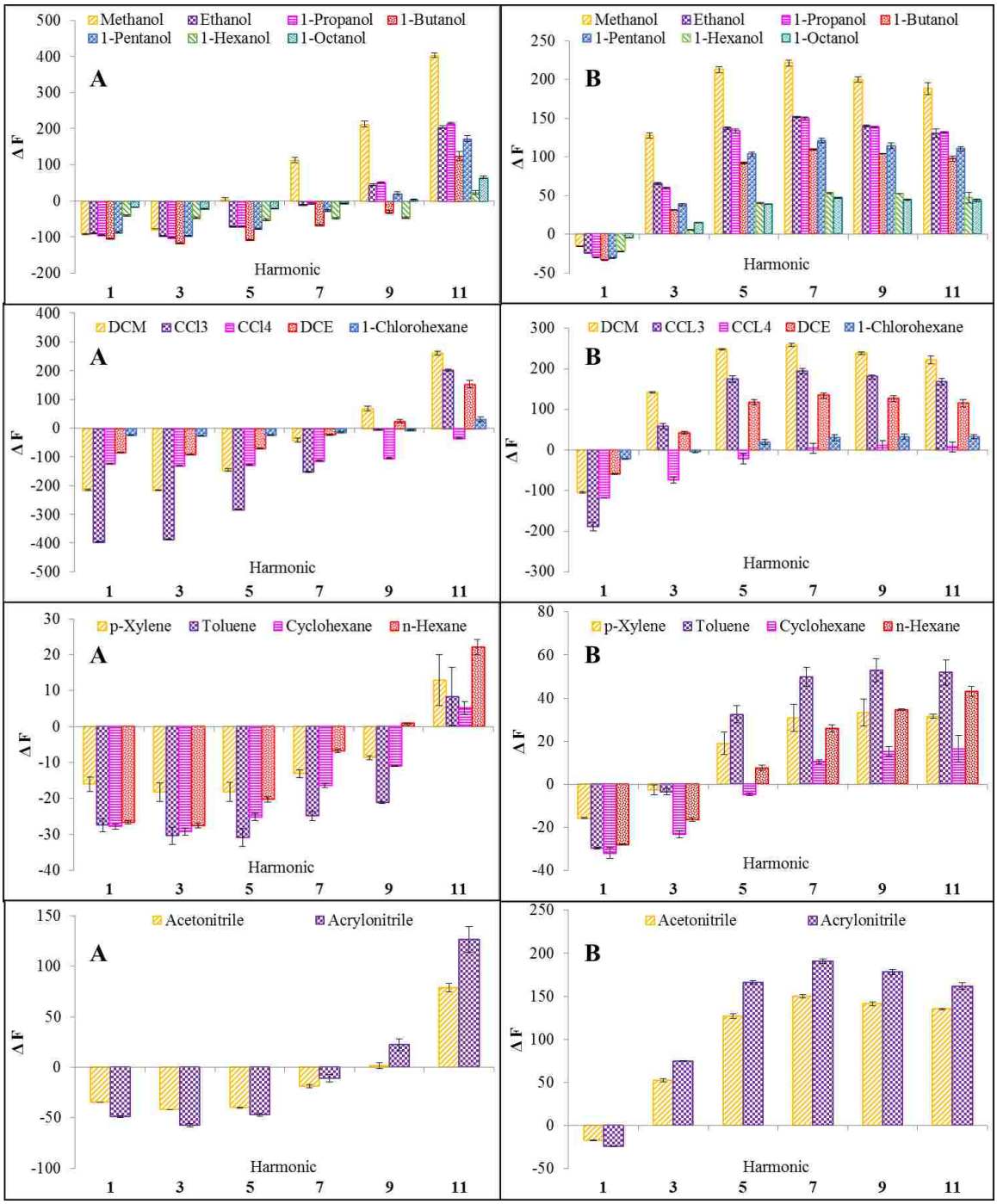

Figure 2.5 Δ*f* (Hz) response patterns for each class of vapors (in descending order n-alcohols, chlorohydrocarbons, hydrocarbons, and nitriles) are shown for a A) 3 minute [OMIm][Br] coating based sensor and B) 3 minute [OMIm][SCN] coating based sensor. The vapor partial pressure for all analytes is fixed at $p_a/p_o = 0.2$. Error bars represent the standard deviations of three replicate measurements.

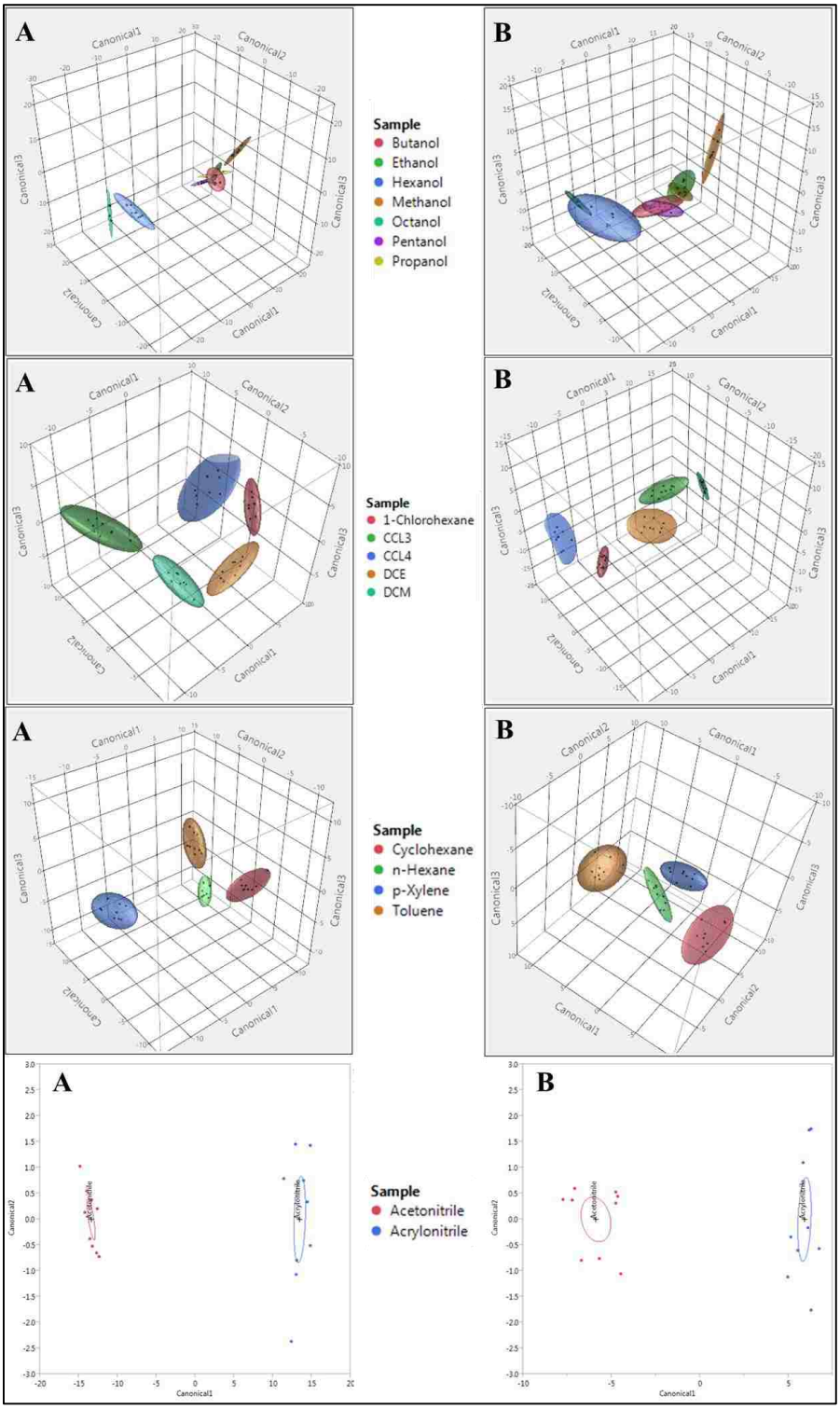

Figure 2.6 QDA canonical plots for each class of organic vapors (in descending order n-alcohols, chlorohydrocarbons, hydrocarbons, and nitriles) with respect to a VSA comprised of either a 3 minute coating of A) [OMIm][Br] or B) [OMIm][SCN]

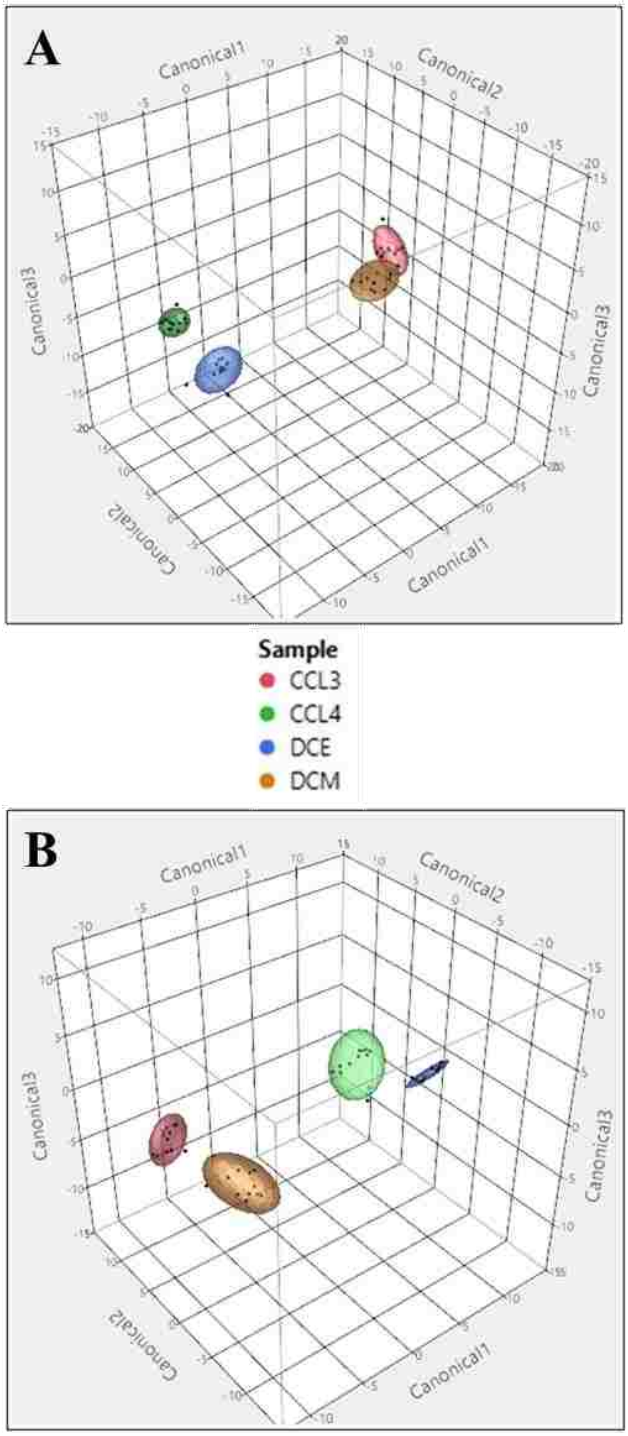

Figure 2.7 QDA canonical plots for chlorohydrocarbons at low concentrations (p_a/p_o = 0.02, 0.05, 0.10, 0.15) with respect to a VSA comprised of either a 3 minute coating of A) [OMIm][Br] or B) [OMIm][SCN].

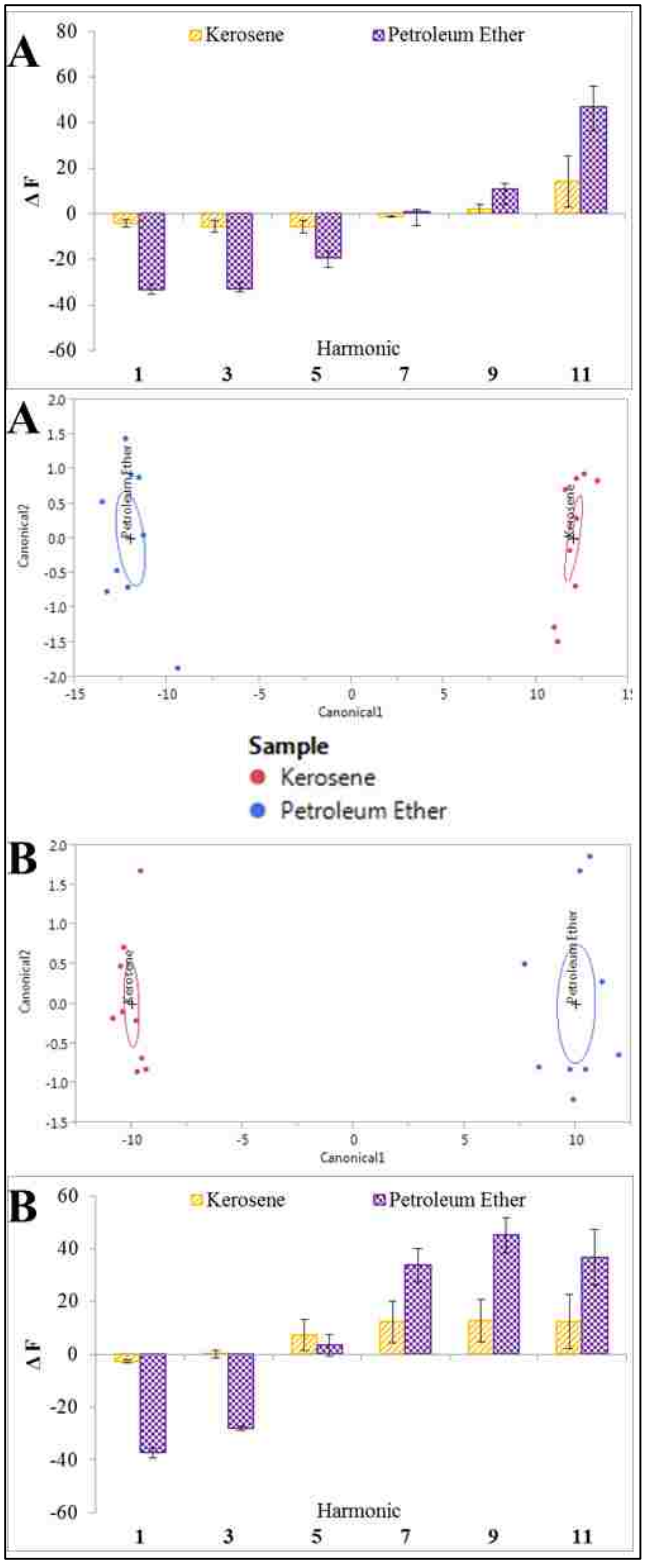

Figure 2.8 Sensor response, *Δf* (Hz), and QDA canonical plots for two complex mixtures of hydrocarbons, i.e petroleum ether and kerosene with respect to a VSA comprised of either a 3 minute coating of A) [OMIm][Br] or B) [OMIm][SCN]

2.4 Conclusion

In summary, I have demonstrated the concept of using a QCM-D based virtual sensor array for facile discrimination of a wide range of organic vapors. The most commonly used sensor arrays utilize multiple sensor elements coated with recognition elements that possess different binding affinities to different analytes. In this chapter, I sought to present an entirely fresh perspective for use of QCM sensor arrays, i.e. the use of material properties (viscoelasticity and film thickness) as the discriminating factor in contrast to chemical affinity. Four QCM-D sensors were prepared by coating two ILs which differ in anion, at two thicknesses, and were subsequently exposed to 18 different analytes belonging to the same or different homologous series. Changes in frequencies at different harmonics were monitored. Data acquired at multiple harmonics were analyzed using PCA and DA, which provided highly accurate identification of closely related compounds within a class. Additionally, upon analyses of the complete set of 18 analytes at multiple concentrations for interclass discrimination, accuracies ranged from 97.6%-99.4% for the four VSAs tested. When applied to discrimination of two similar complex mixtures, accuracies of 100% were achieved. This level of accuracy for this approach is truly promising for discrimination of closely related and chemically distinct analytes, as well as complex mixtures. Furthermore, by use of only a single sensor, I have decreased the sensor array preparative time and material cost, while simultaneously increasing data output. Thus, I have introduced a simplistic array method for the QCM-D in the form of a virtual sensor array based on a single QCM-D sensor that permits facile discrimination of organic vapors. Overall, I believe that this approach is a promising alternative (or at least complementary) technique to the conventional MSA approach used for QCM based gas discrimination. Further investigations are underway to ascertain the full potential of this new strategy for vapor phase analyses.

2.5 References

1. Ayad, M. M. & Torad, N. L. Alcohol vapours sensor based on thin polyaniline salt film and quartz crystal microbalance. Talanta 78, 1280–1285 (2009).

2. Hierlemann, A., Weimar, U., Kraus, G., Schweizer-Berberich, M. & Göpel, W. Polymer-based sensor arrays and multicomponent analysis for the detection of hazardous oragnic vapours in the environment. Sens. Actuators B Chem. 26, 126–134 (1995).

3. Stetter, J. R., Jurs, P. C. & Rose, S. L. Detection of hazardous gases and vapors: pattern recognition analysis of data from an electrochemical sensor array. Anal. Chem. 58, 860–866 (1986).

4. Machado, R. F. et al. Detection of Lung Cancer by Sensor Array Analyses of Exhaled Breath. Am. J. Respir. Crit. Care Med. 171, 1286–1291 (2005).

5. Di Natale, C. et al. Lung cancer identification by the analysis of breath by means of an array of non-selective gas sensors. Biosens. Bioelectron. 18, 1209–1218 (2003).

6. Carey, J. R. et al. Rapid Identification of Bacteria with a Disposable Colorimetric Sensing Array. J. Am. Chem. Soc. 133, 7571–7576 (2011).

7. Capone, S. et al. Monitoring of rancidity of milk by means of an electronic nose and a dynamic PCA analysis. Sens. Actuators B Chem. 78, 174–179 (2001).

8. Buratti, S., Benedetti, S., Scampicchio, M. & Pangerod, E. C. Characterization and classification of Italian Barbera wines by using an electronic nose and an amperometric electronic tongue. Anal. Chim. Acta 525, 133–139 (2004).
9. Bello, A. et al. Potentialities of a modified QCM sensor for the detection of analytes interacting via H-bonding and application to the determination of ethanol in bread. Sens. Actuators B Chem. 125, 321–325 (2007).

10. Ponrathnam, T., Cho, J., Kurup, P., Nagarajan, R. & Kumar, J. Investigation of QCM Sensors with Azobenzene Functionalized Coatings for the Detection of Nitroaromatics. J. Macromol. Sci. Part A 48, 1031–1037 (2011).

11. Wang, F., Gu, H. & Swager, T. M. Carbon Nanotube/Polythiophene Chemiresistive Sensors for Chemical Warfare Agents. J. Am. Chem. Soc. 130, 5392–5393 (2008).

12. Rehman, A. et al. Differential Solute Gas Response in Ionic-Liquid-Based QCM Arrays: Elucidating Design Factors Responsible for Discriminative Explosive Gas Sensing. Anal. Chem. 83, 7823–7833 (2011).

13. Bachar, N. et al. Sensor Arrays Based on Polycyclic Aromatic Hydrocarbons: Chemiresistors versus Quartz-Crystal Microbalance. ACS Appl. Mater. Interfaces 5, 11641–11653 (2013).

14. Jin, X., Yu, L., Garcia, D., Ren, R. X. & Zeng, X. Ionic Liquid High-Temperature Gas Sensor Array. Anal. Chem. 78, 6980–6989 (2006).

15. Toniolo, R. et al. Room Temperature Ionic Liquids As Useful Overlayers for Estimating Food Quality from Their Odor Analysis by Quartz Crystal Microbalance Measurements. Anal. Chem. 85, 7241–7247 (2013).

16. Umali, A. P. & Anslyn, E. V. A general approach to differential sensing using synthetic molecular receptors. Curr. Opin. Chem. Biol. 14, 685–692 (2010).

17. Albert, K. J. et al. Cross-Reactive Chemical Sensor Arrays. Chem. Rev. 100, 2595–2626 (2000).

18. Suslick, B. A., Feng, L. & Suslick, K. S. Discrimination of Complex Mixtures by a Colorimetric Sensor Array: Coffee Aromas. Anal. Chem. 82, 2067–2073 (2010).

19. Janzen, M. C., Ponder, J. B., Bailey, D. P., Ingison, C. K. & Suslick, K. S. Colorimetric Sensor Arrays for Volatile Organic Compounds. Anal. Chem. 78, 3591–3600 (2006).

20. Galpothdeniya, W. I. S. et al. Ionic liquid-based optoelectronic sensor arrays for chemical detection. RSC Adv 4, 7225–7234 (2014).

21. Koo, C.-K., Samain, F., Dai, N. & Kool, E. T. DNA polyfluorophores as highly diverse chemosensors of toxic gases. Chem. Sci. 2, 1910 (2011).

22. Kwon, H., Samain, F. & Kool, E. T. Fluorescent DNAs printed on paper: sensing food spoilage and ripening in the vapor phase. Chem. Sci. 3, 2542 (2012).

23. Stetter, J. R. & Penrose, W. R. Understanding Chemical Sensors and Chemical Sensor Arrays(Electronic Noses): Past, Present, and Future. Sens. Update 10, 189 (2002).

24. Reimann, P. & Schütze, A. in Gas Sensing Fundamentals (eds. Kohl, C.-D. & Wagner, T.) 15, 67–107 (Springer Berlin Heidelberg, 2013).

25. Schutze, A., Gramm, A. & Ruhl, T. Identification of Organic Solvents by a Virtual Multisensor System With Hierarchical Classification. IEEE Sens. J. 4, 857–863 (2004).

26. Ankara, Z., Kammerer, T., Gramm, A. & Schütze, A. Low power virtual sensor array based on a micromachined gas sensor for fast discrimination between H2, CO and relative humidity. Sens. Actuators B Chem. 100, 240–245 (2004).

27. Sim, C. O. et al. Chemometric Classification of Herb – Orthosiphon stamineus According to Its Geographical Origin Using Virtual Chemical Sensor Based Upon Fast GC. Sensors 3, 458–471 (2003).

28. Chen, X. et al. A study of an electronic nose for detection of lung cancer based on a virtual SAW gas sensors array and imaging recognition method. Meas. Sci. Technol. 16, 1535–1546 (2005).

29. Staples, E. J. & Viswanathan, S. Ultrahigh-speed chromatography and virtual chemical sensors for detecting explosives and chemical warfare agents. IEEE Sens. J. 5, 622–631 (2005).

30. Ding, B., Kim, J., Miyazaki, Y. & Shiratori, S. Electrospun nanofibrous membranes coated quartz crystal microbalance as gas sensor for NH3 detection. Sens. Actuators B Chem. 101, 373–380 (2004).

31. Liang, C., Yuan, C.-Y., Warmack, R. J., Barnes, C. E. & Dai, S. Ionic Liquids: A New Class of Sensing Materials for Detection of Organic Vapors Based on the Use of a Quartz Crystal Microbalance. Anal. Chem. 74, 2172–2176 (2002).

32. Regmi, B. P. et al. A novel composite film for detection and molecular weight determination of organic vapors. J. Mater. Chem. 22, 13732 (2012).

33. Regmi, B. P. et al. Molecular weight sensing properties of ionic liquid-polymer composite films: theory and experiment. J Mater Chem C 2, 4867–4878 (2014).

34. Jin, X., Huang, Y., Mason, A. & Zeng, X. Multichannel Monolithic Quartz Crystal Microbalance Gas Sensor Array. Anal. Chem. 81, 595–603 (2009).

35. Makino, W., Kishikawa, R., Mizoshiri, M., Takeda, S. & Yao, M. Viscoelastic properties of room temperature ionic liquids. J. Chem. Phys. 129, 104510 (2008).

36. Yamaguchi, T., Miyake, S. & Koda, S. Shear Relaxation of Imidazolium-Based Room-Temperature Ionic Liquids. J. Phys. Chem. B 114, 8126–8133 (2010).

37. Ghosh, S. K., Ostanin, V. P. & Seshia, A. A. Anharmonic Surface Interactions for Biomolecular Screening and Characterization. Anal. Chem. 83, 549–554 (2011).

38. Ghosh, S. K., Ostanin, V. P. & Seshia, A. A. Anharmonic Interaction Signals for Acoustic Detection of Analyte. Anal. Chem. 82, 3929–3935 (2010).

39. Malmström, J., Agheli, H., Kingshott, P. & Sutherland, D. S. Viscoelastic Modeling of Highly Hydrated Laminin Layers at Homogeneous and Nanostructured Surfaces: Quantification of Protein Layer Properties Using QCM-D and SPR. Langmuir 23, 9760–9768 (2007).

40. Stengel, G., Höök, F. & Knoll, W. Viscoelastic Modeling of Template-Directed DNA Synthesis. Anal. Chem. 77, 3709–3714 (2005).

41. Rodahl, M. et al. Simultaneous frequency and dissipation factor QCM measurements of biomolecular adsorption and cell adhesion. Faraday Discuss. 107, 229–246 (1997).

42. Chen, H., Su, X., Neoh, K.-G. & Choe, W.-S. QCM-D Analysis of Binding Mechanism of Phage Particles Displaying a Constrained Heptapeptide with Specific Affinity to SiO 2 and TiO 2. Anal. Chem. 78, 4872–4879 (2006).

43. Brewer, S. H., Glomm, W. R., Johnson, M. C., Knag, M. K. & Franzen, S. Probing BSA Binding to Citrate-Coated Gold Nanoparticles and Surfaces. Langmuir 21, 9303–9307 (2005).

44. Hierlemann, A. & Gutierrez-Osuna, R. Higher-Order Chemical Sensing. Chem. Rev. 108, 563–613 (2008).

45. Jaworek, A. Electrospray droplet sources for thin film deposition. J. Mater. Sci. 42, 266–297 (2007).

46. Lide, D. R. CRC Handbook of Chemistry and Physics, 85th Edition. (CRC Press, 2004).

47. McHale, G., Lücklum, R., Newton, M. I. & Cowen, J. A. Influence of viscoelasticity and interfacial slip on acoustic wave sensors. J. Appl. Phys. 88, 7304 (2000).

48. Vogt, B. D., Lin, E. K., Wu, W. & White, C. C. Effect of Film Thickness on the Validity of the Sauerbrey Equation for Hydrated Polyelectrolyte Films. J. Phys. Chem. B 108, 12685–12690 (2004).

49. Tan, F. & Huang, X.-H. Relations between Mass Change and Frequency Shift of a QCM Sensor in Contact with Viscoelastic Medium. Chin. Phys. Lett. 30, 50701 (2013).

50. Dixon, M. C. Quartz Crystal Microbalance with Dissipation Monitoring: Enabling Real-Time Characterization of Biological Materials and Their Interactions. J. Biomol. Tech. JBT 19, 151–158 (2008).

51. Benedetti, T. M. & Torresi, R. M. Rheological Changes and Kinetics of Water Uptake by Poly(ionic liquid)-Based Thin Films. Langmuir 29, 15589–15595 (2013).

52. Vergara, A. et al. Chemical gas sensor drift compensation using classifier ensembles. Sens. Actuators B Chem. 166–167, 320–329 (2012).

53. Beckers, N. A., Taschuk, M. T. & Brett, M. J. Selective room temperature nanostructured thin film alcohol sensor as a virtual sensor array. Sens. Actuators B Chem. 176, 1096–1102 (2013).

54. Ziyatdinov, A. & Perera-Lluna, A. Data Simulation in Machine Olfaction with the R Package Chemosensors. PLoS ONE 9, e88839 (2014).

55. Xing Chen et al. A Non-invasive Detection of Lung Cancer Combined Virtual Gas Sensors Array with Imaging Recognition Technique. in 5873–5876 (IEEE, 2005).

56. Mazzone, P. J. et al. Diagnosis of lung cancer by the analysis of exhaled breath with a colorimetric sensor array. Thorax 62, 565–568 (2007).

57. García, M., Aleixandre, M., Gutiérrez, J. & Horrillo, M. C. Electronic nose for wine discrimination. Sens. Actuators B Chem. 113, 911–916 (2006).

58. Santos, J. P. et al. SAW sensor array for wine discrimination. Sens. Actuators B Chem. 107, 291–295 (2005).

59. Xu, X., Cang, H., Li, C., Zhao, Z. K. & Li, H. Quartz crystal microbalance sensor array for the detection of volatile organic compounds. Talanta 78, 711–716 (2009).

60. Rakow, N. A., Sen, A., Janzen, M. C., Ponder, J. B. & Suslick, K. S. Molecular Recognition and Discrimination of Amines with a Colorimetric Array. Angew. Chem. Int. Ed. 44, 4528–4532 (2005).

CHAPTER 3. QCM VIRTUAL SENSOR ARRAY: VAPOR IDENTIFICATION AND MOLECULAR WEIGHT APPROXIMATION

3.1 Introduction

Development of the sensor array concept has provided a powerful analytical approach for detection and discrimination of volatile organic compounds (VOCs). Such analyses are important for ambient air monitoring,[1, 2] biomedical diagnostics,[3] food quality assurance,[4-6] and military and civilian counterterrorism.[7-9] Moreover, as our understanding of the far reaching health and environmental impacts of organic vapors has evolved, so has the number of viable methods for VOC analysis. While such methods vary greatly, each should have the important properties of simplicity, sensitivity, and selectivity.

Among the various methods employed for VOC analyses, quartz crystal microbalance (QCM) based sensor arrays have been recognized as simple, inexpensive, and amenable to miniaturization. Furthermore, the sensitivity and selectivity of such arrays can be controlled by judicious selection of chemosensitive adlayers. As a result, materials with easily alterable properties that facilitate optimal array responses are highly sought. Organic salts with depressed melting points have proven to be particularly attractive. Specifically, ionic liquids (ILs) and solid phase organic salts termed as a Group of Uniform Materials Based on Organic Salts (GUMBOS) are two classes of materials which embody simple synthesis and broad chemical diversity with untold potential for sensing applications.[9-14] Indeed, simply by varying counter ions, material properties such as (1) melting point, (2) solubility, (3) polarity, (4) viscosity, and (5) toxicity can be easily manipulated. Moreover, these materials show reversible capture of organic vapors and are amenable to development of binary blends using polymers. Such blends can be used to enhance or modulate sensor response. In this regard, we have previously demonstrated that IL-polymer composite-coated QCM sensors exhibit stable

dual-parameter response (i.e. change in frequency (Δ*f)* and change in dissipation (Δ*D*) due to the viscoelastic properties of the coatings.[15, 16] More importantly, we have shown that the ratio of the modulated dual parameter response allows molecular weight approximation of adsorbed pure organic vapors.[15, 16] While quite promising, these studies only facilitate molecular weight based discrimination. Thus, identification of same molecular weight compounds i.e. closely related isomers, would prove problematic, and necessitate additional methodologies. In order to extend the utility of our previous studies, I propose herein the fabrication of a multifunctional sensor array. If successful, such an impactful strategy in a sensor array would have great potential for increasing the diversity of analytical information output, i.e. discrimination of analytes as well as approximation of their respective molecular weights.

Generally speaking, most QCM based sensor arrays have employed a standard multisensor array (MSA) approach. [9, 12, 14, 17-25] In contrast, I have introduced a technique for using a dynamically operated single sensor which acts as a sensor array. In this regard, I have previously demonstrated successful fabrication of QCM based virtual sensor arrays (VSAs) using a viscoelastic material.[26] Briefly, ionic liquid coated QCM sensors were exposed to a range of different organic vapors and the frequency shifts (Δ*f)* at multiple harmonics were measured. Thus, each harmonic functions as a virtual sensor. Using QCM-D, different responses at multiple harmonics can be easily recorded simultaneously upon interaction of an analyte with the ionic liquid coating material. Due to inherent viscoelastic properties of the coating, both increases and decreases of Δf were exhibited depending on the analyte, harmonic number, and film thickness. When responses across multiple harmonics were taken in aggregate, analyte specific response patterns were generated and could be analyzed using statistical methods. I note that Q-sense markets their instrument with the ability to excite various harmonics. However to date, variable response at multiple harmonics of the QCM-D instrument has never been

exploited as a sensor array with the exception of my previous work.[26] In this regard, the majority of applications that employ multiple harmonics concern modeling studies, or sensor sensitivity, but never in the form of a sensor array. [27-31] This approach, while quite simple, proved to be highly effective for discrimination of distinct, as well as closely related organic vapors using the quartz crystal microbalance with dissipation (QCM-D). Significant advantages arise when using a VSA scheme in comparison to MSAs. In particular, limitations such as stringent selection of multiple coating materials based on chemical affinity, requirement of multiple readout electronics, and signal drift issues that deteriorate the performance of MSAs are alleviated.[32, 33] Thus, researchers are embracing the development of VSAs to circumvent these concerns.[32, 34-36] I desire to further expand my QCM VSA technique by exploiting the unique properties of composite materials to facilitate two dimensional analyses. It should be noted, that the potential for molecular weight approximation by VSA, is negated by using only ionic liquid chemosensitive layers, as previously published[26]. Therefore, in this study, a binary blend composed of ionic liquids and polymer was explored as an alternative chemosensitive layer for molecular weight approximation using VSAs.

3.1.1 Approach

In this chapter, I present the first fabrication of a sensor array with capabilities for approximating molecular weights of adsorbed analytes. In this regard, the development of QCM VSAs employing a binary blend of ionic liquid and polymer as a chemosensitive adlayer is introduced. The unique properties of these materials suitably modulate sensor response allowing for measurement of stable resonance frequency and dissipation shift (Δf and ΔD). Moreover, the ratio of change in two parameters ($\frac{\Delta f}{\Delta D}$), can be directly correlated with molecular weight of adsorbed vapors under low to moderate loadings as previously described by us. [15, 16] Notably, such blends have been found to exhibit

viscoelastic behavior.[16] This makes such materials particularly amenable to the presented virtual sensor array approach. The composite films utilized in this study consisted of a binary blend of the ionic liquid, 1-hexyl-3-methylimidazolium bis(trifluoromethylsulfonyl)imide ([HMIm][NTf_2]), and the polymer polymethylmethacrylate (PMMA). It should be noted that this adlayer employs a very low viscosity ionic liquid, which contrasts with previously reported highly viscous/ solid phase ionic liquids and GUMBOS that were employed for applications involving molecular weight approximations.[15, 16] The present composite material was investigated using three distinct film thicknesses. Each individual sensor was then exposed to organic vapors and the frequency and dissipation shift over multiples harmonics was monitored. Due to the viscoelastic properties of this composite material, all combinations of Δf and ΔD were exhibited. Multiple harmonic data resulting from the best thickness of composite material were then examined using statistical methods. Each parameter was analyzed separately to ascertain capability for discrimination. Additionally, the $\frac{\Delta f}{\Delta D}$ ratio was analyzed using the 1st harmonic to obtain optimal molecular weight approximations. To evaluate this concept, as well as demonstrate the innate selectivity of my method, I assessed a set of closely related alcohols including isomers. Alcohols are volatile solvents and important pollutants, which are ubiquitously found in civilian and industrial settings and thus represent an important class of VOCs. It should be noted that I am using simple composites, with no additional modifications, to discriminate between a homologous series, as well as isomers which exhibit very similar characteristics and the same molecular weight. Thus, this is a very simplistic approach, especially when compared to some of the synthetic materials employed for QCM based methods.[37, 38] Upon evaluation of the resultant data, this method was found to be exceedingly promising for simultaneous discrimination and molecular weight approximation of closely

related organic vapors. While we have previously presented molecular weight approximation using the QCM, this concept has never been employed in a sensor array scheme. In this chapter, I further extend my study to demonstrate the first example of a sensor array which allows molecular weight determination, discrimination of closely related organic vapors over multiple concentrations, and discrimination of isomers. Coincidentally, this chapter also is a report of the first fabrication of a dissipation based virtual sensor array.

3.1.2 Theory of QCM based Molecular Weight Approximation

We have previously reported the use of ionic liquid –polymer composite coated QCM sensors for molecular weight (MW) approximation of VOCs. [15, 16] Therein, a relationship was determined between resonance frequency (Δf), motional resistance (ΔR) / dissipation (ΔD) and MW of VOCs.[16] Motional resistance and dissipation are equivalent parameters and thus can be used interchangeably. The relationship is denoted below in equation 3.1:

$$1) \quad \mathrm{MW} = \frac{-\Delta f}{k'\Delta R^2 + k\Delta R} \qquad (3.1),$$

In this equation, MW is molecular weight; Δf is change in resonance frequency; ΔR is change in motional resistance; k' and k are coating dependent constants. Typically, k' is small with low motional resistance change and thus equation 3.1 can be reduced to equation 3.2.

$$2) \quad \frac{\Delta f}{\Delta R} = -k\mathrm{MW} \qquad (3.2),$$

Thus, for composite coated QCM sensors the ratio of Δf to ΔR or alternatively Δf to ΔD is found to correlate with molecular weight of absorbed VOCs. Such a relationship allows approximation of MW of VOCs. Finally, we note that this relationship has not been found to be true for pure ionic liquids.

3.1.3 Theory of QCM based Virtual Sensing

I have previously reported the fabrication and theory of QCM virtual sensor arrays.[26] QCM virtual sensing is based on dynamic operation of a single QCM sensor coated with a viscoelastic chemosensitive material. In this regard, a single sensor coated with a thin film of viscoelastic material when measured at multiple harmonics yields several quasi-independent sensor responses. Changes in sensor response at different harmonics are due to changes in mass and viscoelastic contributions as a result of perceived variations in film thickness. In fact, measurements of a fixed film thickness at multiple harmonics have an equivalency with measurements of multiple film thicknesses at a single harmonic. This is recognized when one considers the following equation:

$$\delta = \sqrt{\frac{2\eta}{\rho\omega}} \quad where, \quad \omega = 2\pi f \qquad (3.3),$$

where δ is penetration depth, i.e. the distance at which the amplitude of the wave decreases to 1/e of its value at the surface, η is the viscosity of the coating; ρ is the density of the coating; ω is angular frequency, and *f* is frequency. Therefore, as frequency increases/decreases, the penetration depth of the acoustic wave decreases/increases. As a result of this changing penetration depth, perceived film thickness changes. It is well known from the Sauerbrey equation, that thin, rigid films exhibit the most Sauerbrey like behavior, while thick less rigid films exhibit more viscoelastic behavior, resulting in deviations from ideal sauerbrey behavior. Such

behavior allows large variations in sensor response to be achieved based on film thickness, viscoelasticity, and harmonics employed.[26, 39, 40] It should be noted that the same effect could be accomplished by employing several physical sensors however it is more efficient to use a single sensor operated at multiple harmonics.

3.2 Experimental Section

3.2.1 Reagents and Materials

The composite chemosensitive adlayers used in the present study consists of IL [HMIm][NTf_2] and PMMA. PMMA (molecular weight ~500,000 Da) was obtained from Polysciences, Inc. (Warrington, PA, USA). Anhydrous methanol, anhydrous ethanol, anhydrous 1-propanol, anhydrous 2-propanol, anhydrous 1-butanol, anhydrous 2-butanol, anhydrous 3-methyl-1-butanol, and anhydrous 1-hexanol, 1-chlorohexane, 1-methylimidazole and lithium bis(trifluoromethylsulfonyl)imide ($LiNTf_2$) were obtained from Sigma-Aldrich (St. Louis, MO, USA). Dichloromethane (DCM) was obtained from Macron Fine Chemicals (Center Valley, PA, USA). All chemicals were used as received without further purification.

3.2.2 Instrumentation

The QCM-D E4 system and gold sensors were obtained from Q-Sense AB (Gothenburg, Sweden). Each QSX 301 sensor is a gold-coated AT-cut quartz crystal with a diameter of 14 mm and 5MHz fundamental frequency. Readout equipment (Model 5878) as well as mass flow controllers (Model 5850E) were obtained from Brooks Instrument, LLC (Hatfield, PA, USA).

3.2.3 Synthesis of Ionic Liquid

The IL [HMIm][NTf_2] was synthesized using a previously reported method.[41, 42] Briefly, a mixture containing equimolar amounts 1-methylimidazole and 1-chlorohexane was refluxed at 70°C for 48 hours. The product was isolated and subsequently washed with ethyl acetate several times. Finally, the product was rotovaped to obtain 1-hexyl-3-

methylimidazolium chloride ([HMIm][Cl]), a light yellow highly viscous liquid. [HMIm][Cl] and [Li][NTf_2] were dissolved in water at a 1:1.1 mole ratio and stirred overnight to facilitate ion exchange. The product was then washed with water to remove lithium chloride (LiCl) byproduct and then lyophilized to obtain [HMIm][NTf_2] as a pale yellow, less viscous liquid.

3.2.4 Preparation of Stock Solutions

Stock solutions of [HMIm][NTf_2] (1 mg mL^{-1}) and PMMA (0.5 mg mL^{-1}) were prepared in DCM using 20 mL borosilicate glass scintillation vials. Chemical structures are shown in Scheme B1.

3.2.5 Preparation of Sensing Films

All composite thin films utilized in these studies were prepared using an electrospray technique. Each film was coated onto a clean quartz crystal resonator (QCR) using the same coating parameters, specifically, 1) voltage of 2.9 V, 2) current of 3 A, 3) flow rate of 100 μL/min and 4) working distance of 7 cm. The working distance is the distance between the nozzle and QCR surface. Variations in coating thicknesses were achieved solely by changing the electrospray time period.

3.2.6 Film Characterization

Films were imaged using a JEOL JSM-6390 Scanning Electron Microscope (SEM) in high vacuum mode. Energy Dispersive X-ray Spectroscopy (EDS) was performed using an EDAX APPOLLO X instrument.

3.2.7 QCM-D Data Acquisition

The present study was performed on a flow type system, as depicted in supporting information (Scheme B2). This system consists primarily of the computer interface, QCM-D, two independent gas flow channels, i.e. one channel for sample vapors and another channel for carrier gas, in combination with their respective mass flow controllers. Prior to data acquisition, the system was purged with ultrapure argon to

achieve a stable frequency and dissipation baseline. Chemical vapors were introduced via bubbling of argon gas through the sample reservoir in order to generate a sample assumed to be at saturated vapor pressure. Sample flow is diluted as the sample channel and carrier channel merge, thus yielding percentages of the respective saturated vapor pressure (SVP) represented here in terms of partial pressure, p_a/p_0 = 0.2, 0.3, 0.4. Digital mass flow controllers were used to control flow rate for each channel, while the total flow rate was adjusted to 100 sccm. Both channels are mixed over a 1 m length of tubing and vapors are passed over the QCM sensor crystal within the flow module. Flow module temperature was precisely regulated at 22 °C. Sample vapors were removed by purging the system with ultrapure argon until recovery of the baseline.

3.2.8 Data Analysis

Predictive models were developed independently using each of the three parameters tested, i.e. Δf alone, ΔD alone, or $\frac{\Delta f}{\Delta D}$ values. First, principal component analysis (PCA) was performed in order to reduce the dimensionality of the original data set. The resultant principal components were used as input variables to discriminant analysis (DA) in order to quantitatively distinguish among and specifically identify the various test analytes. Input variables for each DA corresponded to the number of PCs required to constitute 99% of the variability in the original data set. A cross validation method was used to estimate classification error rates for each model.

3.3 Results and Discussion

3.3.1 Preparation and Characterization of Sensing Films

Composite films were deposited onto the QCR surface using an electrospray. These films were then imaged using SEM and EDS. Representative micrographs for two different films, corresponding to a thin and thick coating, are shown in Figure B1. Based

on observation of these SEM images, it is evident that the films are heterogeneous and comprise isolated islands/droplets of varying sizes. SEM images further show that the surface coverage increases with coating time. These EDS images were acquired to obtain elemental compositions of the films. Upon close examination of each isolated mass, two distinct regions were observed, a circular central portion and an irregularly shaped peripheral region. It can be discerned that the central circular portion in each case is primarily ionic liquid and the peripheral region is primarily polymer by comparison of the SEM images and EDS composition analyses. This inference is supported by the high relative intensities of ionic liquid constituent elements in the circular region and the high polymer constituents in the peripheral region. I therefore concluded that the coating is not only spatially heterogeneous, but also compositionally heterogeneous.

3.3.2 Examination of the Effect of Film Thickness on Gas-sensing Response of Ionic Liquid-Polymer Composites

In order to examine whether sensor response for composite-based sensors exhibits similar thickness dependencies to those coated with pure ionic liquid, (as reported previously[26]), several sensors employing varying film thicknesses were investigated. Three QCRs were coated with a binary blend of [HMIm][NTf_2]-PMMA to acquire three different film thicknesses with corresponding frequency change of ~ -2500 Hz, ~ -3,500 Hz, and ~ -16000 Hz, respectively. This change in frequency represents the 1^{st} harmonic change in frequency between the coated and uncoated QCR and corresponds to different film thicknesses. It should be noted that this material is one of many possible combinations of ionic liquid and polymer, and in this regard, other specifically tailored composites could be employed to enhance sensitivity if required for a particular application. However, a major advantage of this approach is that judicious selection of the ionic liquid was not required as is typically the case with QCM sensor arrays. Furthermore, employing ionic liquids with pronounced chemical affinities is likely to

deteriorate molecular weight approximation. Herein, I seek to demonstrate the simplicity of this method through proof of concept. Each sensor was exposed to various alcohol vapors at three different concentrations (p_a/p_0 = 0.2, 0.3, 0.4 where p_a/p_0 = 0.2 corresponds to approximately 100 ppm for the least volatile analyte, hexanol, and 500 ppm for the most volatile analyte methanol) and responses with respect to each parameter (Δf, ΔD, and $\frac{\Delta f}{\Delta D}$) were measured in triplicate. Sensor response with regard to each parameter is depicted in Figure 3.1. Each sensor exhibited a stable baseline and responses were found to be stable, reproducible, and reversible as depicted in Figure B2. In agreement with theory, both positive and negative responses are observed.[40] Moreover, response pattern was observed to change with alteration in film thickness as shown in Figure 3.1. Such thickness dependent responses suggest that ionic liquid-polymer composites are suitable for fabrication of VSAs. Furthermore, based on responses obtained from these experiments, Δf and ΔD, as conventionally used parameters seem most suitable for discrimination of the closely related set of alcohols including positional isomers, as compared to $\frac{\Delta f}{\Delta D}$. This result is truly logical, as the ratio of $\frac{\Delta f}{\Delta D}$ responses for composite materials is known to correlate with molecular weight of pure vapor phase analytes.[15, 16] As a result, isomers should exhibit similar response for the parameter $\frac{\Delta f}{\Delta D}$, as depicted in Figure 3.1. While molecular weight approximation using the $\frac{\Delta f}{\Delta D}$ parameter is feasible, discrimination of isomers for such systems is problematic, and thus necessitates a different strategy. In this regard, the presented VSA technique is particularly promising since it is amenable to discrimination using approriate parameters (Δf and ΔD), while simultaneously facilitating molecular weight approximation using data obtained from a single collection step.

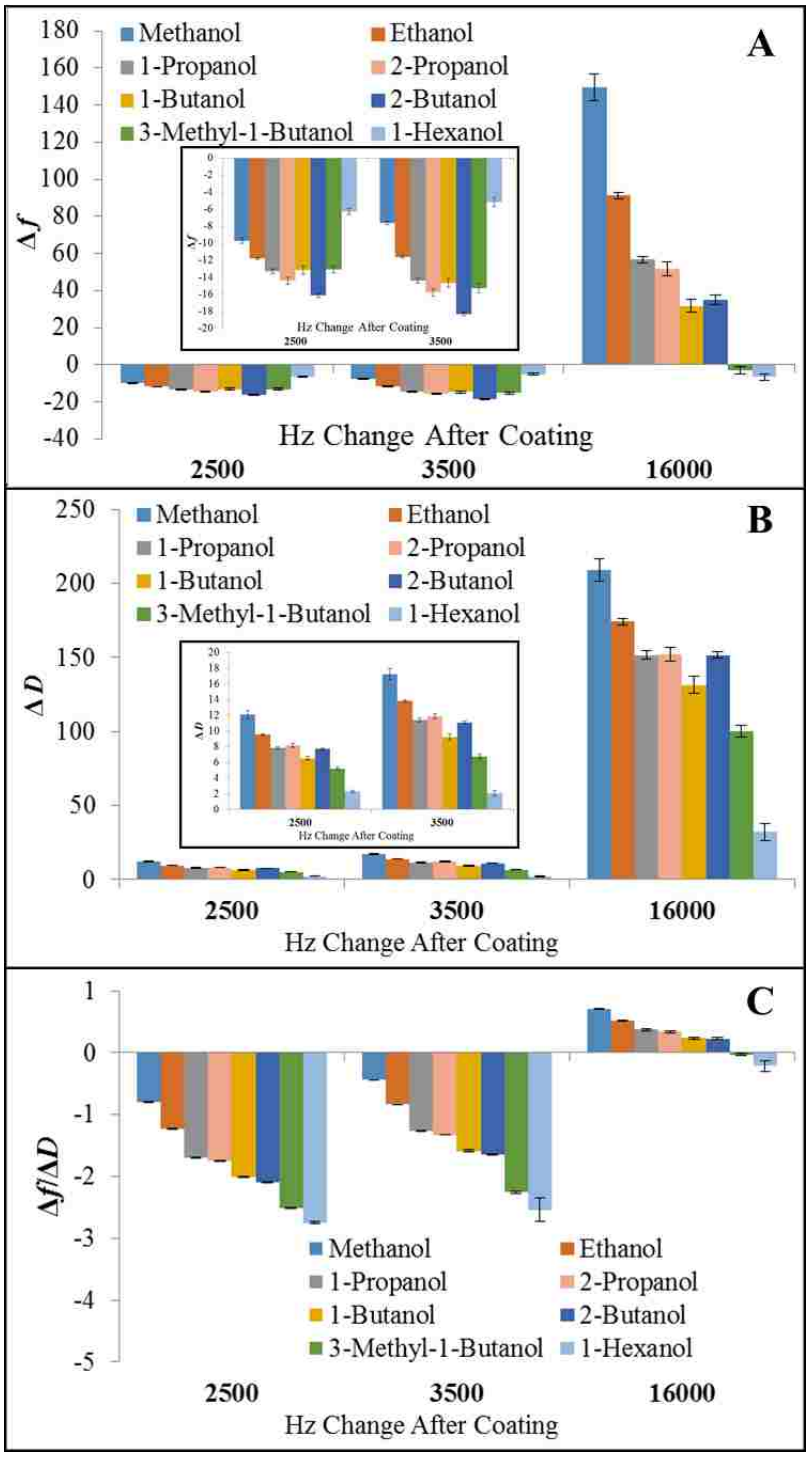

Figure 3.1 Sensor response at fundamental frequency (1st harmonic) across multiple film thicknesses at pa/p0=0.2. A) Change in frequency B) Change in dissipation C) Change in frequency/Change in dissipation. Insets depict sensor response at 2500 Hz and 3500 Hz. Error bars represent three replicate measurements.

3.3.3 Fabrication and Evaluation of a Virtual Sensor Array for Discrimination and Molecular Weight Approximation

In order to fabricate viable VSAs, the previously coated QCRs corresponding to ~ -2500 Hz, and ~ -3,500 Hz were employed. These QCRs were selected because the respective films were of suitable thickness to obtain multiple harmonics with the thinnest film (~ -2500 Hz), exhibiting five harmonics and a film of intermediate thickness (~ -3500 Hz) exhibiting four harmonics. This corresponds to 5 and 4 virtual sensors respectively. The thickest film (~ -16000 Hz) exhibited only one harmonic and thus was not suitable for fabrication of virtual sensor arrays. Each QCR was installed into the QCM-D and exposed to a set of alcohols and isomers at varying concentrations (p_a/p_0 = 0.2, 0.3, 0.4). By use of this instrumentation, it is possible to measure the resonance frequency and dissipation for up to seven different harmonics (odd harmonics from 1st through 13th). The frequency and dissipation at a particular harmonic are simultaneously measured, while different harmonics are successively probed within a range of milliseconds.[43] In this manner, multiple harmonic data was collected for each of the QCRs, effectively creating two separate virtual sensor arrays. Although responses for ~ -2500 Hz, and ~ -3,500 Hz based sensors were similar in sensitivity, ~ -2500 Hz exhibited more harmonics or virtual sensors. Thus, only the ~ -2500 Hz based VSA was selected for further studies. For clarity, Figure 3.2 depicts the VSA response with respect to the parameters Δf, and ΔD at a single concentration p_a/p_0= 0.2 The parameter $\frac{\Delta f}{\Delta D}$ is excluded for discriminatory purposes since molecular weight dependencies would make this parameter ineffectual (Figure B3). As seen with pure ionic liquids,[26] responses vary across harmonics, i.e. each virtual sensor yields a quasi-independent response. Responses were found to be stable, reversible, and reproducible across all harmonics. (Figure B2) When taken in aggregate, the patterns for these closely related analytes show slight to extreme

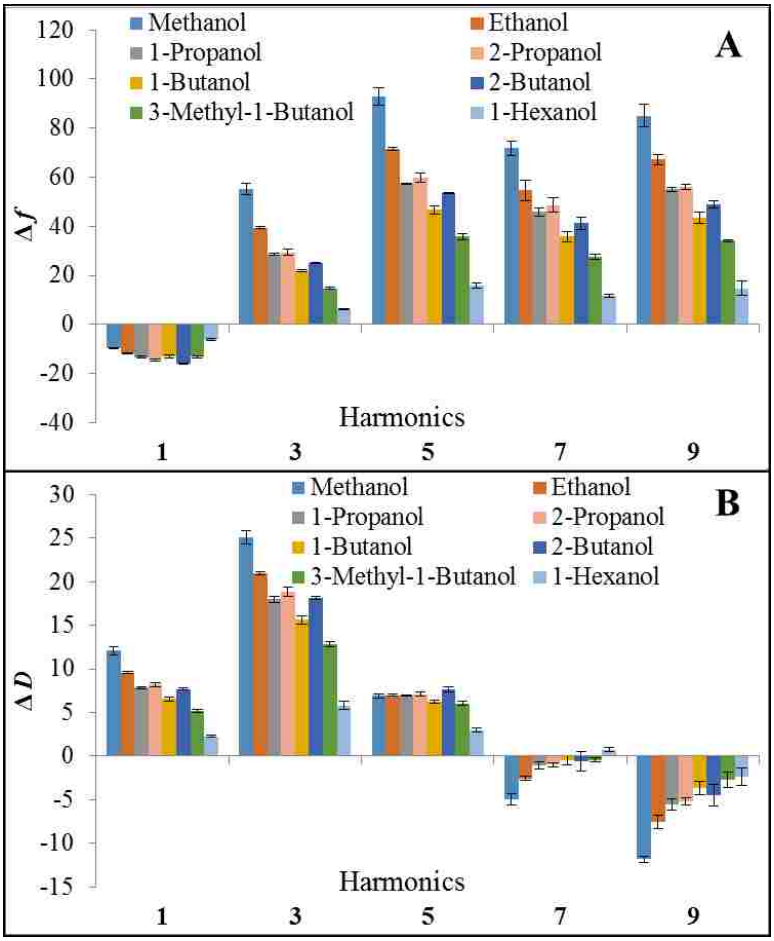

Figure 3.2 Sensor response patterns at different harmonics for each alcohol with respect to the parameters A) Δf and B) ΔD which constitute a virtual sensor array. The vapor partial pressure for all analytes is fixed at p_a/p_0 =0.2. Error bars represent the standard deviations of three replicate measurements.

variations depending on harmonic and measured parameter. Each pattern is noted to exhibit cross reactive elements and is analyte specific, satisfying two requirements for effective use of sensor arrays. More importantly, isomers yield unique response patterns for each parameter tested, which demonstrates the ability of the VSA to distinguish these closely related analytes. Moreover, VSA pattern similarity, in the case of resonance frequency for the set of alcohols, is consistent with the pattern similarity presented for arrays based on chemical affinity.[14] I note that resonance frequency and dissipation vary in different ways with increasing harmonic (thickness) which is in full agreement with and

well supported by data in the literature.[40] Overall, these results seem promising for discrimination of set of closely related alcohols.

3.3.4 Evaluation of a Virtual Sensor Array for Discrimination of Alcohols and Isomers

To assess the discriminatory power of the developed VSA, two statistical approaches were employed. In this regard, principal component analysis (PCA), allows a qualitative assessment of discriminatory power via the use of score plots. In order to quantitate discrimination power, the second approach, discriminant analysis, uses the resultant principal components as inputs for classification of analytes using a cross validation method. Figure 3.3 contains quadratic discriminant analysis (QDA) canonical plots analyzed with respect to the parameters Δf, and ΔD across three concentrations (pa/p0 = 0.2, 0.3, 0.4). In each analysis, three replicate measurements for each analyte at each concentration were considered for a total of 72 measurements. This data set was baseline shifted to account for positive and negative responses and normalized to account for concentration related magnitude increases. When examining these plots, good discriminatory capability is typically signified by spatial separation of different analytes and good clustering between replicate measurements of the same analyte. In this regard, the plot corresponding to the parameter Δf, should represent superior discrimination as compared to the parameter ΔD. In fact, accuracies of 100% and 97.3% were achieved for the parameters Δf, and ΔD respectively. For the parameter of ΔD, with slightly diminished identification accuracy, two samples of 1-propanol were confused for 2-propanol. Overall, each parameter is highly successful in discriminating a set of alcohols and isomers. In order to approximate molecular weight of the vapor phase analytes, the normalized Δf and the normalized ΔD data from the previous analysis step were used to calculate the $\frac{\Delta f}{\Delta D}$ ratio. From the Sauerbrey equation, Δf is proportional to

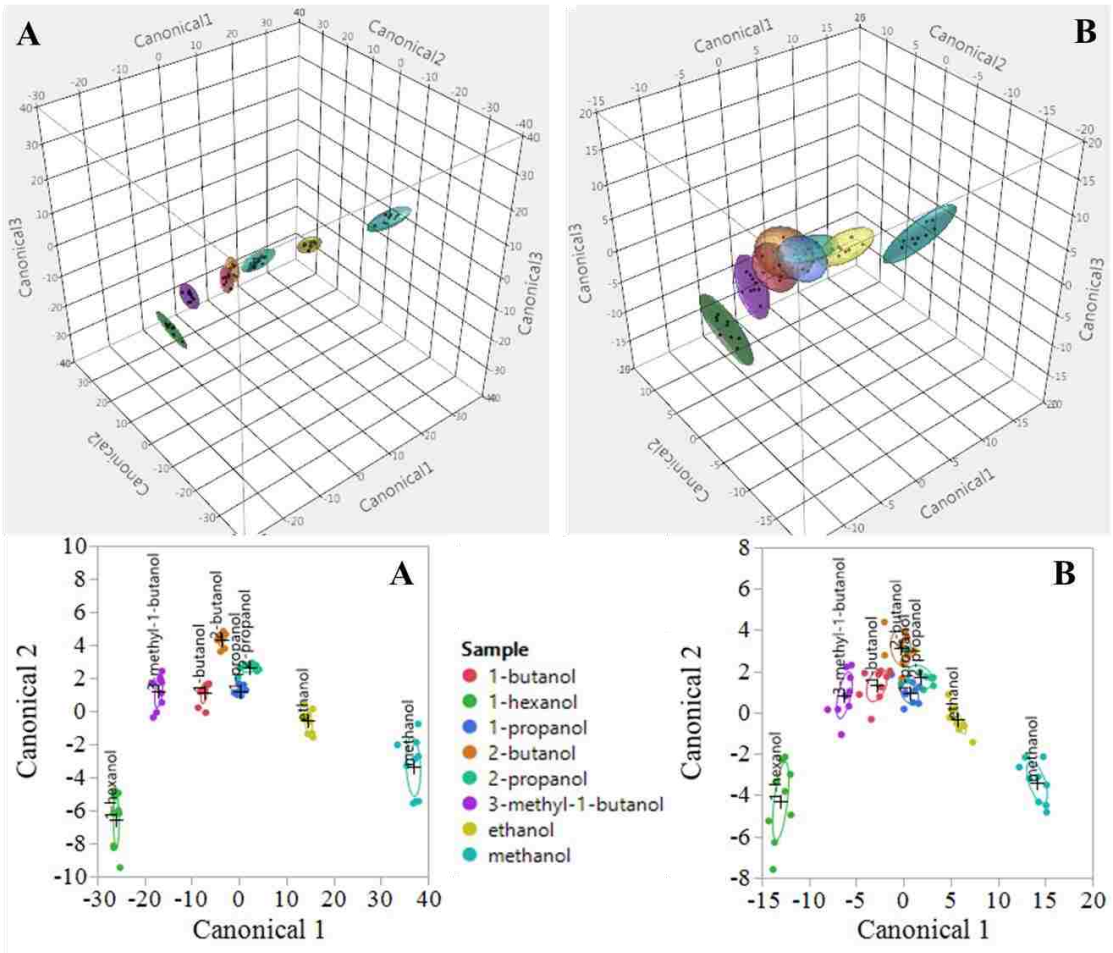

Figure 3.3 QDA canonical plots for a set of alcohols, with respect to parameters A) Δ*f* and B) Δ*D*. Plots consider either data set (Δ*f,* or Δ*D* values for each analyte measured across three concentrations (p_a/p_0 = 0.2, 0.3, 0.4) in triplicate. Thus 9 measurements per analyte and 72 total measurements) normalized for concentration.

mass change on the surface, while we have found that for ionic-liquid polymer blends, with low to moderate vapor sorption conditions, Δ*D* is proportional to moles adsorbed to the surface. The $\frac{\Delta f}{\Delta D}$ data were plotted against molecular weight for all analytes, which is depicted in Figure 3.4. These plots consist of three replicate measurements at 3 concentrations (pa/p0 = 0.2, 0.3, 0.4) for each analyte. (72 total measurements). A reasonably linear correlation between sensor response and molecular weight is achieved for all analytes with an R-squared value of 0.976. As expected, isomers exhibit close overlap since the molecular weight is identical. Notably, some spread in the

individual sample clusters is observed due to varying concentration. While the overall molecular weight approximation for the 72 samples is reasonably good (R^2=0.976), it is possible to further enhance correlation for these approximations. Towards this aim, another analysis was performed based on the raw data without normalization and baseline shifting. In this way, it is possible to determine not only the analyte identity, but also the concentration of the analyte. This type of analysis would be highly desirous for determination of unknowns, where not only the identity but also the concentration of the unknown is important. Figure 3.5 depicts PCA score plots across multiple concentrations (pa/p0 = 0.2, 0.3, 0.4) with respect to parameters Δf, and ΔD. PCA score plots are presented here for ease of visual interpretation, while the corresponding linear

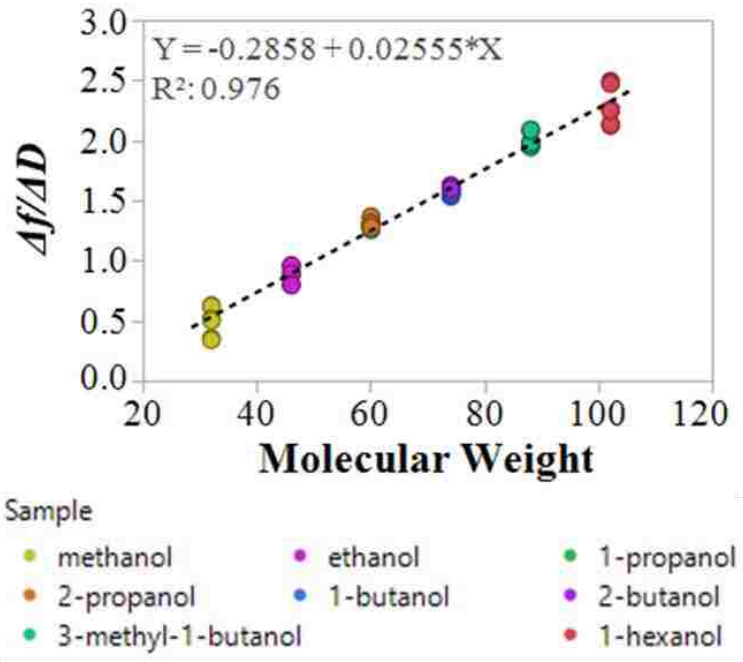

Figure 3.4 Molecular weight approximation of alcohols using the $\frac{\Delta f}{\Delta D}$ values calculated from the normalized data set.($\frac{\Delta f}{\Delta D}$ values calculated using normalized Δf divided by normalized ΔD for each measurement) Nine measurements represented by dots (each alcohol measured across three concentrations (p_a/p_0 = 0.2, 0.3, 0.4) in triplicate**)** are depicted for each alcohol at for a total of 72 measurements.

discriminant analysis (LDA) canonical plots are presented in Figure B4. LDA is used in this analysis as opposed to QDA in deference to the low sample size for each analyte. Examination of these plots shows that Δf exhibits good clustering and spatial separation between each analyte, while ΔD exhibits fair clustering and some spatial separation. Typically, increasing concentration has a linear effect on sensor response for individual analytes and this is depicted by the arrows. Qualitatively the parameter Δf appears to yield better discriminatory power.Moreover, the parameter Δf exhibits superior quantitative discriminatory power as compared to the parameter ΔD, with classification accuracies of 100% and 98.7%, respectively. Overall Δf still proves to be the best parameter for discrimination of this set of alcohols and isomers, whether or not identifying concentration is a concern. Once the identity of an analyte and its concentration has been determined, it is then possible to fit the data to a corresponding concentration specific molecular weight approximation. Figure 3.6 depicts plots of $\frac{\Delta f}{\Delta D}$ ratio at the first harmonic versus molecular weight at each concentration independently. Again, an excellent correlation between sensor response and molecular weight of analytes is observed. In fact, the linear correlation is enhanced with each plot exhibiting an $R^2 \approx 0.99$ Notably, the slope of the correlation varies gradually depending on concentration, with the lowest concentration exhibiting the highest slope and the highest concentration exhibiting the lowest slope. As a result, superimposition of these plots will exhibit the cluster spreading seen in Figure 3.4. Moreover, for the tested data set, it seems that as concentration increases, so does the quality of the molecular weight correlation due to increased overlap between the isomers. This is attributed to increased concentration overcoming sorption variation due to factors such as volatility and chemical affinity differences. Nonetheless, the presented data deconvolution thoroughly resolves the previous spreading issue and allows for excellent molecular weight

approximation across all concentrations. When taken in aggregate, these presented analyses are extremely promising for discrimination and molecular weight approximation of a set of alcohols and isomers, whether used for determination of analyte identity, concentration, or molecular weight.

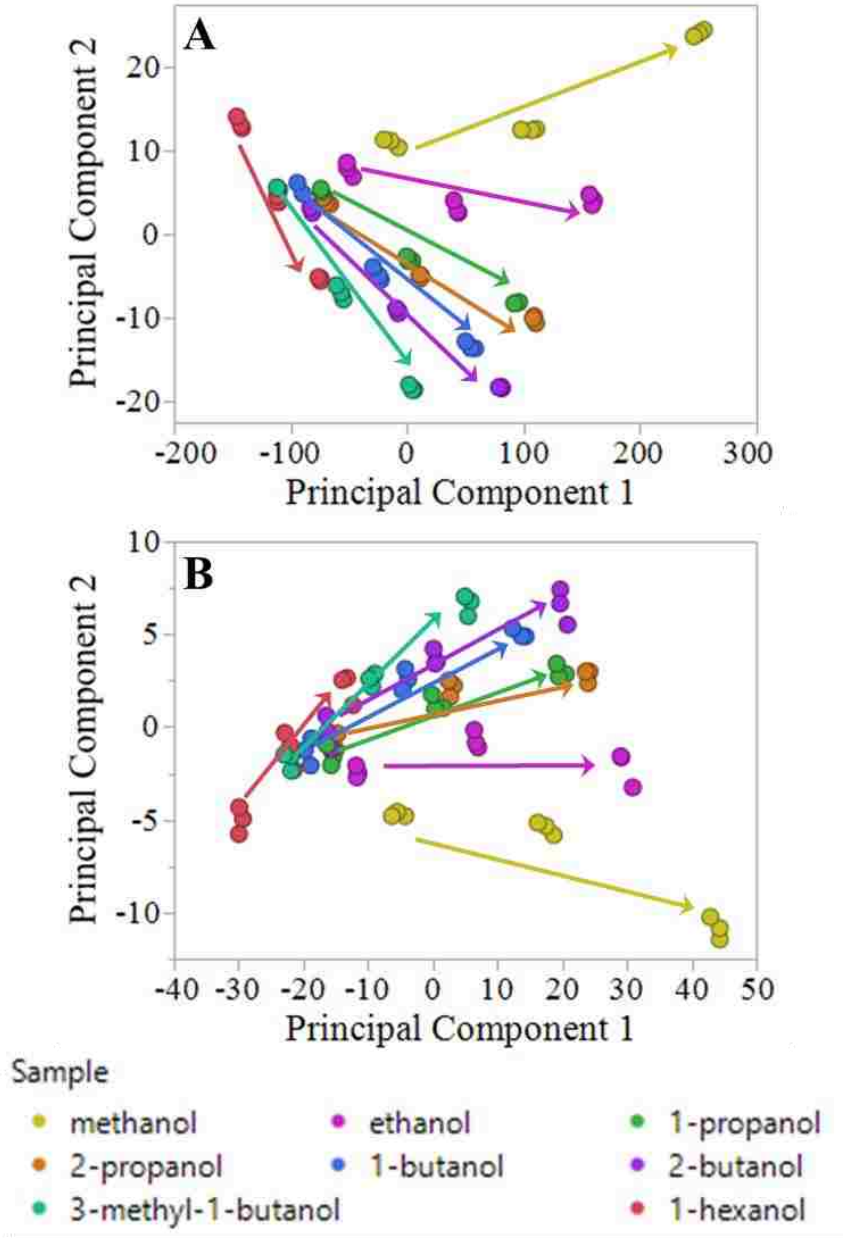

Figure 3.5 PCA score plots for a set of alcohols, measured in triplicate across multiple concentrations (p_a/p_0 =0.2, 0.3, 0.4) with respect to parameters A) Δ*f* and B) Δ*D* Arrows depict direction of increasing concentration.

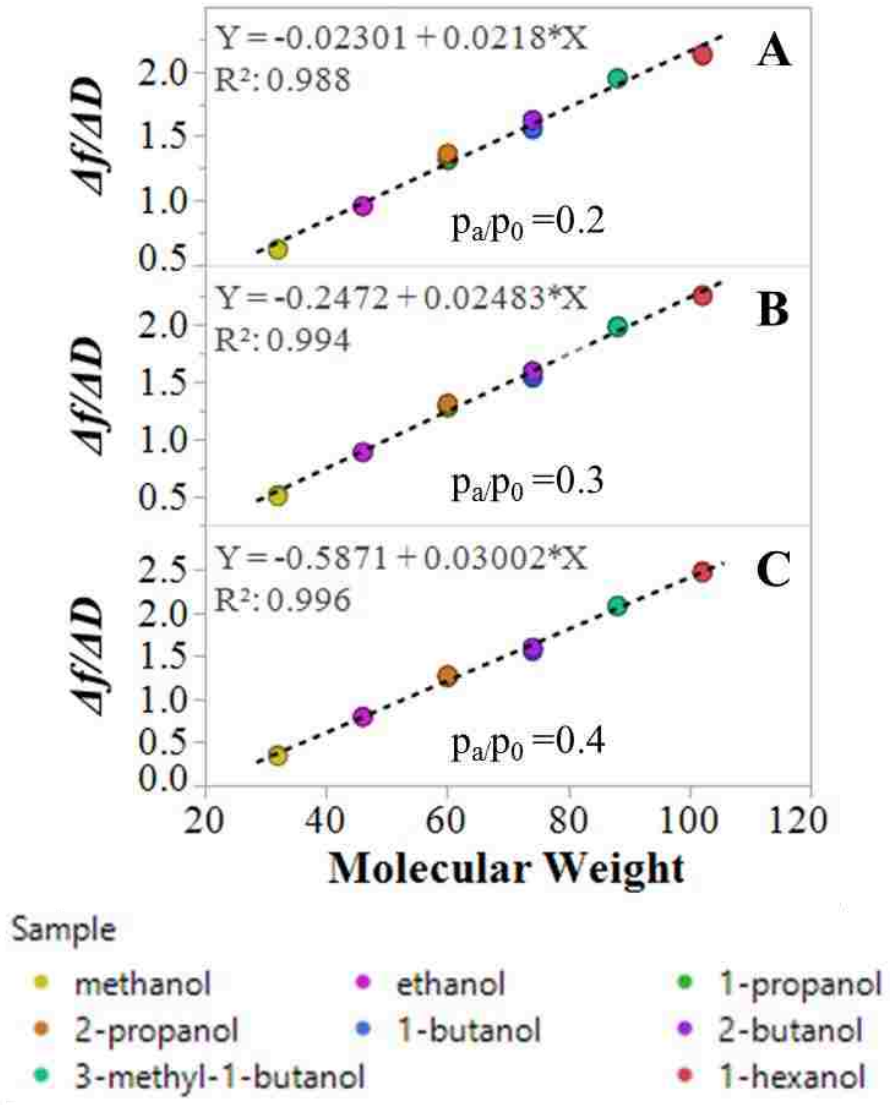

Figure 3.6 Molecular weight approximation of alcohols accounting for variation in concentration. Three replicate measurement dots are depicted for each alcohol at a single concentration for a total of 24 measurements in plot A) p_a/p_0 =0.2, B) p_a/p_0 =0.3, and C) p_a/p_0 =0.4 respectively.

3.4 Conclusion

In conclusion, I have presented a relatively simple method for increasing the diversity of analytical information output of QCM based sensor arrays. As such, I have developed a QCM VSA with two dimensional analysis capability, i.e. identification of analytes, as well as approximation of molecular weights. This is a first for a relatively

simple measurement technique such as QCM-D. In this regard, two types of analyses are presented: 1) identification of analyte and 2) identification of analyte as well as concentration of closely related alcohols. In each instance, excellent accuracy was achieved with the parameter, Δf, providing superior discrimination power. The $\frac{\Delta f}{\Delta D}$ ratio was used for molecular weight approximation and excellent correlations were obtained. In aggregate, the analyses presented herein are extremely promising for discrimination and molecular weight approximation of organic vapors, whether determining analyte identity, concentration, or molecular weight. Moreover this method seems promising for discrimination of vapor phase isomers. Further investigations are under way to ascertain the full potential of this approach.

3.5 References

1. Ayad, M. M. & Torad, N. L. Alcohol vapours sensor based on thin polyaniline salt film and quartz crystal microbalance. Talanta 78, 1280–1285 (2009).

2. Karousos, N. G., Aouabdi, S., Way, A. S. & Reddy, S. M. Quartz crystal microbalance determination of organophosphorus and carbamate pesticides. Anal. Chim. Acta 469, 189–196 (2002).

3. Yakovleva, M. E., Moran, A. P., Safina, G. R., Wadström, T. & Danielsson, B. Lectin typing of Campylobacter jejuni using a novel quartz crystal microbalance technique. Anal. Chim. Acta 694, 1–5 (2011).

4. Bello, A. et al. Potentialities of a modified QCM sensor for the detection of analytes interacting via H-bonding and application to the determination of ethanol in bread. Sens. Actuators B Chem. 125, 321–325 (2007).

5. Capone, S. et al. Monitoring of rancidity of milk by means of an electronic nose and a dynamic PCA analysis. Sens. Actuators B Chem. 78, 174–179 (2001).

6. Buratti, S., Benedetti, S., Scampicchio, M. & Pangerod, E. C. Characterization and classification of Italian Barbera wines by using an electronic nose and an amperometric electronic tongue. Anal. Chim. Acta 525, 133–139 (2004).

7. Ponrathnam, T., Cho, J., Kurup, P., Nagarajan, R. & Kumar, J. Investigation of QCM Sensors with Azobenzene Functionalized Coatings for the Detection of Nitroaromatics. J. Macromol. Sci. Part A 48, 1031–1037 (2011).

8. Wang, F., Gu, H. & Swager, T. M. Carbon Nanotube/Polythiophene Chemiresistive Sensors for Chemical Warfare Agents. J. Am. Chem. Soc. 130, 5392–5393 (2008).

9. Rehman, A. et al. Differential Solute Gas Response in Ionic-Liquid-Based QCM Arrays: Elucidating Design Factors Responsible for Discriminative Explosive Gas Sensing. Anal. Chem. 83, 7823–7833 (2011).

10. Liang, C., Yuan, C.-Y., Warmack, R. J., Barnes, C. E. & Dai, S. Ionic Liquids: A New Class of Sensing Materials for Detection of Organic Vapors Based on the Use of a Quartz Crystal Microbalance. Anal. Chem. 74, 2172–2176 (2002).

11. Goubaidoulline, I., Vidrich, G. & Johannsmann, D. Organic Vapor Sensing with Ionic Liquids Entrapped in Alumina Nanopores on Quartz Crystal Resonators. Anal. Chem. 77, 615–619 (2005).

12. Jin, X., Yu, L., Garcia, D., Ren, R. X. & Zeng, X. Ionic Liquid High-Temperature Gas Sensor Array. Anal. Chem. 78, 6980–6989 (2006).

13. Xu, X. et al. Ionic liquids used as QCM coating materials for the detection of alcohols. Sens. Actuators B Chem. 134, 258–265 (2008).

14. Toniolo, R. et al. Room Temperature Ionic Liquids As Useful Overlayers for Estimating Food Quality from Their Odor Analysis by Quartz Crystal Microbalance Measurements. Anal. Chem. 85, 7241–7247 (2013).

15. Regmi, B. P. et al. A novel composite film for detection and molecular weight determination of organic vapors. J. Mater. Chem. 22, 13732 (2012).

16. Regmi, B. P. et al. Molecular weight sensing properties of ionic liquid-polymer composite films: theory and experiment. J Mater Chem C 2, 4867–4878 (2014).

17. Bachar, N. et al. Sensor Arrays Based on Polycyclic Aromatic Hydrocarbons: Chemiresistors versus Quartz-Crystal Microbalance. ACS Appl. Mater. Interfaces 5, 11641–11653 (2013).

18. Umali, A. P. & Anslyn, E. V. A general approach to differential sensing using synthetic molecular receptors. Curr. Opin. Chem. Biol. 14, 685–692 (2010).

19. Albert, K. J. et al. Cross-Reactive Chemical Sensor Arrays. Chem. Rev. 100, 2595–2626 (2000).

20. Suslick, B. A., Feng, L. & Suslick, K. S. Discrimination of Complex Mixtures by a Colorimetric Sensor Array: Coffee Aromas. Anal. Chem. 82, 2067–2073 (2010).

21. Hierlemann, A., Weimar, U., Kraus, G., Schweizer-Berberich, M. & Göpel, W. Polymer-based sensor arrays and multicomponent analysis for the detection of hazardous oragnic vapours in the environment. Sens. Actuators B Chem. 26, 126–134 (1995).

22. Janzen, M. C., Ponder, J. B., Bailey, D. P., Ingison, C. K. & Suslick, K. S. Colorimetric Sensor Arrays for Volatile Organic Compounds. Anal. Chem. 78, 3591–3600 (2006).

23. Galpothdeniya, W. I. S. et al. Ionic liquid-based optoelectronic sensor arrays for chemical detection. RSC Adv 4, 7225–7234 (2014).

24. Koo, C.-K., Samain, F., Dai, N. & Kool, E. T. DNA polyfluorophores as highly diverse chemosensors of toxic gases. Chem. Sci. 2, 1910 (2011).

25. Kwon, H., Samain, F. & Kool, E. T. Fluorescent DNAs printed on paper: sensing food spoilage and ripening in the vapor phase. Chem. Sci. 3, 2542 (2012).

26. Speller, N. C. et al. Rational Design of QCM-D Virtual Sensor Arrays Based on Film Thickness, Viscoelasticity, and Harmonics for Vapor Discrimination. Anal. Chem. 87, 5156–5166 (2015).

27. Granéli, A., Edvardsson, M. & Höök, F. DNA-Based Formation of a Supported, Three-Dimensional Lipid Vesicle Matrix Probed by QCM-D and SPR. ChemPhysChem 5, 729–733 (2004).

28. Höök, F. & Kasemo, B. in Piezoelectric Sensors (eds. Steinem, C. & Janshoff, A.) 5, 425–447 (Springer Berlin Heidelberg, 2007).

29. Lubarsky, G. V., Davidson, M. R. & Bradley, R. H. Hydration–dehydration of adsorbed protein films studied by AFM and QCM-D. Biosens. Bioelectron. 22, 1275–1281 (2007).

30. Patel, A. R., Kerwin, B. A. & Kanapuram, S. R. Viscoelastic characterization of high concentration antibody formulations using quartz crystal microbalance with dissipation monitoring. J. Pharm. Sci. 98, 3108–3116 (2009).

31. Muller, J. B. A., Smith, C. E., Newton, M. I. & Percival, C. J. Evaluation of coated QCM for the detection of atmospheric ozone. The Analyst 136, 2963 (2011).

32. Reimann, P. & Schütze, A. in Gas Sensing Fundamentals (eds. Kohl, C.-D. & Wagner, T.) 15, 67–107 (Springer Berlin Heidelberg, 2013).

33. Vergara, A. et al. Chemical gas sensor drift compensation using classifier ensembles. Sens. Actuators B Chem. 166–167, 320–329 (2012).

34. Beckers, N. A., Taschuk, M. T. & Brett, M. J. Selective room temperature nanostructured thin film alcohol sensor as a virtual sensor array. Sens. Actuators B Chem. 176, 1096–1102 (2013).

35. Ziyatdinov, A. & Perera-Lluna, A. Data Simulation in Machine Olfaction with the R Package Chemosensors. PLoS ONE 9, e88839 (2014).

36. Xing Chen et al. A Non-invasive Detection of Lung Cancer Combined Virtual Gas Sensors Array with Imaging Recognition Technique. in 5873–5876 (IEEE, 2005). doi:10.1109/IEMBS.2005.1615826

37. Yuan-Yuan, L. et al. QCM Coated with Self-assembled Cystine-bearing 1,3-Bridged Calix[4]arenes for Recognizing Gas-phase Butylamines. Chin. J. Chem. 23, 571–575 (2005).

38. Latif, U., Rohrer, A., Lieberzeit, P. A. & Dickert, F. L. QCM gas phase detection with ceramic materials—VOCs and oil vapors. Anal. Bioanal. Chem. 400, 2457–2462 (2011).

39. Vogt, B. D., Lin, E. K., Wu, W. & White, C. C. Effect of Film Thickness on the Validity of the Sauerbrey Equation for Hydrated Polyelectrolyte Films. J. Phys. Chem. B 108, 12685–12690 (2004).

40. McHale, G., Lücklum, R., Newton, M. I. & Cowen, J. A. Influence of viscoelasticity and interfacial slip on acoustic wave sensors. J. Appl. Phys. 88, 7304 (2000).

41. Berton, P., Regmi, B. P., Spivak, D. A. & Warner, I. M. Ionic liquid-based dispersive microextraction of nitrotoluenes in water samples. Microchim. Acta 181, 1191–1198 (2014).

42. Huddleston, J. G. et al. Characterization and comparison of hydrophilic and hydrophobic room temperature ionic liquids incorporating the imidazolium cation. Green Chem. 3, 156–164 (2001).

43. Dixon, M. C. Quartz Crystal Microbalance with Dissipation Monitoring: Enabling Real-Time Characterization of Biological Materials and Their Interactions. J. Biomol. Tech. JBT 19, 151–158 (2008).

CHAPTER 4. ASSESSMENT OF QCM ARRAY SCHEMES FOR MIXTURE IDENTIFICATION: CITRUS SCENTED ODORS

4.1 Introduction

One approach to discriminating complex mixtures of volatile organic compounds (VOCs) that is gaining popularity is use of cross-reactive sensor arrays (CRSAs).[1-6] The advantage of CRSAs lies in their use to identify and discriminate complex samples, without the need for identification of individual VOCs. In fact, this operating principle is similar to that of using the mammalian nose, which is held as the gold standard. As a result, this approach has been applied to fabrication of gas sensing arrays using various combinations of transducers and recognition elements.[7-9] Among possible combinations, quartz-crystal microbalance (QCM) transducers, coupled with ionic liquids as recognition elements, have proven increasingly attractive.[3,5,10-13] As a transducer, the QCM is sensitive, offers potential for miniaturization,[14] and is amenable to fabrication of sensor arrays. Moreover, ionic liquids (ILs), as recognition elements, have been demonstrated to be promising sensing materials for detection and discrimination of a wide range of organic vapors,[3,11,14-17] ILs, which are defined as organic salts with melting points below 100 °C, are highly tunable, possess low vapor pressure, and allow reversible capture of organic vapors. ILs have also been shown to possess viscoelastic behavior,[16,18,19,26] a property which plays a critical role in the present studies. Notably, IL based QCM sensor arrays have great potential to satisfy the requirements of simple, rapid, reproducible and reliable systems for discrimination of complex mixtures.[3,11,20,21]

By convention, multisensor arrays (MSA) based on chemical affinity have been employed for applications using QCM based CRSAs. In such schemes, each sensor contains a unique cross-reactive recognition element. Upon exposure to complex mixtures, differential sensor responses are exhibited and subsequently used to generate analyte specific patterns. Such patterns are then analyzed using statistical methods

(e.g., principal component analysis (PCA), discriminant analysis (DA), artificial neural networks (ANN), cluster analysis (CA), etc.) to predict the utility of the array for identification/ discrimination. However, I have recently introduced an alternative strategy for a virtual sensor array (VSA) based on a single sensor, viscoelasticity, film thickness, and harmonics that exhibits significant advantages as compared to MSAs.[10] In this regard, cost, complexity, and problems associated with sensor drift are minimized in VSAs. However, chemical affinity is lost as a discriminatory factor. Naturally, questions arise as to whether these two schemes are 1) comparable for a given application and 2) can be used as complementary approaches.

Herein, I detail a comparative study between QCM array sensing schemes for complex mixture identification. Hence, the utility of MSA and VSA schemes for citrus odor recognition is directly compared. Furthermore, I introduce, for the first time, a complementary approach that incorporates the two sensing schemes, i.e. use of chemical affinity and viscoelastic discriminatory factors, to rapidly enhance the information density of QCM based sensor arrays. In this regard, we introduce a QCM based Virtual multisensor array (V-MSA) for complex mixture discrimination. Thus, I ultimately compare the performance of MSAs, VSAs, and V-MSAs, using statistical analysis to reveal the best array strategy for complex mixture identification. As a proof of concept, a set of citrus odors, represented by aroma profiles of five essential oils, were chosen as representative complex mixtures. Essential oils are produced by plants, and are responsible for the characteristic flavor and odors of particular species. As a result, these oils are important stocks for the food, pharmaceutical, and perfume industries.[22,23] Odors emitted from essential oils are highly complex mixtures of VOCs. In fact, a common scent, such as one derived from an orange essential oil may contain more than 300 VOCs although only a small fraction of these are truly responsible for the scent

commonly identify as orange.[23] Hence, odors are challenging targets for accurate identification and discrimination using conventional approaches.[2]

4.2 Approach

4.2.1 Array Fabrication

In this study one MSA, four VSAs and eleven V-MSAs were fabricated using ILs immobilized as thin films onto QCM-D transducers. Ionic liquids were chosen as promising chemosensitive materials for odor recognition based on work in the field by Nakamoto and colleagues, who have demonstrated that lipids have favorable aroma/ odor sensing properties.[22,24-26] Since lipids are composed of a polar head group(s) and an aliphatic tail(s), four ionic liquids, 1-nonyl-3-methylimidazolium thiocyanate ([C_9MIm][SCN]), 1-nonyl-3-methylimidazolium bromide ([C_9MIm][Br]), 1-octenyl-3-pyridinium bromide ([C_8Pyr][Br]), and 1-undecenyl-3-pyridinium bromide ([C_{11}Pyr][Br]) were chosen for odor sensing since each IL contains a polar head group represented by the charged imidazolium/pyridinium group and anion and aliphatic tails represented by varying length carbon side chains (saturated and unsaturated). Structures of these four ILs are displayed in Scheme 1. Each of the four sensors acquired by coating four quartz crystal using these different ionic liquid, were installed into the instrument simultaneously. Measurements were taken concurrently for each sensor across multiple harmonics to create one master data set. Subsequently, fabrication of each sensor array scheme was accomplished by considering appropriate measurements from the master data set. The MSA comprises four sensors with coatings [C_9MIm][SCN], [C_9MIm][Br], [C_8Pyr][Br], and [C_{11}Pyr][Br] respectively, where only the response at the first harmonic (i.e fundamental frequency) was used for data analysis. This is consistent with the standard operation of QCM MSAs in the literature. Four VSAs were employed using the same sensors from the MSA, only individually. In this regard, measurements across all harmonics for an individual sensor were considered for analysis as performed in a

previous publication.[27] Finally, to test the utility of these two schemes as complementary methods, multiple V-MSAs were fabricated by considering the aggregate of measurements from all four sensors over all harmonics and these data were analyzed. It should be noted that all measurements considered for each array were taken concurrently. Therefore, any variation in identification accuracy is a result of the scheme as tested and not to differing experimental procedure or conditions. For clarity a scheme of each array type is depicted in Figure 4.2.

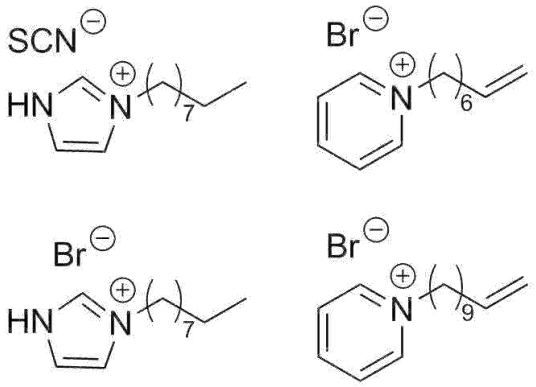

Figure 4.1 Chemical structures of organic salt adlayers**.**

4.2.2 QCM Virtual Sensor Arrays

Development of QCM based virtual sensor arrays has been detailed in a previous publication.[27] For clarification, a brief synopsis is provided here. Briefly, a QCM sensor coated with a viscoelastic material is dynamically operated to obtain analyte specific response patterns, which can be used for identification purposes. Such patterns are obtained by exploiting the effects of film thickness, harmonics, and viscoelasticity on sensor response of the QCM. It is known from the Sauerbrey equation that thin and rigid

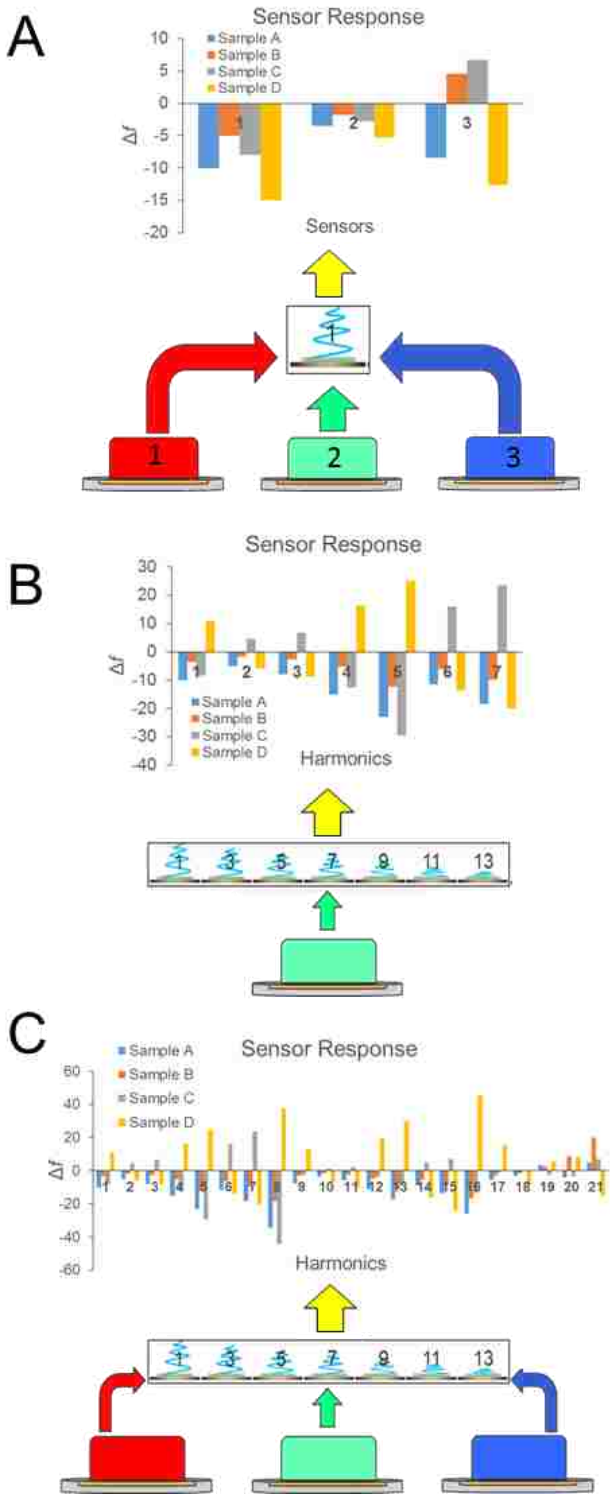

Figure 4.2 QCM array sensing schemes A) MSA B) VSA and C) V-MSA. Where red, green, and blue sensors represent physical sensors. Smaller odd numbered sensors represent harmonics.

films exhibit best Sauerbrey like behavior. However, as film thickness increases, deviations from ideal Sauerbrey behavior occur due to increasing viscoelastic effects on sensor response. It is also known that such deviations can be further enhanced depending on the viscoelastic properties of the coating material to obtain all combinations of positive and negative sensor response. In my previous studies, this relationship was exploited to create sensor arrays by performing measurements across multiple harmonics. This strategy is based on the observation that change in sensor response at different harmonics is due to changes in mass and viscoelastic contributions as a result of perceived variations in film thickness. In fact, measurements of a fixed film thickness at multiple harmonics can be viewed as equivalent to measurements of multiple film thicknesses at a single harmonic. This idea is rationalized using the following equation:

$$\delta = \sqrt{\frac{2\eta}{\rho\omega}} \quad where, \quad \omega = 2\pi f \qquad (4.1)$$

where δ is penetration depth, i.e. the distance at which the amplitude of the wave decreases to 1/e of its value at the surface; η is the viscosity of the coating; ρ is the density of the coating; ω is angular frequency, and *f* is frequency.[10,28,29]

4.2.3 QCM Virtual Multisensor Arrays

Herein, I introduce the first example of a QCM virtual multisensor array scheme. This scheme is based on employing the multisensory array and virtual sensor array schemes in a complementary fashion. Notably, the multisensor array scheme is based on employing multiple sensors, which differ, based on chemical affinity. In contrast, the virtual sensor array scheme is based on dynamic operation of a single sensor, which elicits differential response based on harmonics, film thickness, and viscoelasticity.

Thus, the logical conclusion is that the schemes are not required to be mutually exclusive. In fact, since each scheme employs different discriminatory factors, it should be expected that the combination (V-MSA) should yield more discriminatory information. In this regard, the V-MSA scheme should exhibit enhanced data density, which should result in more accurate analyses than either the MSA or VSA alone.

4.3 Experimental Section

4.3.1 Reagents and Materials

Four ILs, i.e. [C_9MIm][SCN], [C_9MIm][Br], [C_8Pyr][Br] and [C_{11}Pyr][Br], were used to prepare quartz crystal coatings in the present studies and were synthesized using previously documented procedures.[27,30] Foods brand 100% pure essential oils were purchased from Whole Foods Inc, i.e. lemon, lime, orange, lemon eucalyptus, and lemongrass. All oils were used as received without further purification. Dichloromethance was purchased from Macron Fine Chemicals (Center Valley, PA, USA) and used without further purification.

4.3.2 Preparation of Stock Solutions

Stock solutions of [C_9MIm][SCN], [C_9MIm][Br], [C_8Pyr][Br] and [C_{11}Pyr][Br] (1 mg mL-1) were prepared in dichloromethane (DCM) using 20 mL borosilicate glass scintillation vials.

4.3.3 Preparation of Sensing Films

Electrospray was used for deposition of thin films. All films were coated using the same parameters: deposition time of 1.5 min, flowrate of 100 µl/ min, current of 3 Amps, voltage of 2.9 V, and a working distance of 7 cm. After coating, all films were blown with nitrogen and stored in a desiccator. The change in frequency between coated and uncoated crystal was found to be ~ -1000 Hz at the fundamental frequency.

4.3.4 QCM-D Data Acquisition

The flow type system used to perform these experiments consists of two independent gas flow channels i.e., one channel for sample odors and another channel for carrier gas. As a first step in data collection, ultrapure argon is purged through the system to obtain a stable baseline frequency. Odors are introduced via bubbling of argon gas through the sample reservoir, which was filled with the pure essential oil of interest, in order to generate a sample of saturated vapor pressure. As the sample channel and carrier channel merge, the sample flow is diluted yielding percentages of the respective saturated vapor pressure (SVP). (e.g. 10% 50%, 75%, 100% of saturated vapor pressure) The flow rate was controlled by digital mass flow controllers and adjusted to a total flow rate of 100 sccm. After sufficient mixing over the length of the tubing (1m), the vapors are passed over the QCM sensor crystal placed inside a flow module. The chamber temperature was precisely regulated (22°C). Finally, to remove sample vapors, the system was purged with ultrapure argon until recovery of the baseline. A schematic of the experimental system is depicted in Figure C10.

4.3.5 Data Analysis

A single data set was generated from these experiments and used to develop statistical models for assessing the identification accuracies of each of the arrays. In this regard, independent predictive models were developed using frequency change (Δf) response values appropriate for a particular array scheme (VSA, MSA, V-MSA). In order to reduce the dimensionality of the data set, principal component analysis (PCA) was performed. Subsequently, discriminant analysis was performed using PCA indices (accounting for 99% of variance in the original data set) as input variables to quantitatively access the ability of each array for identification of selected odors. In this regard, linear discriminant analysis (LDA) and quadratic discriminant analysis (QDA) using cross-validation were used to obtain classification error rates for all models.

4.4 Results and Discussion

4.4.1 Sensor Response of ILs to Odors

Four QCM sensors coated with [C_9MIm][SCN], [C_9MIm][Br], [C_8Pyr][Br], and [C_{11}Pyr][Br] respectively, were installed into a flow type system. Subsequently all sensors were introduced to a set of five citrus scented odors (lemon, lime, orange, lemon eucalyptus, lemongrass) selected for comparative assessment of complex mixture identification ability. This set consists of chemically distinct and closely related odors generated by essential oils. All sensors were exposed to three different concentrations (10%, 20%, 40% of SVP) of the respective odors for 30s intervals and Δf at each harmonic was measured. Each sensor was found to exhibit stable baseline, and reversible capture. (Figure C1-C9) Moreover, sensor responses were found to be stable and reproducible. Figure 4.3 depicts sensor response for all sensors across multiple harmonics when exposed to each of the five citrus scented odors. As in my previous study,[27] cross-reactive responses to different analytes were obtained by simply changing harmonics of the same sensor. This suggests that each sensor has potential for not only fabrication of MSAs, but also VSA and V-MSAs. As expected, positive and negative shifts in resonant frequency were obtained. Such shifts can be attributed to relative changes in the mass and viscoelastic contributions of the chemosensitive film to sensor response. In this regard, response variability is primarily governed by film viscoelasticity and penetration depth with changing harmonic. These dependencies have been described in previous publication.[27] Overall, the differential sensing patterns obtained for each sensor seem promising for fabrication of sensor arrays.

4.4.2 Evaluation of a Multisensor Array for Odor Recognition

Fabrication of an MSA was performed in the traditional fashion. In this regard, an MSA consisted of all four chemically distinct sensors, specifically [C_9MIm][SCN], [C_9MIm][Br], [C_8Pyr][Br], and [C_{11}Pyr][Br]. Only measurements taken at the fundamental frequency

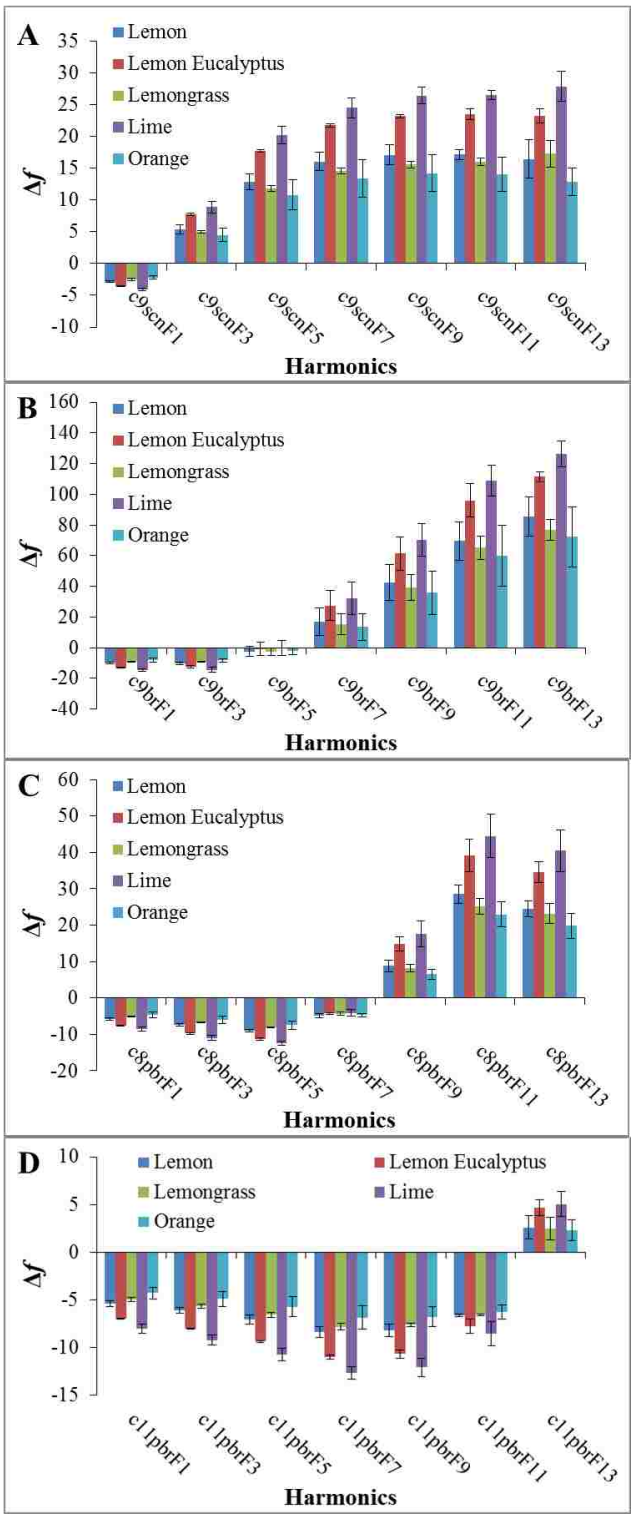

Figure 4.3 Sensor response of citrus type odors at multiple harmonics at 20% of SVP for A) [C_9MIm][SCN], B) [C_9MIm][Br], C) [C_8Pyr][Br], and D) [C_{11}Pyr][Br]. Error bars represents standard deviation for three replicate measurements.

(first harmonic) for each sensor were considered for MSA performance evaluation. As a result, the data matrix consisted of Δ*f* values, where the columns represented each of the chemically distinct sensors and the rows represented each of the odors tested at three concentrations (10%, 20%, and 40% of SVP). Three replicate measurements were considered for each odor, giving a total of 9 measurements per sample.(4 columns x 45 rows) A canonical plot for this MSA is depicted in Figure 4.4, wherein ellipses represent 95% confidence. Qualitatively, high level discrimination is typically represented by good clustering within a sample and spatial separation between samples. Therefore, the high degree of overlap exhibited in this plot suggests less than optimal accuracy. This is quantitatively supported, by classification results using LDA with the cross validation method, where an accuracy of 84.5% was achieved. This corresponds to 7 total misclassifications. As suggested by examination of the plot, two major groups of odor confusion were exhibited. The first group contains 5 instances of confusion between lemon, lemongrass, and orange odors, while the second group consists of 2 instances between lime and lemon eucalyptus odors. Typically classification accuracies can be improved by employing quadratic discriminant analysis (QDA). This method allows for better approximation of decision boundaries resulting in better classification. However, it can only be employed when the number of sensors are less than the number of sample measurements for a single analyte. Upon employing QDA on the same data set, an accuracy of 91.2% corresponding to 4 misclassifications, was achieved. Overall, this level of accuracy suggests that the multisensor array as presented is a reasonable method for odor identification. Incidentally, including additional sensors as is done in some studies should further enhance accuracy.[3,11] Yet, when compared to methods presented herein, addition of more sensors could be disadvantageous as it increases experimental time, materials cost, and complexity when using the current system.

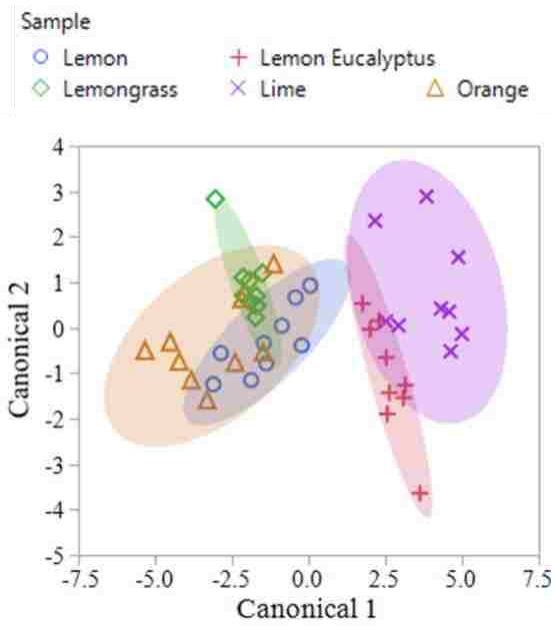

Figure 4.4 Canonical plot for identification of five citrus type odors with respect to a 4 sensor MSA. Plot considers 45 total measurements consisting of three replicate measurements at three concentrations for each odor (9 measurements per sample).

4.4.3 Evaluation of Virtual Sensor Arrays for Odor Recognition.

To examine the utility of VSAs for applications in complex mixture identification, each sensor was analyzed as an independent system. In this regard, an individual sensor, coated with a single ionic liquid and its respective multiple harmonic data (frequency change at different harmonics) would constitute an array. The analyte-selective sensing patterns generated by measurements at multiple harmonics are subsequently used for data analysis. Thus, the data matrix would consist of Δf values where the columns represented each of the harmonics and the rows represented each of the odors tested (7 columns x 45 rows). Three replicate measurements were considered for each odor. Each ionic liquid was tested as a separate VSA. Figure 4.5 depicts canonical plots for each of the 4 VSAs tested, where ellipses represent 95% confidence. Al-though the discriminating factors for the two array sensing schemes (MSA and VSA) are different, it is interesting to see that the same overlaps between

certain odors are present. This would suggest that both array types yield comparable information. This is further supported when considering the identification accuracies obtained via LDA. In this regard, accuracies of 88.9%, 73.4%, 80%, 73.4% were acquired for [C_9MIm][SCN], [C_9MIm][Br], [C_8Pyr][Br], and [C_{11}Pyr][Br] based VSAs, respectively. Furthermore, these accuracies can be enhanced by employing QDA. In this

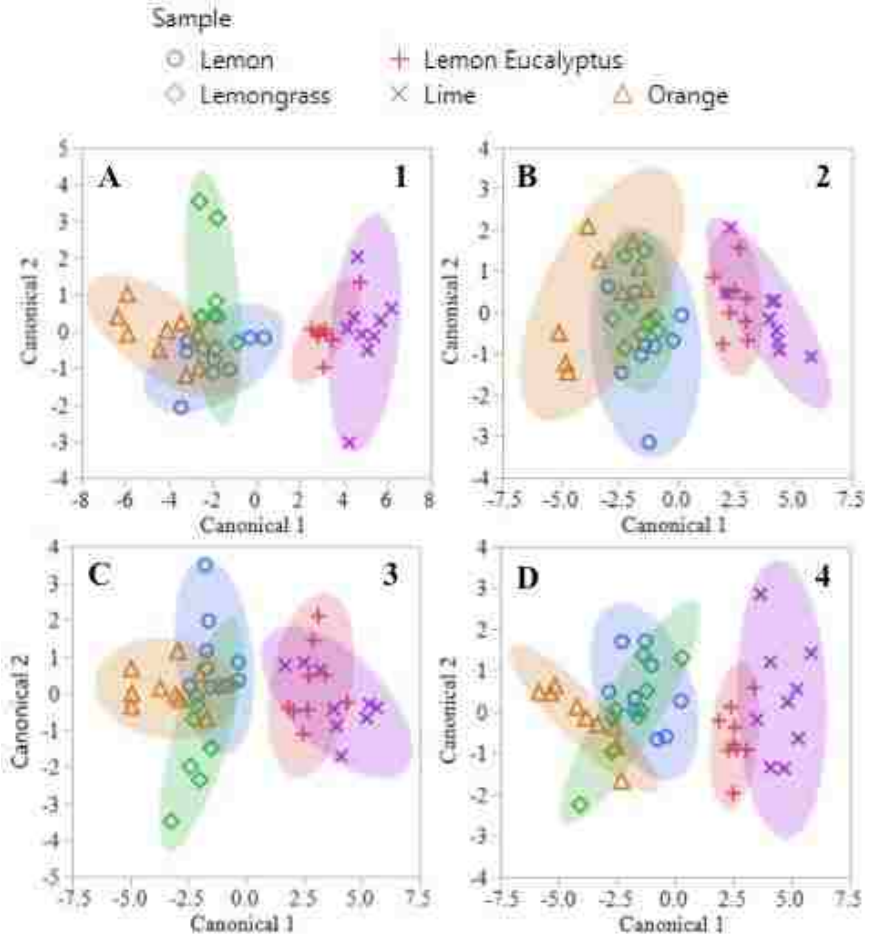

Figure 4.5 Canonical plots for identification of five citrus type odors with respect to four VSAs based on A) [C_9MIm][SCN] B) [C_9MIm][Br] C) [C_8Pyr][Br], and D) [C_{11}Pyr][Br] respectively. Each Plot considers 45 total measurements consisting of three replicate measurements at three concentrations for each odor (9 measurements per sample).

regard, accuracies of 97.8%, 91.2%, 97.8%, and 97.8% were obtained for [C_9MIm][SCN], [C_9MIm][Br], [C_8Pyr][Br], and [C_{11}Pyr][Br] based VSAs, respectively.

Thus, depending on sensor composition, the accuracies obtained are comparable or better than the presented MSA. However, when considering the ease of implementation and significant advantages that arise when using a VSA, this method may have better utility for certain applications. Although, these accuracies represent a vast improvement compared to earlier results (MSA), further optimization would be needed to obtain 100% accuracy.

4.4.4 Evaluation of Virtual Multisensor Sensor Arrays for Odor Recognition

Thus far, evaluation of data presented herein, supports the assertion that MSAs and VSAs can be used interchangeably. Notably, such array schemes are not mutually exclusive. In addition, the discriminating factor for each scheme is quite different. Thus, it is reasonable to expect that the two schemes could be complementary. Since a VSA is based on dynamic operation of a single sensor and an MSA is based on utility of multiple chemically distinct sensors, a complementary system could consist of several dynamically operated sensors, which are chemically distinct. In order to assess the utility of using the MSA and VSA methods as complementary methods, several V-MSAs were fabricated using previously collected data. First, a set of V-MSAs, consisting of two sensors, was fabricated. In this regard, response data for two chemically distinct sensors at all harmonics were considered, effectively combining each of the array schemes. By combining the two schemes, the response output has been augmented 2 fold in comparison to a VSA and 7 fold when compared to 2-sensor MSA. In terms of dimensions, the resultant data matrix consisted of 14 columns representing the harmonics (i.e 2 VSAs or 7 harmonics per sensor) and 45 rows representing three replicate tests at three concentrations of 5 odors. Figure 4.6 is a depiction of canonical plots for the six possible 2-sensor V-MSA combinations derived from the four chemically distinct sensors (1- [C_9MIm][SCN], 2- [C_9MIm][Br], 3- [C_8Pyr][Br], and 4- [C_{11}Pyr][Br]). While it is challenging to discern qualitative differences between these plots, quantitative

accuracies showed a marked increase in identification capability for each of the two sensor V-MSAs. In this regard, LDA accuracies of 97.8%, 100%, 97.8%, 93.4%, 84.5% and 93.4% were obtained for sensor combination A) 1-2 B) 1-3 C) 1-4 D) 2-3 E) 2-4 and F) 3-4, respectively. It should be noted that these accuracies are obtained through LDA since QDA is not applicable for this system given that the number of sensors are more than the number of measurements per sample. Therefore, performance comparisons should be made by considering the LDA results for the previous array sensing schemes, which indicates that the V-MSA method is very promising. Moreover, there is a trend in accuracies for the V-MSAs comprised of 2 chemical sensors that can be predicted by considering their constituent VSA accuracies. In this regard, V-MSAs comprising more accurate VSA sensors yield higher identification accuracies, while V-MSAs comprising less accurate VSA sensors yield lower accuracies. This can be clearly seen when examining V-MSA B, which is comprised of a [C_9MIm][SCN] VSA (88.9%) and a [C_8Pyr][Br] VSA (80%) to V-MSA E, which consists of a [C_9MIm][Br] VSA (73.4%) and a [C_{11}Pyr][Br] VSA (73.4%). The former combination comprises the most accurate VSAs and exhibits the highest accuracy V-MSA (100%) as compared to the latter combination, which comprises the least accurate VSAs and exhibits the lowest accuracy V-MSA (84.5%). While these results are quite reasonable, it is still possible to further enhance the discriminatory power and identification accuracies of V-MSAs. In this regard, a set of V-MSAs consisting of three chemical sensors was fabricated. Figure 4.7 is a depiction of LDA canonical plots for 4 possible combinations of V-MSAs (comprised of three chemical sensors) derived from the four chemically distinct sensors (1- [C_9MIm][SCN], 2- [C_9MIm][Br], 3- [C_8Pyr][Br], and 4- [C_{11}Pyr][Br]).For each array, the resultant data matrix consisted of 21 columns representing the harmonics and 45 rows representing three replicate tests at three concentrations of 5 odors. This corresponds to a 3-fold enhancement of data output as compared to a VSA and a 7-fold enhancement as

compared to a 3 sensor MSA. Again, LDA was employed using the cross validation method, and accuracies of 100%, 97.8%, 100%, 97.8% were obtained for sensor combination A) 1-2-3 B) 1-2-4 C) 1-3-4 D) 2-3-4, respectively. Interestingly, two observations can be made when examining the resultant plots and accuracies. When considering the plots, it is clear that the addition of a 3rd sensor to the V-MSA, significantly enhances spatial separation and clustering of individual samples. In fact, the degree of overlap displayed in these plots is by far the least when compared to any of the previous sensing schemes. Qualitatively, this agrees with the excellent identification accuracies obtained. When considering accuracies, it is clear that addition of an extra sensor further enhances V-MSA results as would be expected from comparing the V-MSA comprised of 2 sensors to the single sensor VSA. Notably, sensor combinations, which were 100% accurate in the two-sensor iteration, retained their level of accuracy upon addition of a third sensor as would be expected. Moreover, two sensor combinations which were less accurate exhibited an increase in accuracy upon addition of a third sensor. Such results suggest that even the least accurate systems can be suitably optimized by addition of a single sensor. Finally, a V-MSA was fabricated by using all four ionic liquid sensors, and statistical analysis was used to measure identification accuracy. The resultant data matrix of this array consisted of 28 columns, representing the harmonics and 45 rows, representing three replicate tests at three concentrations of 5 odors. Apparently, this corresponds to a 4-fold enhancement of data output as compared to a VSA and a 7-fold enhancement as compared to a 4 sensor MSA. Figure 4.8 is a canonical plot for the 4 sensor V-MSA comprised of four chemically distinct sensors (1- [C_9MIm][SCN], 2- [C_9MIm][Br], 3- [C_8Pyr][Br], and 4- [C_{11}Pyr][Br]). In comparison to plots generated from previous sensing schemes, it is easy to see that clustering within a sample and spatial separation between samples is significantly improved. Qualitatively, this plot should represent a significant increase in odor using the

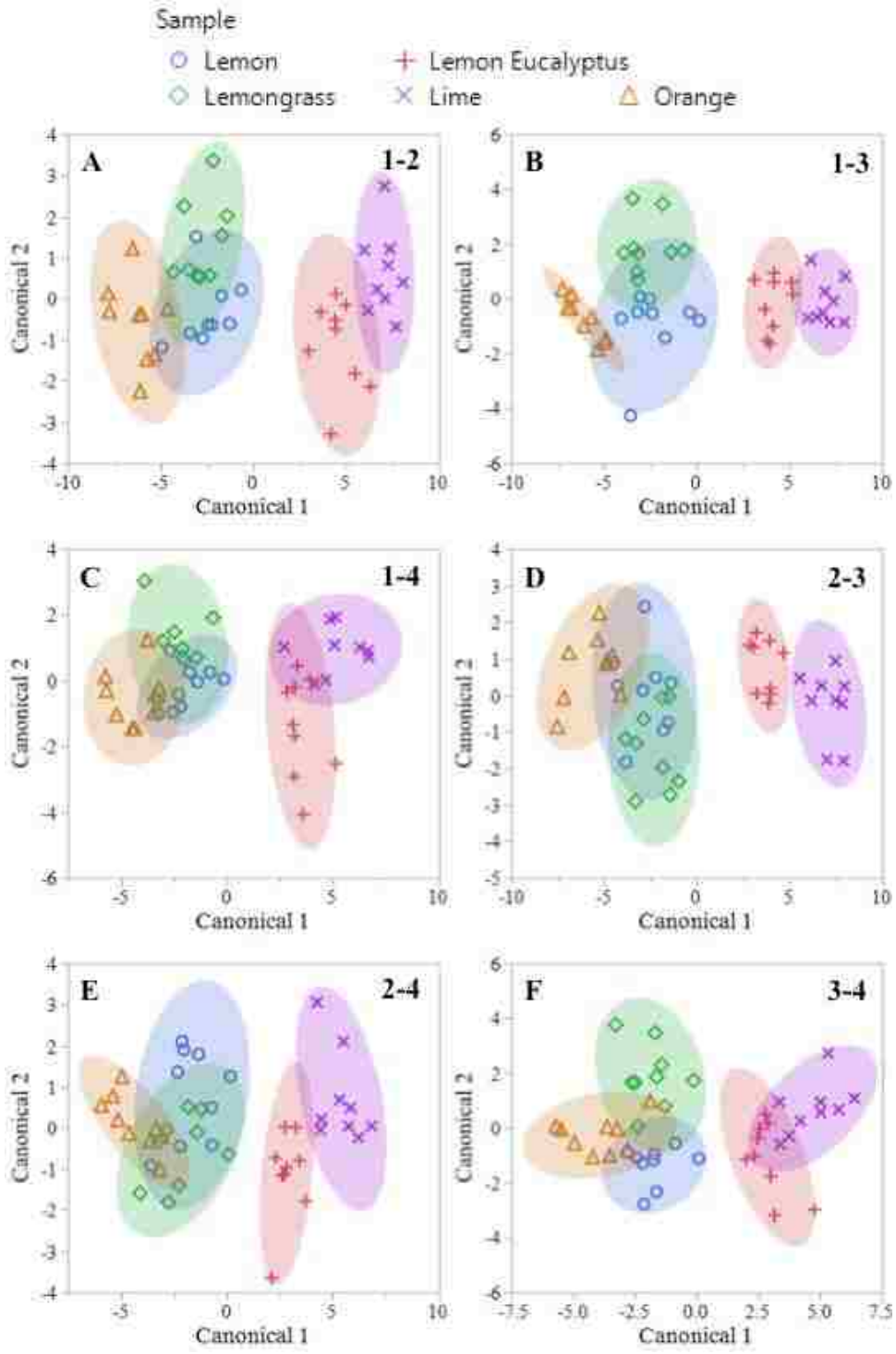

Figure 4.6 Canonical plots for identification of five citrus type odors with respect to several two sensor V-MSAs based on combinations of 1- [C_9MIm][SCN], 2- [C_9MIm][Br], 3- [C_8Pyr][Br], and 4- [C_{11}Pyr][Br]) where arrays consist of sensors A) 1-2 B) 1-3 C) 1-4 D) 2-3 E) 2-4 and F) 3-4 respectively. Each Plot considers 45 total measurements consisting of three replicate measurements at three concentrations for each odor (9 measurements per sample).

cross validation method. This result is truly logical based on results from the three sensor V-MSA. Taken in aggregate, the results herein extoll the effectiveness of the new V-MSA scheme. Hence, I have proven that the V-MSA is an excellent approach identification accuracy, as sample overlap is almost nonexistent. This supposition is supported quantitatively, where an odor identification accuracy of 100% was obtained

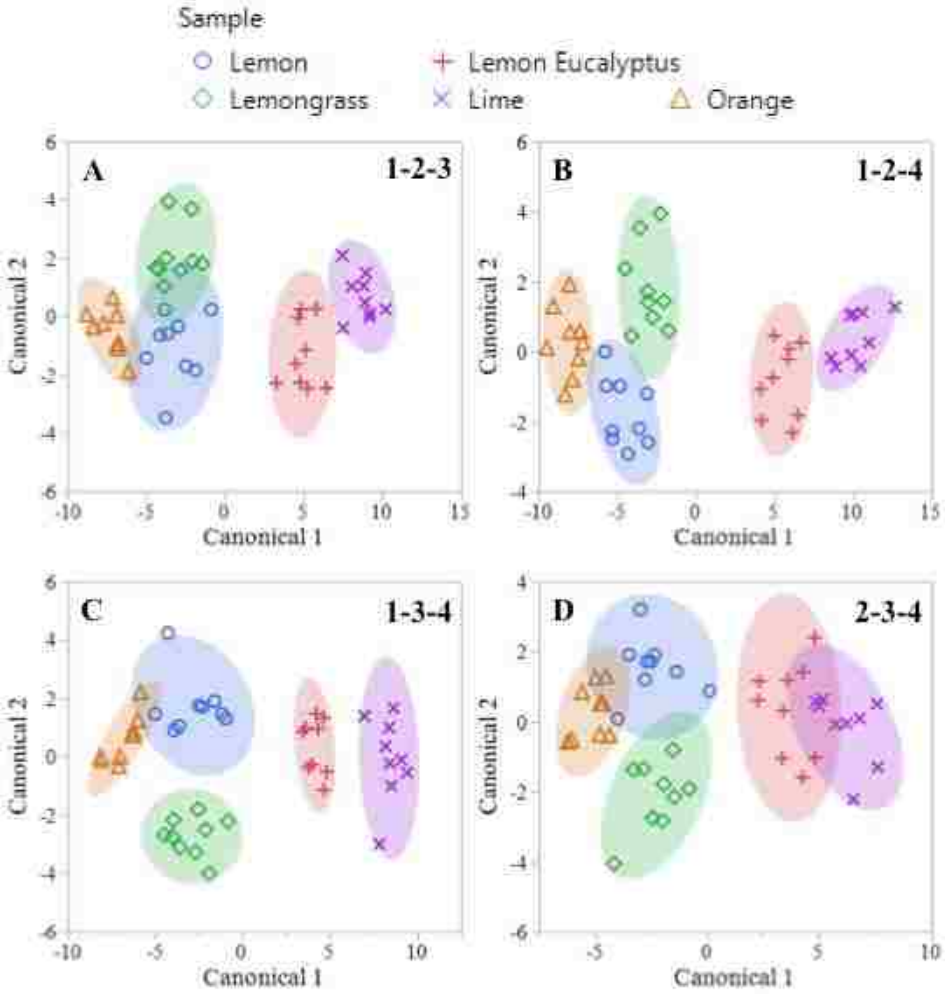

Figure 4.7 Canonical plots for identification of five citrus type odors with respect to several three sensor V-MSAs based on combinations of 1- [C_9MIm][SCN], 2- [C_9MIm][Br], 3- [C_8Pyr][Br], and 4- [C_{11}Pyr][Br]) where arrays consist of sensors A) 1-2-3 B) 1-2-4 C) 1-3-4 D) 2-3-4 respectively. Each Plot considers 45 total measurements consisting of three replicate measurements at three concentrations for each odor (9 measurements per sample).

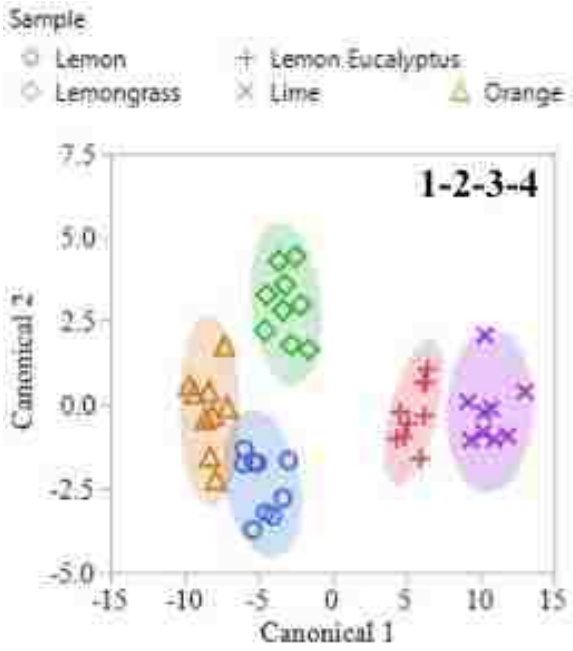

Figure 4.8 Canonical plot for identification of five citrus type odors with respect to a four sensor V-MSA comprised of sensors 1-2-3-4 where 1- [C_9MIm][SCN], 2- [C_9MIm][Br], 3- [C_8Pyr][Br], and 4- [C_{11}Pyr][Br]. Plot considers 45 total measurements consisting of three replicate measurements at three concentrations for each odor (9 measurements per sample).

for complex mixtures analysis. High discrimination accuracy was acquired as the number of sensors were increased within a given V-MSA scheme.

4.5 Conclusion

In conclusion, a comparative study to assess the utility of QCM array sensing schemes for complex mixture identification was performed by employing four chemically distinct ionic liquids. It was observed that MSA and VSA schemes could be used interchangeably since accuracy levels were comparable. However, the VSA scheme is potentially more promising than MSA in terms of cost, labor, and time expenditure. Furthermore, a new sensing scheme based on complementary use of MSA and VSA schemes was introduced. In this regard, multiple V-MSAs were systematically developed and analyzed using two, three, and four ionic liquid based sensors. After comparing

results, it is clear that the V-MSA scheme is extremely promising as compared to existing QCM sensing schemes. It is also apparent from this scheme that increased data density is important for achieving highly accurate identification of complex mixtures. Overall, these studies are particularly promising for use of QCM sensor arrays in applications involving odor recognition. Potential examples of such applications would include: quality control of perfume/ scents and vapor phase assessment of food quality. Currently, additional studies are underway to ascertain the full potential of this method with regard to complex mixture analysis.

4.6 References

1. Carey, J. R. et al. Rapid Identification of Bacteria with a Disposable Colorimetric Sensing Array. J. Am. Chem. Soc. 133, 7571–7576 (2011).

2. Suslick, B. A., Feng, L. & Suslick, K. S. Discrimination of Complex Mixtures by a Colorimetric Sensor Array: Coffee Aromas. Anal. Chem. 82, 2067–2073 (2010).

3. Toniolo, R. et al. Room Temperature Ionic Liquids As Useful Overlayers for Estimating Food Quality from Their Odor Analysis by Quartz Crystal Microbalance Measurements. Anal. Chem. 85, 7241–7247 (2013).

4. Capone, S. et al. Monitoring of rancidity of milk by means of an electronic nose and a dynamic PCA analysis. Sens. Actuators B Chem. 78, 174–179 (2001).

5. Galpothdeniya, W. I. S. et al. Ionic liquid-based optoelectronic sensor arrays for chemical detection. RSC Adv 4, 7225–7234 (2014).

6. Kwon, H., Samain, F. & Kool, E. T. Fluorescent DNAs printed on paper: sensing food spoilage and ripening in the vapor phase. Chem. Sci. 3, 2542 (2012).

7. Albert, K. J. et al. Cross-Reactive Chemical Sensor Arrays. Chem. Rev. 100, 2595–2626 (2000).

8. Askim, J. R., Mahmoudi, M. & Suslick, K. S. Optical sensor arrays for chemical sensing: the optoelectronic nose. Chem. Soc. Rev. 42, 8649 (2013).

9. Stetter, J. R. & Penrose, W. R. Understanding Chemical Sensors and Chemical Sensor Arrays(Electronic Noses): Past, Present, and Future. Sens. Update 10, 189 (2002).

10. Speller, N. C. et al. Rational Design of QCM-D Virtual Sensor Arrays Based on Film Thickness, Viscoelasticity, and Harmonics for Vapor Discrimination. Anal. Chem. 87, 5156–5166 (2015).

11. Jin, X., Yu, L., Garcia, D., Ren, R. X. & Zeng, X. Ionic Liquid High-Temperature Gas Sensor Array. Anal. Chem. 78, 6980–6989 (2006).

12. Rehman, A. et al. Differential Solute Gas Response in Ionic-Liquid-Based QCM Arrays: Elucidating Design Factors Responsible for Discriminative Explosive Gas Sensing. Anal. Chem. 83, 7823–7833 (2011).

13. Xu, X. et al. Ionic liquids used as QCM coating materials for the detection of alcohols. Sens. Actuators B Chem. 134, 258–265 (2008).

14. Jin, X., Huang, Y., Mason, A. & Zeng, X. Multichannel Monolithic Quartz Crystal Microbalance Gas Sensor Array. Anal. Chem. 81, 595–603 (2009).

15. Xu, X., Cang, H., Li, C., Zhao, Z. K. & Li, H. Quartz crystal microbalance sensor array for the detection of volatile organic compounds. Talanta 78, 711–716 (2009).

16. Liang, C., Yuan, C.-Y., Warmack, R. J., Barnes, C. E. & Dai, S. Ionic Liquids: A New Class of Sensing Materials for Detection of Organic Vapors Based on the Use of a Quartz Crystal Microbalance. Anal. Chem. 74, 2172–2176 (2002).

17. Regmi, B. P. et al. Molecular weight sensing properties of ionic liquid-polymer composite films: theory and experiment. J Mater Chem C 2, 4867–4878 (2014).

18. Makino, W., Kishikawa, R., Mizoshiri, M., Takeda, S. & Yao, M. Viscoelastic properties of room temperature ionic liquids. J. Chem. Phys. 129, 104510 (2008).

19. Yamaguchi, T., Miyake, S. & Koda, S. Shear Relaxation of Imidazolium-Based Room-Temperature Ionic Liquids. J. Phys. Chem. B 114, 8126–8133 (2010).

20. Ide, J., Nakamoto, T. & Moriizumi, T. in Olfaction and Taste XI (eds. Kurihara, K., Suzuki, N. & Ogawa, H.) 727–730 (Springer Japan, 1994).

21. Berger, R. G. Flavours and Fragrances: Chemistry, Bioprocessing and Sustainability. (Springer Science & Business Media, 2007).

22. Moriizumi, T., Nakamoto, T. & Sakuraba, Y. in Olfaction and Taste XI (eds. Kurihara, K., Suzuki, N. & Ogawa, H.) 694–698 (Springer Japan, 1994).

23. Vogt, B. D., Lin, E. K., Wu, W. & White, C. C. Effect of Film Thickness on the Validity of the Sauerbrey Equation for Hydrated Polyelectrolyte Films. J. Phys. Chem. B 108, 12685–12690 (2004).

24. McHale, G., Lücklum, R., Newton, M. I. & Cowen, J. A. Influence of viscoelasticity and interfacial slip on acoustic wave sensors. J. Appl. Phys. 88, 7304 (2000).

25. Hasan, F. et al. Ionic liquids as buffer additives in ionic liquid-polyacrylamide gel electrophoresis separation of mixtures of low and high molecular weight proteins. RSC Adv 5, 69229–69237 (2015).

CHAPTER 5. QCM VIRTUAL MULTISENSOR ARRAY FOR FUEL DISCRIMINATION AND DETECTION OF GASOLINE ADULTERATION

5.1 Introduction

Since the mid -19th century, petroleum based fuels have been the energy source of choice for meeting energy requirements worldwide. In this regard, gasoline, and diesel have proven to be globally important fuels, for transportation purposes.[1,2] As a result, illegal adulteration of such fuels can be a lucrative endeavor. This illegal activity is typically spurred by price disparities between petroleum based fuels and commonly available adulterants, such as industrial solvents.[3,4] In this regard, the cost difference is normally driven by differential taxation between fuels and potential adulterants. [3,4] Unfortunately, adulteration can have significant economic and environmental impacts. Such impacts include increased toxic emissions, lost taxes, and consumer vehicle malfunctions.[3-8] Thus there is a need for simplistic cost effective methods for detection of fuel adulteration.

Numerous analytical techniques have been employed to detect fuel adulteration. In fact, the American Society for Testing and Materials International (ASTM) has documented several methods that have been accepted as global standards.[3] These include a number of physicochemical property based tests as well as more sophisticated analytical approaches. In this regard, relative density measurements, and evaporation/distillation methods are among the simplest approaches. However these approaches are often not sufficient for detecting low level adulteration or adulteration with naturally occurring fuel constituents such as hydrocarbon solvents.[3] More complex analytical methods such as gas chromatography-mass spectrometry (GC-MS) or implementation of dye markers are more reliable.[3,9] However, these approaches are typically expensive, time consuming or require significant expertise to achieve accurate results.[3,8] Due to these limitations, researchers are developing novel systems or

application of novel techniques for detection of fuel adulteration. In this regard, all advanced research can be divided into two main categories 1) application of new techniques to traditional analytical approaches or 2) implementation of new instrumental approaches. With regard to the former category, the vast majority of reports in literature employ statistical analyses of data to enhance traditional approaches such as distillation and gas chromatography based methods.[10-14] In each case, statistical techniques are employed to simplify data analyses and enhance accuracy of detection. This approach addresses some of the limitations of traditional techniques such as the requirement for lengthy analysis time. With regard to the latter category, several new methods have been developed for detection of gasoline adulteration which are mostly based on applying new instrumental approaches. In this regard, several spectroscopy and spectrometry based methods have been reported recently.[8,15-25] In the present study, an alternative method for fuel discrimination and detection of gasoline adulteration, based on the quartz crystal microbalance (QCM), is introduced. Similar to some of the spectroscopy based methods, advantages of this approach include, lack of sample preparation, and prompt nondestructive analyses.

The QCM is a simple yet sensitive analytical tool primarily used as a mass detection device. However, as a physical event transducer, this device is particularly amenable to the fabrication of sensors and sensor arrays. [26-35] In this regard, a gas phase QCM sensor is typically comprised of a chemosensitive layer immobilized onto the quartz crystal resonator surface (QCR). The chemosensitive adlayer, which directly affects sorption properties, imparts sensitivity and selectivity to the sensor. As a gravimetric transducer, the QCM converts the sorption event into a quantifiable electronic signal. When several sensors employing different chemosensitive adlayers are utilized in tandem, a mutisensor array (MSA) is developed. MSAs represent the most prevalent examples of QCM sensor arrays in literature, [30-32,36-44] however such systems

suffer from limitations when trying to discriminate numerous closely related highly complex mixtures. Recently, I introduced an alternative scheme called a virtual sensor array (VSA) based on the dynamic operation of a signal sensor that utilizes harmonics, film thickness, and viscoelasticity to generate differential responses.[45] While powerful for discriminating closely related pure analytes, using single chemosensitive material, this scheme can also suffer some accuracy limitations when analyzing multiple highly complex mixtures. To address the limitations experienced by the MSA and VSA schemes, I introduced a new scheme that combines the MSA and VSA scheme, termed a Virtual Multisensor array (V-MSA). This new scheme is based on dynamic operation of multiple sensors, and exhibits multifold enhancement of data density when compared to its component schemes. It was found that enhanced data density was a key factor in accurate discrimination of volatile complex mixtures. Hence, I further explore the utility of this newly reported sensing scheme (V-MSA) by assessing its potential for fuel discrimination and detection of gasoline adulteration.

Herein, a new approach for fuel discrimination based on employing the quartz crystal microbalance is introduced. In this regard, the development and implementation of a QCM V-MSA, employing organic salts (OSs) as recognition elements, for discrimination of pure and adulterated fuel samples is described. OSs, particularly Ionic liquids and Group of Uniform Materials based on Organic Salts (GUMBOS), have proven promising chemosensitive adlayers for gas phase QCM sensors and sensor arrays.[31,32,45-48] Moreover, OSs exhibit viscoelasticity and favorable sorption properties, which are vital for fabrication of V-MSAs. [35,49,50] As a proof of concept, this system was initially employed to discriminate between four petroleum based fuels, specifically petroleum ether, gasoline, kerosene and diesel, which represent the most chemically distinct complex mixtures assessed. Subsequently, this array was used to discriminate more closely related complex mixtures represented by gasoline grades (Exxon Regular,

Exxon Plus, Exxon Supreme). Finally the system was utilized to detect adulteration of gasoline by common industrial solvents (methanol, ethanol, xylenes, and toluene) with varying adulterant concentration (v/v ratios 1%,10%,20%,40%). This study is the first report of a QCM sensor array for applications in fuel discrimination and detection of gasoline adulteration.

5.2 Experimental Section

5.2.1 Reagents and Materials

Four OSs, named 1-octyl-3-methylimidazolium bromide ([C_8MIm][Br]), 1-decyl-3-methylimidazolium bromide ([C_{10}MIm][Br]), 1-dodecyl-3-methylimidazolium bromide ([C_{12}MIm][Br]), 1-hexadecyl-3-methylimidazolium bromide ([C_{16}MIm][Br]) were used to prepare coatings on the quartz crystal resonators utilized in these studies. These ILs were synthesized using previously documented procedures.[51,52] Fuel samples were purchased from a local Exxon Gas station in Baton Rouge, Louisiana. Dichloromethane was obtained from Malindkroft fine chemicals, Xylenes were obtained from Fischer Scientific while Toluene, Anhydrous Methanol and Anhydrous Ethanol were obtained from Sigma Aldrich. All materials were used as is, without any further purification.

5.2.2 Preparation of Stock Solutions

Stock solutions of [C_8MIm][Br], [C_{10}MIm][Br], [C_{12}MIm][Br], and [C_{16}MIm][Br] (1 mg mL-1) were prepared in dichloromethane (DCM) using 20 mL borosilicate glass scintillation vials.

5.2.3 Preparation of Sensing Films

All films were coated on the QCR using electrospray deposition under the same parameters. A flowrate of 100 µl/ min, current of 3 Amps, voltage of 2.9 V, and a working distance of 7 cm were used. After coating, nitrogen gas was blown on all films, and films were stored in a desiccator. Change in frequency between coated and uncoated crystal was found to be ~ -2000 Hz at the fundamental frequency.

5.2.4 Preparation of Fuel Samples

All fuel samples (non adulterated samples) were prepared by introducing 10 mL of the respective sample into a 20 mL borosilicate glass scintillation vials.

5.2.5 Preparation of Adulterated Samples

All adulterated samples were prepared in 20 mL borosilicate glass scintillation vials using Exxon regular gasoline and the chosen adulterant. Adulterated samples of gasoline were prepared by calculating the appropriate v/v ratio (1%,10%,20%,40%) for a 10 mL sample.

5.2.6 Array Fabrication

In this chapter, a V-MSA was fabricated using OSs immobilized as thin films onto QCM-D transducers. In this regard, four QCRs were coated with ionic liquids: 1-octyl-3-methylimidazolium bromide ([C_8MIm][Br]), 1-decyl-3-methylimidazolium bromide ([C_{10}MIm][Br]), 1-dodecyl-3-methylimidazolium bromide ([C_{12}MIm][Br]), 1-hexadecyl-3-methylimidazolium bromide ([C_{16}MIm][Br]) respectively. These materials were selected as a simple representation of a homologous series of organic salts. A bromide counter ion was chosen due to high sensitivity that halide containing ionic liquids exhibit towards alcohols.[46] As chain length increases within the series, viscosity increases resulting in two of the four OSs being solid phase. Structures of the four OSs are displayed in Figure D1. Subsequently, the four sensors coated with these four OSs were installed into the QCM-D and concurrent measurements were recorded for all sensors across multiple harmonics. This effectively creates a master data set which represents a virtual mutisensor array (V-MSA), i.e. measurements from several dynamically operated, chemically distinct sensors.

The operating principle of the V-MSA, is based on an amalgamation of the MSA and VSA schemes i.e dynamic operation of chemically distinct sensors. In this regard, sensor response is dependent upon five parameters: chemical affinity, viscoelasticity,

film thickness, harmonics and nature of analyte. Thus it is possible to obtain combinations of positive and negative differential sensor response as seen in previous publications.[45]

5.2.7 Data Acquisition

A system consisting of two independent gas flow channels (one channel for sample odors and another channel for carrier gas) was used to perform this experiment. As a first step in data collection, a stable baseline was obtained by purging the system with ultrapure argon. Subsequently, fuel samples were introduced via bubbling of argon gas through the sample reservoir, which was filled with the sample of interest, to generate a sample of saturated vapor pressure. As the sample channel and carrier channel merge, the sample flow is diluted yielding percentages of the respective saturated vapor pressure (SVP). (e.g. 10%, 20%, 40% of SVP) The flow rate was controlled by digital mass flow controllers and adjusted to a total flow rate of 100 sccm. After mixing over the 1 meter length of the tubing, the vapors flow over the QCM sensor crystals placed inside a flow modules. Chamber temperature was precisely regulated (22°C). Finally, to remove sample vapors, the system was purged with ultrapure argon until recovery of the baseline. A schematic of the experimental system is depicted in Figure D2 of the appendix.

5.2.8 Data Analysis

Data sets consisting of Δf responses, generated from these experiments were used to develop statistical models for assessing the identification accuracies of the V-MSA. As a first step in analysis, PCA was employed to reduce the dimensionality of the data set. Thereafter, the principal components accounting for 99% of variance in the original data set were used as input variables for linear discriminant analysis. Quantitative assessment of classification accuracy was obtained via of the use of LDA coupled with leave one out cross validation.

5.3 Results and Discussion

5.3.1 Fuel Discrimination using a QCM V-MSA

After installing the four sensors into the QCM-D, all sensors were exposed to four hydrocarbon fuels (petroleum, gasoline, kerosene and diesel) at multiple concentrations to assess suitability of the system for discrimination between complex hydrocarbon mixtures. Each fuel was exposed at three different concentrations (10%, 20%, 40% of SVP) for an exposure time of 1 minute. Measurements of Δ*f* at each harmonic were acquired, and each sensor was found to exhibit stable baseline and reproducible responses with reversible capture. (Supporting information figure D3-D6) Figure 5.1 depicts sensor response of each sensor for the four hydrocarbon fuels. As in my previous work, positive and negative responses were obtained via measurement at

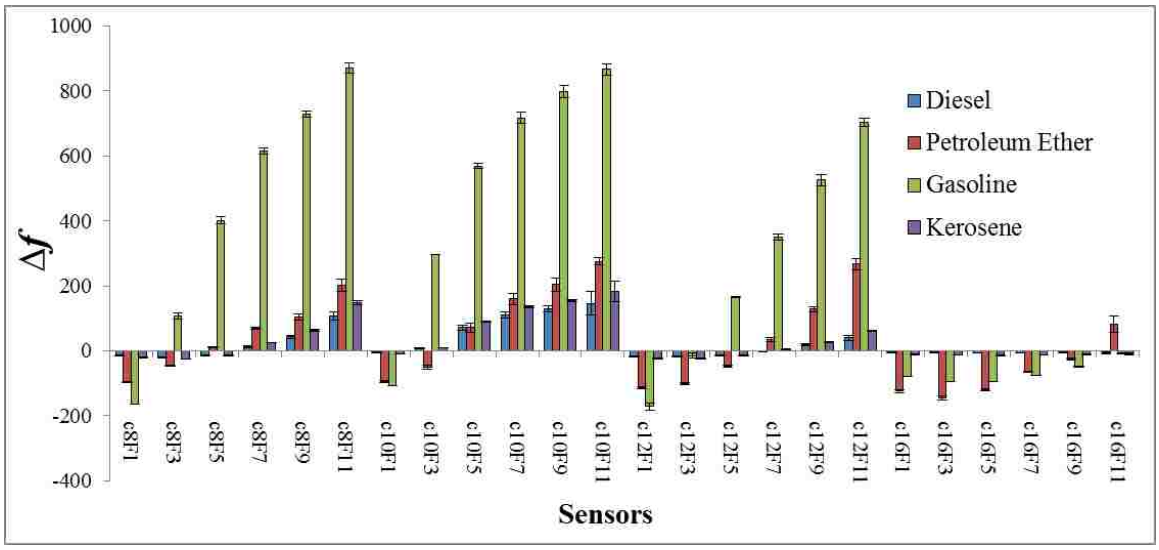

Figure 5.1 Multiple harmonic sensor response of ionic liquids [C_8MIm][Br], [C_{10}MIm][Br], [C_{12}MIm][Br], [C_{16}MIm][Br] to four hydrocarbon fuels at 20% of SVP. Responses considered in aggregate constitute a V-MSA. For clarity X-axis labels are in the form, C_nF_n where C_n represents ionic liquid cation and F_n represents harmonic number. Error bars represent three replicate measurements.

multiple harmonics. Moreover, each fuel mixture exhibited an analyte specific response pattern which is promising for identification of each complex mixture. Overall, gasoline

generally exhibits the greatest sensor response and this is likely due to the presence of ethanol within the mixture. This is particularly promising for further studies in this chapter. To assess the capability of the V-MSA for discrimination between the four different fuels, principal component analysis (PCA) and linear discriminant analysis (LDA) were employed.The data matrix consisted of Δf values where the columns represented each of the sensors and the rows represented each of the fuels tested across three concentrations (20%, 30%, and 40% of SVP). Three replicate measurements were considered for each sample for a total of 9 measurements per sample. (24 columns x 36 rows) A canonical plot for the V-MSA is depicted in figure 5.2,

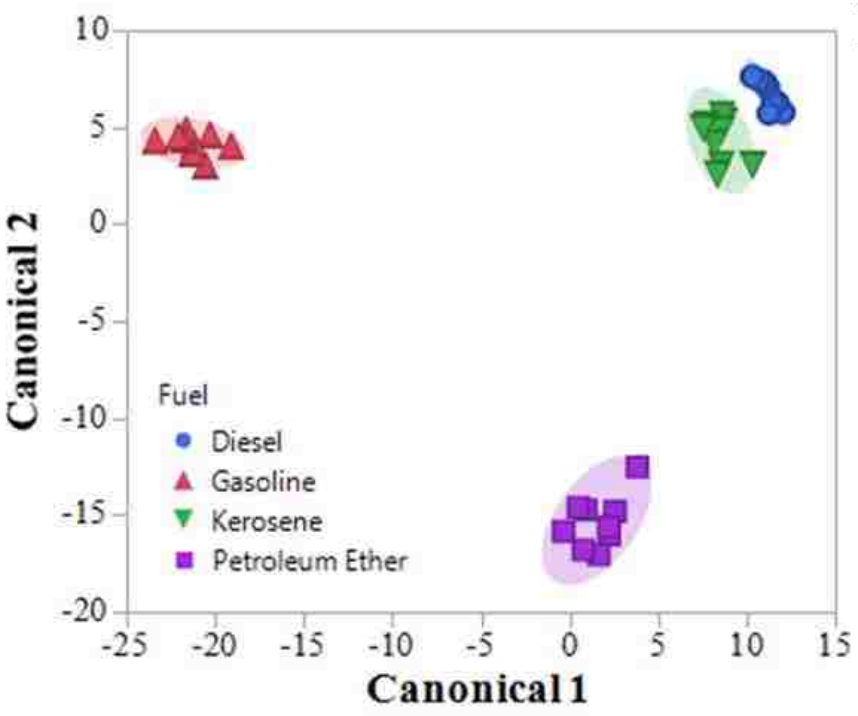

Figure 5.2 LDA canonical plot for discrimination of four hydrocarbon fuels using a V-MSA. Plots considers a data set of Δf values for each sample measured across three concentrations (p_a/p_0 = 0.2, 0.3, 0.4) in triplicate (9 measurements per sample for 36 total measurements).

wherein ellipses represent 95% confidence. From a quick visual assessment of this figure, it is easy to identify that each sample is well discriminated. A quantitative assessment of identification accuracy was obtained using the cross validation method. In this regard, each sample was correctly identified yielding 100% accurate discrimination of the hydrocarbon fuels. These results demonstrate that utilizing a QCM V-MSA is a promising approach for discrimination of hydrocarbon fuels. Since gasoline proved to be the most sensitive fuel for the array as configured, further studies were conducted with gasoline. This result is to be expected as halide containing organic salts were shown be sensitive to alcohols,[46] and gasoline contains a significant concentration of ethanol (10-15%v/v).

5.3.2 Gasoline Grade Discrimination using a QCM V-MSA

To further benchmark the capabilities of the fabricated V-MSA, three closely related hydrocarbon fuels were chosen for discrimination. In this regard, three gasoline grades, Exxon Regular, Exxon Plus, and Exxon Supreme, were chosen to establish whether the V-MSA could accurately distinguish between each sample. As described in the previous section, all sensors were exposed to each gasoline grade at varying concentrations for exposure times of 1 minute per sample. Measurements of Δf at each harmonic were acquired to construct a data matrix of 24 columns x 27 rows. In this regard, three replicate measurements of each gasoline grade across three concentrations (20%, 30%, and 40% of SVP) were tested for a total of 9 measurements per sample. Figure 5.3 depicts sensor response of each sensor to the gasoline grades. Notably each gasoline grade yields a specific response pattern. However it is easy to discern that the responses are much more similar than the previously tested fuels in figure 5.1. This result is expected as these samples are much more closely related. Figure 5.4 depicts a canonical plot for identification of the three gasoline grades.

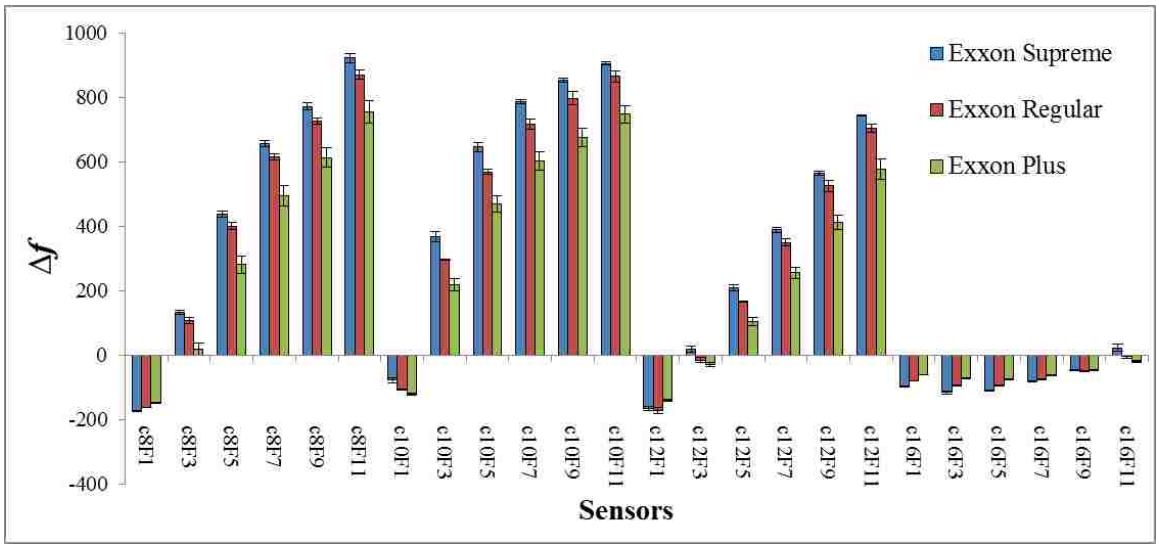

Figure 5.3 Multiple harmonic sensor response of organic salts [C_8MIm][Br], [C_{10}MIm][Br], [C_{12}MIm][Br], [C_{16}MIm][Br] to three gasoline grades at 20% of SVP. Responses considered in aggregate constitute a V-MSA. For clarity X-axis labels are in the form, C_nF_n where C_n represents ionic liquid cation and F_n represents harmonic number. Error bars represent three replicate measurements

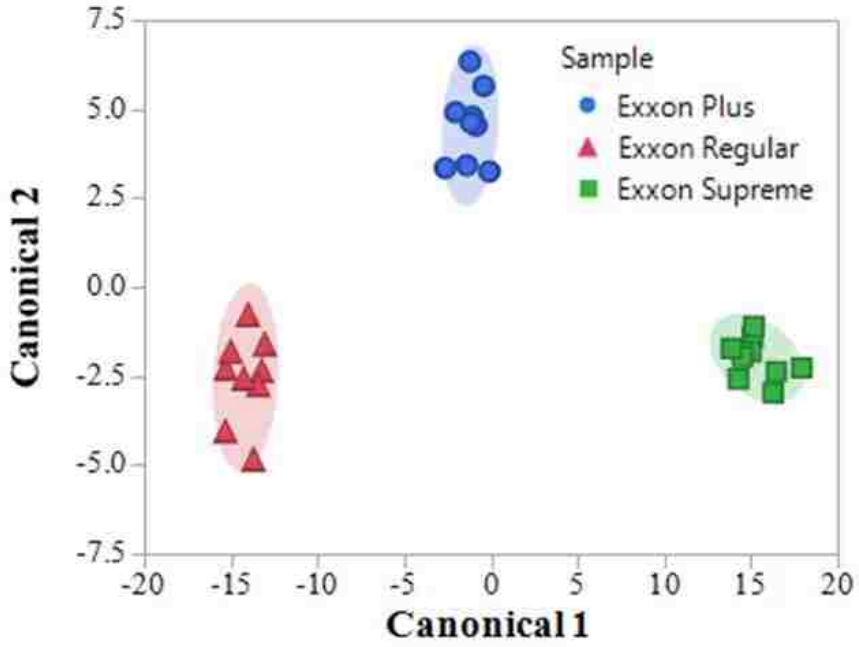

Figure 5.4 LDA canonical plot for discrimination of three gasoline grades using a V-MSA. Plots considers a data set of ∆f values for each sample measured across three concentrations (pa/p0 = 0.2, 0.3, 0.4) in triplicate (9 measurements per sample for 27 total measurements.)

Although these samples are more closely related than the previously tested fuels, 100% accurate discrimination was attained via the cross validation method. Such results

revealed that the V-MSA approach is a very promising tool for discrimination of gasoline samples, which is essential for detecting gasoline adulteration.

5.3.3 Detection of Gasoline Adulteration using a QCM V-MSA

To assess the capability of the V-MSA to be used for gasoline adulteration, four common industrial solvents (methanol, ethanol, xylene and toluene) were tested as gasoline adulterants. In this regard, Exxon Regular gasoline was adulterated with each solvent (adulterant) at four v/v ratios (1%, 10%, 20%, 40%). As performed previously, each sample was exposed for 1 minute three different concentrations (20%, 30%, 40% of SVP) and three replicate measurements were considered for each sample. Figures 5.5-5.8 depict sensor response for each adulterated sample. To assess the capability of the V-MSA to detect gasoline adulteration a data matrix considering all gasoline grades (Exxon Regular, Plus and Supreme) and adulterated samples was constructed (24 columns x 171 rows). Figure 5.9 depicts canonical plots for detection of gasoline adulteration using a V-MSA. Canonical 1 and 2 successfully discriminates between adulterated and unadulterated gasoline samples. Moreover, canonical 2 and 3 accurately discriminates between samples adulterated by xylene and toluene. Finally canonical 3 and 4 successfully classifies samples adulterated by methanol and ethanol. Overall 100% accurate determination of gasoline adulteration as well as the nature of the adulterant over multiple v/v ratios was achieved. These results are very promising for the development of QCM based methods for adulteration screening of gasoline and other important petroleum based fuels.

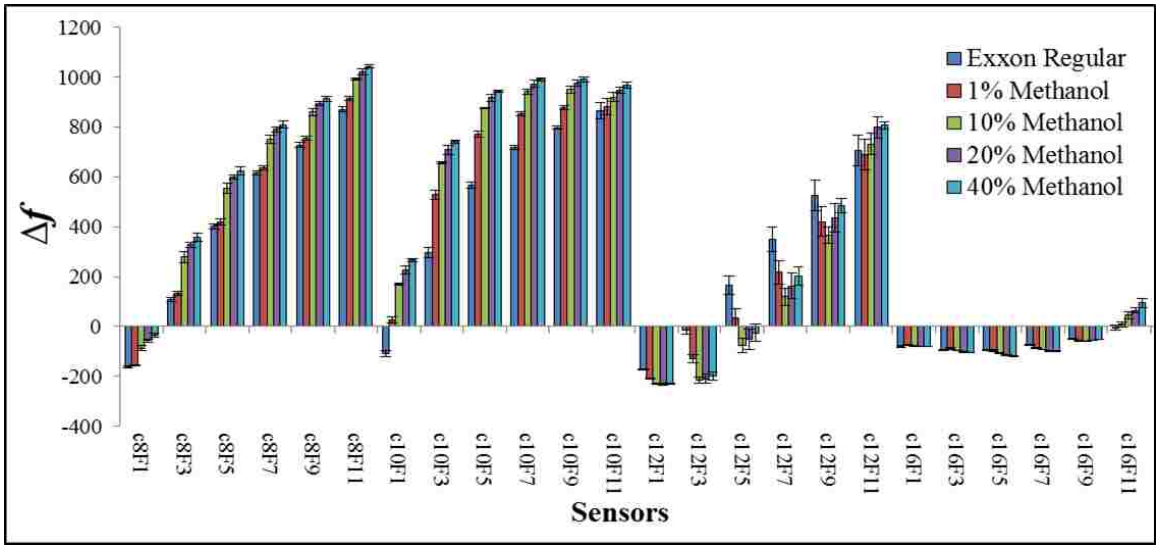

Figure 5.5 Multiple harmonic sensor response of organic salts [C_8MIm][Br], [C_{10}MIm][Br], [C_{12}MIm][Br], [C_{16}MIm][Br] exposed to Exxon regular Gasoline adulterated with methanol at five v/v ratios (0%, 1%, 10%, 20% 40%) at 20% of SVP. Responses considered in aggregate constitute a V-MSA. For clarity X-axis labels are in the form, C_nF_n where C_n represents ionic liquid cation and F_n represents harmonic number. Error bars represent three replicate measurements

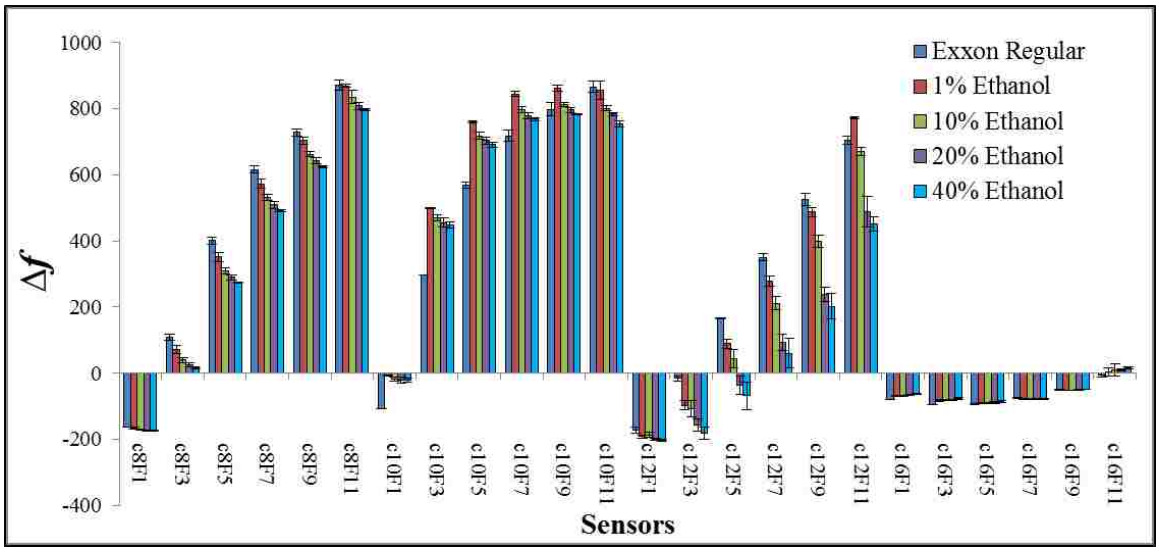

Figure 5.6 Multiple harmonic sensor response of organic salts [C_8MIm][Br], [C_{10}MIm][Br], [C_{12}MIm][Br], [C_{16}MIm][Br] exposed to Exxon regular Gasoline adulterated with ethanol at five v/v ratios (0%, 1%, 10%, 20% 40%) at 20% of SVP. Responses considered in aggregate constitute a V-MSA. For clarity X-axis labels are in the form, C_nF_n where C_n represents ionic liquid cation and F_n represents harmonic number. Error bars represent three replicate measurements.

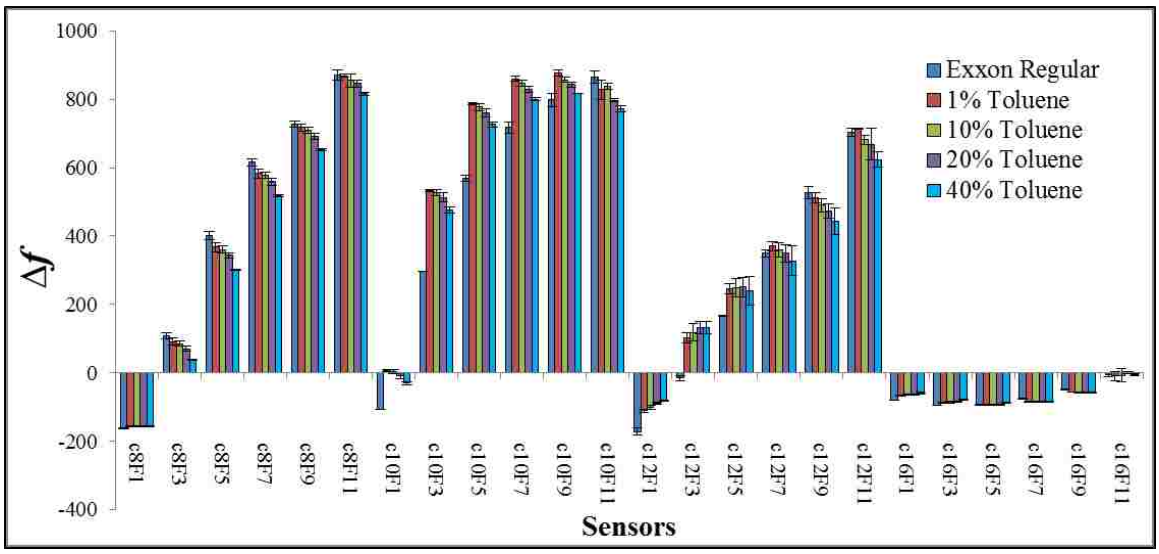

Figure 5.7 Multiple harmonic sensor response of organic salts [C_8MIm][Br], [C_{10}MIm][Br], [C_{12}MIm][Br], [C_{16}MIm][Br] exposed to Exxon regular Gasoline adulterated with toluene at five v/v ratios (0%, 1%, 10%, 20% 40%) at 20% of SVP. Responses considered in aggregate constitute a V-MSA. For clarity X-axis labels are in the form, C_nF_n where C_n represents ionic liquid cation and F_n represents harmonic number. Error bars represent three replicate measurements.

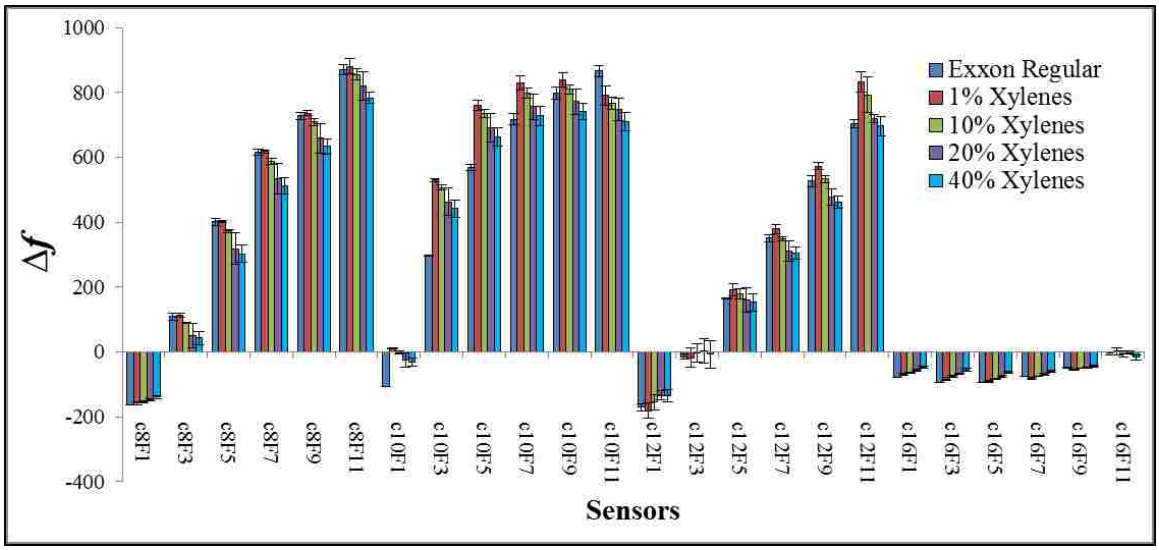

Figure 5.8 Multiple harmonic sensor response of organic salts [C_8MIm][Br], [C_{10}MIm][Br], [C_{12}MIm][Br], [C_{16}MIm][Br] exposed to Exxon regular Gasoline adulterated with xylenes at five v/v ratios (0%, 1%, 10%, 20% 40%) at 20% of SVP. Responses considered in aggregate constitute a V-MSA. For clarity X-axis labels are in the form, C_nF_n where C_n represents ionic liquid cation and F_n represents harmonic number. Error bars represent three replicate measurements.

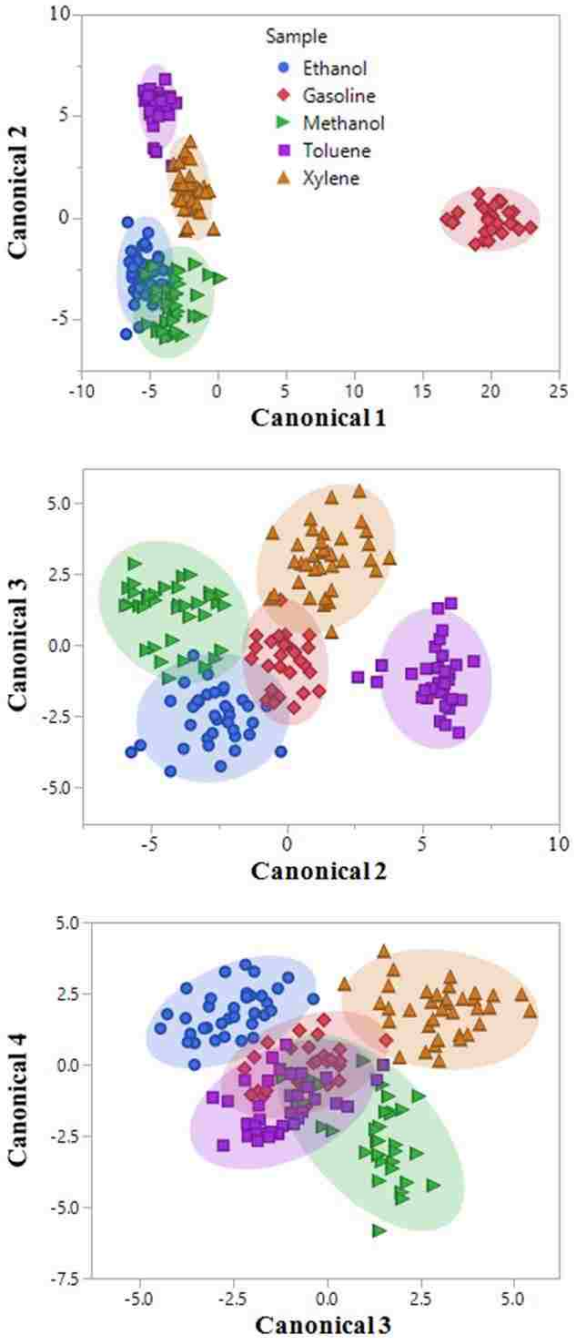

Figure 5.9 LDA canonical plots for detection of gasoline adulteration using a V-MSA. Plots considers a data set of Δf values for each sample measured across three concentrations (pa/p0 = 0.2, 0.3, 0.4) in triplicate. Adulterated samples denoted Methanol, Ethanol, Toluene and Xylene are Exxon Regular gasoline adulterated at four v/v ratios (1%, 10%, 20% 40%). (36 measurements per adulterant type for 144 total measurements) Additionally the sample termed gasoline considers all measurements of Exxon Regular, Exxon Plus and Exxon Supreme.(9 measurements per grade for 27 total measurements) The plot considers 9 measurements per sample for a total of 171 measurements.

5.4 Conclusion

This work is a description of the development and implementation of a QCM V-MSA for fuel discrimination and detection of gasoline adulteration. In this regard, a V-MSA was fabricated using organic salts as chemosensitive adlayers. Initially, the system was used to successfully discriminate between four petroleum based fuels (Petroleum Ether, Gasoline, Kerosene and Diesel). Subsequently, the V-MSA was used to discriminate between, more closely related, gasoline grades. Finally, the system was employed to detect and determine the nature of gasoline adulteration by several common industrial solvents across four v/v ratios (1%, 10%, 20%, 40%). All analyses were accomplished with 100% accuracy as determined via LDA employing the cross validation method. These studies are very promising for implementation of QCM V-MSAs for quality control applications and are an interesting benchmark. Further studies are underway to ascertain the full potential of this approach.

5.5 References

1. Dahl, C. & Sterner, T. Analysing gasoline demand elasticities: a survey. Energy Econ. 13, 203–210 (1991).

2. Dahl, C. A. Measuring global gasoline and diesel price and income elasticities. Energy Policy 41, 2–13 (2012).

3. Garg, N., Mohan, S., Pal, A. & Mishra, R. S. Fuel Adulteration, Problem and Mitigation Strategies: A Review. Methods 48, 51 (2015).

4. Kalligeros, S., Zannikos, F., Stournas, S. & Lois, E. Fuel adulteration issues in Greece. Energy 28, 15–26 (2003).

5. Obeidat, S. M., Al-Ktash, M. M. & Al-Momani, I. F. Study of Fuel Assessment and Adulteration Using EEMF and Multiway PCA. Energy Fuels 28, 4889–4894 (2014).

6. Mendes, G. & Barbeira, P. J. S. Detection and quantification of adulterants in gasoline using distillation curves and multivariate methods. Fuel 112, 163–171 (2013).

7. Barbeira, P. J. S., Pereira, R. C. C. & Corgozinho, C. N. C. Identification of Gasoline Origin by Physical and Chemical Properties and Multivariate Analysis. Energy Fuels 21, 2212–2215 (2007).

8. Koshets, I. A., Kazantseva, Z. I., Shirshov, Y. M., Cherenok, S. A. & Kalchenko, V. I. Calixarene films as sensitive coatings for QCM-based gas sensors. Sens. Actuators B Chem. 106, 177–181 (2005).

9. Pereira, R. C. C., Skrobot, V. L., Castro, E. V. R., Fortes, I. C. P. & Pasa, V. M. D. Determination of Gasoline Adulteration by Principal Components Analysis-Linear Discriminant Analysis Applied to FTIR Spectra. Energy Fuels 20, 1097–1102 (2006).

10. Aleme, H. G., Costa, L. M. & Barbeira, P. J. S. Determination of gasoline origin by distillation curves and multivariate analysis. Fuel 87, 3664–3668 (2008).

11. de Oliveira, F. S., Gomes Teixeira, L. S., Ugulino Araujo, M. C. & Korn, M. Screening analysis to detect adulterations in Brazilian gasoline samples using distillation curves. Fuel 83, 917–923 (2004).

12. McConnell, V. D. & Schwab, R. M. The Impact of Environmental Regulation on Industry Location Decisions: The Motor Vehicle Industry. Land Econ. 66, 67 (1990).

13. Bourgeois, W., Romain, A.-C., Nicolas, J. & Stuetz, R. M. The use of sensor arrays for environmental monitoring: interests and limitations. J. Environ. Monit. 5, 852 (2003).

14. Current, R. B. C. T. EPA Proposes Mandatory Methane Reduction Despite Declining Emissions. Policy (2015).

15. Hagleitner, C., Lange, D., Hierlemann, A., Brand, O. & Baltes, H. CMOS single-chip gas detection system comprising capacitive, calorimetric and mass-sensitive microsensors. IEEE J. Solid-State Circuits 37, 1867–1878 (2002).

16. Balabin, R. M. & Safieva, R. Z. Gasoline classification by source and type based on near infrared (NIR) spectroscopy data. Fuel 87, 1096–1101 (2008).

17. Fernandes, H. L., Jr, I. M. R., Pasquini, C. & Rohwedder, J. J. R. Simultaneous determination of methanol and ethanol in gasoline using NIR spectroscopy: Effect of gasoline composition. Talanta 75, 804–810 (2008).

18. Gentry, S. J. & Jones, T. A. The role of catalysis in solid-state gas sensors. Sens. Actuators 10, 141–163 (1986).

19. Flumignan, D. L., Boralle, N. & Oliveira, J. E. de. Screening Brazilian commercial gasoline quality by hydrogen nuclear magnetic resonance spectroscopic fingerprintings and pattern-recognition multivariate chemometric analysis. Talanta 82, 99–105 (2010).

20. Gaião, E. da N. et al. An inexpensive, portable and microcontrolled near infrared LED-photometer for screening analysis of gasoline. Talanta 75, 792–796 (2008).

21. Kaiser, C. R., Borges, J. L., dos Santos, A. R., Azevedo, D. A. & D′Avila, L. A. Quality control of gasoline by 1H NMR: Aromatics, olefinics, paraffinics, and oxygenated and benzene contents. Fuel 89, 99–104 (2010).

22. Monteiro, M. R. et al. Study of Brazilian Gasoline Quality Using Hydrogen Nuclear Magnetic Resonance (1 H NMR) Spectroscopy and Chemometrics. Energy Fuels 23, 272–279 (2009).

23. Tan, K. M. et al. Toward the Development of Raman Spectroscopy as a Nonperturbative Online Monitoring Tool for Gasoline Adulteration. Anal. Chem. 85, 1846–1851 (2013).

24. Teixeira, L., Oliveira, F., Dossantos, H., Cordeiro, P. & Almeida, S. Multivariate calibration in Fourier transform infrared spectrometry as a tool to detect adulterations in Brazilian gasoline. Fuel 87, 346–352 (2008).

25. Ayad, M. M. & Torad, N. L. Alcohol vapours sensor based on thin polyaniline salt film and quartz crystal microbalance. Talanta 78, 1280–1285 (2009).

26. Ding, B., Kim, J., Miyazaki, Y. & Shiratori, S. Electrospun nanofibrous membranes coated quartz crystal microbalance as gas sensor for NH3 detection. Sens. Actuators B Chem. 101, 373–380 (2004).

27. Di Natale, C. et al. Lung cancer identification by the analysis of breath by means of an array of non-selective gas sensors. Biosens. Bioelectron. 18, 1209–1218 (2003).

28. Bello, A. et al. Potentialities of a modified QCM sensor for the detection of analytes interacting via H-bonding and application to the determination of ethanol in bread. Sens. Actuators B Chem. 125, 321–325 (2007).

29. Rehman, A. et al. Differential Solute Gas Response in Ionic-Liquid-Based QCM Arrays: Elucidating Design Factors Responsible for Discriminative Explosive Gas Sensing. Anal. Chem. 83, 7823–7833 (2011).

30. Jin, X., Yu, L., Garcia, D., Ren, R. X. & Zeng, X. Ionic Liquid High-Temperature Gas Sensor Array. Anal. Chem. 78, 6980–6989 (2006).

31. Toniolo, R. et al. Room Temperature Ionic Liquids As Useful Overlayers for Estimating Food Quality from Their Odor Analysis by Quartz Crystal Microbalance Measurements. Anal. Chem. 85, 7241–7247 (2013).

32. Liang, C., Yuan, C.-Y., Warmack, R. J., Barnes, C. E. & Dai, S. Ionic Liquids: A New Class of Sensing Materials for Detection of Organic Vapors Based on the Use of a Quartz Crystal Microbalance. Anal. Chem. 74, 2172–2176 (2002).

33. Regmi, B. P. et al. A novel composite film for detection and molecular weight determination of organic vapors. J. Mater. Chem. 22, 13732 (2012).

34. Regmi, B. P. et al. Molecular weight sensing properties of ionic liquid-polymer composite films: theory and experiment. J Mater Chem C 2, 4867–4878 (2014).

35. Bachar, N. et al. Sensor Arrays Based on Polycyclic Aromatic Hydrocarbons: Chemiresistors versus Quartz-Crystal Microbalance. ACS Appl. Mater. Interfaces 5, 11641–11653 (2013).

36. Speller, N. C. et al. Rational Design of QCM-D Virtual Sensor Arrays Based on Film Thickness, Viscoelasticity, and Harmonics for Vapor Discrimination. Anal. Chem. 87, 5156–5166 (2015).

37. Umali, A. P. & Anslyn, E. V. A general approach to differential sensing using synthetic molecular receptors. Curr. Opin. Chem. Biol. 14, 685–692 (2010).

38. Albert, K. J. et al. Cross-Reactive Chemical Sensor Arrays. Chem. Rev. 100, 2595–2626 (2000).

39. Suslick, B. A., Feng, L. & Suslick, K. S. Discrimination of Complex Mixtures by a Colorimetric Sensor Array: Coffee Aromas. Anal. Chem. 82, 2067–2073 (2010).

40. Hierlemann, A., Weimar, U., Kraus, G., Schweizer-Berberich, M. & Göpel, W. Polymer-based sensor arrays and multicomponent analysis for the detection of hazardous oragnic vapours in the environment. Sens. Actuators B Chem. 26, 126–134 (1995).

41. Janzen, M. C., Ponder, J. B., Bailey, D. P., Ingison, C. K. & Suslick, K. S. Colorimetric Sensor Arrays for Volatile Organic Compounds. Anal. Chem. 78, 3591–3600 (2006).

42. Galpothdeniya, W. I. S. et al. Ionic liquid-based optoelectronic sensor arrays for chemical detection. RSC Adv 4, 7225–7234 (2014).

43. Koo, C.-K., Samain, F., Dai, N. & Kool, E. T. DNA polyfluorophores as highly diverse chemosensors of toxic gases. Chem. Sci. 2, 1910 (2011).

44. Kwon, H., Samain, F. & Kool, E. T. Fluorescent DNAs printed on paper: sensing food spoilage and ripening in the vapor phase. Chem. Sci. 3, 2542 (2012).

45. Xu, X. et al. Ionic liquids used as QCM coating materials for the detection of alcohols. Sens. Actuators B Chem. 134, 258–265 (2008).

46. Xu, X., Cang, H., Li, C., Zhao, Z. K. & Li, H. Quartz crystal microbalance sensor array for the detection of volatile organic compounds. Talanta 78, 711–716 (2009).

47. Goubaidoulline, I., Vidrich, G. & Johannsmann, D. Organic Vapor Sensing with Ionic Liquids Entrapped in Alumina Nanopores on Quartz Crystal Resonators. Anal. Chem. 77, 615–619 (2005).

48. Makino, W., Kishikawa, R., Mizoshiri, M., Takeda, S. & Yao, M. Viscoelastic properties of room temperature ionic liquids. J. Chem. Phys. 129, 104510 (2008).

49. Yamaguchi, T., Miyake, S. & Koda, S. Shear Relaxation of Imidazolium-Based Room-Temperature Ionic Liquids. J. Phys. Chem. B 114, 8126–8133 (2010).

CHAPTER 6. CONCLUSIONS AND FUTURE WORK

6.1 Conclusions

VOCs are a ubiquitous class of organic chemicals emitted from numerous sources, both natural and artificial. Due to the health and environmental impact of VOCs, as well as the characteristic nature of VOC emissions, analyses of this class of chemicals has proven increasingly important. Hence, there is a need for simple yet inexpensive methods to perform VOC analyses. In this regard, gas sensor technology has garnered much interest in recent years. Typically, such sensors are comprised of a chemosensitive material coupled with an appropriate transducer. In fact, this dissertation employed sorption based gas sensors, comprised of organic salts based recognition elements and a QCM transducer. Organic salts, specifically ionic liquids and GUMBOS are attractive chemosensitive materials due to favorable properties including simple synthesis, tunable physicochemical properties, and negligible vapor pressure. Among transducers, the QCM is lauded for its simplistic operation and excellent sensitivity. While such sensors are promising for detection of VOCs, they are typically inefficient for discrimination of VOCs. Hence, sensor arrays are employed. In Chapter 1, an introduction to VOCs, gas sensors and sensor arrays, statistical analysis, and relevant background of the QCM is presented.

The theory of QCM virtual sensing, fabrication of QCM virtual sensor arrays, discrimination of 18 VOCs, and real samples are presented in chapter 2. These studies introduce the first example of a virtual sensing scheme for the QCM. Furthermore, sensor arrays employing this scheme were designed and implemented to discriminate between several closely related homologous series of VOCs. Additionally discrimination between two related real samples was tested. The success of this foundational study led to further research in this area, as well as development of another powerful sensing scheme.

In chapter 3, design and implementation of a QCM VSA for discrimination and molecular weight approximation of VOCs is presented. These studies are the first example of a sensor array with molecular weight approximation capabilities. Notably, a homologous series of alcohols including isomeric alcohols were discriminated and the molecular weight approximated in a single experimental step. This was accomplished using the favorable properties of an ionic liquid-polymer composite chemosensitive layer. These studies are a foundational step towards the development of a QCM based system that could be an inexpensive niche alternative to mass spectrometry.

A comparative assessment of the alternative virtual sensor array scheme and the traditional multisensor array scheme for complex volatile mixture analysis is presented in Chapter 4. Additionally, a new sensing scheme called the virtual multisensor array, which is a combination of the VSA and MSA schemes, is introduced. In this regard, each array was utilized to discriminate between five complex volatile mixtures represented by citrus type odors. The classification accuracy for each array was assessed to determine the most useful array sensing approach for complex mixture analysis. These studies further examined the utility of each array type, and introduced a very powerful method, in the form of the V-MSA, for discriminating between volatile complex mixtures.

In the previous chapter, it was discovered that the V-MSA approach is a powerful technique for analyzing volatile complex mixtures. In chapter 5, the V-MSA approach was tested for analyzing a real world application. Hence, the VMSA was utilized to identify petroleum based fuels, gasoline grades, and adulterated gasoline. These studies are the first example of a QCM sensor array applied towards fuel related issues. The excellent results of these studies suggest that this simplistic technique could hold great promise for real world applications. Overall, the culmination of studies presented in this dissertation represents a great step in advancement of QCM based measurements within the field of measurement science.

6.2 Future Work

The work within this dissertation has demonstrated the utility of novel QCM based array sensing schemes employing organic salts. While this work is primarily focused on the development of novel sensor arrays, there are a host of areas where further investigation could be undertaken. Such areas include 1) development of novel chemosensitive materials, 2) further enhancement of existing approaches to incorporate new analytical techniques, and 3) optimization of existing approaches for different applications.

With regard to development of chemosensitive materials, novel materials could be developed to enhance sensitivity and selectivity of the sensors that comprise the presented array sensing schemes. Furthermore, materials could be designed to exhibit specific viscoelastic properties that could be employed to systematically alter sensor response over multiple harmonics in a precise fashion or be used to effectively model each system. Finally other classes of materials could be investigated to ascertain their effectiveness as chemosensitive adlayers in virtual sensing.

In chapter 2, a VSA which can identify VOCs and approximate their molecular weight was developed. This function is rather similar to mass spectrometry. The limitation of this technique is that molecular weight approximation is only possible for pure analytes. Thus analyzing mixtures of VOCs would prove problematic. However if this technique was coupled with gas chromatography, this problem could be readily solved. In this regard, GC could be used to separate volatile mixtures and pure analytes could be introduced to the QCM for identification and molecular weight approximation. This function is analogous to a vastly less expensive niche GC-MS. The coupling of these two systems would represent an enhancement of a presented virtual sensing approach with an additional analytical technique.

Finally, the presented sensing approaches could be optimized for specific applications using a combination of chemosensitive material development and technique enhancement. Moreover virtual sensing in liquid based applications could be investigated. In particular the liquid analog of the electronic nose, i.e the electronic tongue could be developed using a QCM virtual array approach.

APPENDIX A: SUPPORTING INFORMATION FOR CHAPTER TWO

Working Principle of QCM-D

A typical QCM comprises a thin wafer of AT-cut quartz crystal that is inserted between two metallic electrodes. When an external voltage is applied across the quartz crystal, as a result of the piezoelectric characteristics of the quartz, the crystal undergoes thickness shear vibrations. The antinodes of the standing shear wave lie at the surfaces of the crystal, while one or more nodes lie in the bulk of the crystal. In fact, the crystal can be sequentially excited at different harmonics and in this regard, only odd harmonics are possible since the antinodes are always at the surfaces. The resonance frequency and amplitude of the shear waves undergo changes when passing through the coating material immobilized onto the crystal surface. Although different interface electronics are available for QCM measurements, a relatively new approach based on impulse-excitation techniques introduced by Kasemo and coworkers has proven very useful in recent years.[1-3] The QCM instrument based on the impulse-excitation technique is called the quartz crystal microbalance with dissipation monitoring (QCM-D). The QCM-D measures frequency shift (Δf) and dissipation shift (ΔD) at up to seven different harmonics.

In a majority of studies, the QCM has been used only as a mass sensor which is based on the original findings of Sauerbrey who showed that the decrease in resonance frequency is directly related to the mass adsorbed onto the surface.[4] However, the Sauerbrey relationship is only valid for thin, rigid, and uniform films where the dissipation will be negligible. In the case of thick and/or viscoelastic coatings, Δf and ΔD depend on both the mass and the viscoelastic properties of the coating materials. Several researchers have presented details on how the mass and viscoelasticity influence sensor responses, and more detailed equations in this regard can be found in references

cited therein.[5-8] In this regard, we have recently studied the vapor sensing characteristics of IL or IL/polymer-coated QCM sensors, and have demonstrated that for the same mass of different vapors absorbed, the effect on viscoelasticity of the film is different.[9,10] Therefore, it is rational to conclude that different analytes should give different response patterns when multiple harmonic data from IL-based QCM-D are analyzed with suitable pattern recognition techniques. Furthermore, it follows that it should be possible to create sensor arrays by exploiting the viscoelastic properties of the coating materials, rather than primarily using chemical affinity as a factor for chemical discrimination.

Experimental Section

Reagents and Materials

The ILs, 1-octyl-3-methylimidazolium bromide ([OMIm][Br]) or 1-octyl-3-methylimidazolium thiocyanate ([OMIm][SCN]), were used to prepare coatings in the present studies. Anhydrous acetonitrile, anhydrous acrylonitrile, anhydrous chloroform (CCL3), anhydrous carbon tetrachloride (CCL4), anhydrous dicholoroethane (DCE), 1-chlorohexane, anhydrous toluene, anhydrous 1-butanol, 1-pentanol, 1-propanol, anhydrous 1-hexanol, 1-octanol, p-xylene, n-hexane, cyclohexane, methanol were obtained from Sigma-Aldrich (St. Louis, MO, USA). Dichloromethane (DCM) was obtained from Avantor Performance Materials, Inc. (Center Valley, PA, USA). Absolute ethanol was obtained from Pharmco Products, Inc. (Brookfield, CT, USA). All chemicals were used as received without any further purification. The QCM-D E4 system and gold-coated AT-cut quartz crystals with a diameter of 14 mm and a fundamental frequency of 5 MHz were purchased from Q-Sense AB (Gothenburg, Sweden). Readout equipment (Model 5878) as well as mass flow controllers (Model 5850E) were obtained from Brooks Instrument, LLC (Hatfield, PA, USA).

Synthesis of Ionic Liquids

The IL [OMIm][Br] utilized here was synthesized by alkylation of methyl imidazole, using 1-bromooctane. Briefly, a mixture containing a 1:1.1 ratio of 1-methylimidazole to 1-bromooctane in methanol was refluxed at 70 °C for 72 hours to directly generate the ionic liquid. This ionic liquid was then used to synthesize [OMIm][SCN] via a simple anion exchange reaction. This was achieved by dissolving [OMIm][Br] and KSCN in acetonitrile using a 1:2 mole ratio and stirring for 48 hours to facilitate ion exchange. The byproducts, KBr and excess KSCN, were then filtered from solution. The solution, which contained the product, was placed on a rotary evaporator to remove excess acetonitrile. Next, the product was redissolved into cooled dichloromethane (4°C). The remaining solid byproduct was again filtered. After rotary evaporation to remove the excess DCM, [OMIm][SCN] was obtained. The EDS spectra of these compounds are shown in figure A2, while the structures are shown in scheme A1.

Film Preparation

In these studies, a solution containing IL (1mg/mL) in DCM was used for electrospraying. The optimized electrospray parameters chosen to prepare these coatings were 1) voltage of 2.8 V, 2) current of 3 Amps, and 3) flow rate of 100 μL/min. The working distance between the nozzle and the quartz crystal resonator (QCR) was set at 7 cm. These parameters were chosen because they allowed a sufficient mass of materials to be coated onto the gold surface, while enabling evaporation of the organic solvent during prolonged coating times. In order to obtain films of different thicknesses, only the coating time was changed while maintaining other parameters constant.

2.3 Film Characterization

Films were imaged using a JEOL JEM-6610LV Scanning Electron Microscope (SEM) in high vacuum mode. Energy Dispersive X-ray Spectroscopy (EDS) was performed with the same microscopy system using an EDAX instrument.

Table A1 Analytes and their physical properties

Table 1. Analytes and their physical properties

Class	Compound	Molecular Weight	Vapor Pressure (kPA @ 25°C)	Dielectric Constant (Ambient Temperature)	Density (g/mL @ 20 or 25°C)
n-Alcohols					
	Methanol	32.04	16.9	33.0	0.791 (20°C)
	Ethanol	46.06	7.87	25.3	0.789 (20°C)
	1-Propanol	60.09	2.76	20.8	0.799 (25°C)
	1-Butanol	74.12	0.86	17.8	0.809 (20°C)
	1-Pentanol	88.14	0.25	15.1	0.814 (20°C)
	1-Hexanol	102.1	0.11	13.0	0.813 (20°C)
	1-Octanol	130.2	0.01	10.3	0.826 (25°C)
Chloromethanes					
	Dichloromethane	84.93	58.2	8.93	1.326 (20°C)
	Chloroform	119.3	26.2	4.80	1.478 (25°C)
	Carbon Tetrachloride	153.8	15.2	2.23	1.594 (20°C)
	1,2 -Dichloroethane	98.95	10.6	10.42	1.175 (20°C)
	1-Chlorohexane	120.6	-	-	0.878 (20°C)
Aromatic Hydrocarbons					
	Toluene	92.13	3.79	2.37	0.866 (20°C)
	p-Xylene	106.1	1.19	2.27	0.856 (25°C)
	Cyclohexane	84.15	13.0	2.02	0.773 (25°C)
	n-Hexane	86.17	20.2	1.88	0.660 (25°C)
Nitriles					
	Acetonitrile	41.05	11.9	36.6	0.785 (20°C)
	Acrylonitrile	43.06	14.1	33.0	0.800 (25°C)

Table A2 Discriminant Analysis Classification Accuracy Derived from Cross Validation

Table 2. Discriminant Analysis Classification Acurracy Derived from Cross Validation

VSA	Classification Accuracy (%)			
	[OMIm][Br] 3min	[OMIm][Br] 1min	[OMIm][SCN] 3min	[OMIm][SCN] 1min
Intraclass				
Alcohols	98.4	100	100	100
Chlorohydrocarbons	100	100	100	100
Hydrocarbons	100	100	100	100
Nitriles	100	100	100	100
Low Concentration Chlorohydrocarbons	100	-	100	-
Interclass				
18 Analyte Set (e.g. methanol, ethanol 1-propanol, 1-butanol, 1-pentanol, 1-hexanol, 1-octanol, p-xylene, toluene, cyclohexane, n-hexane, dichloromethane, chloroform, carbon tetratchloride, dichloroethane, 1-chlorohexane, acetonitrile, acrylonitrile)	97.6	100	98.7	100
Complex Mixture				
Petroleum Ether and Kerosene	100	-	100	-

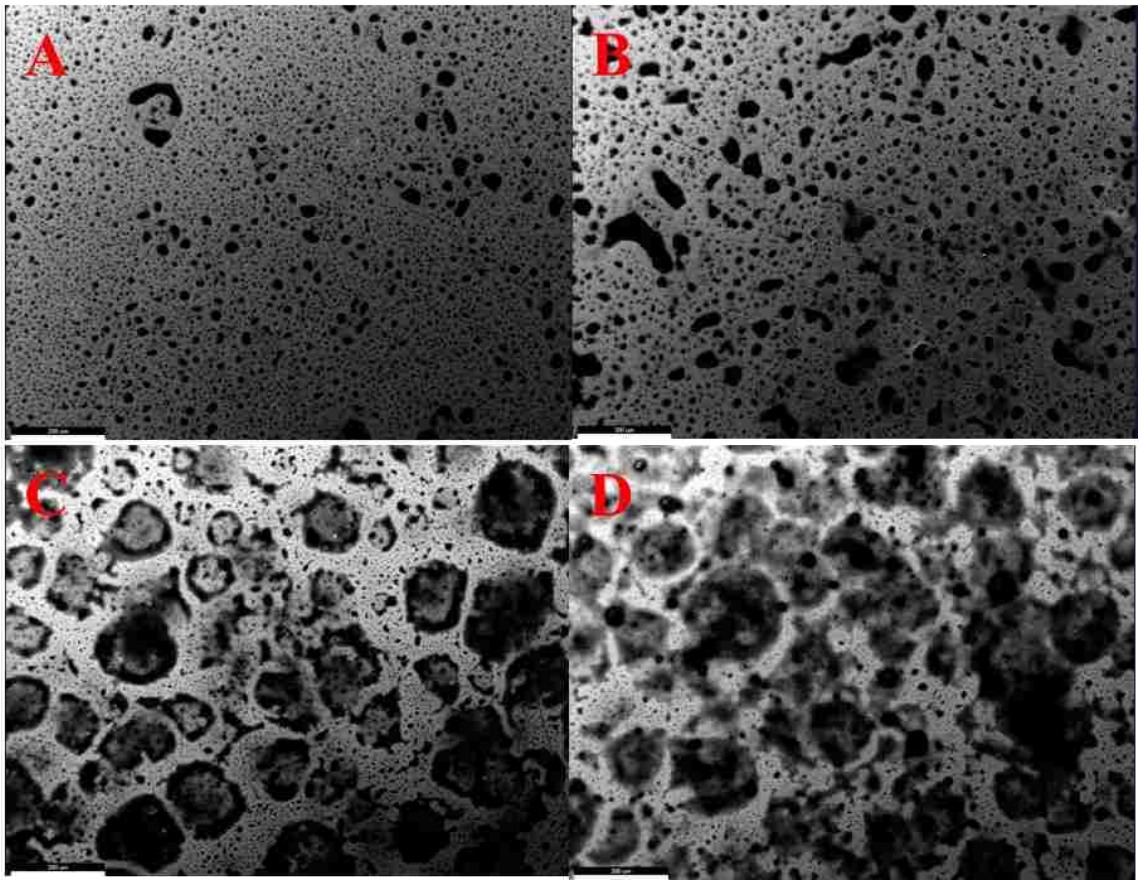

Figure A1. SEM images of A) 1.5 minute [OMIm][SCN] film B) 3 minute [OMIm][SCN] film, C) 1.5 minute [OMIm][Br] film D) 3 minute [OMIm][Br] film. Scale bar represents 200 µm.

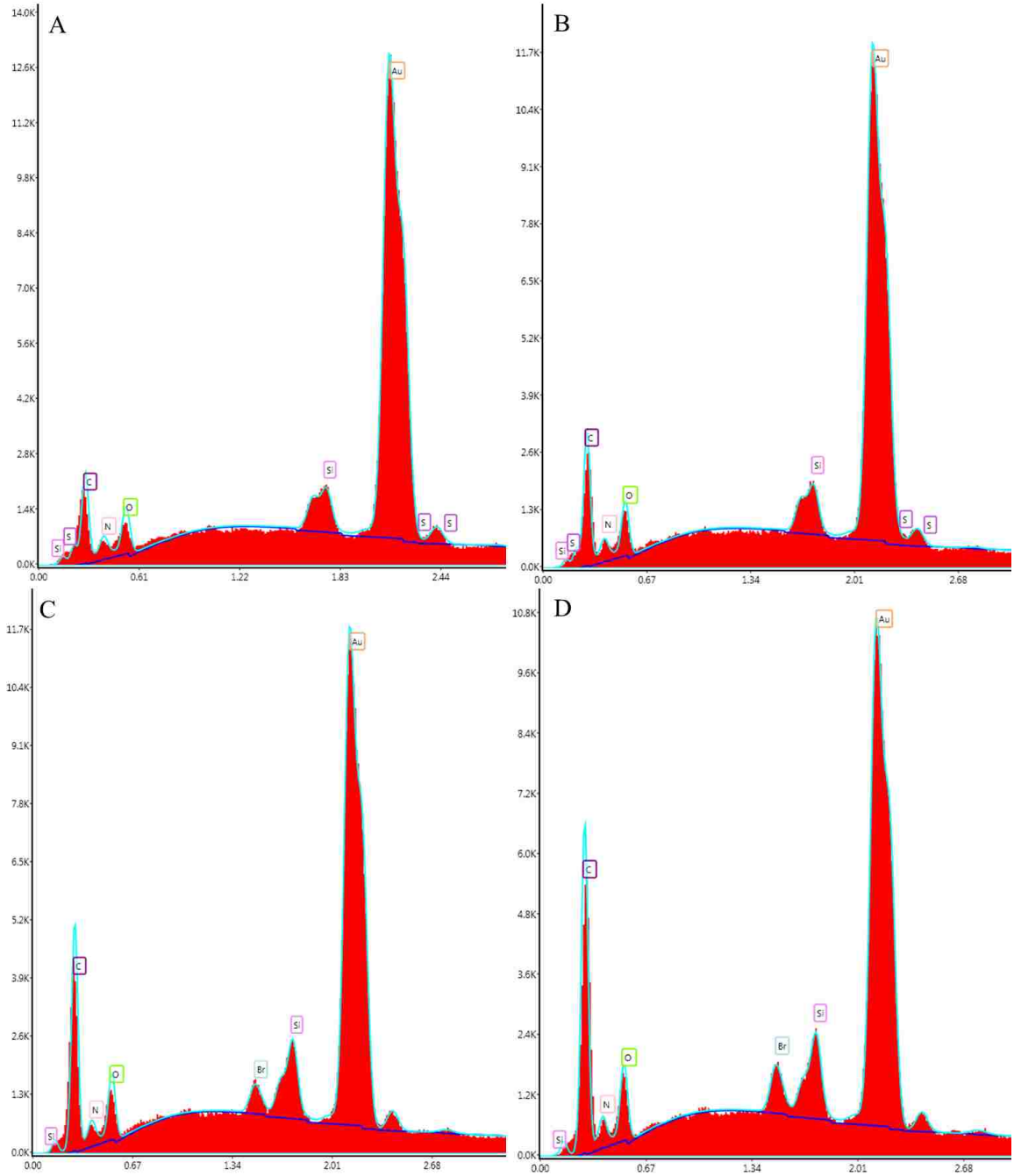

Figure A2. EDS Spectra of A) 1.5 minute [OMIm][SCN] film B) 3 minute [OMIm][SCN] film, C) 1.5 minute [OMIm][Br] film D) 3 minute [OMIm][Br] film representing the relative amount of each element.

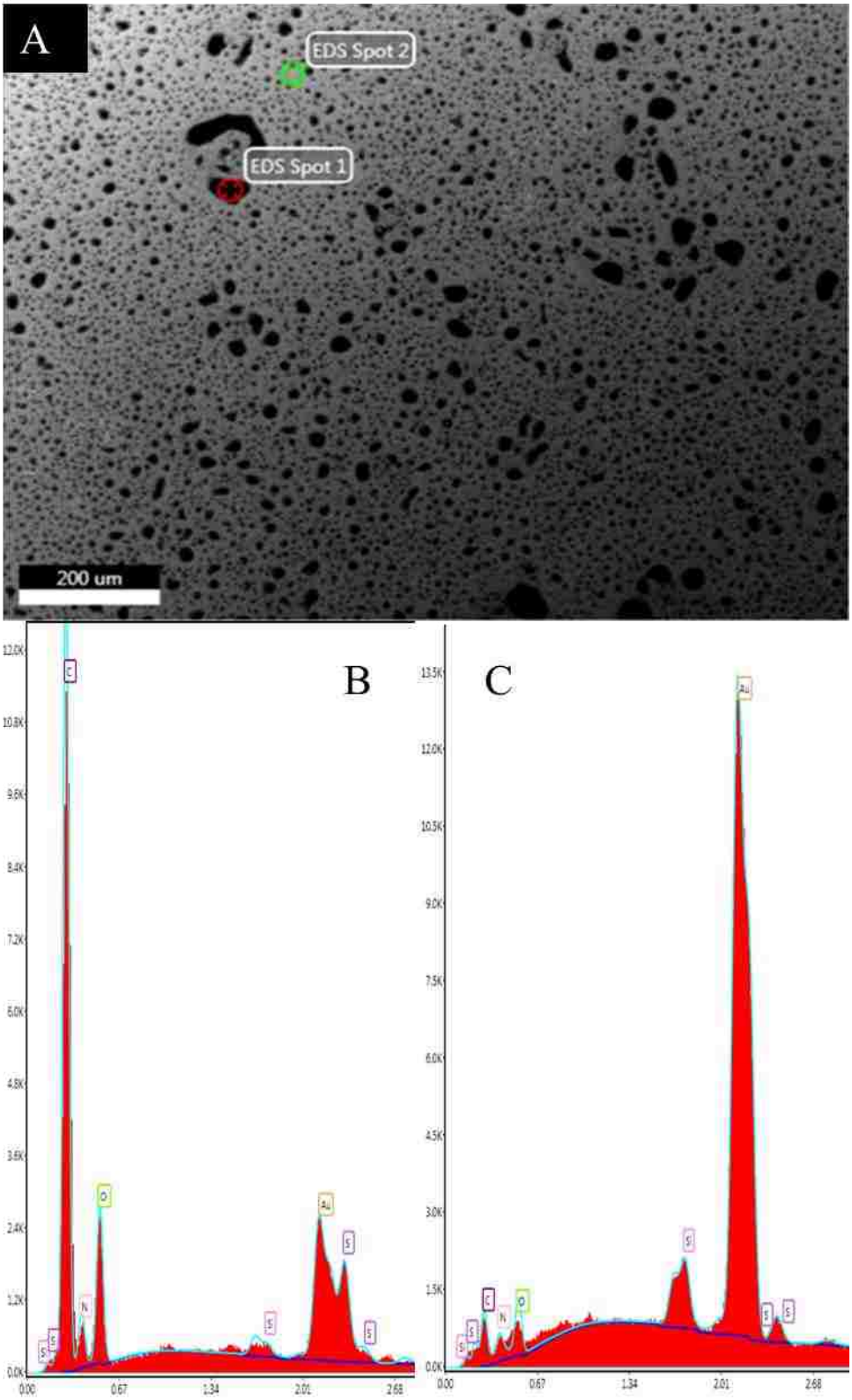

Figure A3. A) SEM Image with two highlighted spots. EDS point analysis spectra of a 1.5 minute [OMIm][SCN] film for B) spot 1, an area which corresponds to ionic liquid and C) spot 2 an area which contains significantly less ionic liquid, i.e. mostly gold surface

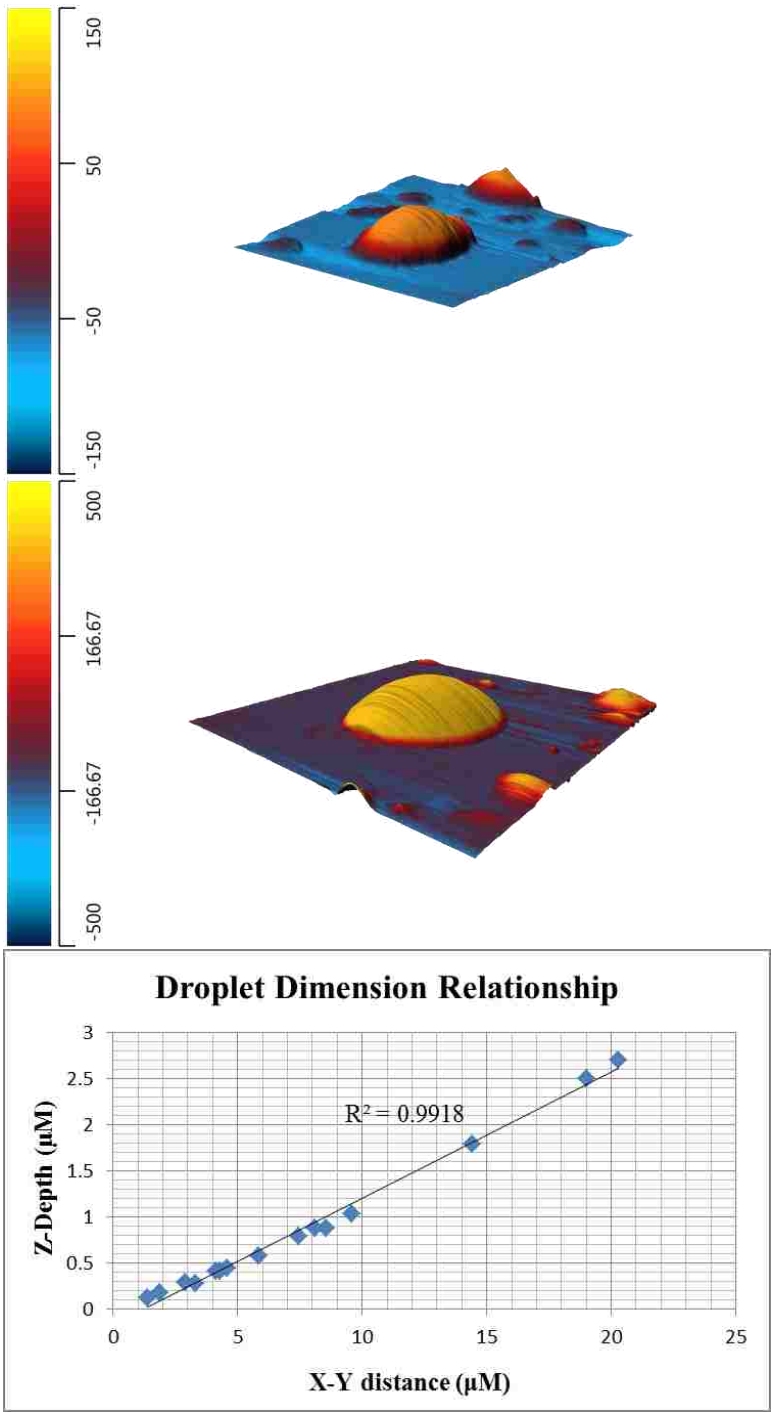

Figure A4. A number of droplets were measured to ascertain the effect of increased droplet size on film thickness via AFM. It was found that X-Y distance of droplet and Z-Depth varied proportionally. As coatings are not homogenous, droplets of varying sizes were measured. A) AFM image of a small droplet. B) AFM image of a large droplet C) Scatter plot of size in the x-y dimesion versus Z-Depth for droplets of varying sizes.

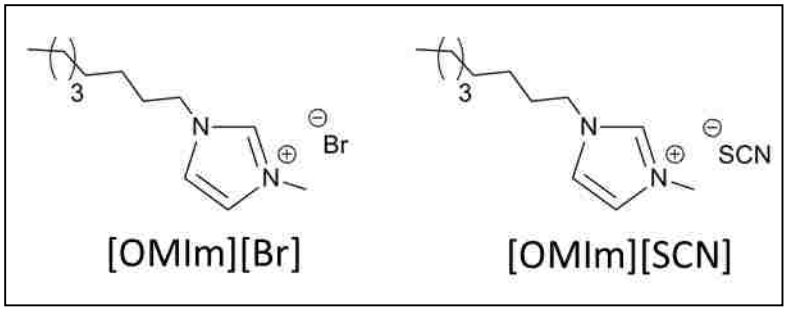

Scheme A1. Chemical structure of [OMIm][Br] and [OMIm][SCN]

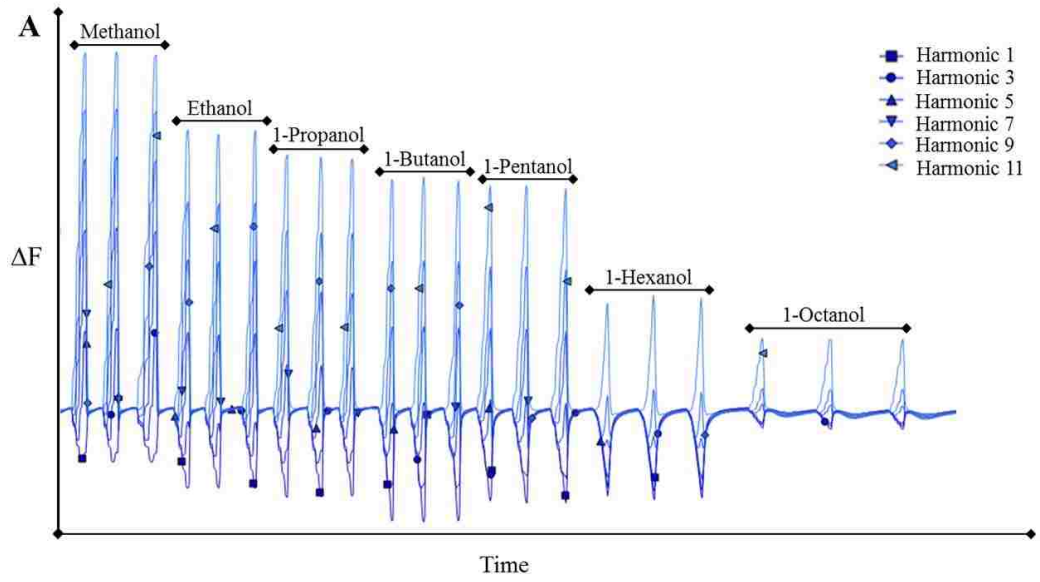

Figure A5. Sensorgrams for the class of alcohols for A) 3 minute [OMIm][Br] film.

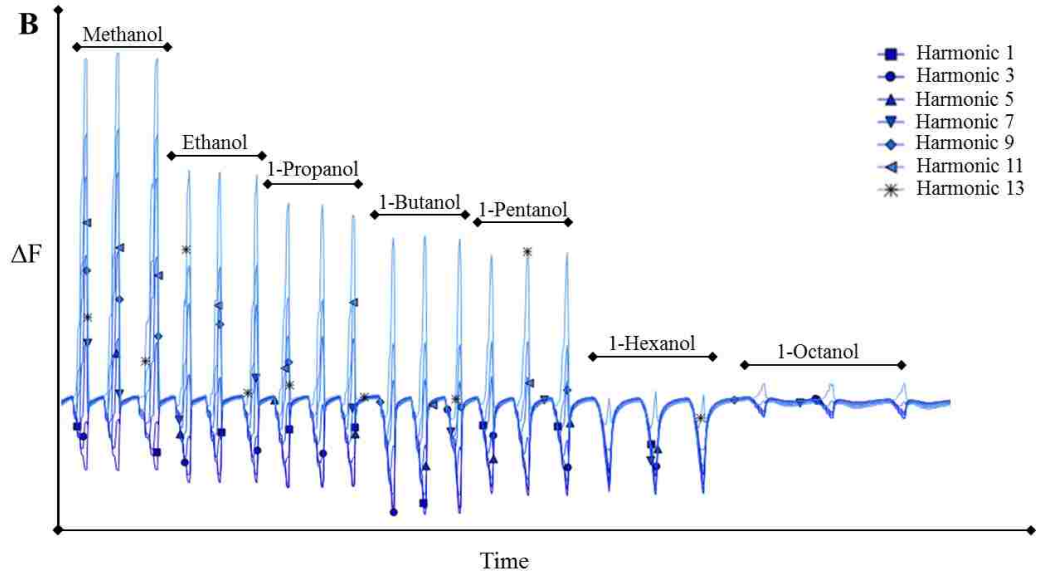

Figure A6. Sensorgrams for the class of alcohols for B) 1.5 minute [OMIm][Br] film

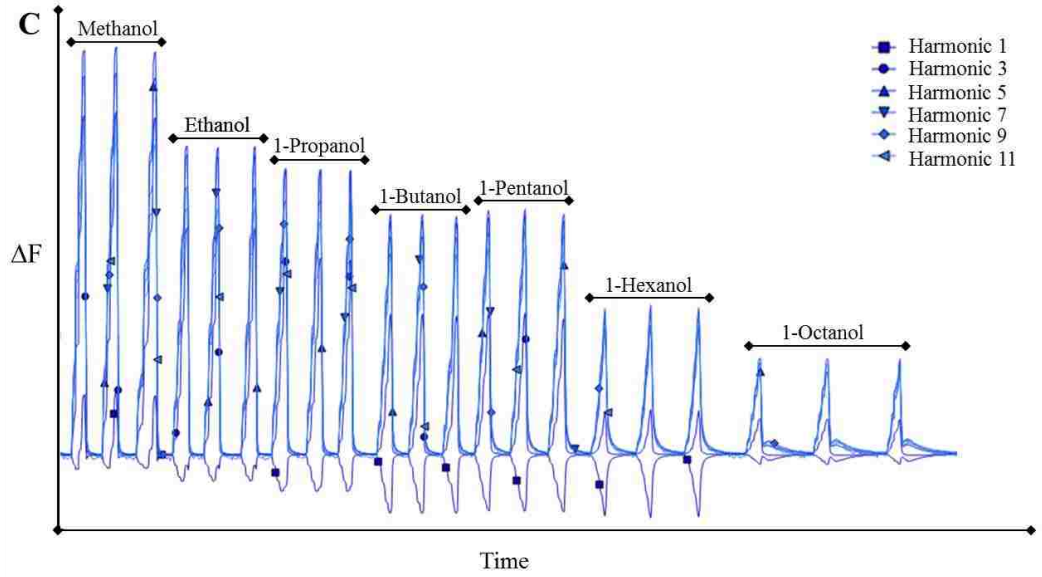

Figure A7. Sensorgrams for the class of alcohols for C) 3 minute [OMIm][SCN] film

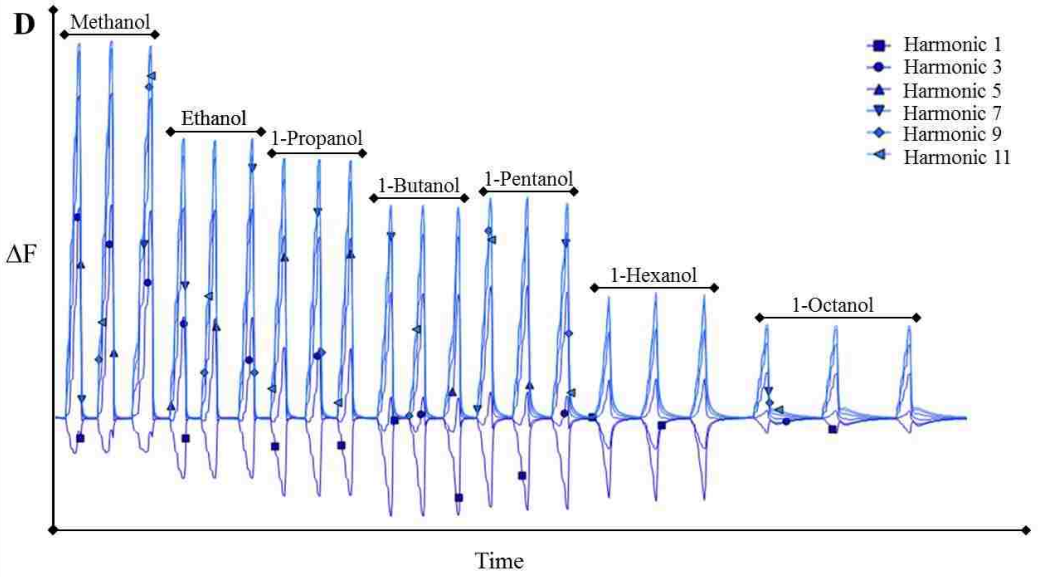

Figure A8. Sensorgrams for the class of alcohols for D) 1.5 minute [OMIm][SCN] film.

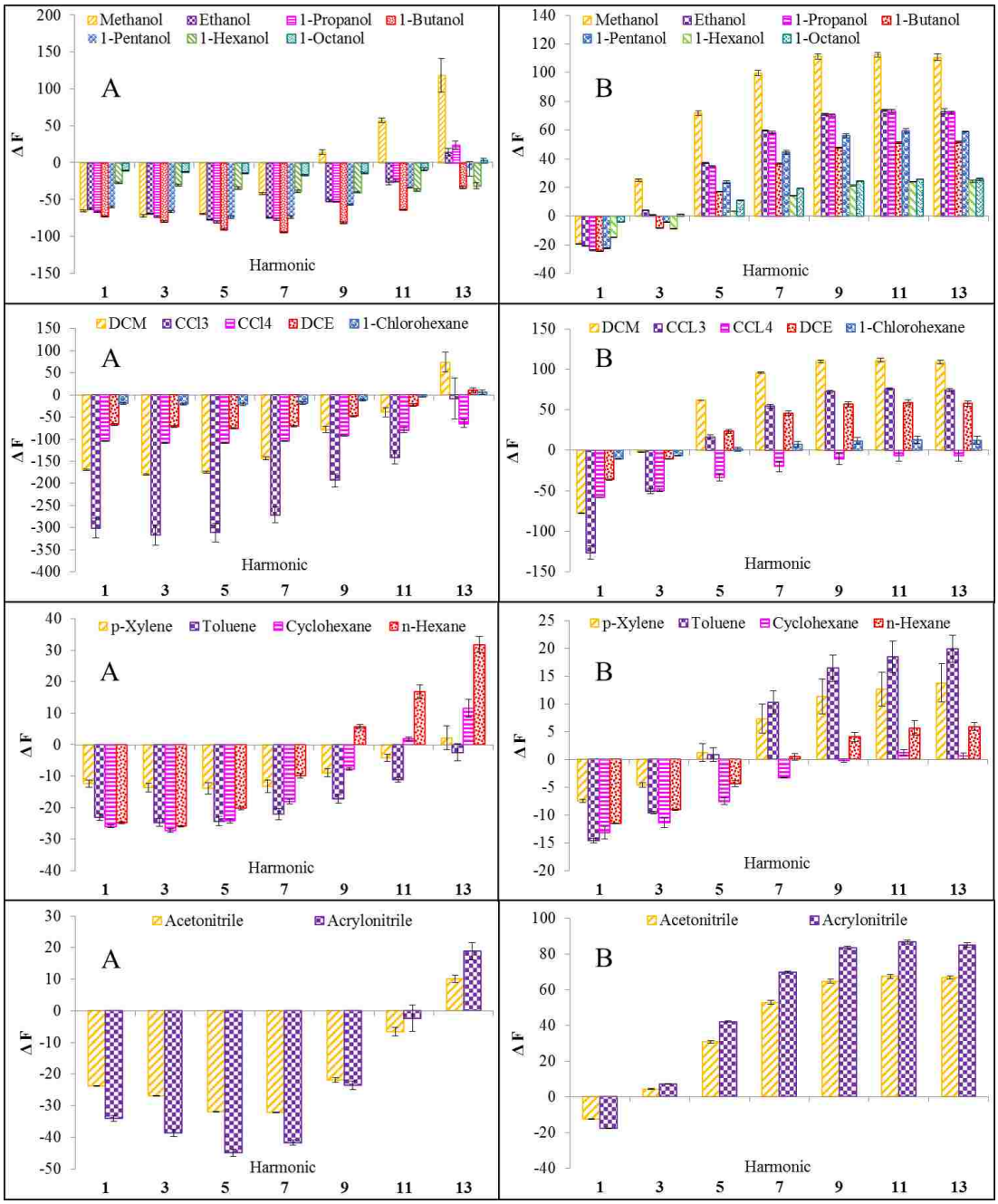

Figure A9. Δ*f* response patterns for each class of vapors (in descending order n-alcohols, chlorohydrocarbons, hydrocarbons, and nitriles) are shown for a A) 1.5 minute [OMIm][Br] coating based sensor and B) 1.5 minute [OMIm][SCN] coating based sensor. The vapor partial pressure for all analytes is fixed at $p_a/p_o = 0.2$. Error bars represent the standard deviations of three replicate measurements.

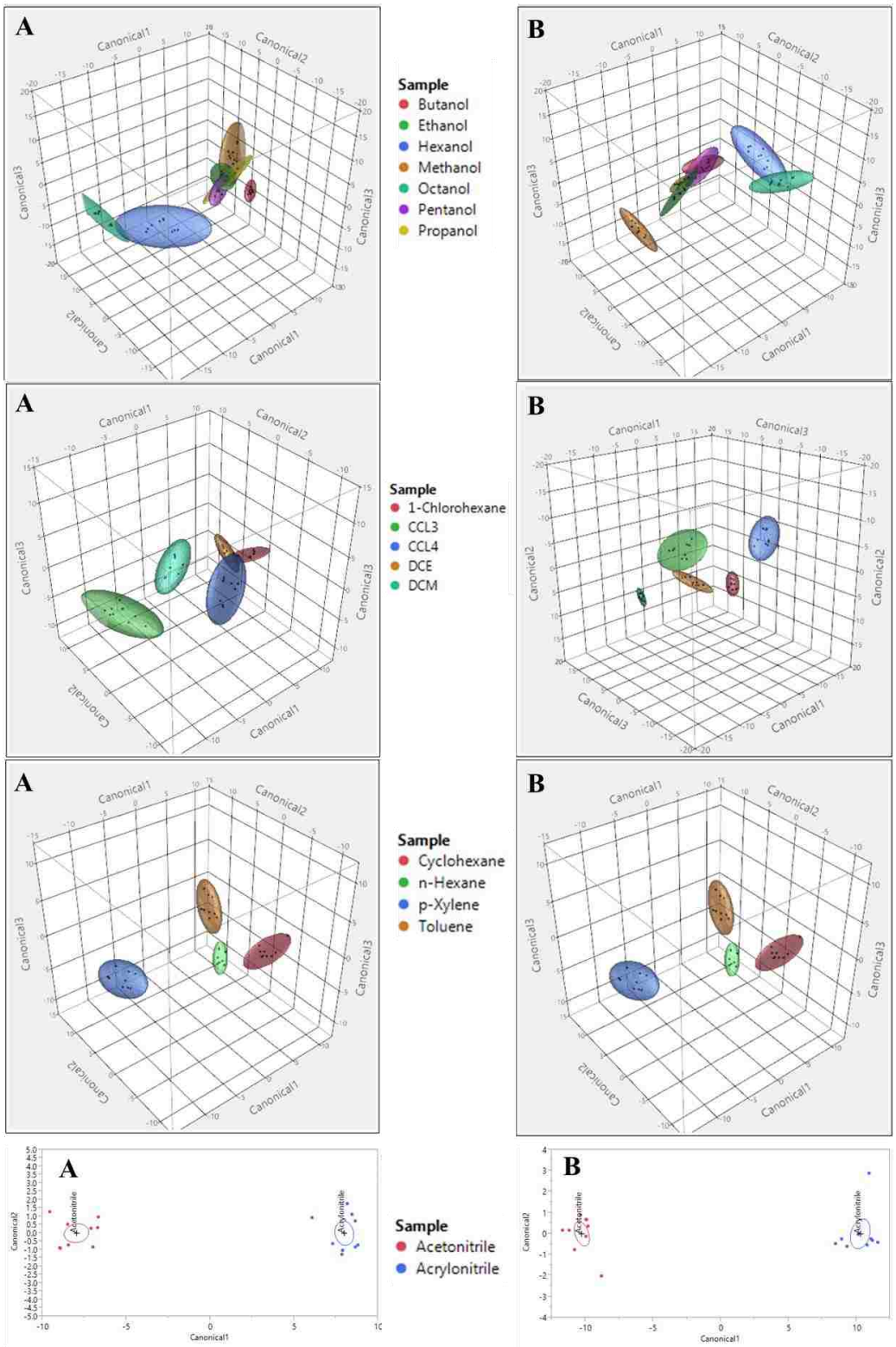

Figure A10. QDA Canonical plots for each class of organic vapors (in descending order n-alcohols, chlorohydrocarbons, nitriles, and hydrocarbons) with respect to a VSA comprised of either a 1.5 minute coating of A) [OMIm][Br] or B) [OMIm][SCN]

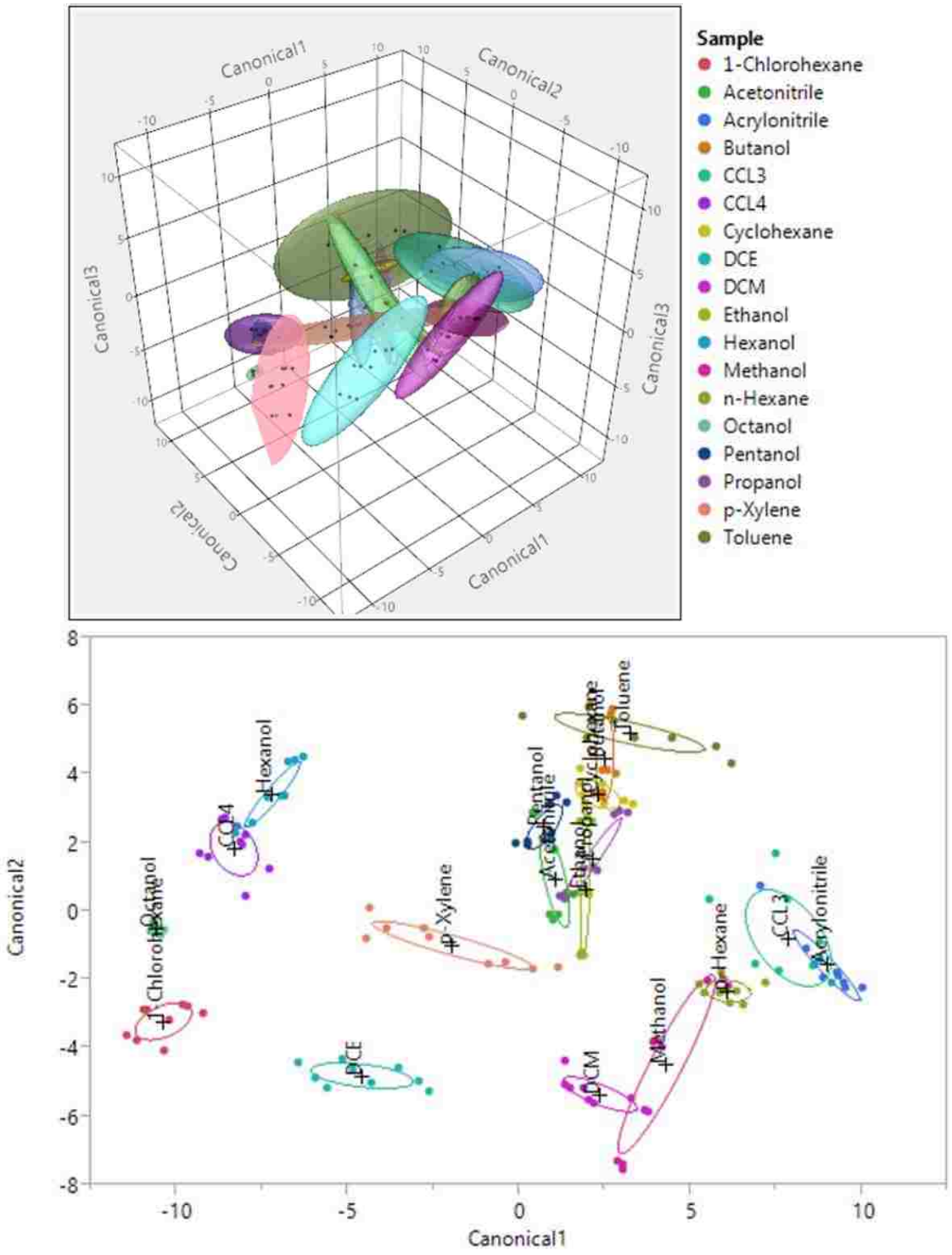

Figure A11. A QDA 3D Canonical plots for the 18 analyte set, over all concentrations, with respect to a VSA comprised of either a 3 minute coating of [OMIm][Br] is presented. To assist visualization a 2D canonical plot is also presented.

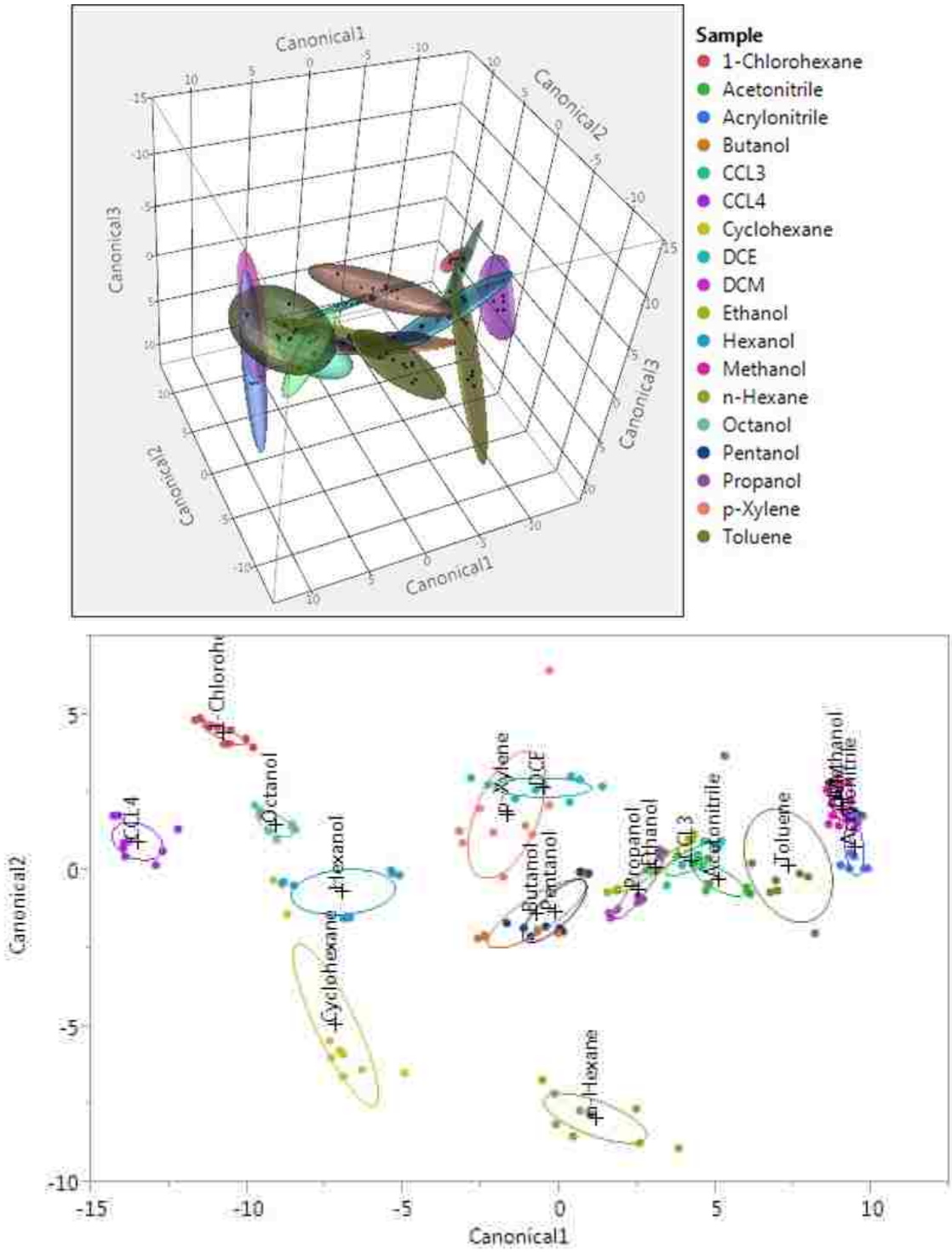

Figure A12. A QDA 3D Canonical plots for the 18 analyte set, over all concentrations, with respect to a VSA comprised of either a 3 minute coating of [OMIm][SCN] is presented. To assist visualization a 2D canonical plot is also presented.

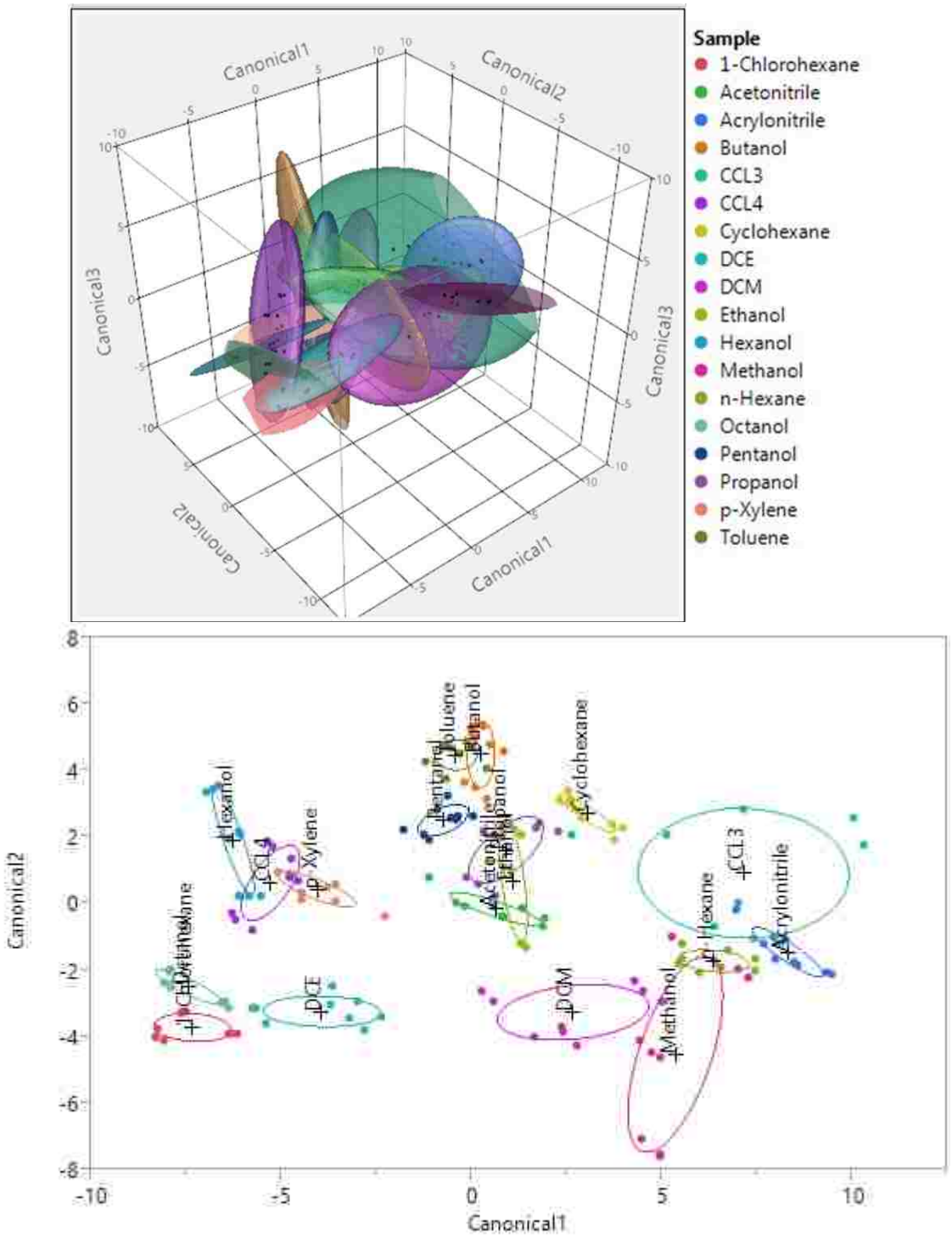

Figure A13. A QDA 3D Canonical plots for the 18 analyte set, over all concentrations, with respect to a VSA comprised of either a 1.5 minute coating of [OMIm][Br] is presented. To assist visualization a 2D canonical plot is also presented.

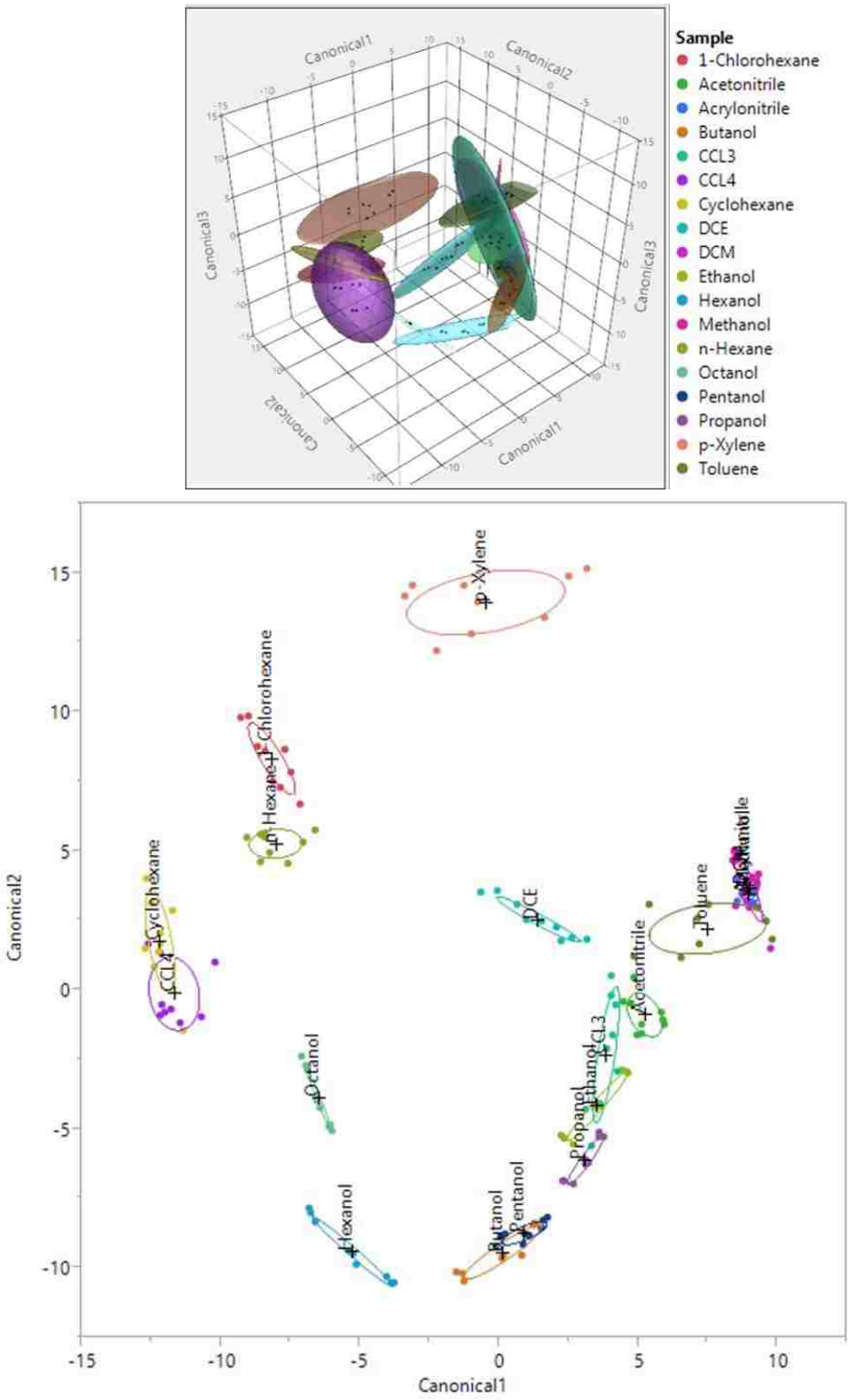

Figure A14. A QDA 3D Canonical plots for the 18 analyte set, over all concentrations, with respect to a VSA comprised of either a 1.5 minute coating of [OMIm][SCN] is presented. To assist visualization a 2D canonical plot is also presented.

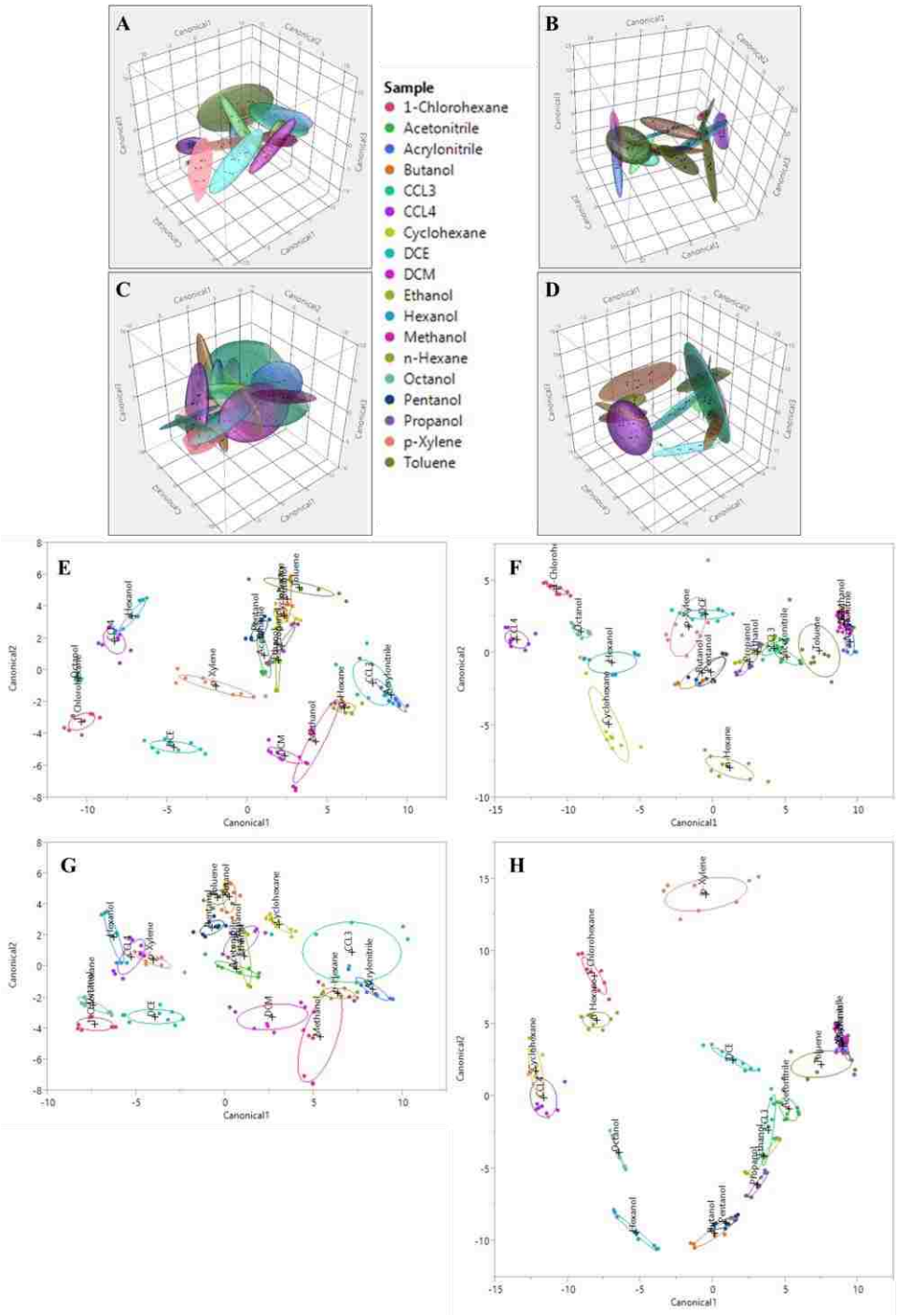

Figure A15. QDA 3D Canonical plots for the 18 analyte set, over all concentrations, with respect to a VSA comprised of either a 3 minute coating of A) [OMIm][Br] or B) [OMIm][SCN] or a 1.5 minute coating of C) [OMIm][Br] or D) [OMIm][SCN]. To assist visualization 2D canonical plots are also presented with respect to a VSA comprised of either a 3 minute coating of E) [OMIm][Br] or F) [OMIm][SCN] or a 1.5 minute coating of G) [OMIm][Br] or H) [OMIm][SCN].

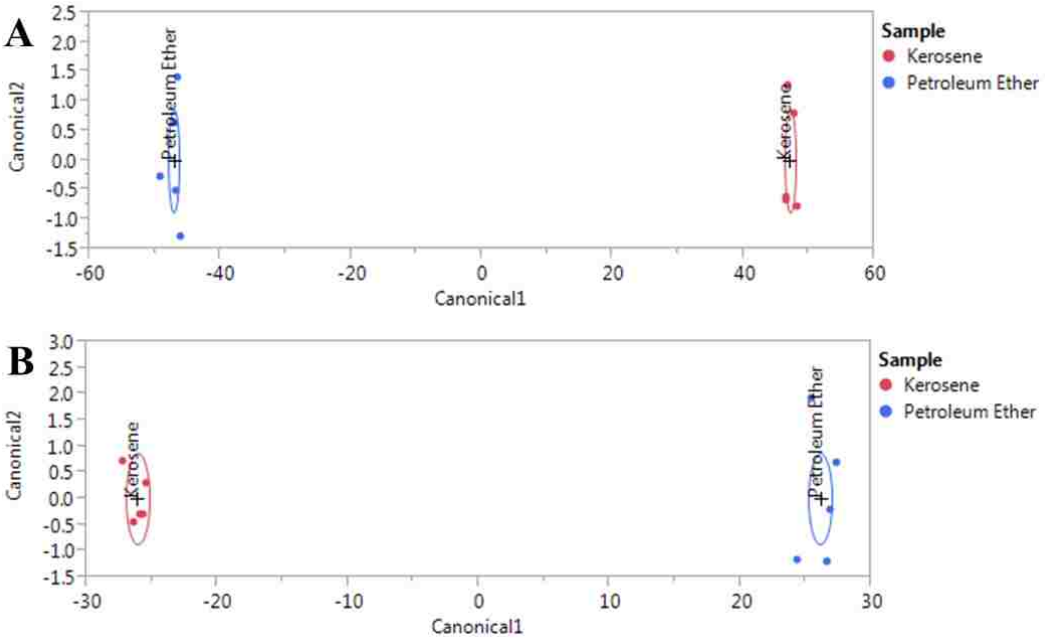

Figure A16. LDA Canonical plots for the real sample, at p_a/p_o =0.2, with respect to a VSA comprised of either a 3 minute coating of A) [OMIm][Br] or B) [OMIm][SCN]. LDA was used for the presented analysis due to small data set size.

APPENDIX B: SUPPORTING INFORMATION FOR CHAPTER THREE

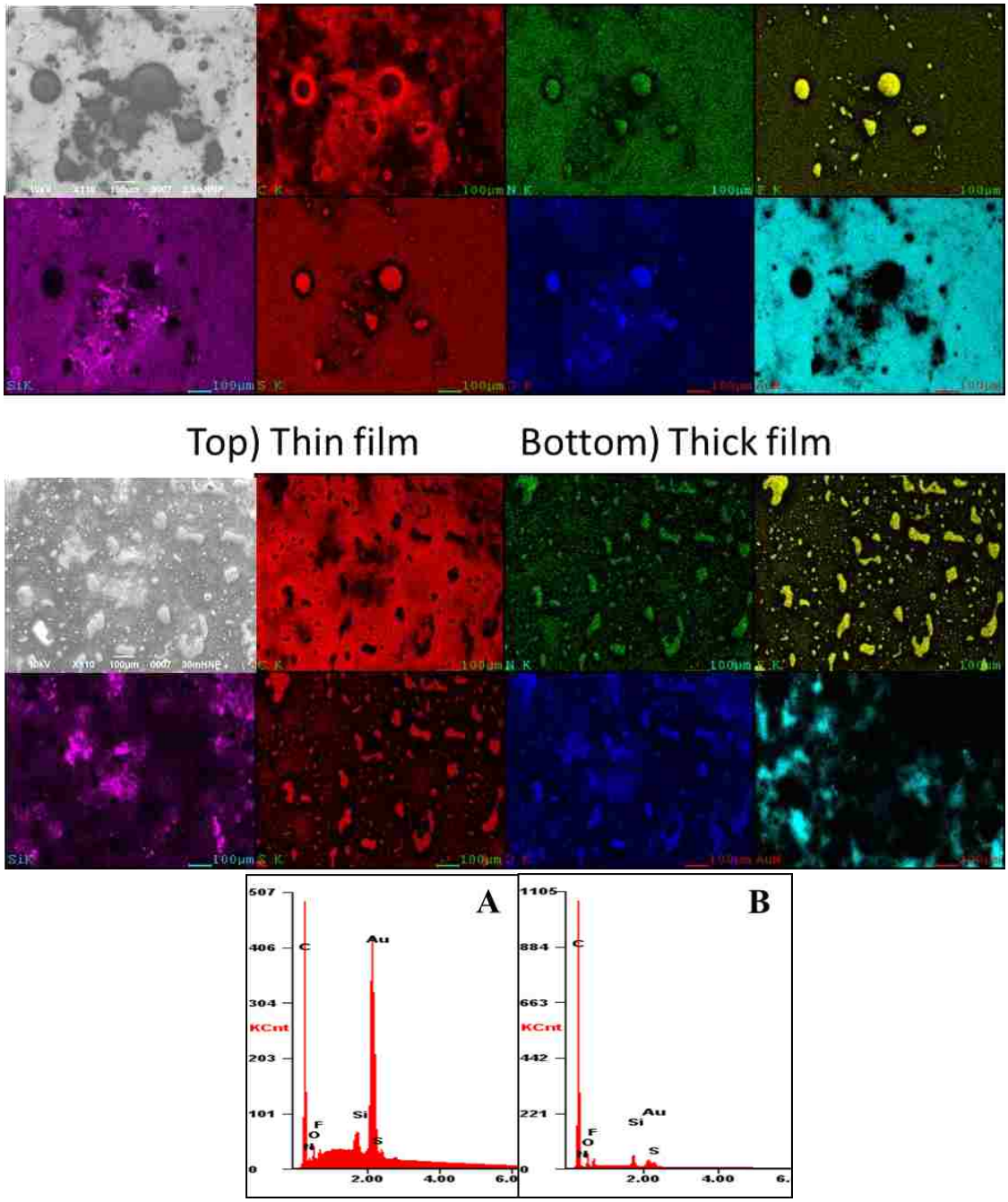

Figure B1. SEM and EDS images of a thin and thick [HMIm][NTf_2]-PMMA coating. Top) Thin film Bottom) Thick film. Scale bar is100 µm. EDS relative intensity spectra in K counts A) Thin [HMIM][NTF_2]-PMMA film, B) Thick [HMIM][NTF_2]-PMMA film

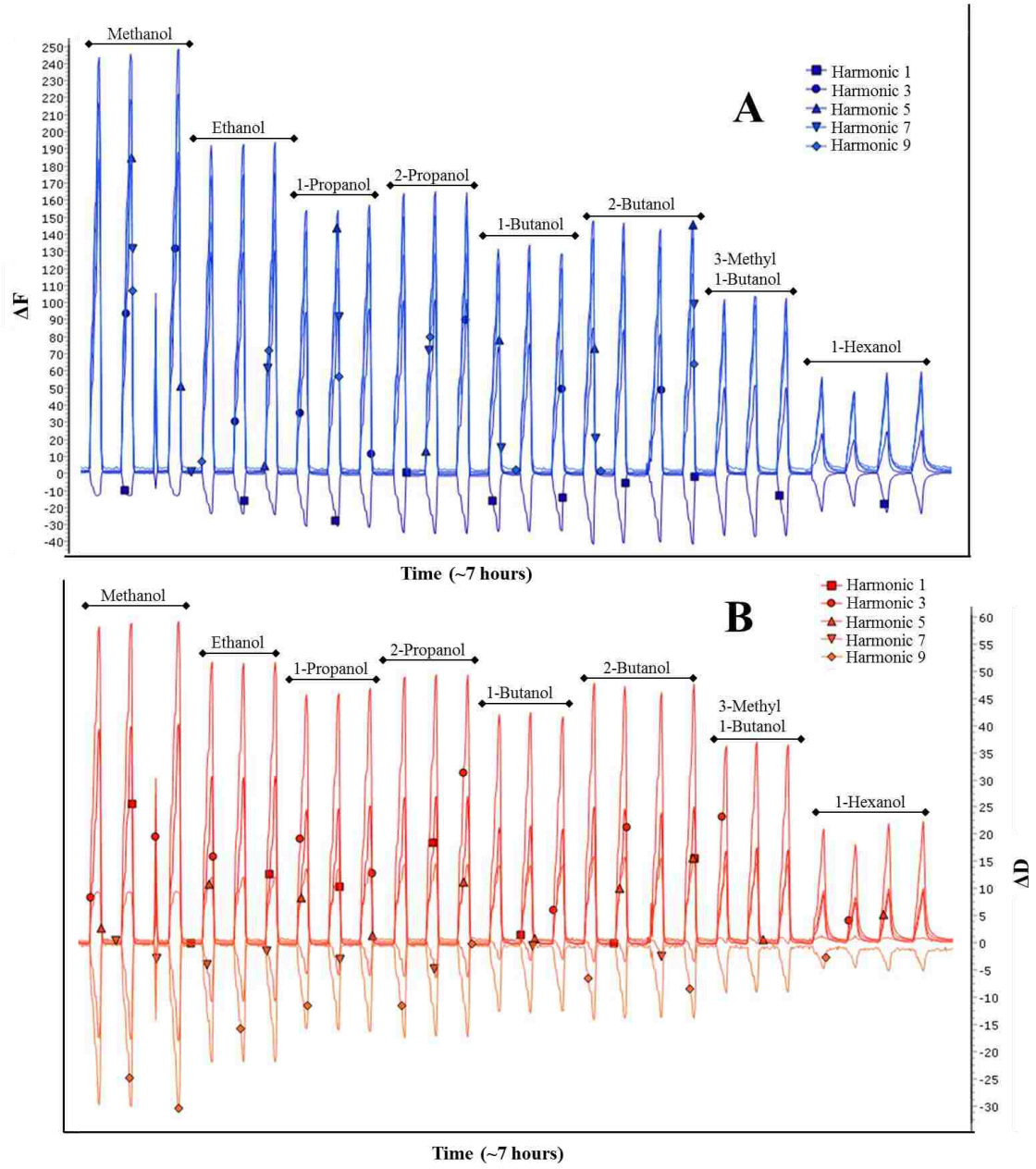

Figure B2. Sensorgrams for a set of 8 alcohols for parameters A) *Δf* and B) *ΔD* at p_a/p_0 =0.2, 0.3,0.4.

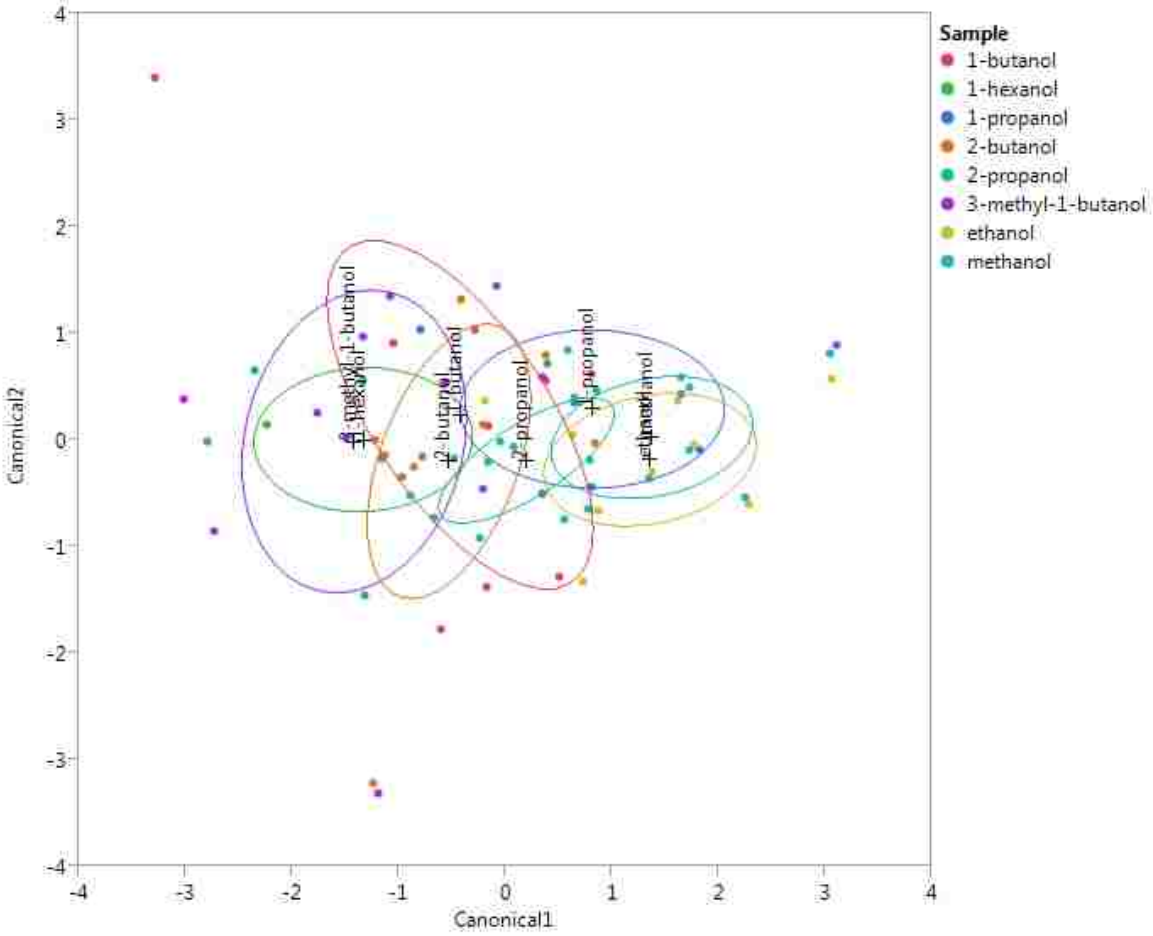

Figure B3. QDA canonical plots for a set of alcohols, p_a/p_0 =0.2, 0.3,0.4, with respect to the parameter $\frac{\Delta f}{\Delta D}$. Plots consider the data set normalized for concentration

APPENDIX C: SUPPORTING INFORMATION FOR CHAPTER FOUR

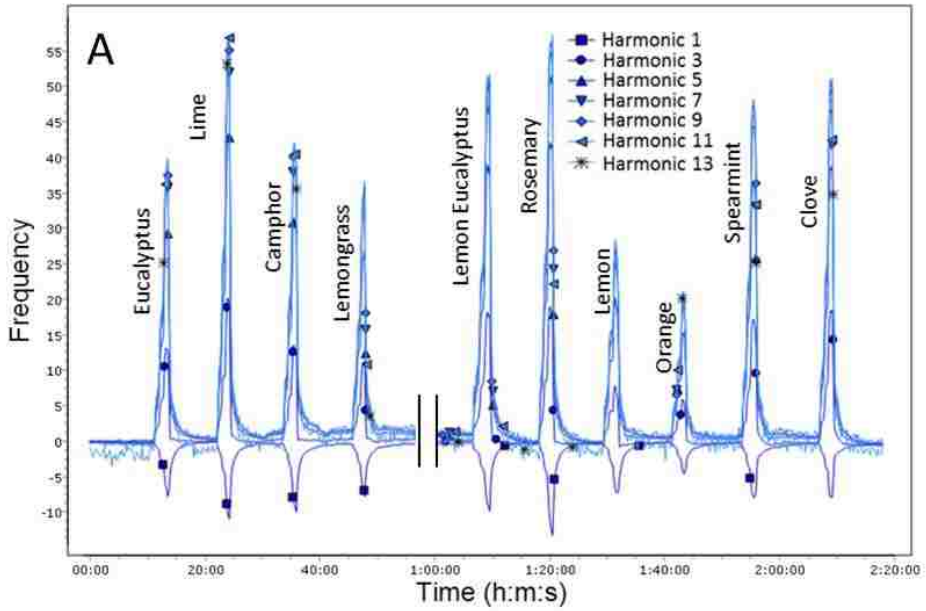

Figure C1. Sensorgrams for a sensor when exposed to 10 different odors. Sensors is coated with ionic liquid 1-nonyl-3-methylimidazolium thiocyanate ([C_9MIm][SCN])

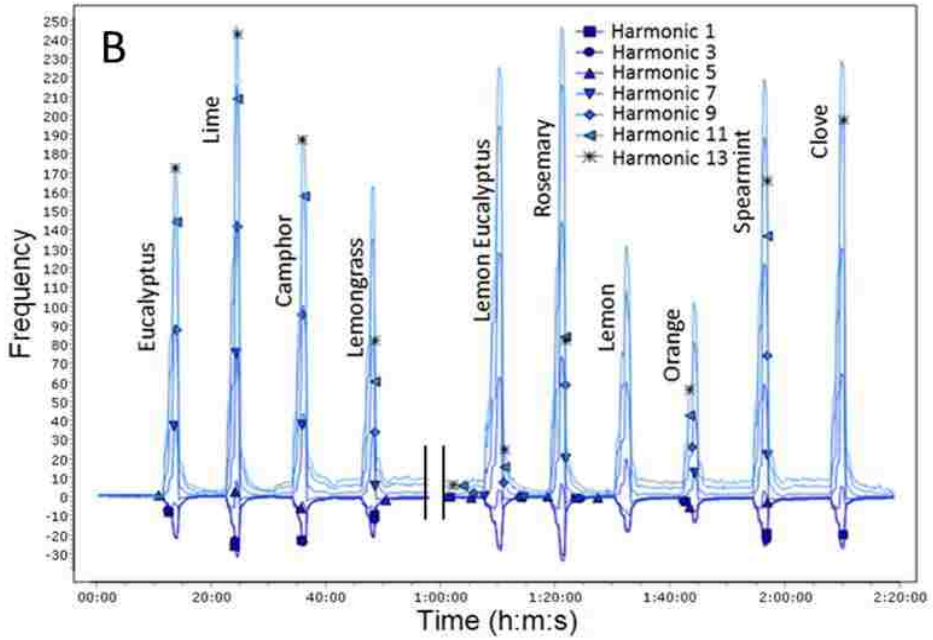

Figure C2. Sensorgrams for a sensor when exposed to 10 different odors. Sensors is coated with ionic liquid 1-nonyl-3-methylimidazolium bromide ([C_9MIm][Br])

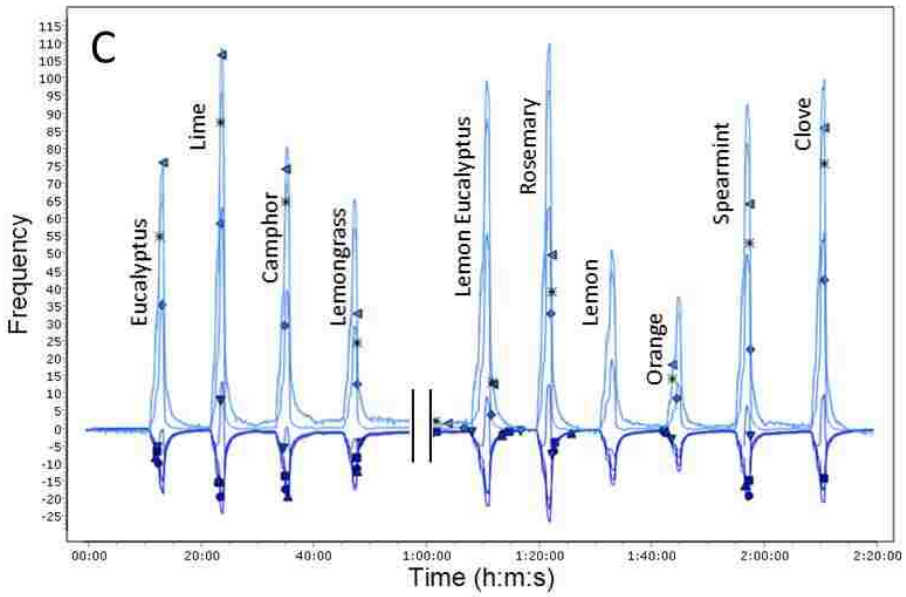

Figure C3. Sensorgrams for a sensor when exposed to 10 different odors. Sensors is coated with ionic liquid 1-octenyl-3-pyridinium bromide ([C_8Pyr][Br])

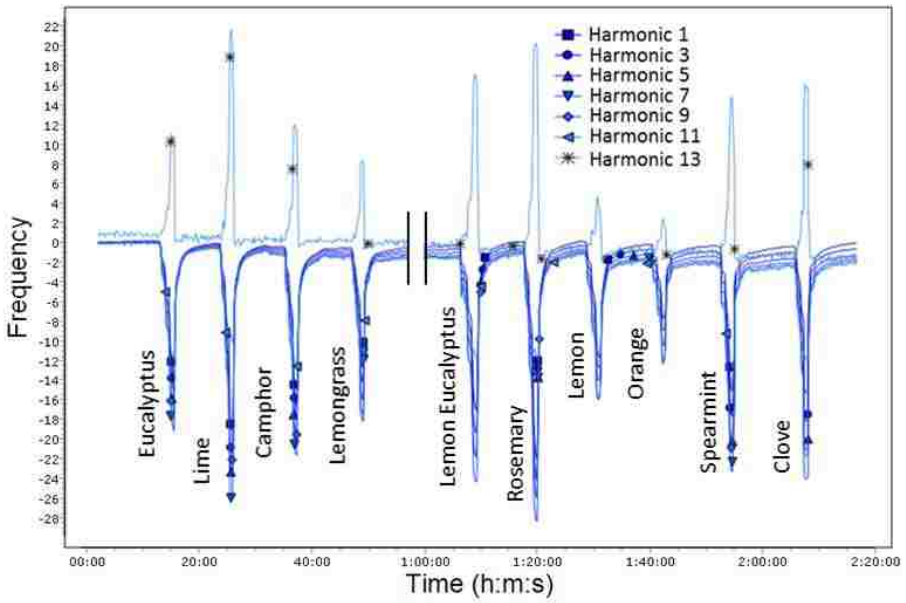

Figure C4. Sensorgrams for a sensor when exposed to 10 different odors. Sensors is coated with ionic liquid 1-undecenyl-3-pyridinium bromide ([C_{11}Pyr][Br]) respectively.

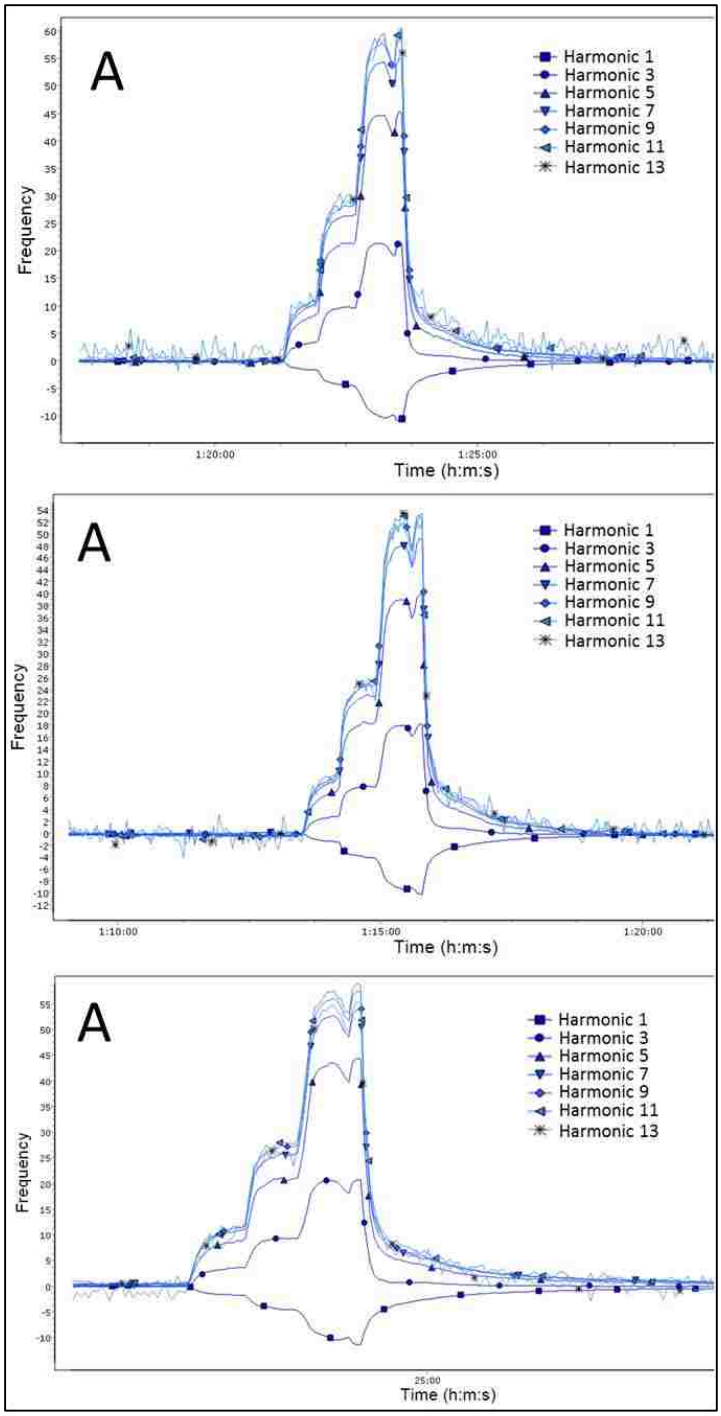

Figure C5. Sensorgrams for three replicate measurements of lime odor at multiple concentrations. Sensor is coated with ionic liquid 1-nonyl-3-methylimidazolium thiocyanate ([C_9MIm][SCN]).

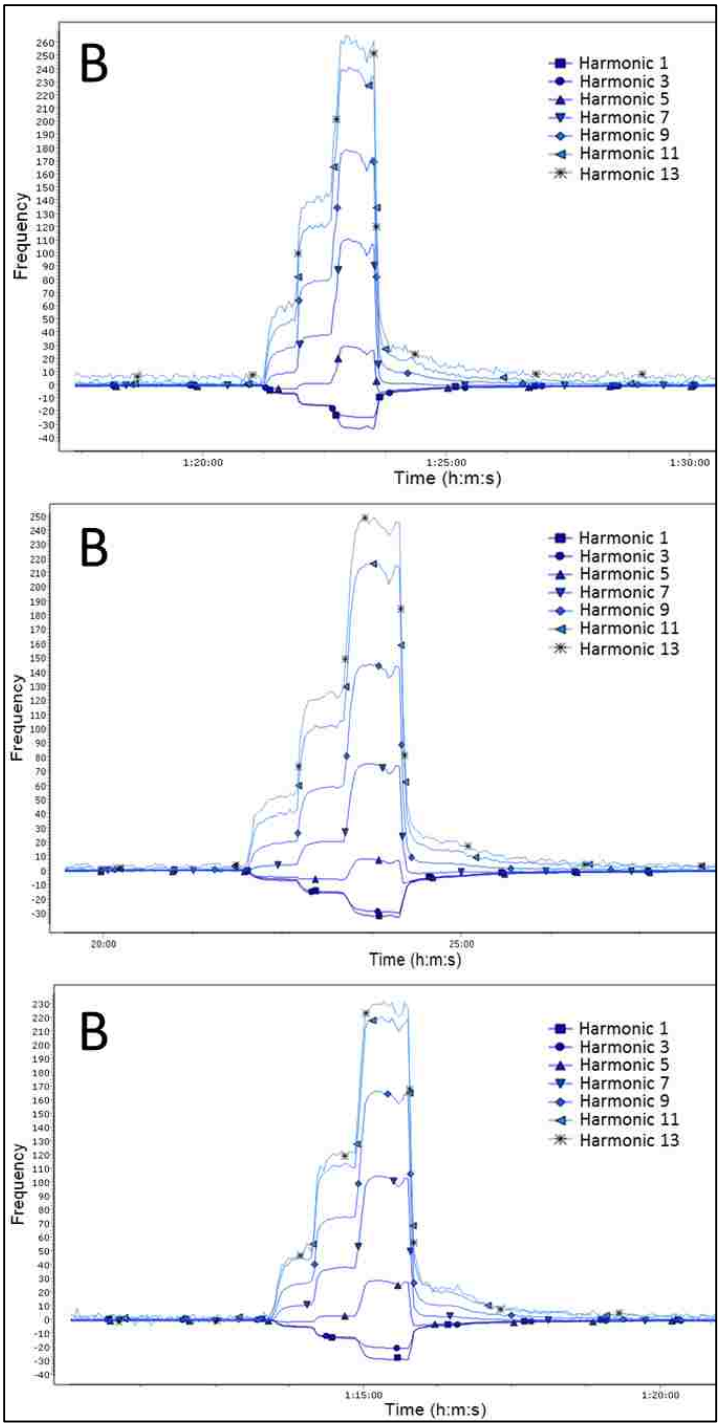

Figure C6. Sensorgrams for three replicate measurements of lime odor at multiple concentrations. Sensor is coated with ionic liquid 1-nonyl-3-methylimidazolium bromide ([C_9MIm][Br]).

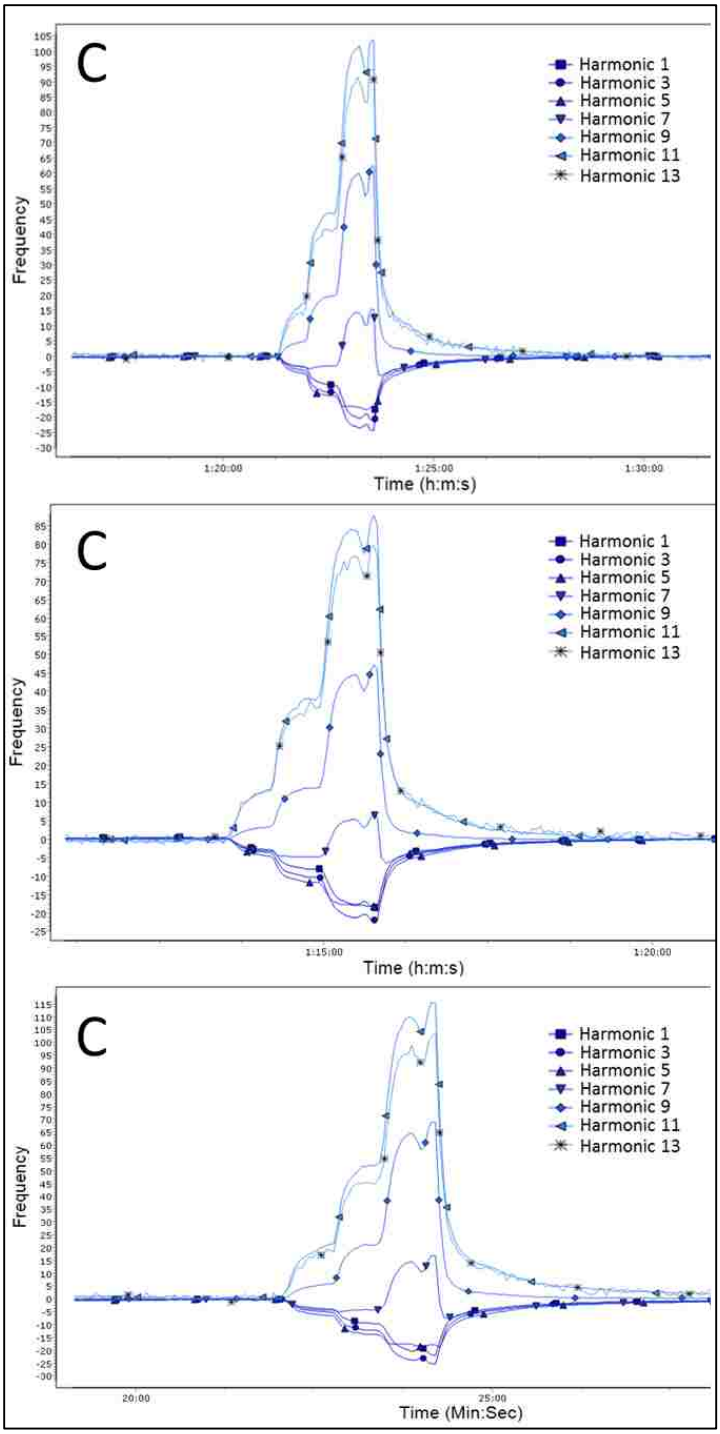

Figure C7. Sensorgrams for three replicate measurements of lime odor at multiple concentrations. Sensor is coated with ionic liquid 1-octenyl-3-pyridinium bromide ([C_8Pyr][Br]).

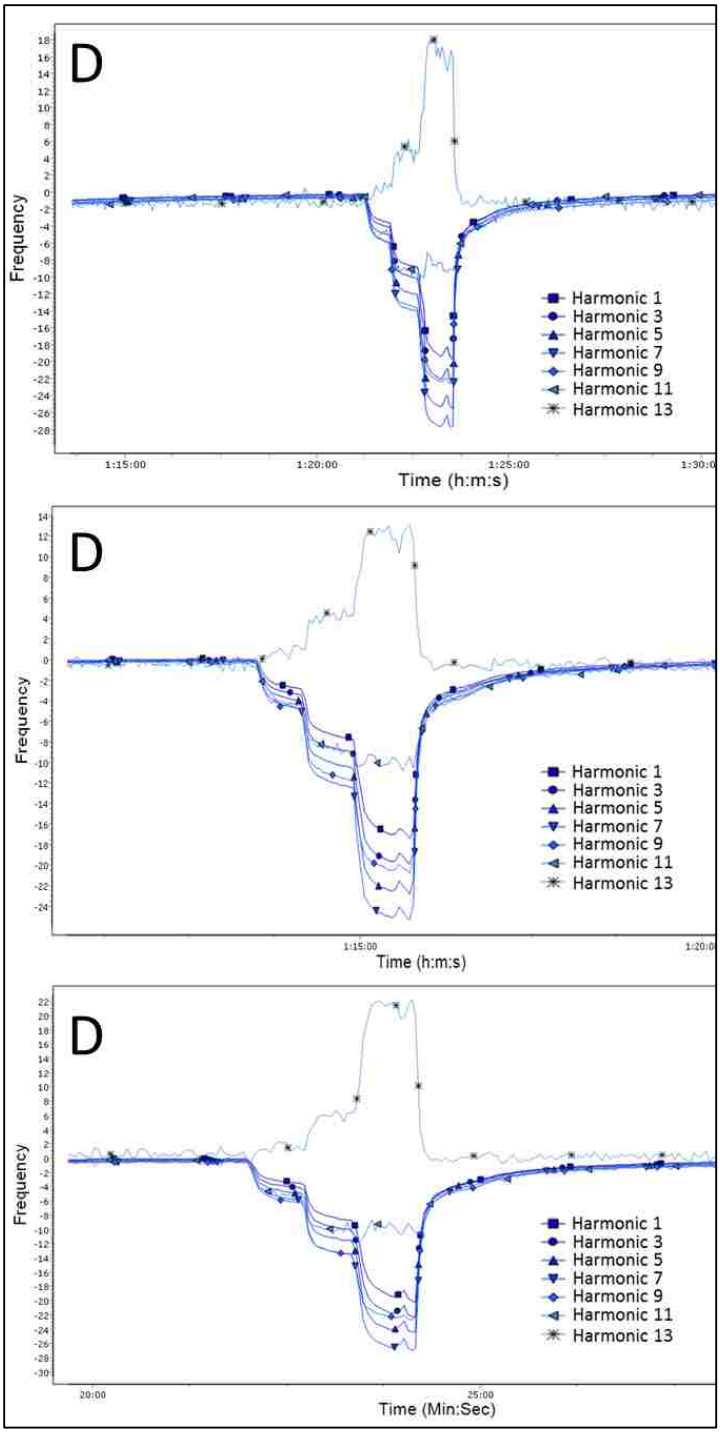

Figure C8. Sensorgrams for three replicate measurements of lime odor at multiple concentrations. Sensor is coated with ionic liquid 1-undecenyl-3-pyridinium bromide ([C_{11}Pyr][Br]).

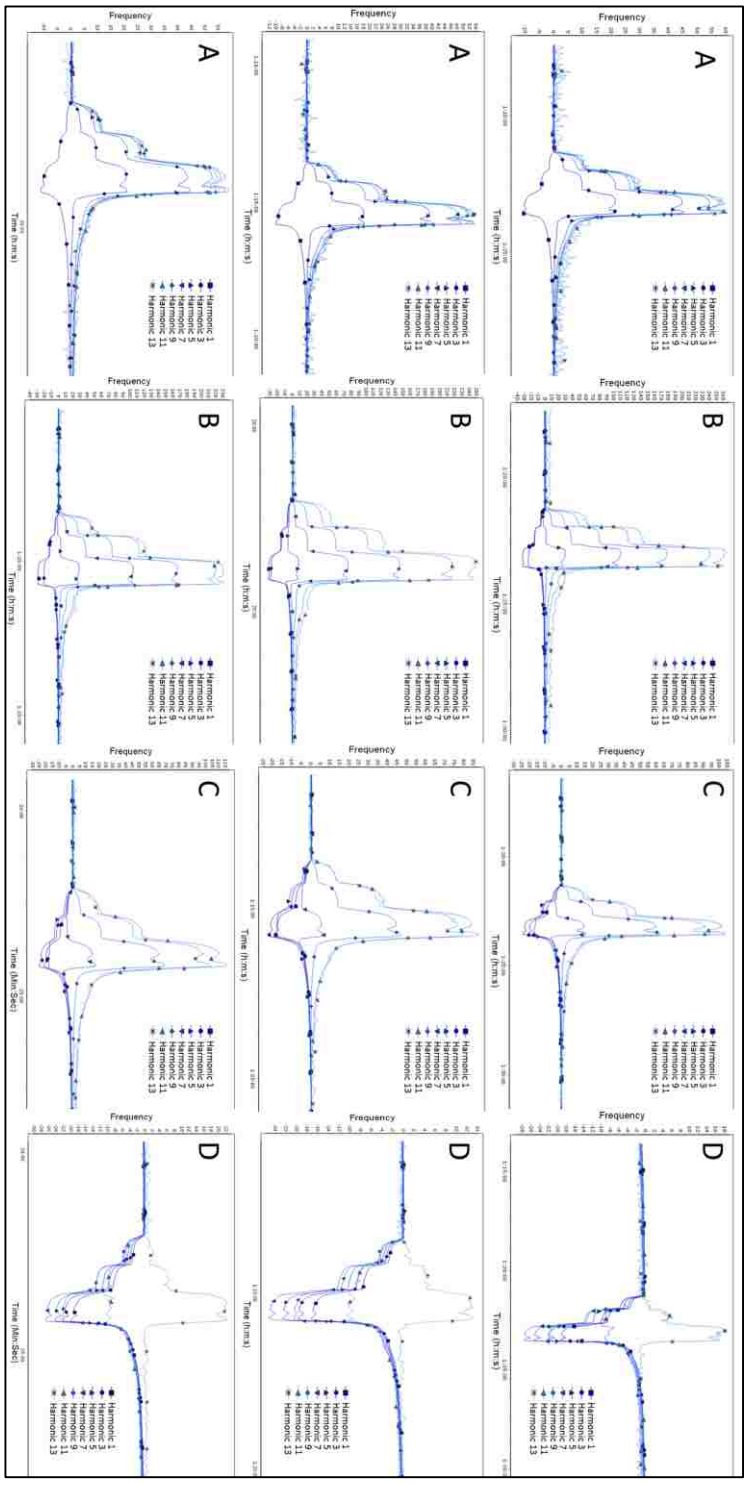

Figure C9. Sensorgrams for three replicate measurements of lime odor at multiple concentrations. Sensors are coated with ionic liquid A) 1-nonyl-3-methylimidazolium thiocyanate ([C_9MIm][SCN]), B) 1-nonyl-3-methylimidazolium bromide ([C_9MIm][Br]), C) 1-octenyl-3-pyridinium bromide ([C_8Pyr][Br]), and D) 1-undecenyl-3-pyridinium bromide ([C_{11}Pyr][Br]) respectively.

.

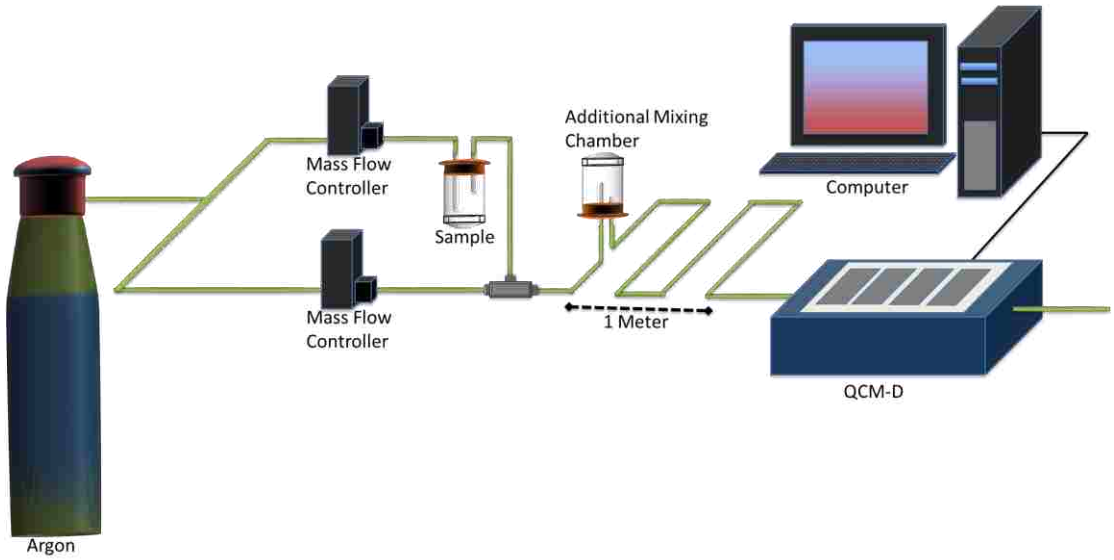

Figure C10. Schematic of the experimental system

APPENDIX D: SUPPORTING INFORMATION FOR CHAPTER FIVE

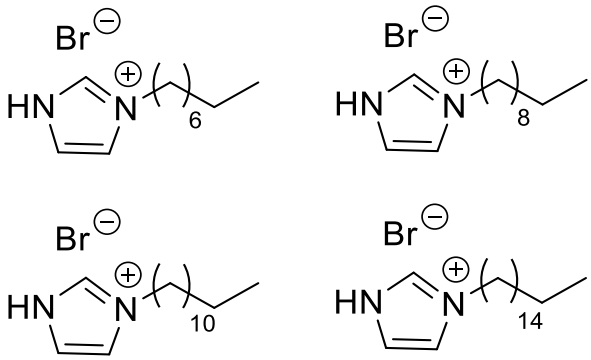

Figure D1. Structures of Organic Salts

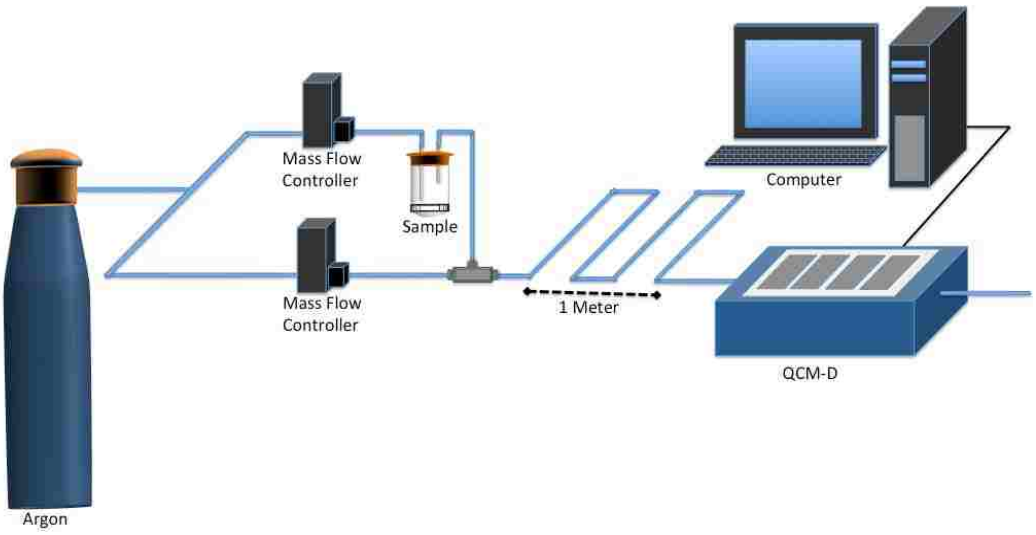

Figure D2. Schematic of the experimental system

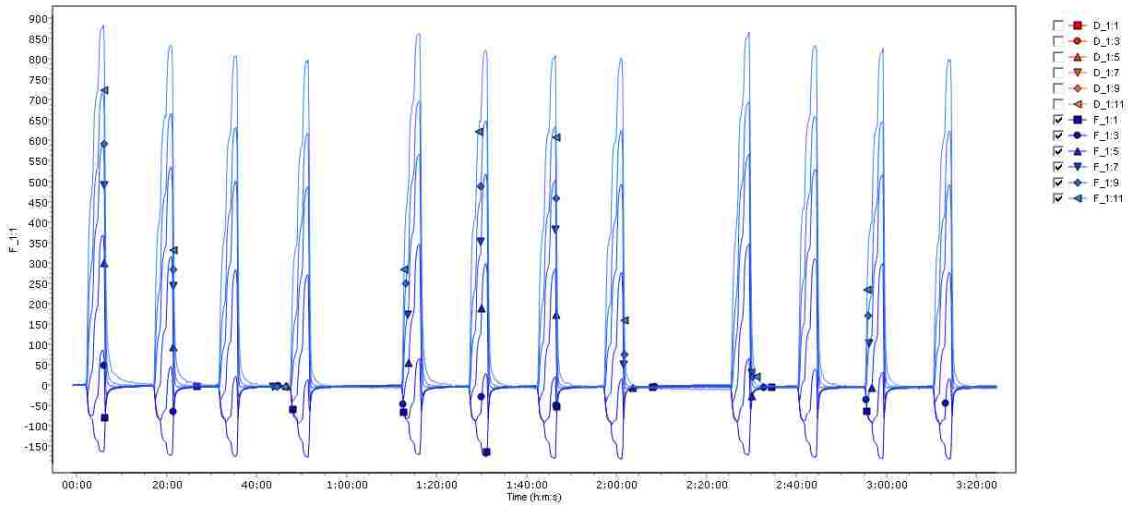

Figure D3. Sensorgrams for three replicate measurements of ethanol adulterated gasoline at multiple concentrations. Sensor is coated with ionic liquid 1-octyl-3-methylimidazolium bromide ([C_8MIm][Br]).

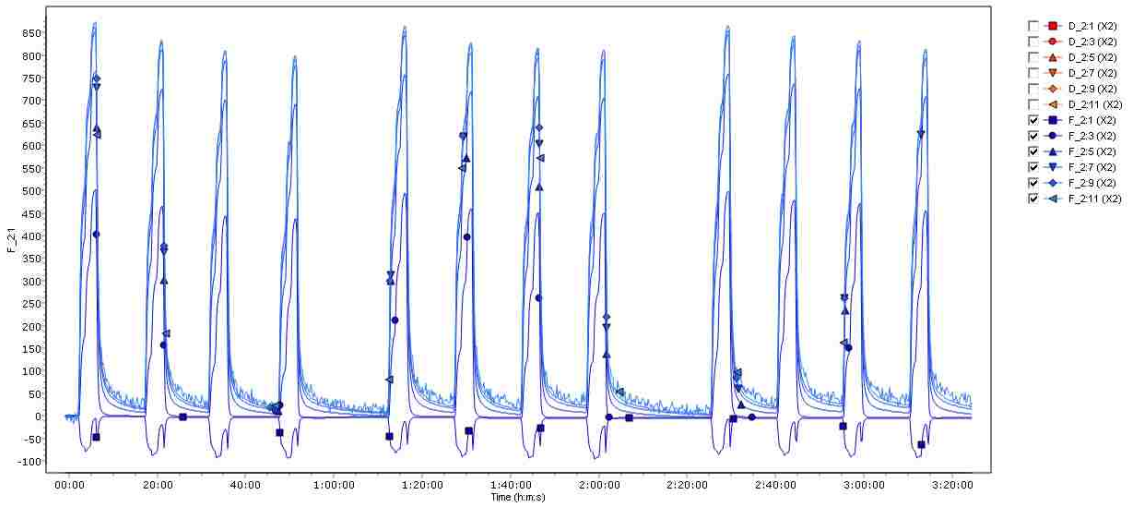

Figure D4. Sensorgrams for three replicate measurements of ethanol adulterated gasoline at multiple concentrations. Sensor is coated with ionic liquid 1-decyl-3-methylimidazolium bromide ([C_{10}MIm][Br]).

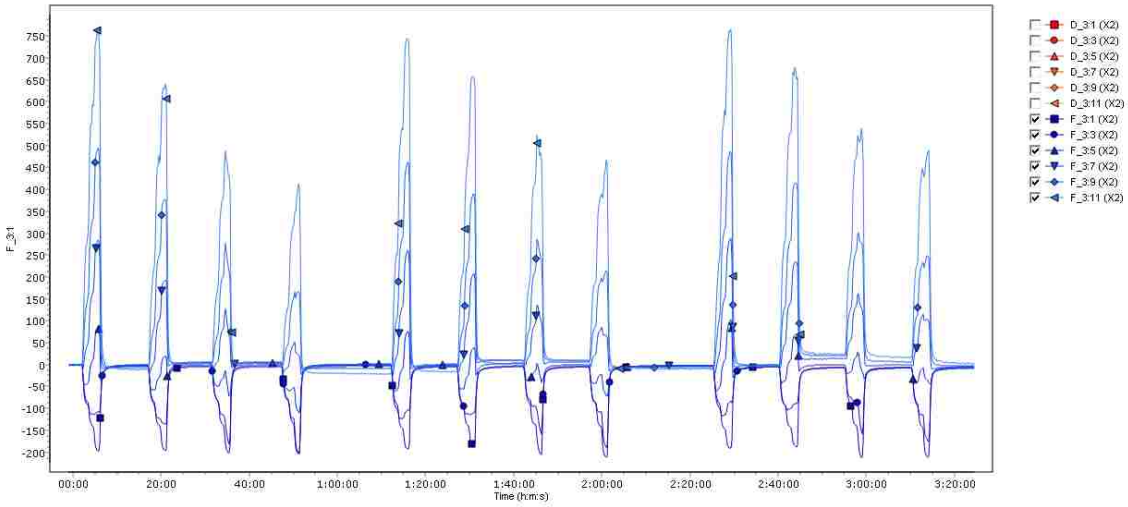

Figure D5. Sensorgrams for three replicate measurements of ethanol adulterated gasoline at multiple concentrations. Sensor is coated with ionic liquid 1-dodecyl-3-methylimidazolium bromide ([C_{12}MIm][Br]).

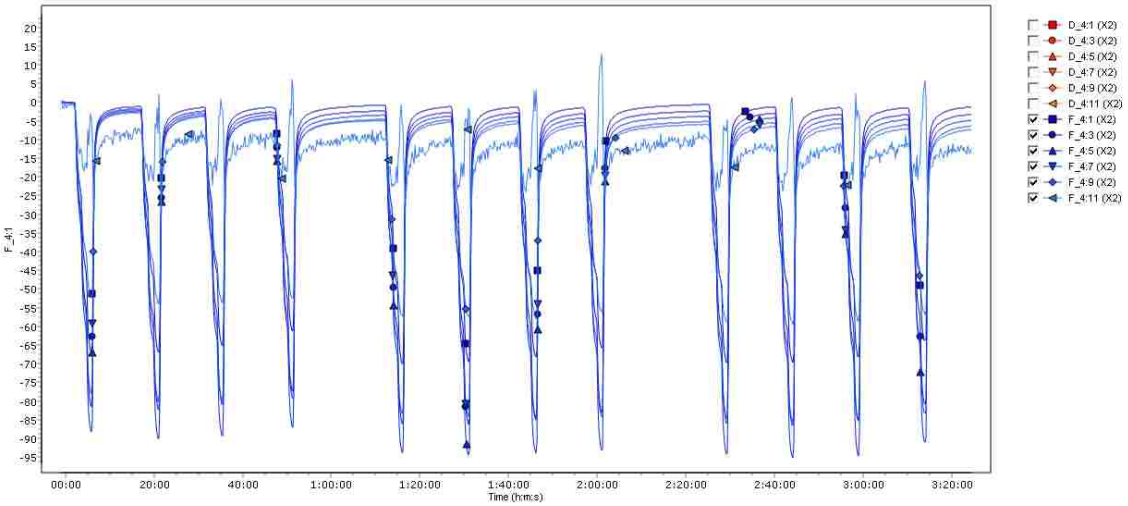

Figure D6. Sensorgrams for three replicate measurements of ethanol adulterated gasoline at multiple concentrations. Sensor is coated with ionic liquid 1-hexadecyl-3-methylimidazolium bromide ([C_{16}MIm][Br]).

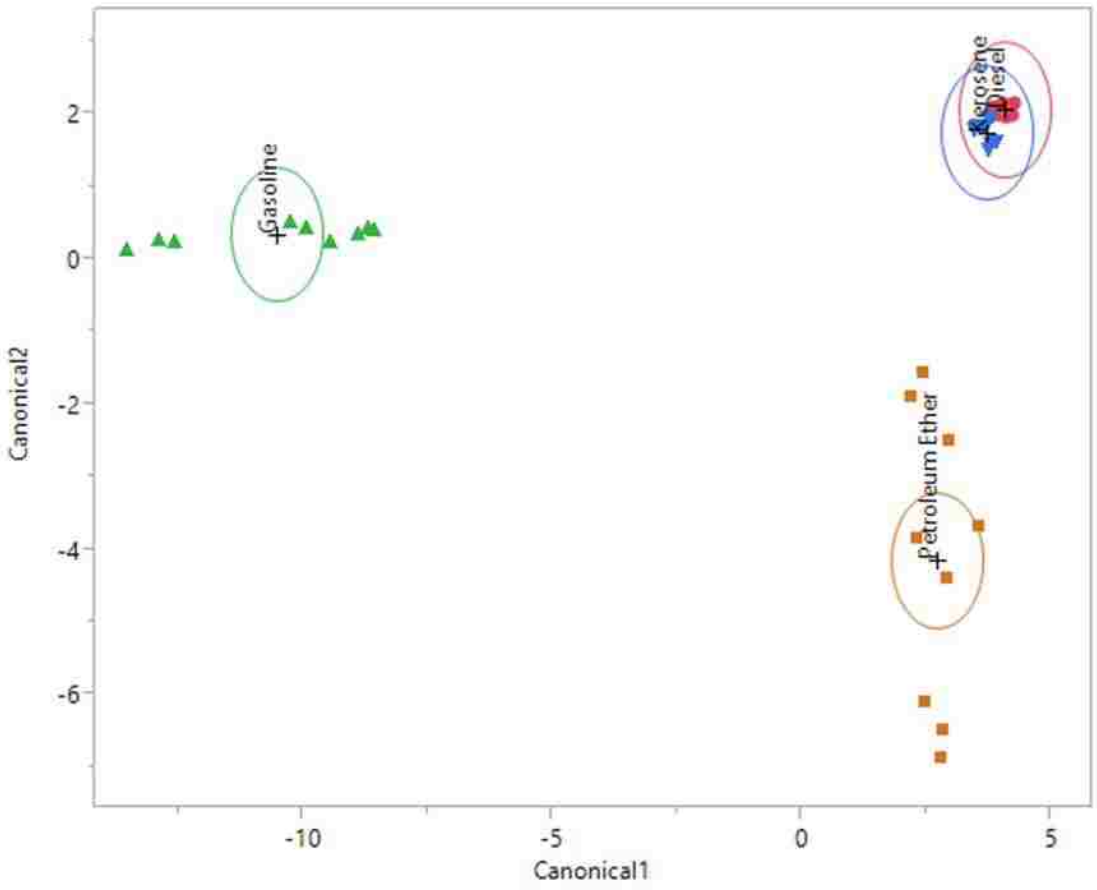

Score Summaries

	Training
Number Misclassified	0
Percent Misclassified	0
-2LogLikelihood	23.15

Training

Counts: Actual Rows by Predicted Columns

	Diesel	Gasoline	Kerosene	Petroleum Ether
Diesel	9	0	0	0
Gasoline	0	9	0	0
Kerosene	0	0	9	0
Petroleum Ether	0	0	0	9

Figure D7. LDA Canonical plot and error rates for fuel discrimination using a 4 sensor MSA

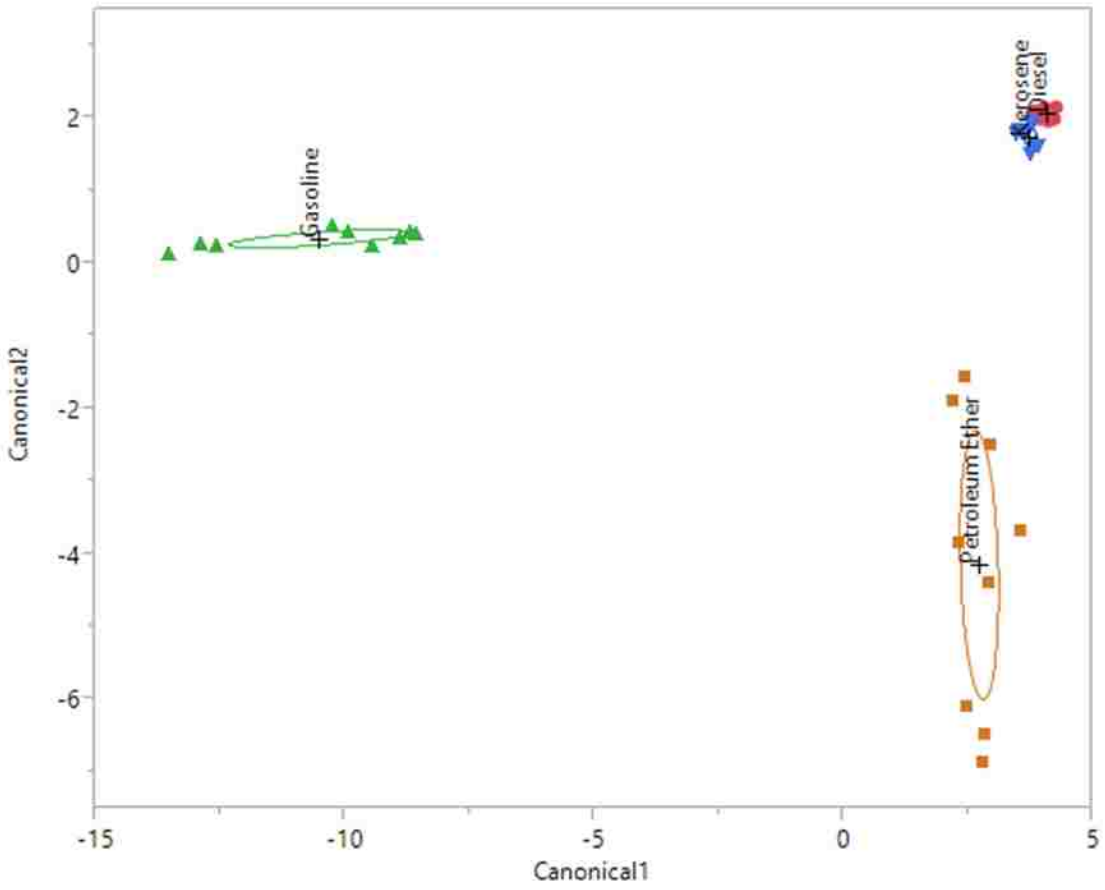

Score Summaries

	Training
Number Misclassified	0
Percent Misclassified	0
-2LogLikelihood	1.061

Training

Counts: Actual Rows by Predicted Columns

	Diesel	Gasoline	Kerosene	Petroleum Ether
Diesel	9	0	0	0
Gasoline	0	9	0	0
Kerosene	0	0	9	0
Petroleum Ether	0	0	0	9

Figure D8. QDA Canonical plot and error rates for fuel discrimination using a 4 sensor MSA

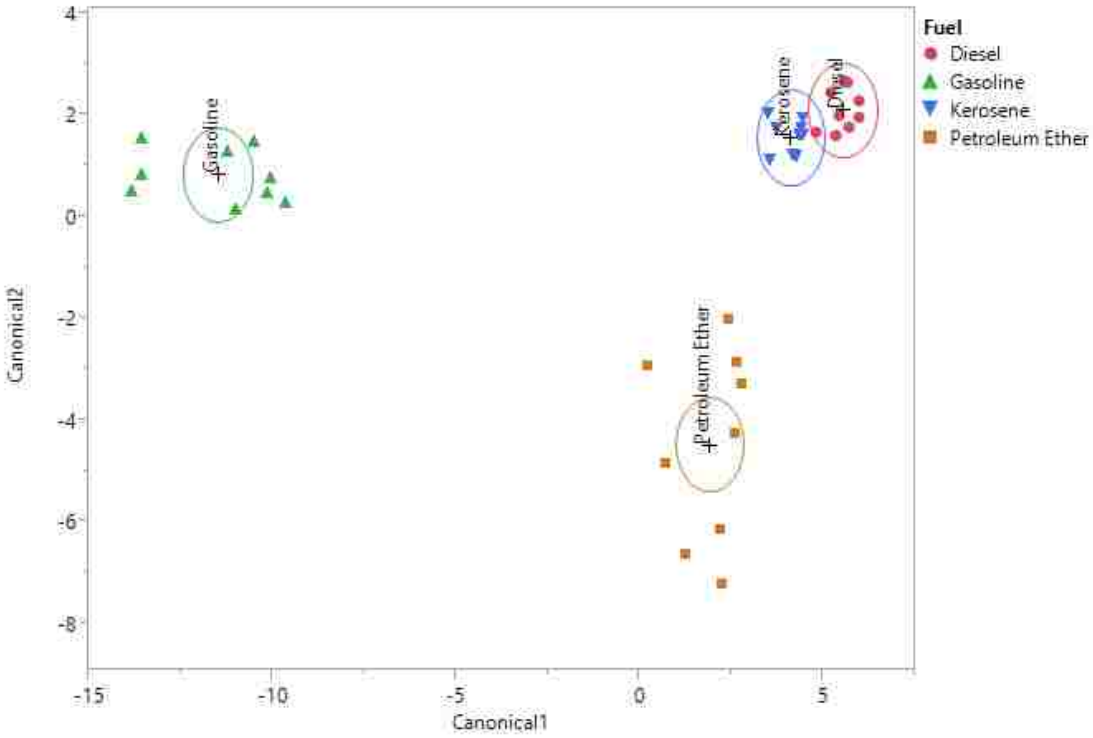

Score Summaries

	Training
Number Misclassified	1
Percent Misclassified	2.778
-2LogLikelihood	7.947

Training

Counts: Actual Rows by Predicted Columns

	Diesel	Gasoline	Kerosene	Petroleum Ether
Diesel	8	0	1	0
Gasoline	0	9	0	0
Kerosene	0	0	9	0
Petroleum Ether	0	0	0	9

Figure D9. LDA Canonical plot and error rates for fuel discrimination using a [C_8MIm][Br] VSA

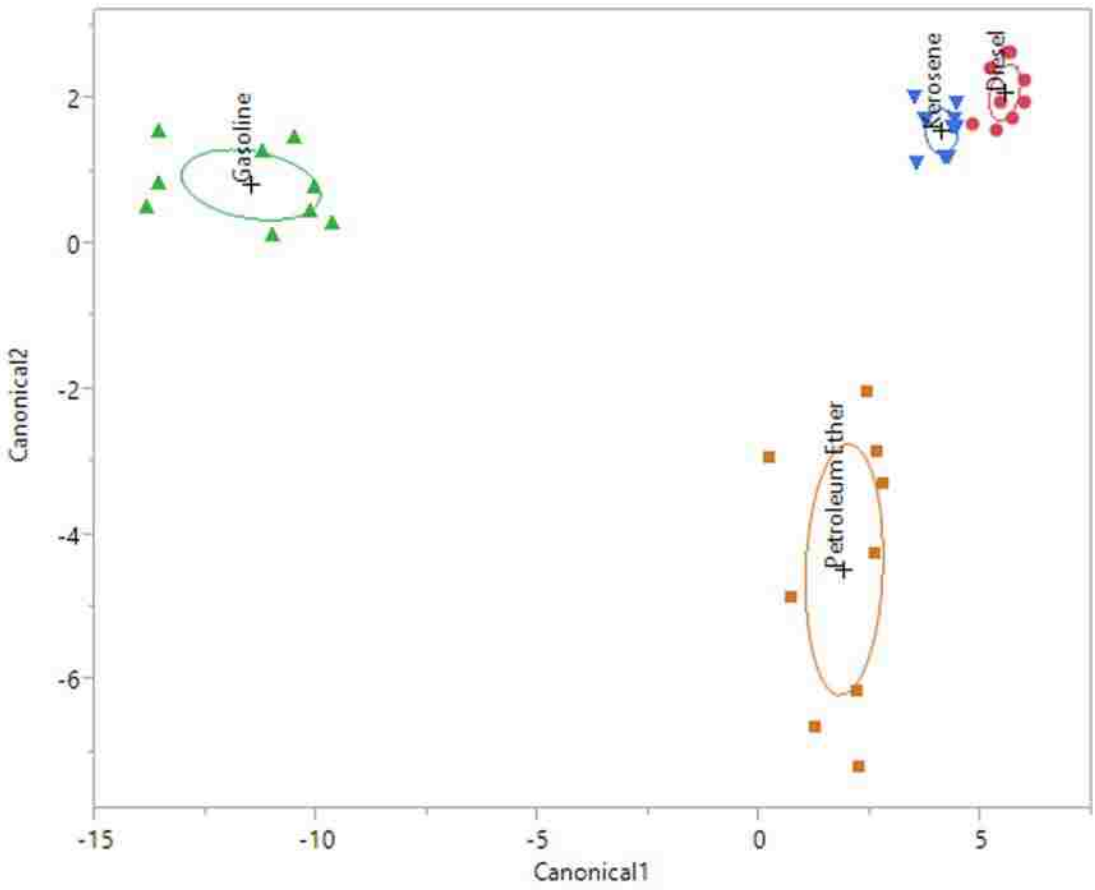

Score Summaries

	Training
Number Misclassified	0
Percent Misclassified	0
-2LogLikelihood	0.028

Training

Counts: Actual Rows by Predicted Columns

	Diesel	Gasoline	Kerosene	Petroleum Ether
Diesel	9	0	0	0
Gasoline	0	9	0	0
Kerosene	0	0	9	0
Petroleum Ether	0	0	0	9

Figure D10. QDA Canonical plot and error rates for fuel discrimination using a $[C_8MIm][Br]$ VSA

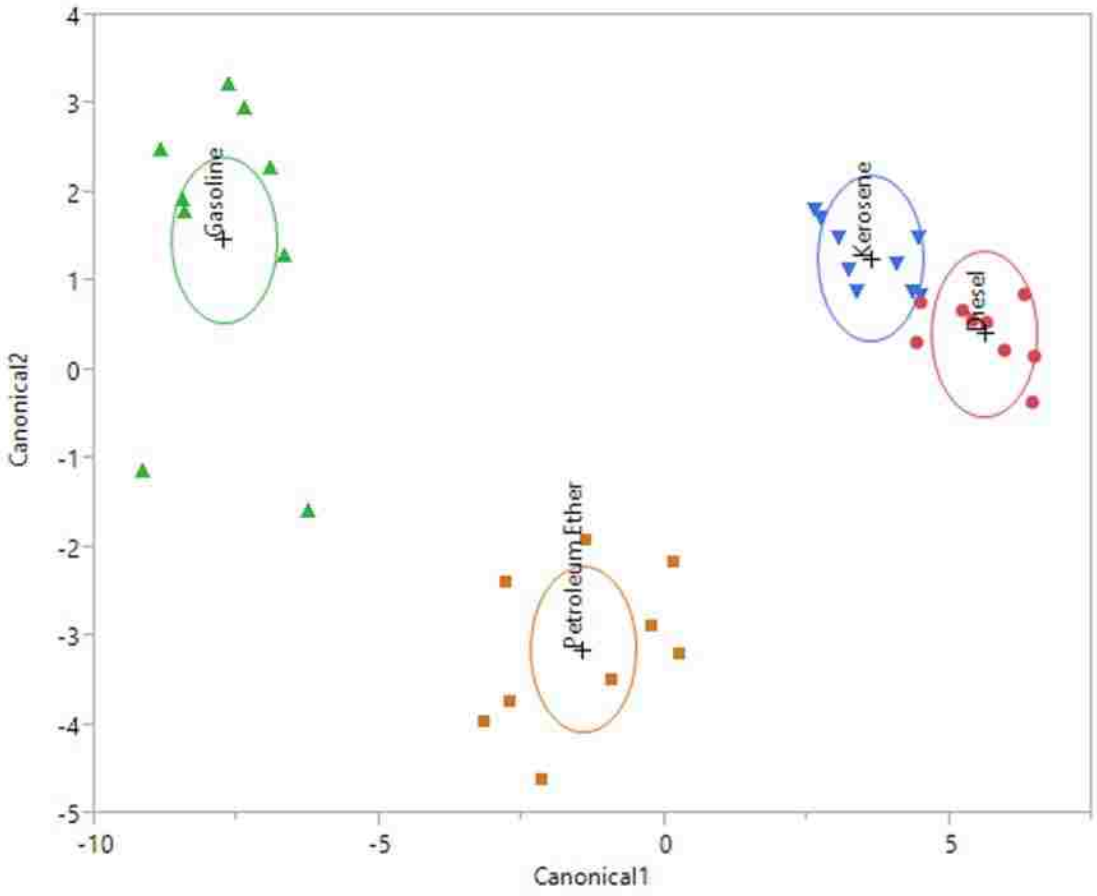

Score Summaries

	Training
Number Misclassified	0
Percent Misclassified	0
-2LogLikelihood	4.964

Training

Counts: Actual Rows by Predicted Columns

	Diesel	Gasoline	Kerosene	Petroleum Ether
Diesel	9	0	0	0
Gasoline	0	9	0	0
Kerosene	0	0	9	0
Petroleum Ether	0	0	0	9

Figure D11. LDA Canonical plot and error rates for fuel discrimination using a $[C_{10}MIm][Br]$ VSA

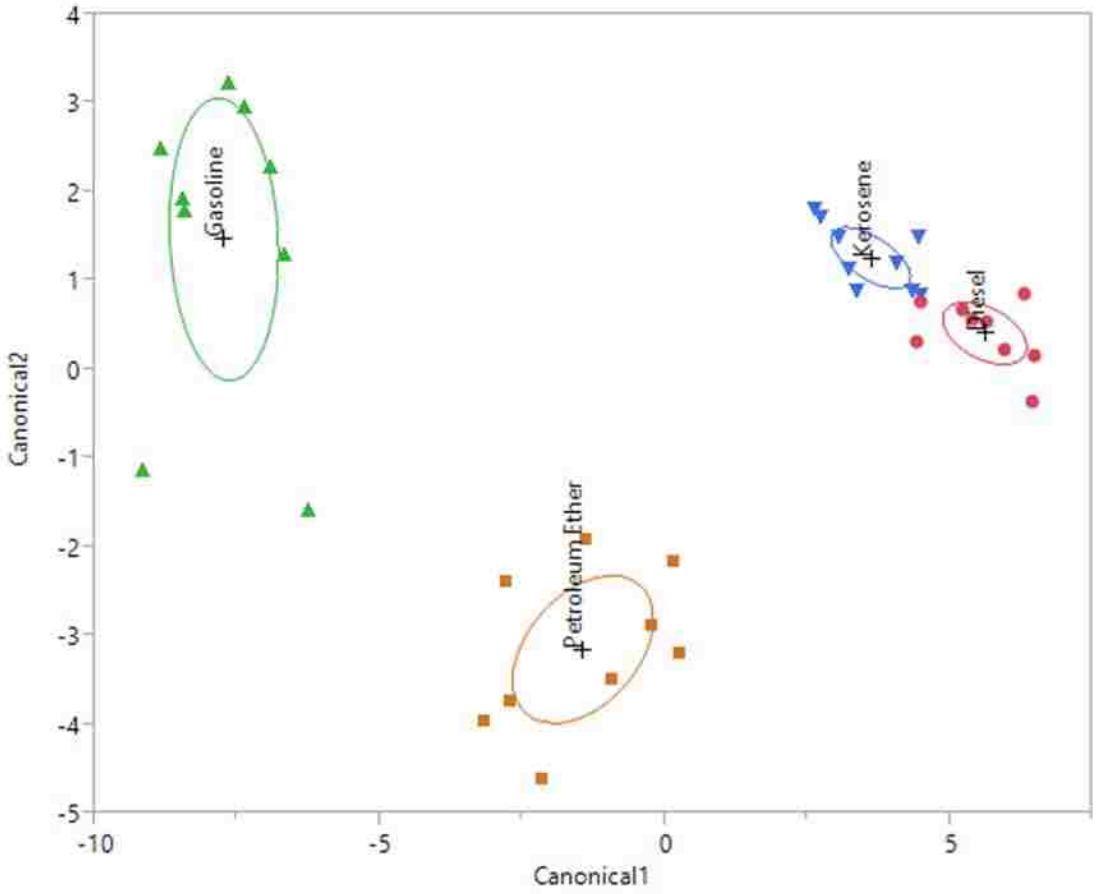

Score Summaries

	Training
Number Misclassified	0
Percent Misclassified	0
-2LogLikelihood	0.093

Training

Counts: Actual Rows by Predicted Columns

	Diesel	Gasoline	Kerosene	Petroleum Ether
Diesel	9	0	0	0
Gasoline	0	9	0	0
Kerosene	0	0	9	0
Petroleum Ether	0	0	0	9

Figure D12. QDA Canonical plot and error rates for fuel discrimination using a $[C_{10}MIm][Br]$ VSA

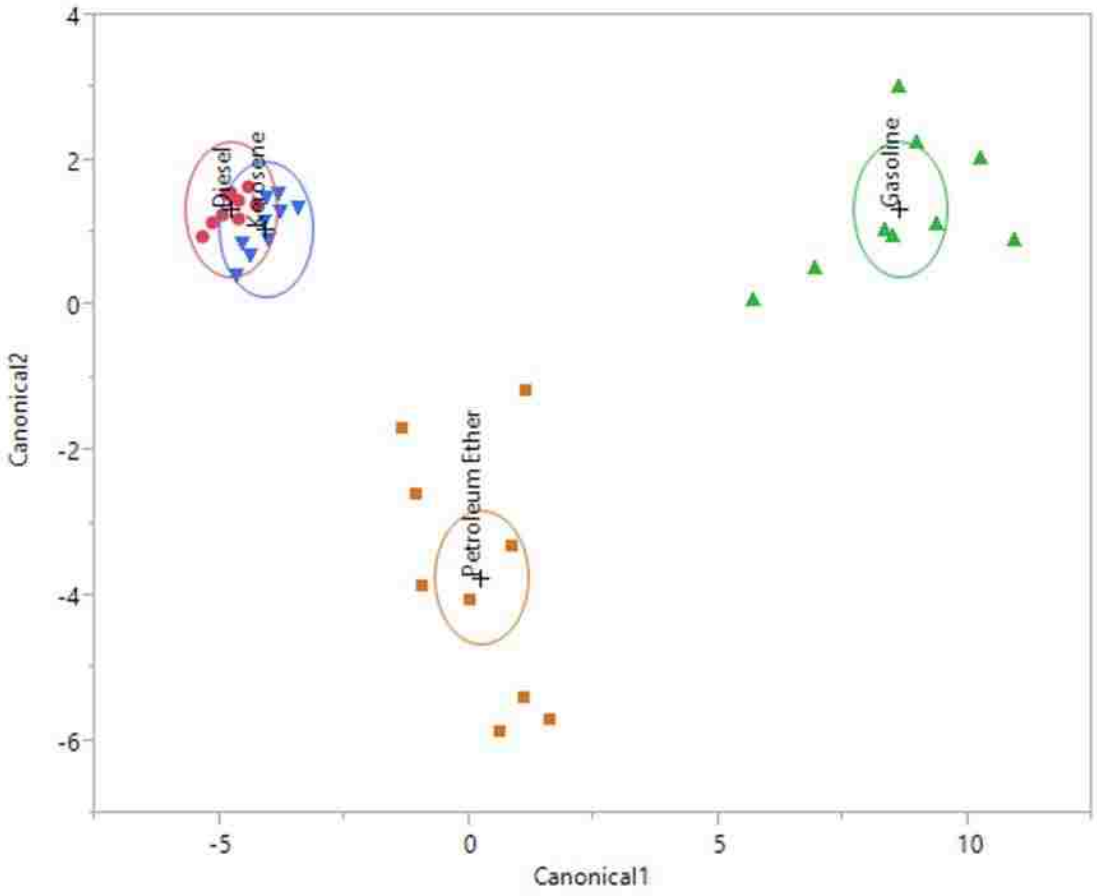

Score Summaries

	Training
Number Misclassified	1
Percent Misclassified	2.778
-2LogLikelihood	20.36

Training

Counts: Actual Rows by Predicted Columns

	Diesel	Gasoline	Kerosene	Petroleum Ether
Diesel	8	0	1	0
Gasoline	0	9	0	0
Kerosene	0	0	9	0
Petroleum Ether	0	0	0	9

Figure D13. LDA Canonical plot and error rates for fuel discrimination using a $[C_{12}MIm][Br]$ VSA

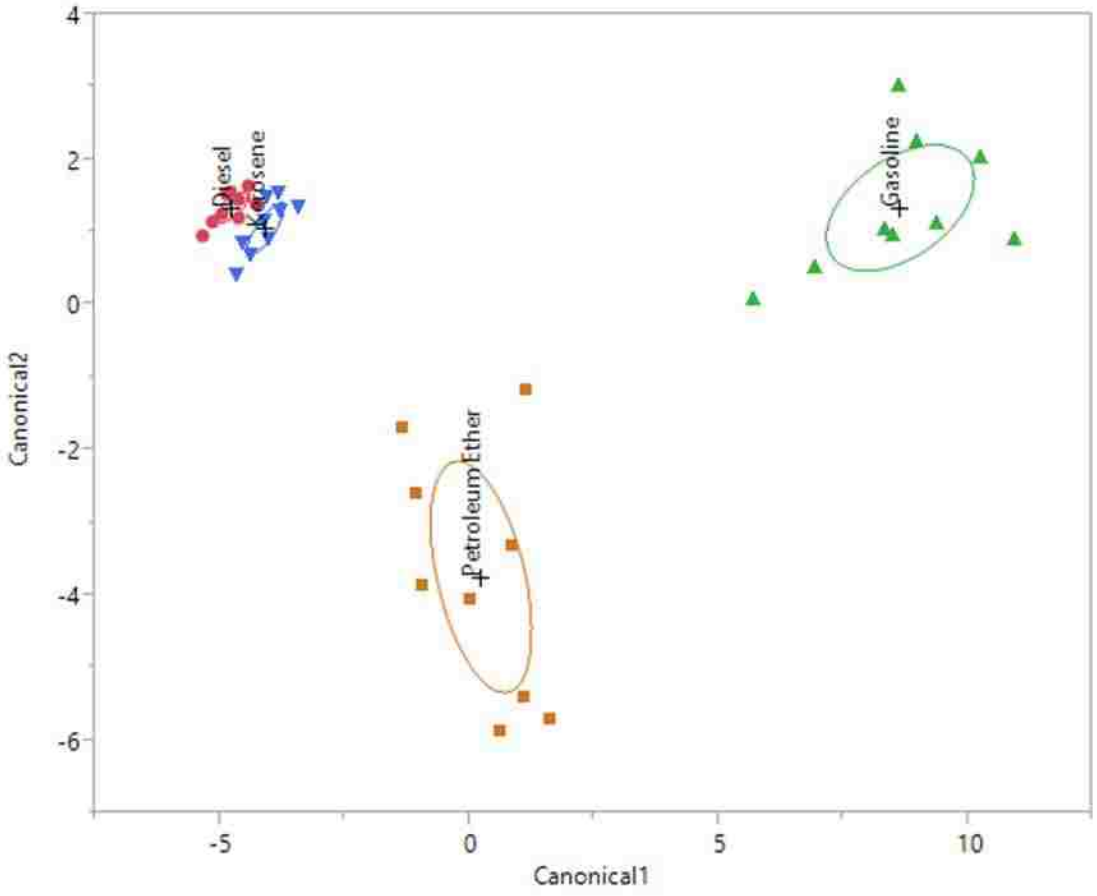

Score Summaries

	Training
Number Misclassified	0
Percent Misclassified	0
-2LogLikelihood	7e-6

Training

Counts: Actual Rows by Predicted Columns

	Diesel	Gasoline	Kerosene	Petroleum Ether
Diesel	9	0	0	0
Gasoline	0	9	0	0
Kerosene	0	0	9	0
Petroleum Ether	0	0	0	9

Figure D14. QDA Canonical plot and error rates for fuel discrimination using a $[C_{12}MIm][Br]$ VSA

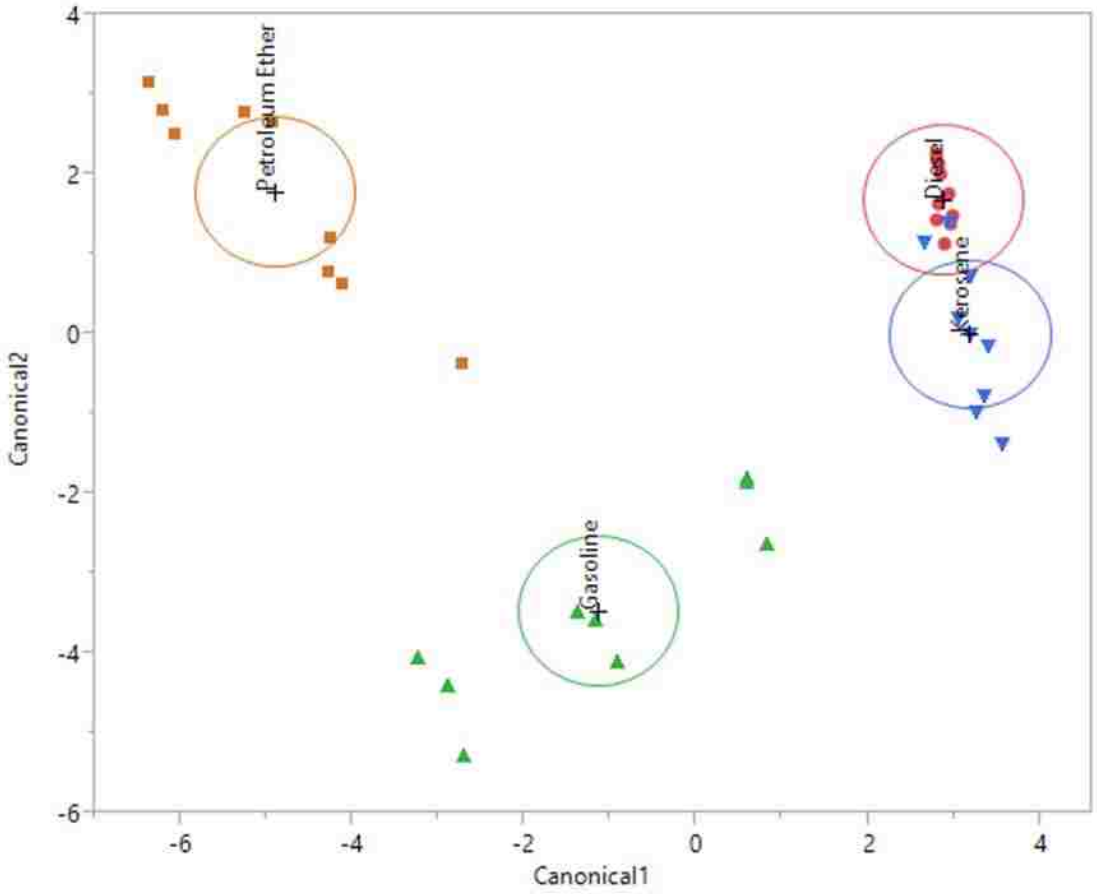

Score Summaries

	Training
Number Misclassified	2
Percent Misclassified	5.556
-2LogLikelihood	11.19

Training

Counts: Actual Rows by Predicted Columns

	Diesel	Gasoline	Kerosene	Petroleum Ether
Diesel	9	0	0	0
Gasoline	0	9	0	0
Kerosene	2	0	7	0
Petroleum Ether	0	0	0	9

Figure D15. LDA Canonical plot and error rates for fuel discrimination using a $[C_{16}MIm][Br]$ VSA

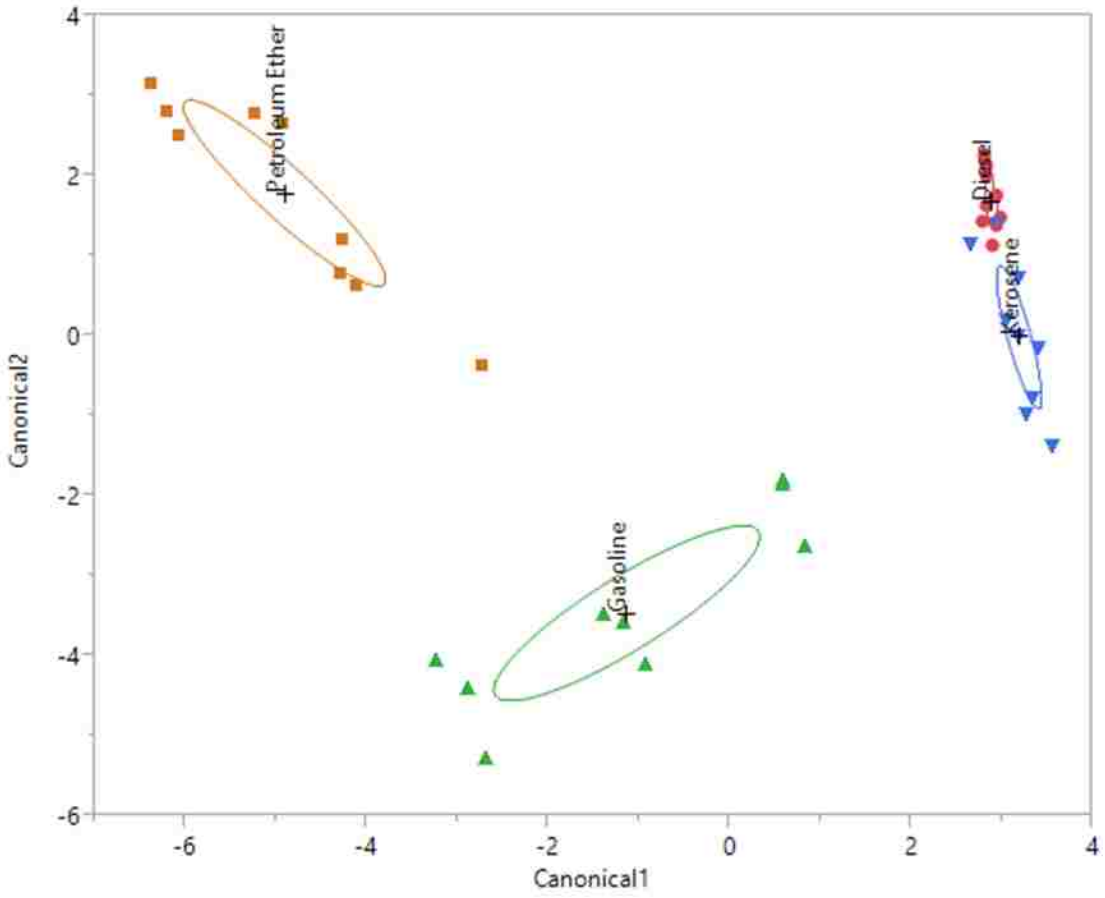

Score Summaries

	Training
Number Misclassified	0
Percent Misclassified	0
-2LogLikelihood	8e-5

Training

Counts: Actual Rows by Predicted Columns

	Diesel	Gasoline	Kerosene	Petroleum Ether
Diesel	9	0	0	0
Gasoline	0	9	0	0
Kerosene	0	0	9	0
Petroleum Ether	0	0	0	9

Figure D16. QDA Canonical plot and error rates for fuel discrimination using a $[C_{16}MIm][Br]$ VSA

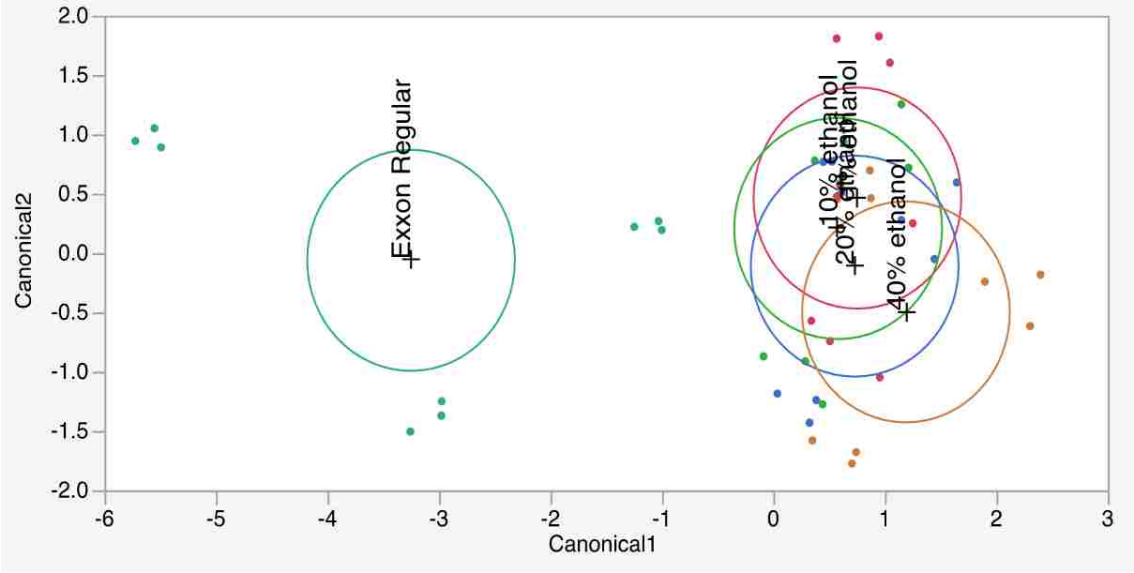

Score Summaries

	Training
Number Misclassified	26
Percent Misclassified	57.78
-2LogLikelihood	104.1

Training

Counts: Actual Rows by Predicted Columns

	1% ethanol	10% ethanol	20% ethanol	40% ethanol	Exxon Regular
1% ethanol	4	2	2	1	0
10% ethanol	4	2	2	1	0
20% ethanol	4	1	1	3	0
40% ethanol	2	1	0	6	0
Exxon Regular	0	3	0	0	6

Figure D17. LDA Canonical plot and error rates for ethanol adulteration discrimination using a 4 sensor MSA

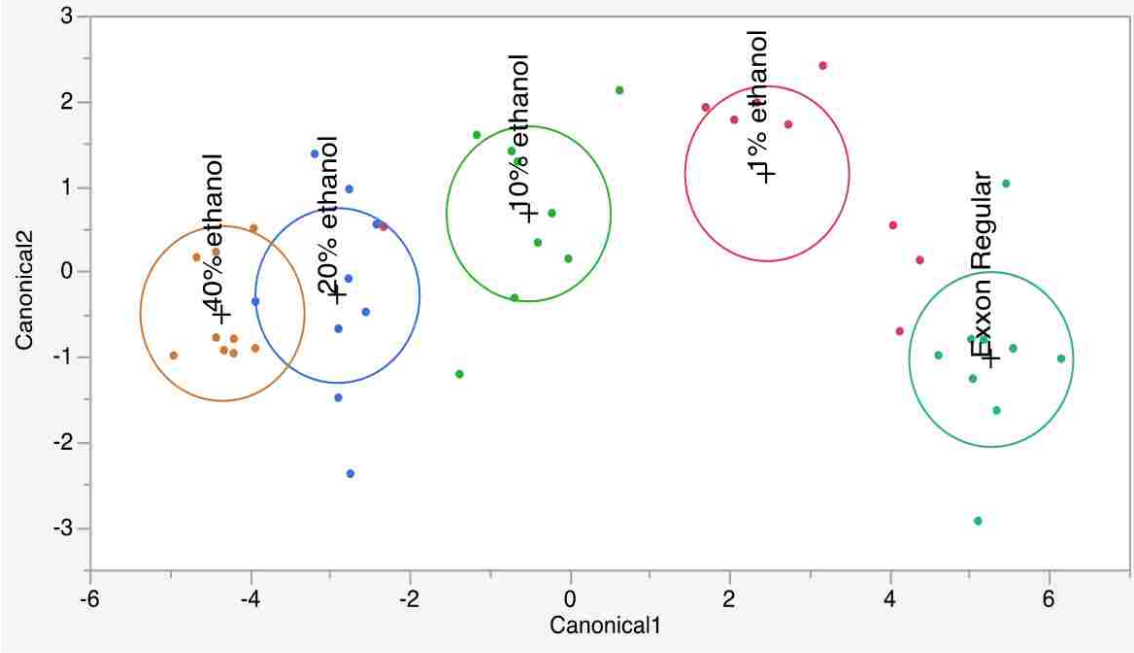

Score Summaries

	Training
Number Misclassified	5
Percent Misclassified	11.11
-2LogLikelihood	49.21

Training

Counts: Actual Rows by Predicted Columns

	1% ethanol	10% ethanol	20% ethanol	40% ethanol	Exxon Regular
1% ethanol	6	0	1	0	2
10% ethanol	0	8	1	0	0
20% ethanol	0	0	8	1	0
40% ethanol	0	0	0	9	0
Exxon Regular	0	0	0	0	9

Figure D18. LDA Canonical plot and error rates for ethanol adulteration discrimination using a [C_8MIm][Br] VSA

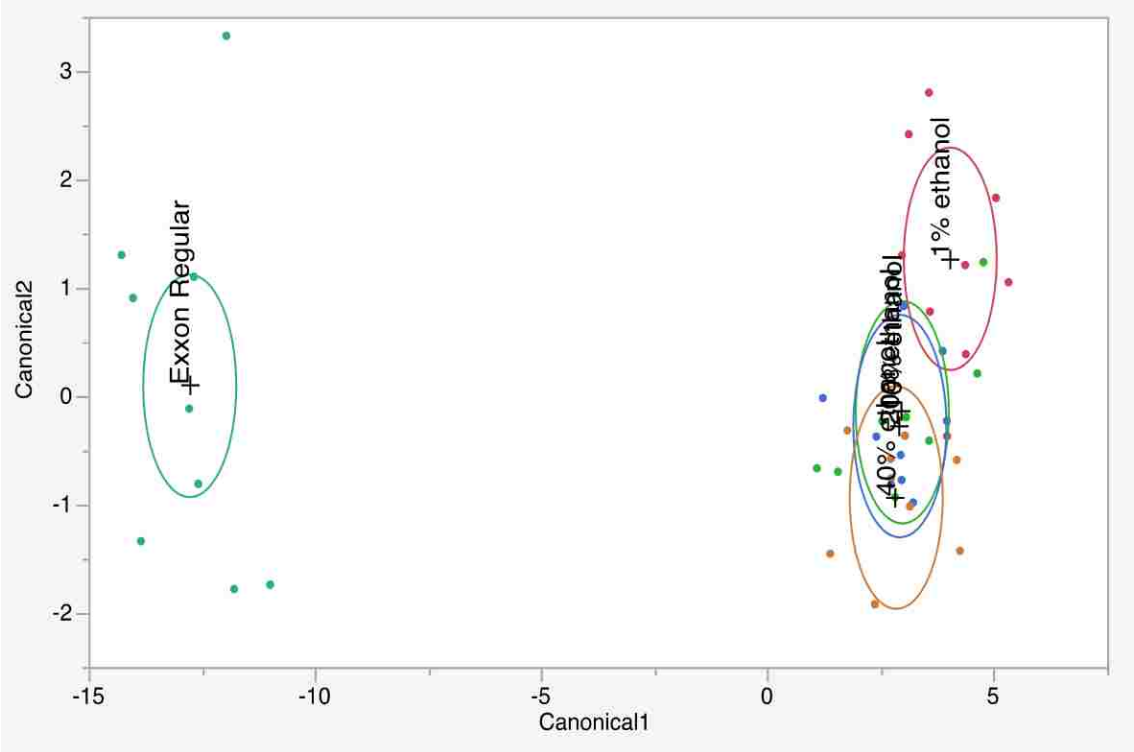

Score Summaries

	Training
Number Misclassified	13
Percent Misclassified	28.89
-2LogLikelihood	65.63

Training

Counts: Actual Rows by Predicted Columns

	1% ethanol	10% ethanol	20% ethanol	40% ethanol	Exxon Regular
1% ethanol	7	1	0	1	0
10% ethanol	2	3	3	1	0
20% ethanol	0	2	5	2	0
40% ethanol	0	0	1	8	0
Exxon Regular	0	0	0	0	9

Figure D19. LDA Canonical plot and error rates for ethanol adulteration discrimination using a [C_{10}MIm][Br] VSA

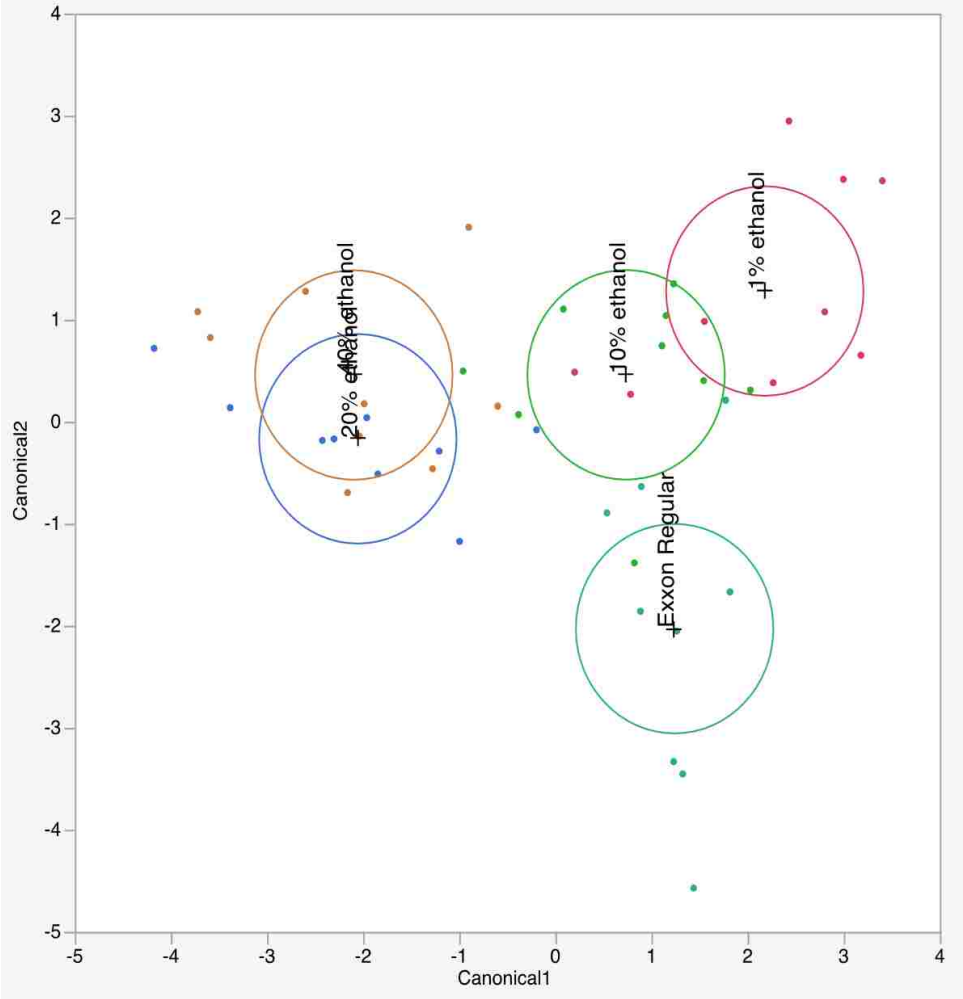

Score Summaries

	Training
Number Misclassified	15
Percent Misclassified	33.33
-2LogLikelihood	51.26

Training

Counts: Actual Rows by Predicted Columns

	1% ethanol	10% ethanol	20% ethanol	40% ethanol	Exxon Regular
1% ethanol	6	3	0	0	0
10% ethanol	2	5	1	0	1
20% ethanol	0	1	6	2	0
40% ethanol	0	0	3	6	0
Exxon Regular	0	2	0	0	7

Figure D20. LDA Canonical plot and error rates for ethanol adulteration discrimination using a [C_{12}MIm][Br] VSA

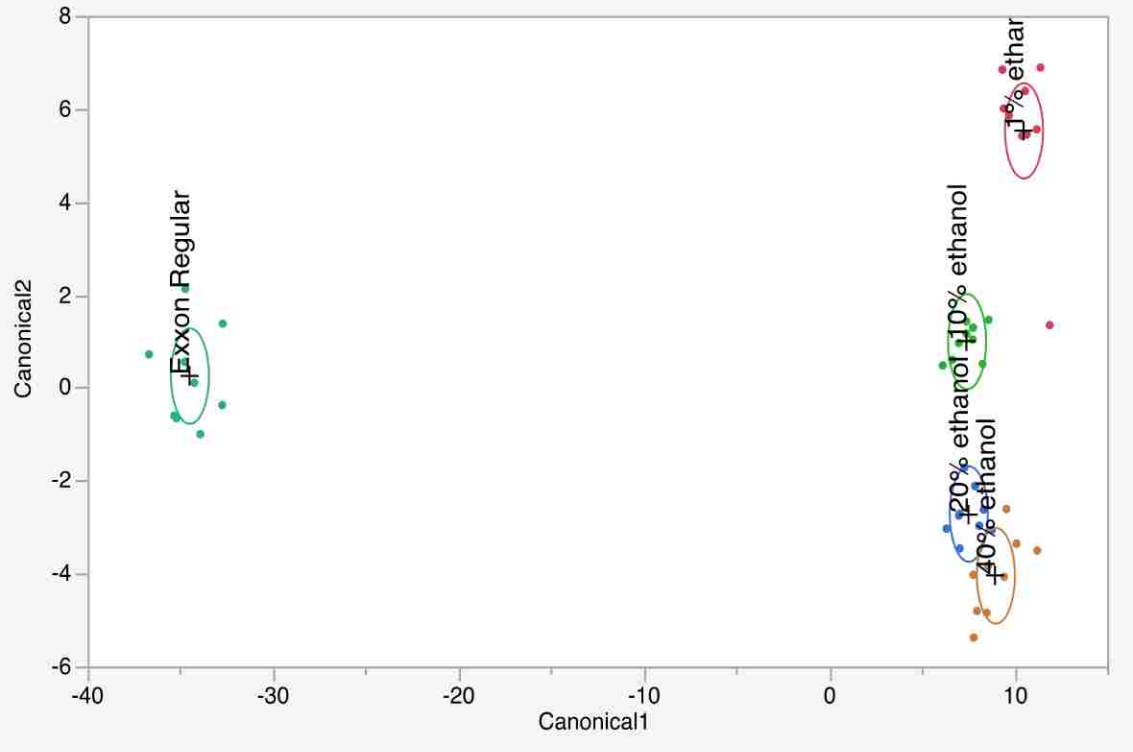

Score Summaries

	Training
Number Misclassified	1
Percent Misclassified	2.222
-2LogLikelihood	3.849

Training

Counts: Actual Rows by Predicted Columns

	1% ethanol	10% ethanol	20% ethanol	40% ethanol	Exxon Regular
1% ethanol	9	0	0	0	0
10% ethanol	0	9	0	0	0
20% ethanol	0	0	9	0	0
40% ethanol	0	0	1	8	0
Exxon Regular	0	0	0	0	9

Figure D21. LDA Canonical plot and error rates for xylenes adulteration discrimination using a four sensor V-MSA

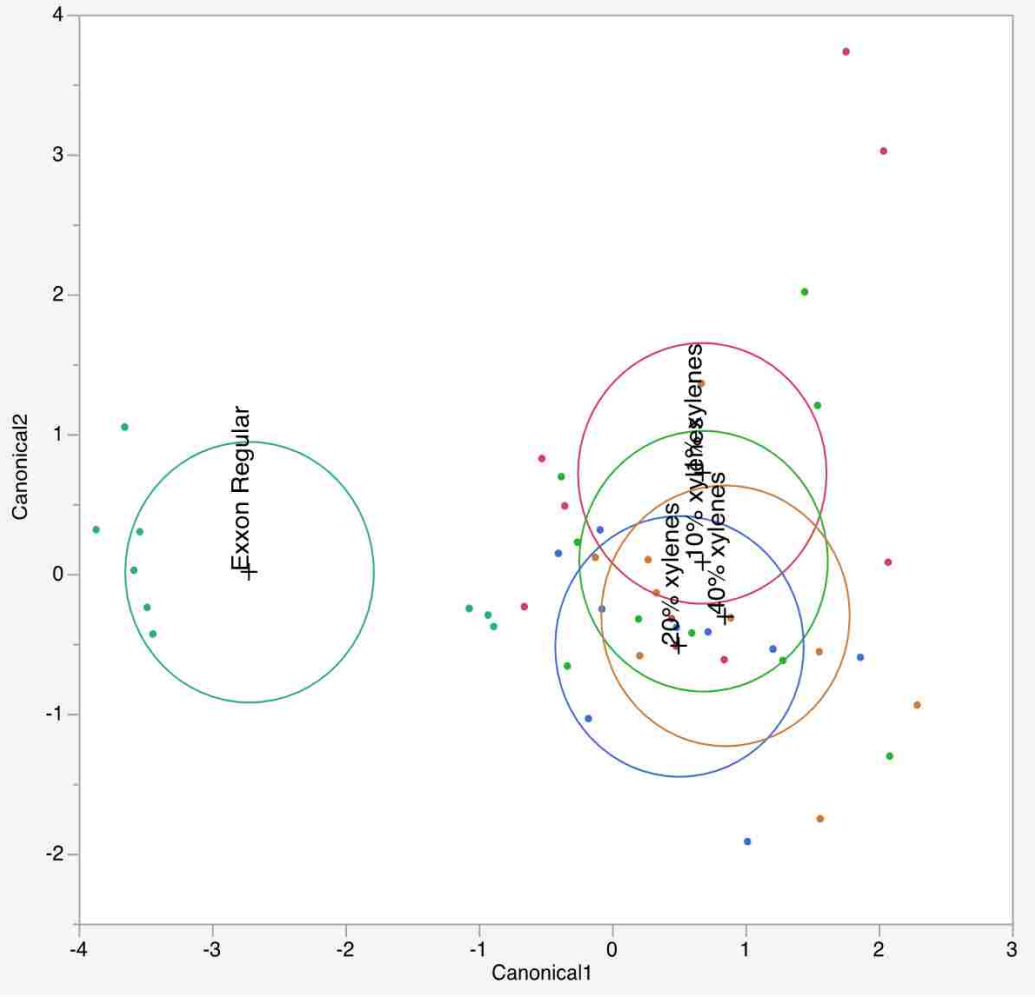

Score Summaries

	Training
Number Misclassified	25
Percent Misclassified	55.56
-2LogLikelihood	102.1

Training

Counts: Actual Rows by Predicted Columns

	1% xylenes	10% xylenes	20% xylenes	40% xylenes	Exxon Regular
1% xylenes	4	1	1	3	0
10% xylenes	3	1	2	3	0
20% xylenes	0	2	4	3	0
40% xylenes	1	2	2	4	0
Exxon Regular	0	0	2	0	7

Figure D22. LDA Canonical plot and error rates for xylenes adulteration discrimination using a four sensor MSA

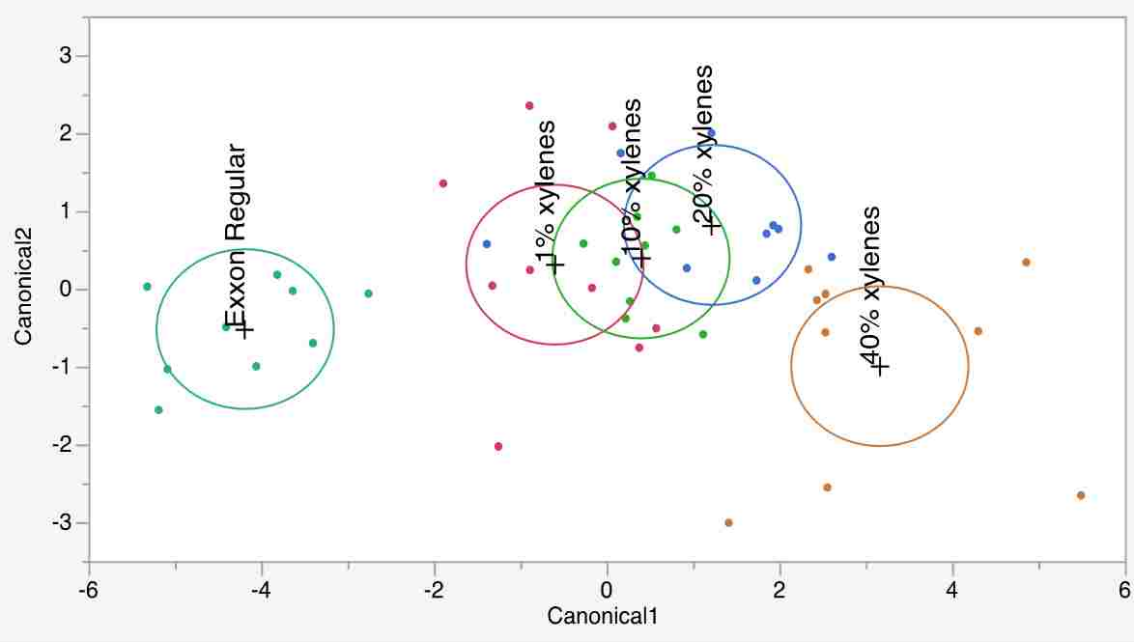

Score Summaries

	Training
Number Misclassified	9
Percent Misclassified	20
-2LogLikelihood	49.95

Training

Counts: Actual Rows by Predicted Columns

	1% xylenes	10% xylenes	20% xylenes	40% xylenes	Exxon Regular
1% xylenes	6	3	0	0	0
10% xylenes	0	7	2	0	0
20% xylenes	1	1	6	1	0
40% xylenes	0	0	1	8	0
Exxon Regular	0	0	0	0	9

Figure D23. LDA Canonical plot and error rates for xylenes adulteration discrimination using a [C_8MIm][Br] VSA

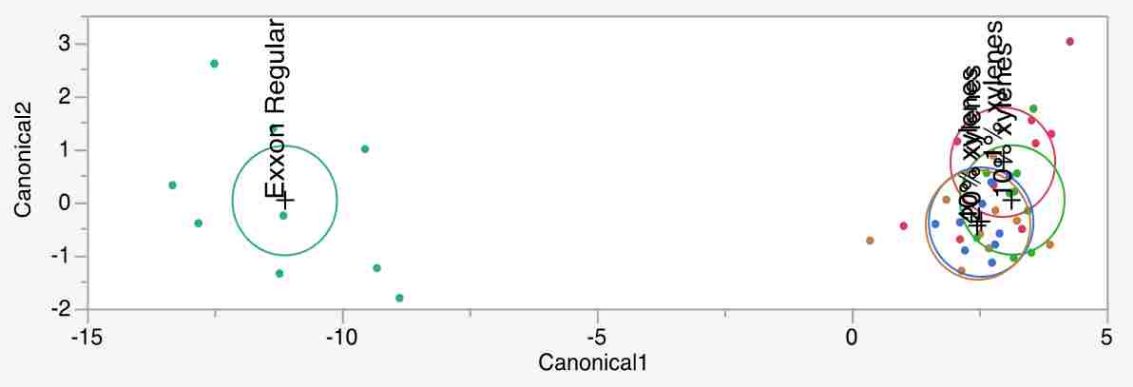

Score Summaries

	Training
Number Misclassified	20
Percent Misclassified	44.44
-2LogLikelihood	86.1

Training

Counts: Actual Rows by Predicted Columns

	1% xylenes	10% xylenes	20% xylenes	40% xylenes	Exxon Regular
1% xylenes	5	0	2	2	0
10% xylenes	2	3	2	2	0
20% xylenes	1	2	4	2	0
40% xylenes	1	3	1	4	0
Exxon Regular	0	0	0	0	9

Figure D24. LDA Canonical plot and error rates for xylenes adulteration discrimination using a [C_{10}MIm][Br] VSA

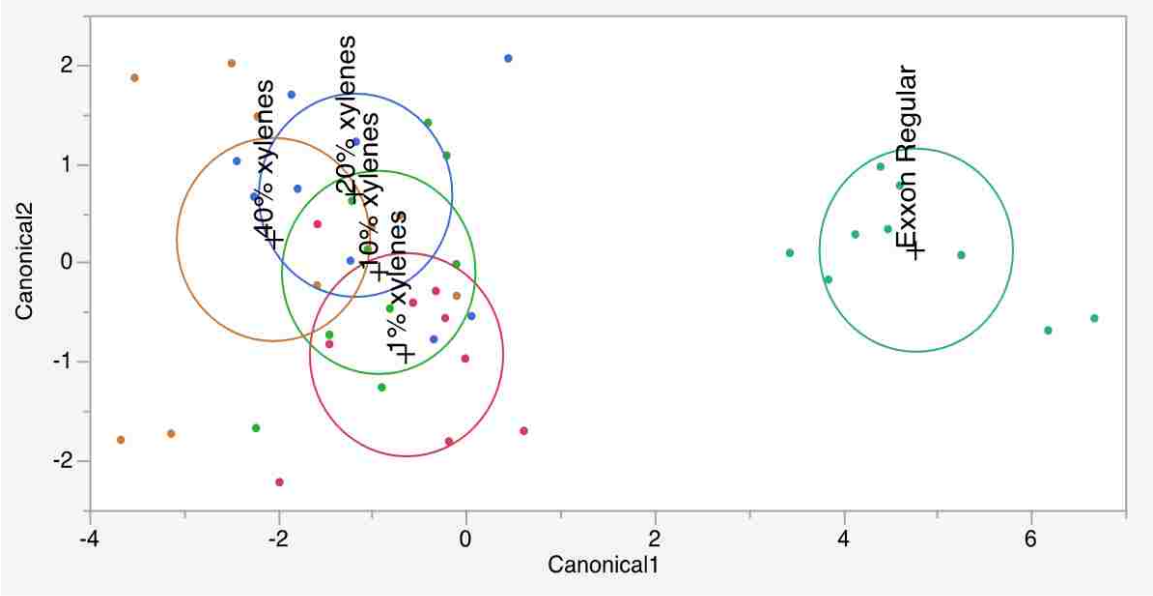

Score Summaries

	Training
Number Misclassified	19
Percent Misclassified	42.22
-2LogLikelihood	77.47

Training

Counts: Actual Rows by Predicted Columns

	1% xylenes	10% xylenes	20% xylenes	40% xylenes	Exxon Regular
1% xylenes	6	2	1	0	0
10% xylenes	3	2	3	1	0
20% xylenes	2	1	4	2	0
40% xylenes	0	2	2	5	0
Exxon Regular	0	0	0	0	9

Figure D25. LDA Canonical plot and error rates for xylenes adulteration discrimination using a [C_{12}MIm][Br] VSA

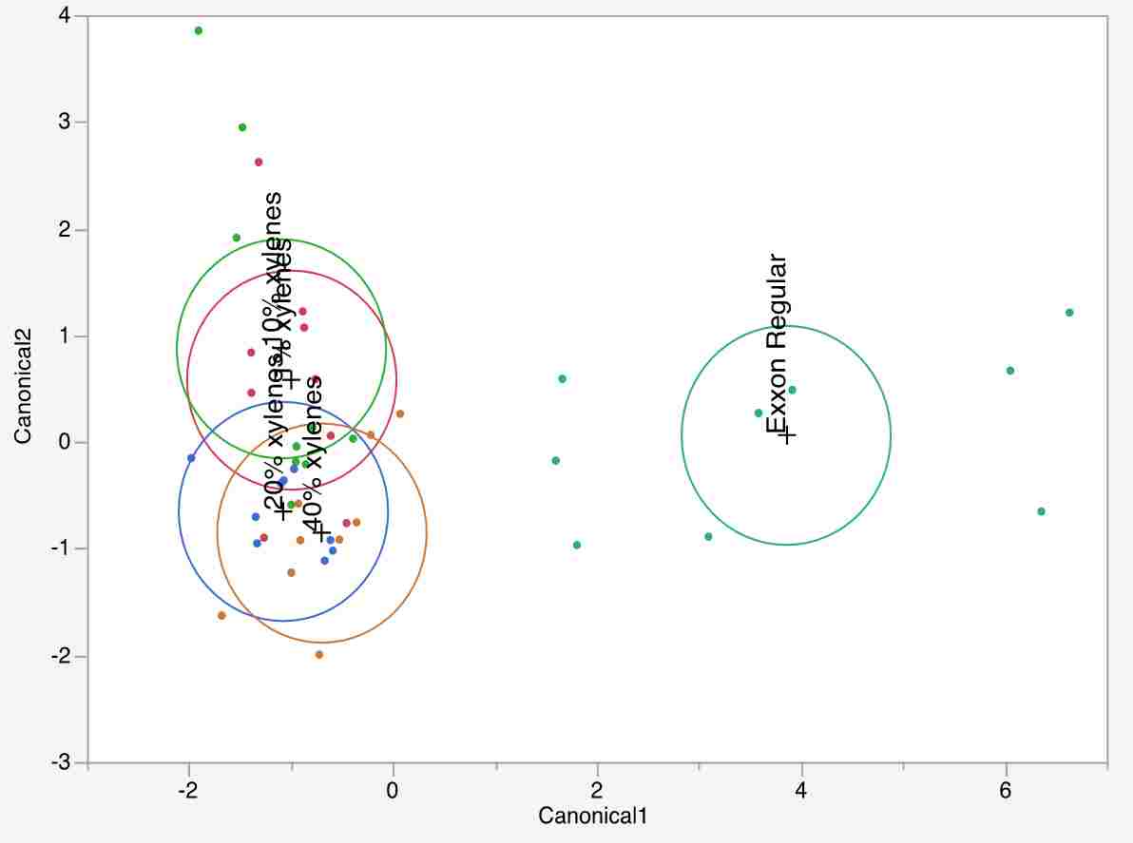

Score Summaries

	Training
Number Misclassified	18
Percent Misclassified	40
-2LogLikelihood	81.07

Training

Counts: Actual Rows by Predicted Columns

	1% xylenes	10% xylenes	20% xylenes	40% xylenes	Exxon Regular
1% xylenes	3	3	1	2	0
10% xylenes	1	3	1	4	0
20% xylenes	0	0	4	5	0
40% xylenes	0	0	1	8	0
Exxon Regular	0	0	0	0	9

Figure D26. LDA Canonical plot and error rates for xylenes adulteration discrimination using a [C_{16}MIm][Br] VSA

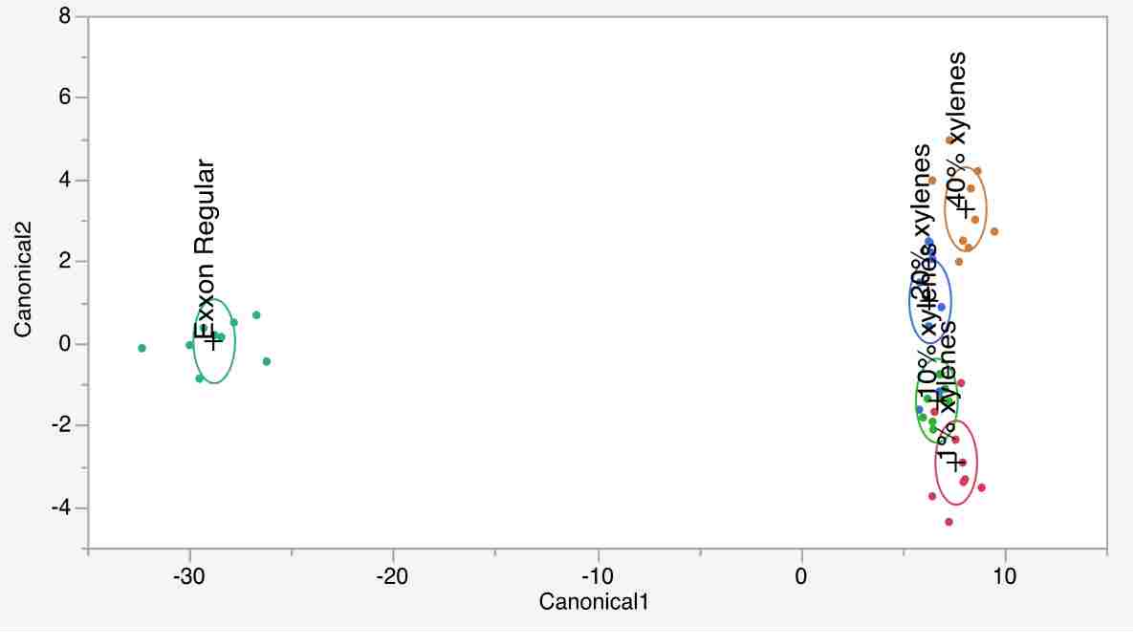

Score Summaries

	Training
Number Misclassified	3
Percent Misclassified	6.667
-2LogLikelihood	16.51

Training

Counts: Actual Rows by Predicted Columns

	1% xylenes	10% xylenes	20% xylenes	40% xylenes	Exxon Regular
1% xylenes	8	1	0	0	0
10% xylenes	0	9	0	0	0
20% xylenes	0	1	8	0	0
40% xylenes	0	0	1	8	0
Exxon Regular	0	0	0	0	9

Figure D27. LDA Canonical plot and error rates for xylenes adulteration discrimination using a a four sensor V-MSA

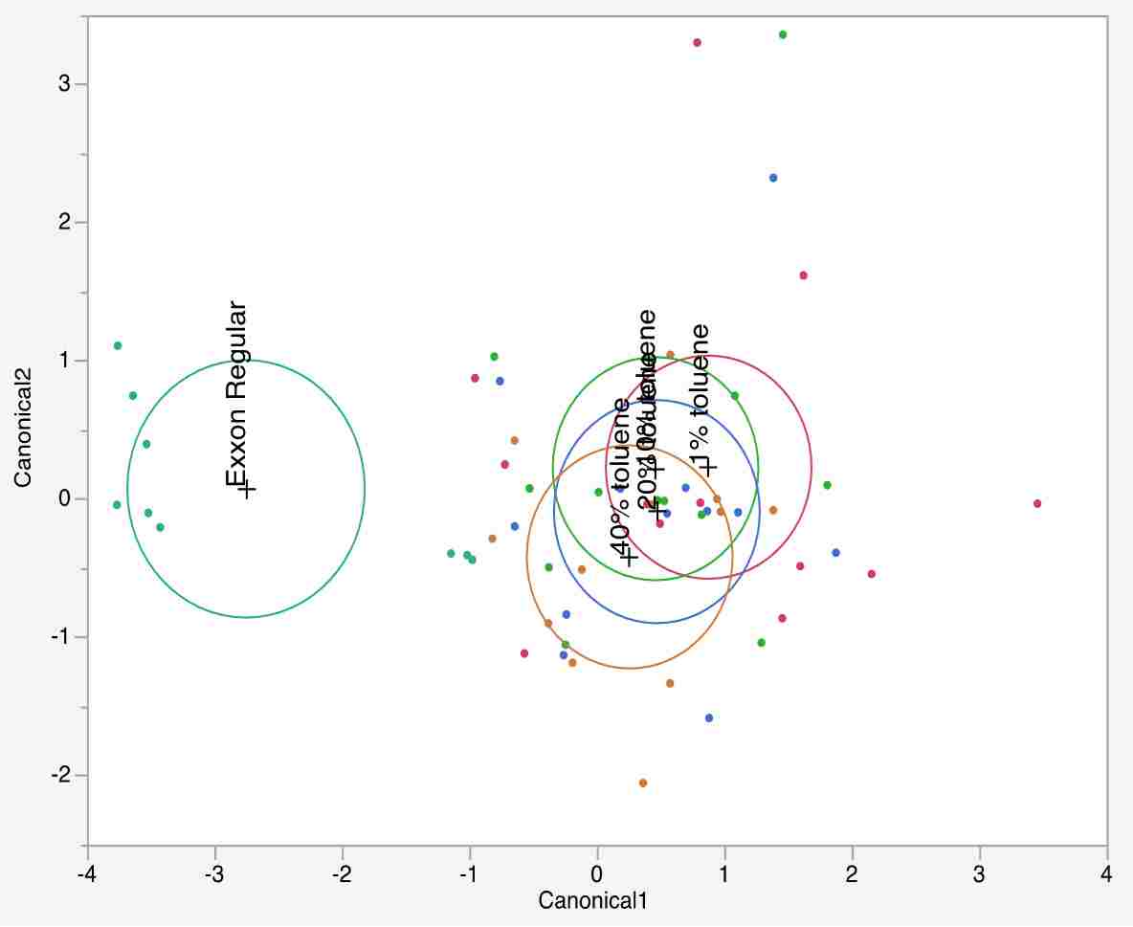

Score Summaries

	Training
Number Misclassified	36
Percent Misclassified	63.16
-2LogLikelihood	139.6

Training

Counts: Actual Rows by Predicted Columns

	1% toluene	10% toluene	20% toluene	40% toluene	Exxon Regular
1% toluene	6	2	1	3	0
10% toluene	6	1	1	4	0
20% toluene	5	1	1	5	0
40% toluene	3	2	0	7	0
Exxon Regular	0	0	0	3	6

Figure D28. LDA Canonical plot and error rates for toluene adulteration discrimination using a four sensor MSA

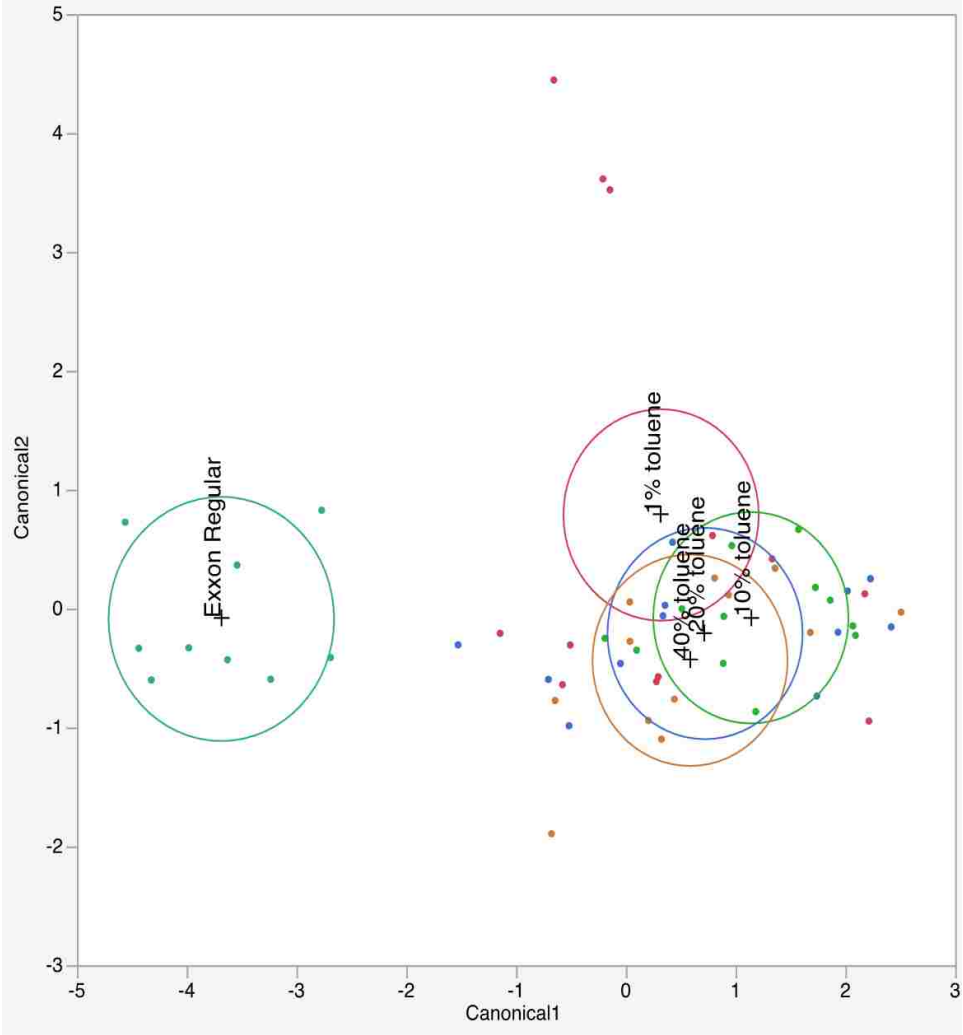

Score Summaries

	Training
Number Misclassified	29
Percent Misclassified	50.88
-2LogLikelihood	122

Training

Counts: Actual Rows by Predicted Columns

	1% toluene	10% toluene	20% toluene	40% toluene	Exxon Regular
1% toluene	3	4	0	5	0
10% toluene	0	7	2	3	0
20% toluene	1	5	1	5	0
40% toluene	0	3	1	8	0
Exxon Regular	0	0	0	0	9

Figure D29. LDA Canonical plot and error rates for toluene adulteration discrimination using a [C_8MIm][Br] VSA

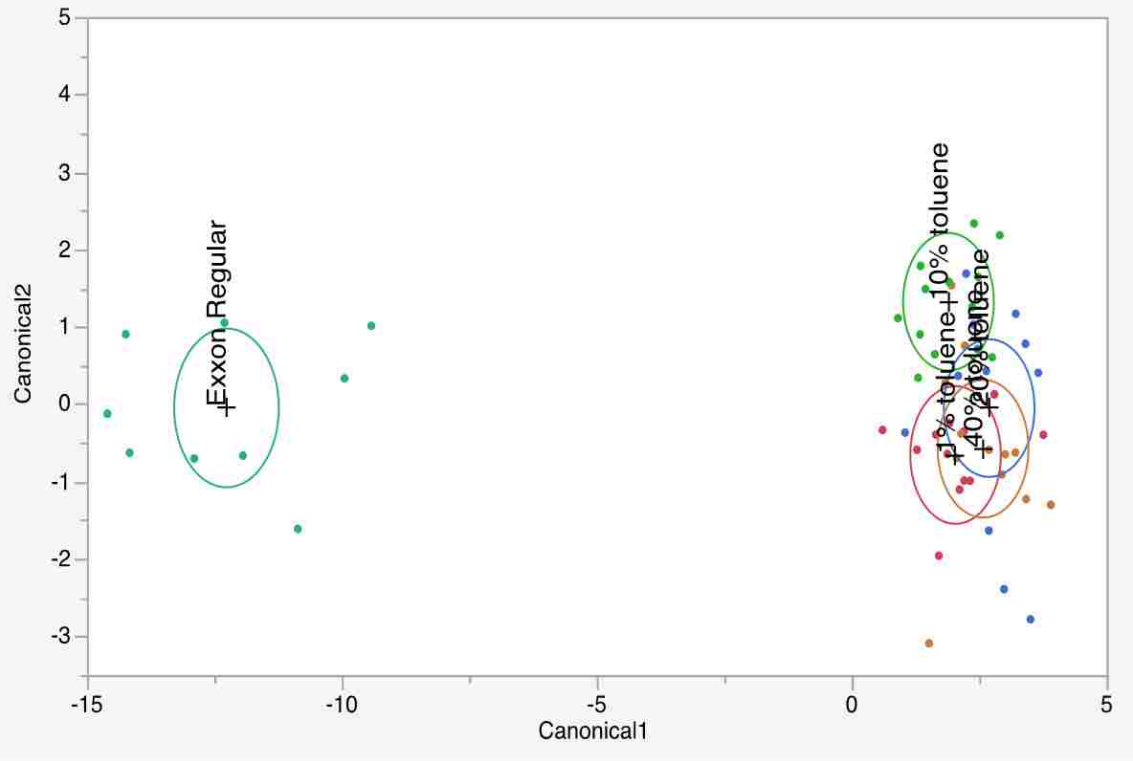

Score Summaries

	Training
Number Misclassified	19
Percent Misclassified	33.33
-2LogLikelihood	96.55

Training

Counts: Actual Rows by Predicted Columns

	1% toluene	10% toluene	20% toluene	40% toluene	Exxon Regular
1% toluene	8	0	1	3	0
10% toluene	0	11	1	0	0
20% toluene	3	3	4	2	0
40% toluene	3	2	1	6	0
Exxon Regular	0	0	0	0	9

Figure D30. LDA Canonical plot and error rates for toluene adulteration discrimination using a [C_{10}MIm][Br] VSA

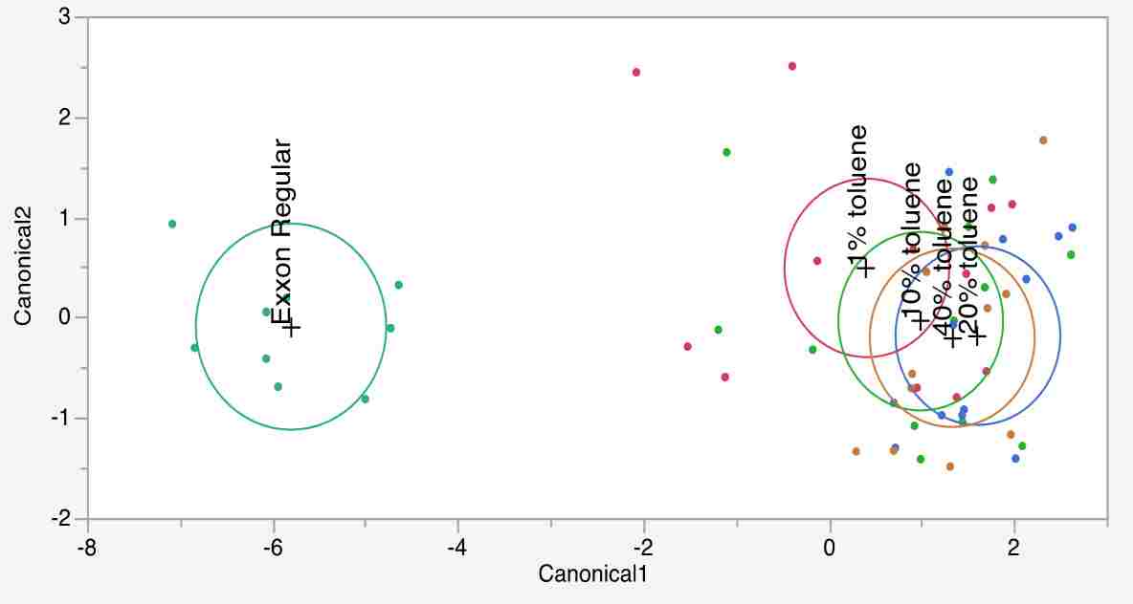

Score Summaries

	Training
Number Misclassified	27
Percent Misclassified	47.37
-2LogLikelihood	119.5

Training

Counts: Actual Rows by Predicted Columns

	1% toluene	10% toluene	20% toluene	40% toluene	Exxon Regular
1% toluene	6	0	4	2	0
10% toluene	2	3	4	3	0
20% toluene	1	1	6	4	0
40% toluene	1	1	4	6	0
Exxon Regular	0	0	0	0	9

Figure D31. LDA Canonical plot and error rates for toluene adulteration discrimination using a [C_{12}MIm][Br] VSA

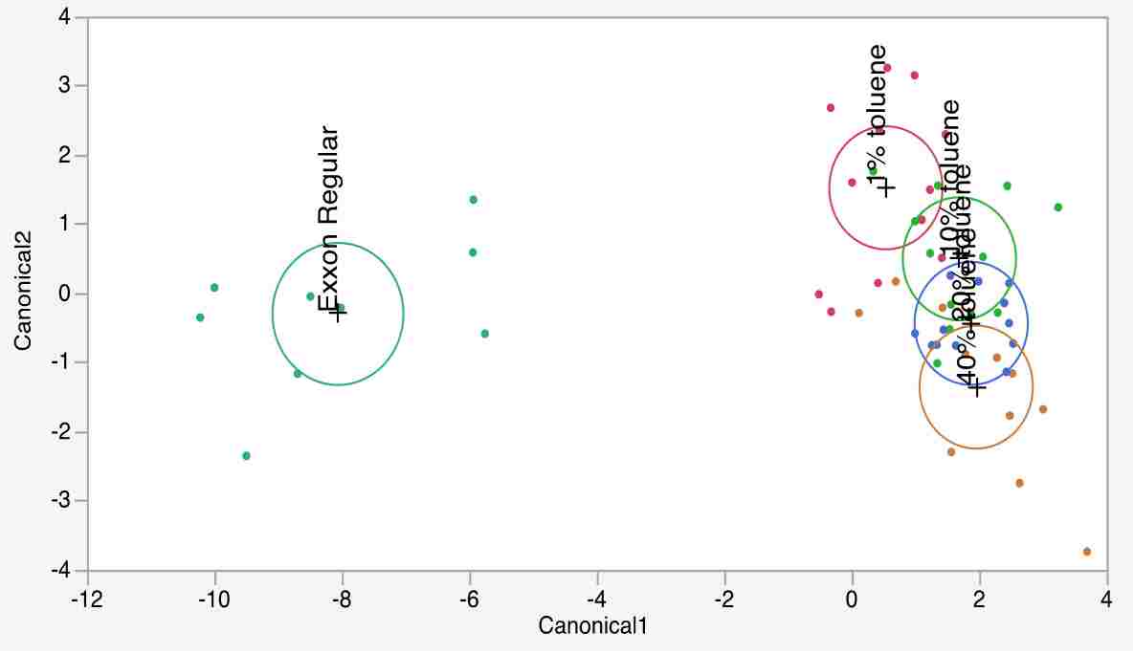

Score Summaries

	Training
Number Misclassified	16
Percent Misclassified	28.07
-2LogLikelihood	79.56

Training

Counts: Actual Rows by Predicted Columns

	1% toluene	10% toluene	20% toluene	40% toluene	Exxon Regular
1% toluene	11	1	0	0	0
10% toluene	3	5	3	1	0
20% toluene	0	1	9	2	0
40% toluene	1	1	3	7	0
Exxon Regular	0	0	0	0	9

Figure D32. LDA Canonical plot and error rates for toluene adulteration discrimination using a [C_{16}MIm][Br] VSA

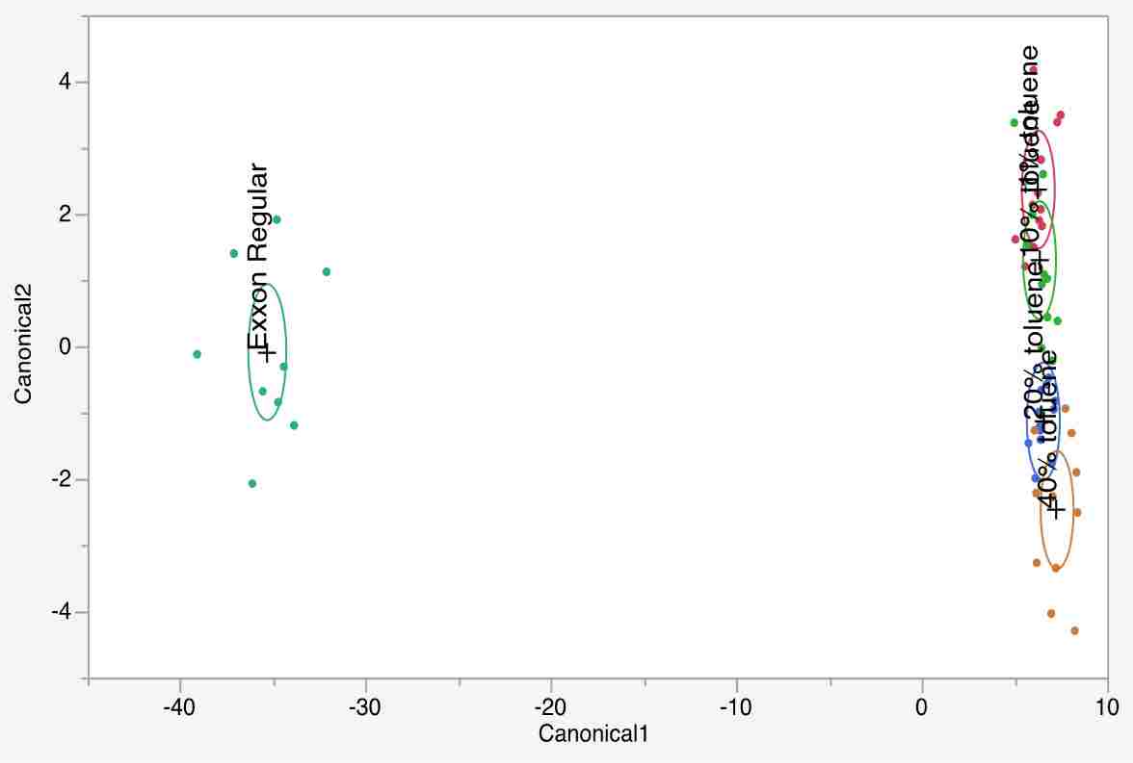

Score Summaries

	Training
Number Misclassified	4
Percent Misclassified	7.018
-2LogLikelihood	24.71

Training

Counts: Actual Rows by Predicted Columns

	1% toluene	10% toluene	20% toluene	40% toluene	Exxon Regular
1% toluene	12	0	0	0	0
10% toluene	0	12	0	0	0
20% toluene	0	0	12	0	0
40% toluene	0	0	4	8	0
Exxon Regular	0	0	0	0	9

Figure D33. LDA Canonical plot and error rates for toluene adulteration discrimination using a four sensor V-MSA

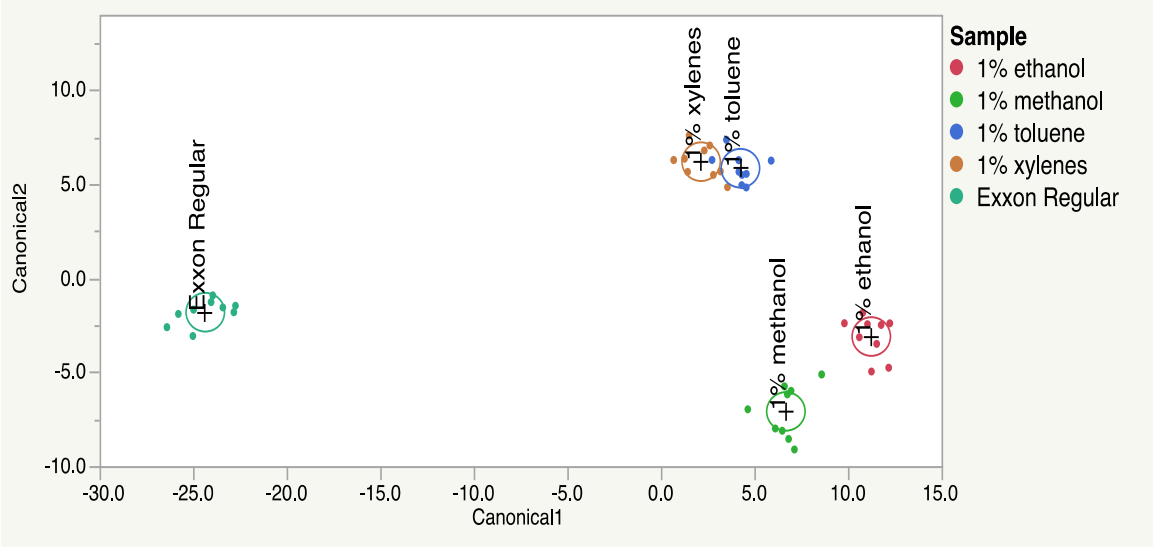

Score Summaries

	Training
Number Misclassified	0
Percent Misclassified	0
-2LogLikelihood	2e-5

Training

Counts: Actual Rows by Predicted Columns

	1% ethanol	1% methanol	1% toluene	1% xylenes	Exxon Regular
1% ethanol	9	0	0	0	0
1% methanol	0	9	0	0	0
1% toluene	0	0	9	0	0
1% xylenes	0	0	0	9	0
Exxon Regular	0	0	0	0	9

Figure D34. LDA Canonical plot and error rates for 1%v/v adulteration discrimination using a four sensor V-MSA

APPENDIX E: LETTER OF PERMISSION

Copyright Clearance Center RightsLink®

Home | Create Account | Help | Live Chat

ACS Publications
Most Trusted. Most Cited. Most Read.

Title: Rational Design of QCM-D Virtual Sensor Arrays Based on Film Thickness, Viscoelasticity, and Harmonics for Vapor Discrimination

Author: Nicholas C. Speller, Noureen Siraj, Bishnu P. Regmi, et al

Publication: Analytical Chemistry

Publisher: American Chemical Society

Date: May 1, 2015

Copyright © 2015, American Chemical Society

LOGIN

If you're a copyright.com user, you can login to RightsLink using your copyright.com credentials. Already a RightsLink user or want to learn more?

PERMISSION/LICENSE IS GRANTED FOR YOUR ORDER AT NO CHARGE

This type of permission/license, instead of the standard Terms & Conditions, is sent to you because no fee is being charged for your order. Please note the following:

- Permission is granted for your request in both print and electronic formats, and translations.
- If figures and/or tables were requested, they may be adapted or used in part.
- Please print this page for your records and send a copy of it to your publisher/graduate school.
- Appropriate credit for the requested material should be given as follows: "Reprinted (adapted) with permission from (COMPLETE REFERENCE CITATION). Copyright (YEAR) American Chemical Society." Insert appropriate information in place of the capitalized words.
- One-time permission is granted only for the use specified in your request. No additional uses are granted (such as derivative works or other editions). For any other uses, please submit a new request.

BACK | CLOSE WINDOW

Copyright © 2016 Copyright Clearance Center, Inc. All Rights Reserved. Privacy statement. Terms and Conditions.
Comments? We would like to hear from you. E-mail us at customercare@copyright.com

VITA

Nicholas C. Speller was born in Norfolk, Virginia to William Speller and Delbra Coutee-Speller. He attended numerous high schools ultimately graduating from Cartersville High School in Cartersville, Ga. Thereafter, he attended Morehouse College, in Atlanta Ga, where he obtained a Bachelors of Science Degree in Biology, and a Bachelors of Science Degree in Chemistry, in May 2011. In August 2011, he joined the Chemistry Department at Louisiana State University as a graduate student. Subsequently, he joined Professor Isiah Warner's research group in Spring of 2012, where he continued his doctoral studies in analytical chemistry. His doctoral studies focused on the design, and implementation of QCM virtual sensor arrays for volatile organic compound analyses. During his time as a graduate student, he received two fellowships including a prestigious NSF graduate research fellowship, published several peer-reviewed manuscripts and has several others under varying stages of preparation and submission. Additionally, he won the James W. Robinson award in analytical chemistry and a RA scholar award. He has presented at multiple conferences and holds memberships in the American Chemical Society (ACS) and the National Organization for the Professional Advancement of Black Chemist and Chemical Engineers (NOBCChE). After graduation he plans on completing a post-doctoral appointment, and thereafter attending medical.